University of Alberta

Development of polymer and lipid based nano-delivery systems for targeted cancer chemotherapy

By

Mostafa Hussein Shahin

A thesis submitted to the Faculty of Graduate Studies and Research

in partial fulfillment of the requirements for the degree of

Doctor of Philosophy

in

Pharmaceutical Sciences

Faculty of Pharmacy and Pharmaceutical Sciences

Fall 2012

Edmonton, Alberta

Dedication

I dedicate this thesis to my beloved father and mother, whose prayers and encouragement gave me hope and strength throughout the Ph D program.

Abstract

Conventional chemotherapy agents can kill tumor cells and inhibit tumor growth, but they produce severe side effects on normal cells at the same time. To shift the balance towards tumoral effects, it would be desirable to direct the anti-cancer drug towards tumor while restricting drug access to normal tissues. The main objective of this thesis was to develop tumor targeted drug delivery system that can take on this task and as a result, improve the specificity and anticancer activity of the incorporated anticancer drugs towards tumor. To this end, lipid and block copolymer based nano-delivery systems of two conventional anti-cancer agents doxorubicin (DOX) and paclitaxel (PTX) are developed, respectively, and modified on their surface with a 12mer breast tumor interacting peptide, namely p160, or its engineered derivatives developed in our research team. The effect of peptide decoration on the specific interaction as well as anti-cancer activity of developed nano-formulations against human breast tumor cells over normal epithelial breast cells or endothelial cells was characterized, in vitro. In this study, micelles of poly(ethylene oxide)-b-poly(ε-caprolactone) were prepared and modified with either c(RGDfK) or p160 and loaded with paclitaxel (PTX). Peptide decoration enhanced the selective cytotoxicity of encapsulated PTX against cancer cells over normal cells. The extent of this increase in cancer cell specificity for encapsulated PTX was more for p160-modified micelles. At the end, the anti-cancer activity of liposomal formulations of DOX, having different density of an engineered breast tumor targeting peptide, namely p-18-4, was assessed in vitro for cellular uptake and selective cytotoxicity, and in vivo using animal model of human breast tumor xenograft and compared to that for liposomal formulations of DOX with no peptide decoration. Liposomal DOX formulations bearing low p18-4 density showed better in vitro selective cytotoxicity and in vivo therapeutic efficacy. Our results points to the potential of p160 and its engineered derivatives as efficient ligands on lipid and block copolymer based nanocarriers for active targeting of anticancer agents to breast

tumors. The results also show the success of this strategy in enhancing the specific anti-cancer effects of the incorporated drug against breast tumor models.

Acknowledgment

I would like to express my deepest gratitude to all of the following people.

- My supervisor Dr. Afsaneh Lavasanifar for giving me the opportunity to pursue my studies in her lab. Her encouragement, guidance and financial and academic support throughout the program enabled me to develop an understanding of the field of targeted nano-carriers and also to develop a deep understanding of the point of my research question. I cannot forget her endless support during the times of hardship that I faced during my Ph D program.
- My supervisory committee members, Dr. Kamaljit Kaur and Dr. Raimer lobenberg for their generous guidance and valuable comments and suggestions.
- My wife Nesrine and my little kids Logean and Mohamed who helped and supported me with all love and patience during the whole time. Without their help, support and passion I would not have been able to complete my advanced studies.
- Dr. Hamid Montazeri, Dr. Samar Hamdy, Dr. Leila Molavi, Ms. Chelcey Dibben, for their sincere help in animal studies.
- Dr John Seubert and Haitham El-sikhry for their help in the fluorescence microscopy imaging experiment.
- Dr Sahar Ahmed, Rania Soudy for their help in the peptide synthesis.
- Ms. Elaine Moase for her help in the cell culture work, and some manuscript proofreading.
- Dr. Vishwa Somayaji for his help with the mass spectrometry.
- Mr. Jeff Turchinsky for helping us to order all the chemicals and supplies needed for my lab.
- All my previous and current lab mates (Dr. Mohammad Vakili, Arash Falamarzian, Nazila Safei Nikouei, Shyam Garg, Hoda Soleymani) for creating a wonderful work environment in the lab.

- Mrs. Joyce Johnson for her help to facilitate all the administrative and paper work need during my studies.

Finally, I would like to thanks all the funding agencies and institutes for their financial support.

- The Egyptian Government Scholarship for supporting me during the first four years of my program.
- The Canadian Institute of Health and Research (CIHR) for supporting me with both Frederick Banting and Charles Best Canada Graduate Scholarship & ICR publication Prize.
- Faculty of Pharmacy and Pharmaceutical Sciences for the Shoppers Drug Mart Scholarship and the Teaching Assistantship.
- Graduate Student Association, University of Alberta for the professional development and travel grant.
- Women and Children Health Research Institute for the travel award.
- American Association of Pharmaceutical Sciences for the travel award.
- Controlled Release Society-Canadian Chapter for the travel award.

Table of Contents:

List of Tables

List of Figures

List of Schemes

List of abbreviations

ABC	ATP-Binding Cassette
ACN	Acetonitrile
AFM	Atomic force microscopy
ANOVA	Analysis of variance
APN	Aminopeptidase-N
ATP	Adenosine-5'-triphosphate
AUC	Area under the curve
BALB	Bagg Albino (inbred research mouse strain)
BCA	Bicinchoninic acid
BCL	α-Benzylcarboxylate ε-caprolactone
BCRP	breast cancer related protein
BOP	benzotriazol-1-yloxy-tris(dimethylamino)-phosphonium hexafluorophosphate
Bu-Li	Butyl Lithium
$CDCL_3$	Deuterated chloroform
CDI	Carbonyldiimidazole
CHOL	Cholesterol
ε-CL	Caprolactone
CMC	Critical micelle concentration
CPP	Cell-penetrating peptide
CPT	Camptothecin
c(RGDfK)	Cyclic(Arginine –Glycine-Aspartic-D-Phenylalanine-Lysine)

CSPG	Chondrointin sulfate proteoglycan
Da	Dalton
DAPI	4’,6-diamidino-2-phenylindole
DCB	dichlorobenzoyl chloride
DCC	N,N’-Dicyclohexylcarbodiimide
DCM	Dichloromethane
DEP	3,3 diethoxy 1-propanol
DIC	N,N-Disopropylcarbodiimide
DiI	*[1,1' - Dioctadecyl - 3,3,3',3' - tetramethylindocarbocyanine iodide]*
DIPEA	Piperidine, N, N diisopropyl ethylamine
DLS	Dynamic light scattering
DMAP	4-Dimethylaminopyridine
DMEM	Dulbecco’s modified eagle medium
DMF	Dimethyl formamide
DMSO	Dimethyl sulfoxide
DNA	Deoxyribonucleic acid
DOPC	Dioleoylphos-phatidylcholine
DOX	Doxorubicin
DPPG	dipalmitoylphosphatidylglycerol
DSC	N , N-Disuccinimidyl carbonate
DSPC	disaturated-phosphatidylcholine
DSPE	1,2-distearoyl-sn-glycero-3-phosphoethanolamine
ECM	Extracellular matrix
EDC	1-Ethyl-3-(3-dimethylaminopropyl) carbodiimide

EDTA	Ethylenediaminetetraacetic acid
EGF	Epidermal growth factor
EGFR	Epidermal growth factor receptors
EMS	Ethyl methane sulfonate
EPR	Enhanced permeation and retention
FACS	Fluorescence activated cell sorter
FBS	Fetal bovine serum
FCS	Fetal calf serum
FDA	Food and drug administration
FdU-NOAC	2’-deoxy-5-fluorouridylyI-N^4-octadecyl-1-βD-
FGFR	fibroblast growth factor receptors
tb-FGF	Truncated basic fibroblast growth factor
FITC	Fluorescein isothiocyanate
Fmoc	9-Fluorenylmethyloxycarbonyl
GDP	Guanosine-5'-diphosphate
GIT	Gastrointestinal tract
GM-CSF	Granulocyte-macrophage colony-stimulating factor
GPC	Gel permeation chromatography
GTP	Guanosine-5'-triphosphate
h	Hour
HB-EGF	Heparin-binding epidermal growth factor
HCTU	(2-(6-chloro-1H-benzotriazole-1-yl)-1,1,3,3-tetramethylaminium hexafluorophosphate)
HIV	Human immunodeficiency virus
HOBt	N-Hydroxybenzotriazole

HPLC	High performance liquid chromatography
HSPC	Hydrogenated soy phosphatidyl choline
HUVEC	Human umbilical vein endothelial cells
IC_{50}	Inhibitory Concentration for 50%
I_e/I_m	Intensity ratio of excimer to monomer
ICAM-1	Intercellular Adhesion Molecule 1
IGFI-R	Insulin-like growth factor I receptor
IPA	Isopropyl alcohol
i.v.	Intravenous
L	Litre
LUV	Large unilamellar vesicles
LVEF	Left ventricular ejection fraction
M	Molar
mAb	Monoclonal antibody
MALDI	Matrix-assisted laser desorption/ionization
MDR	Multidrug resistance
MEGM	Mammary epithelial cell growth medium
MePEO	Methoxy poly(ethylene oxide)
mg	Milligram
min	Minute
mL	Millilitre
MLV	Multi lamellar vesicles
M_n	Number average molecular weight
M_w	Weight average molecular weight
MRP	Multidrug resistance associated protein

MTD	Maximum tolerated dose
MTT	(3-(4,5-Dimethylthiazol-2-yl)-2,5-diphenyltetrazolium bromide
MW	Molecular weight
NCS	Neocarcinostatin
NGR	Asparagine-Glycine-Arginine
NHS	N-hydroxysuccinimide
nm	Nanometer
NMM	N-methyl morpholine
NMP	N-methyl-2-pyrrolidone
NMR	Nuclear magnetic resonance
NOD	Non-obese diabetic
NPC	Nasopharyngeal carcinoma
NRP-1	Neuropilin-1
NSCLC	Non-small cell lung cancer
OLV	Oligolammelar vesicle
PBCL	Poly(α-Benzylcarboxylate ε-caprolactone)
PBS	Phosphate buffer saline
PCCL	Poly(α-carboxylate ε-caprolactone)
PCL	Poly(ε-caprolactone)
PDI	Poly dispersity index
PDLLA	Poly-DL-lactide
PEG	Polyethylene glycol
PEI	Polyethelenimine
PEO	Polyethylene oxide

PEO-b-PBCL	Polyethylene oxide-block-poly(α-benzyl carboxylate-ε-caprolactone)
PEO-b-PCCL	Polyethylene oxide-block-poly(α-carboxyl-ε-caprolactone)
PEO-b-PCL	Polyethylene oxide-block-poly(ε-caprolactone)
PEO-b-P(CL-PTX)	Polyethylene oxide-block-poly(α-carboxyl Paclitaxel-ε-caprolactone)
PGA	Polyglutamic acid
PLA	Poly L-lactide
PLGA	poly(lactic-co-glycolic acid)
PMT	Photomultiplier
PPO	Poly(propylene oxide)
PSC-833	Valspodar
PTX	Paclitaxel
PVC	Polyvinyl chloride
RES	Reticuloendothelial system
RGD	Arginine-Glycine-Aspartic acid
RNA	Ribonucleic acid
RON	Recepteur d'origine nantais
RP-HPLC	Reversed phase high performance liquid chromatography
rpm	Round per minute
s.c.	Subcutaneous
scFv	Single chain variable fragment
SCID	Severe combined immunodeficiency
SD	Standard deviation

SEM	Scanning electron microscopy
SEM	Standard error of mean
siRNA	Small interfering Ribonucleic acid
SMA	Poly(styrene-co-maleic anhydride)
SMANCS	Poly(styrene-co-maleic anhydride) and Neocarcinostatin
SUV	Small unilamellar vesicles
TAT	Trans-activating transcriptional activator
tb-FGF	Truncated basic fibroblast growth factor
TEC	Tumor endothelial cells
TEM	Transmission electron microscopy
TFA	Tri-Flouro acetic acid
THF	Tetrehydrofuran
TIPS	Triisopropyl silane
TLC	Thin layer chromatography
TOF	Time of flight
TNB	5-sulfido-2-nitrobenzoate
TNF-α	Tumor necrosis factor alpha
µL	microlitre
µM	micrometer
UV	Ultraviolet
VEGF	Vascular endothelial growth factor
Vis	Visible

Amino Acid abbreviations

Ala (A)	Alanine
Arg (R)	Arginine
Asn (N)	Asparagine
Asp (D)	Aspartic acid
Cys (C)	Cysteine
Gln (Q)	Glutamine
Glu (E)	Glutamic acid
Gly (G)	Glycine
His (H)	Histidine
Leu (L)	Leucine
Lys (K)	Lysine
Phe (F)	Phenylalanine
Pro (P)	Proline
Tyr (Y)	Tyrosine
Valine (V)	Valine
Trp (W)	Tryptophan
Nle (X)	Norleucine
β-Ala (Z)	β-Alanine
Ile (I)	Isoleucine

Chapter 1
Introduction

1.1 Introduction

1.1.1 Nanotechnology in Cancer therapy: An overview

Cancer is the main cause of death in economically developed countries with an incidence rate of more than twelve million case annually [1]. Current cancer treatment options are restricted to chemotherapy, radiation and surgery [2]. Although conventional cancer treatment options progressed significantly during the last few years, cancer therapy is still far from optimum because it is plagued by several disadvantages that includes; non-specific distribution of the anticancer medication; insufficient concentration of medication reaching the tumor site, unacceptable toxicities, reduced capabilities to evaluate the therapeutic responses and progression of multi drug resistance [3-5]. Therefore, there is an urgent demand for new innovative technologies that could improve the performance of the currently available cancer therapeutics. In recent years, the application of nanotechnology in cancer has received considerable attention in this regard.

Nanotechnology is a new multi-disciplinary approach, which covers a wide range of research areas cutting across the disciplines of engineering, biology, physics and chemistry [6, 7]. Cancer nanotechnology is a revolutionary approach with application in cancer therapy and diagnosis. It offers a new tool

for early diagnosis and detection of cancer, its therapy, prediction of response to therapy, and/or development of personalized cancer treatments [8]. Nano-carriers used for the administration of targeted therapeutics and imaging moieties include but are not limited to liposomes, polymeric micelles, nanoparticles, dendrimers, carbon nanotubes, nanocantilever and quantum dot **(Figure 1-1)** [9, 10]. Several nanotechnology products are currently approved by FDA and are clinically utilized mostly for cancer therapy (**Table 1-1**).

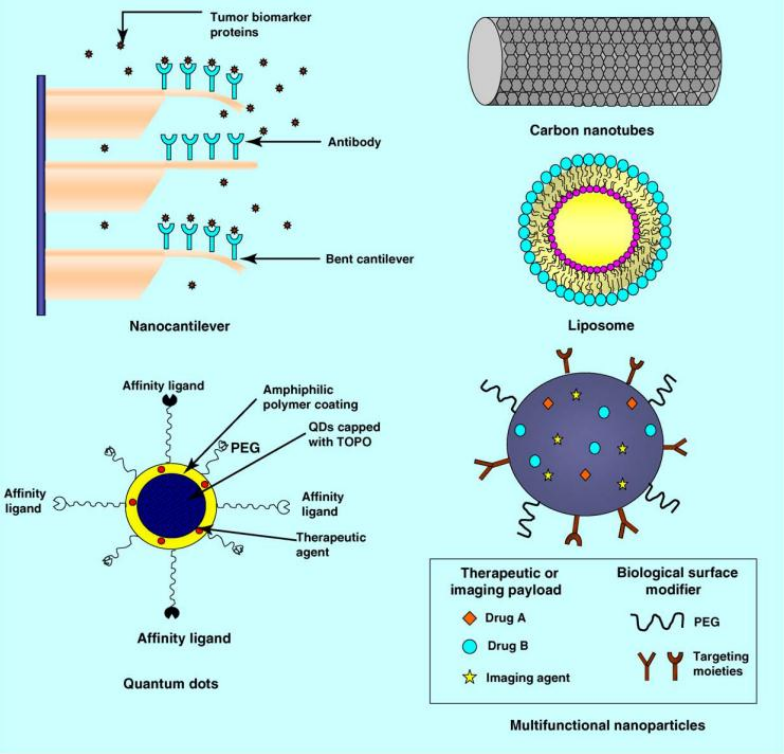

Figure 1-1: Schematics showing the different tools of cancer nanotechnology. Adapted from Ref. [9] with permission.

Table 1-1: Examples of cancer nano-carriers approved and in clinical trials.

Dosage Form	Drug	Name	Indication	Status	Reference
liposomes	Doxorubicin	Doxil	Ovarian cancer, Kaposi Sarcoma, multiple myeloma	approved	[11, 12]
	Doxorubicin	Myocet	Breast Cancer	approved (Europe)	[13]
	Doxorubicin	MCC-465[1]	Gastric cancer	Phase I	[14]
	Doxorubicin	Thermodox[2]	Liver, breast cancer	Phase III	[15, 16]
	Daunorubicin	DaunoXome	Kaposi Sarcoma	approved	[17]
	Cytarabine	DepoCyt	Malignant lymphmatous meningitis	approved	[18-20]
	Lutotecan	OSI-211	Ovarian, small lung cancer	Phase II	[21, 22]
	SN-38	LE-SN38	Colorectal cancer	Phase II	[23]
	Paclitaxel	LEP-ETU	Breast cancer	Phase II	[24]
	Paclitaxel	Endo Tag-1	Pancreatic, Breast cancer	Phase II	[25]
	irinotecan	PEP02	pancreatic cancer	Phase II	[26, 27]
	Cisplatin	Lipoplatin	Various malignancy	Phase III	[28, 29]
	Oxaliplatin	MBP-426	Various malignancies	Phase II	[30, 31]
	CKD-602	S-CKD602	Various malignancies	Phase I/II	[32-35]
Polymeric micelles	Paclitaxel	Genexol-PM	Recurrent Breast cancer	Approved (Korea), Phase II in US	[36-38]
	Paclitaxel	NK105	Stomach cancer	Phase II	[39, 40]

[1] Immunoliposomes tagged with F(ab')2 fragment of human monoclonal antibody GAH.
[2] Thermo-sensitive liposomes contacting DOX.

Dosage Form	Drug	Name	Indication	Status	Reference
	Paclitaxel	Paclical	Ovarian cancer	Phase III	[41, 42]
	Cisplatin	NC-6004	Pancreatic cancer	Phase I/ II	[43, 44]
	DACHPt	NC-4016	Colorectal cancer	Phase I	[45]
	SN-38	NK012	Metastatic breast cancer	Phase II	[46]
Nanoparticles	Paclitaxel	Abraxane (ABI-007)	Breast cancer	Approved	[47-51]
	Docetaxel	BIND-014	Advanced or metastatic cancer	Phase I	[52, 53]
	Docetaxel	Docetaxel-PNP	Various solid malignancies	Phase I	[54]
	Camptothecin	CRLX101	Advanced solid tumors	Phase II	[55-57]
Polymeric conjugates	L-Asparaginase	Oncaspar[1]	Acute Lymphoblastic leukemia	Approved	[58, 59]
	Paclitaxel	Xyotax, Opaxio, CT-2103[2]	Lung cancer, ovarian cancer	Phase III	[60-64]
	Camptothecin	CT-2106[3]	Colon cancer, ovarian cancer	Phase I/II	[65]
	Camptothecin	Pegamotecan	Gastric cancer	Phase II	[66, 67]

[1] PEG-Asparaginase
[2] Polyglutamic acid-Paclitaxel
[3] Polyglutamic acid-Camptothecin

Abraxane ® is the first therapeutic nano-particulate delivery system of paclitaxel (PTX) approved for the treatment of recurrent and metastatic breast cancer. It consists of nanoparticles of human serum albumin (~130 nm in size) physically bound to the PTX (**Figure 1-2**) [68]. This formulation is designed without Cremophor EL that is used in the traditional PTX formulation Taxol®. It targets albumin receptors gp60 localized on the endothelial cells and in the tumor interstitium [69]. Clinically, Abraxane® is well tolerated without corticosteroids or H_1/H_2 blocker pre-medication usually required with Taxol® doses [70]. It has shown significant tumor response in patient with non-small cell lung cancer [71], metastatic breast cancer [72], anal canal, and head and neck cancers [73]. In 2005, Abraxane® was first approved for the treatment of breast cancer after failure of combination chemotherapy for metastatic disease or relapse within 6 months of adjuvant therapy.

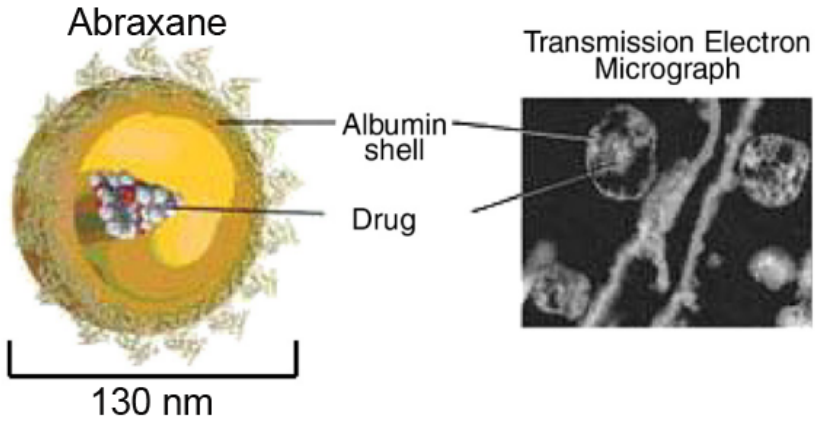

Figure 1-2: Model and transmission electron micrograph of Abraxane® (nab-paclitaxel). Adapted from Ref. [74] with permission.

Two liposomal formulations of doxorubicin (DOX) have been approved for clinical use so far (Doxil® and Myocet®). Doxil® (**Figure 1-3)** is the first FDA approved nano-drug, it a long circulating PEgylated "stealth" liposome containing DOX [75-77]. Doxil® was developed in 1990s by two scientists Martin Woodle and Frank Martin at liposome Technology, Inc. Doxil® is large unilammelar vesicle (LUV) with a size of around 100 nm (**Figure 1-4),** composed of a single lipid bilayer made out of hydrogenated soy phosphatidyl choline (HSPC), cholesterol, $mPEG_{2000}$ distearoyl phosphatidyl ethanolamine ($mPEG_{2000}$-DSPE) (56.4:38:3). This bilayer separates the internal aqueous environment containing DOX from the external medium. DOX is loaded using ammonium sulfate gradient method, in which DOX is precipitated as striated gel of sulfate salt. A protective linear polyethylene glycol (PEG) coating is grafted on the liposome

surface that reduces the interaction between the liposome lipid bilayer and the plasma components. This reduced interaction would be responsible for the stealth effect, remarkable stability in plasma, as well as prolonged plasma half-life. The long plasma residence time has been confirmed in patients with Kaposi sarcoma [78]. Doxil® showed better retention and significant reduction in the volume of distribution for DOX as compared to free drug. This would suggest that DOX is primarily encapsulated inside the liposomes and is released out at a very slow rate. The FDA approved Doxil® for the treatment of ovarian cancer and multiple myeloma in 1995. The first sale of Doxil® in USA and Europe was in 1996 [79]. By 2000, Safra et al. proved that Doxil® has reduced cardiac toxicity in human compared to free DOX based on changes in the left ventricular ejection fraction (LVEF) and clinical follow-up [80].

Figure 1-3: Doxil ® liposomes and its development. Adapted from Ref [81] with permission.

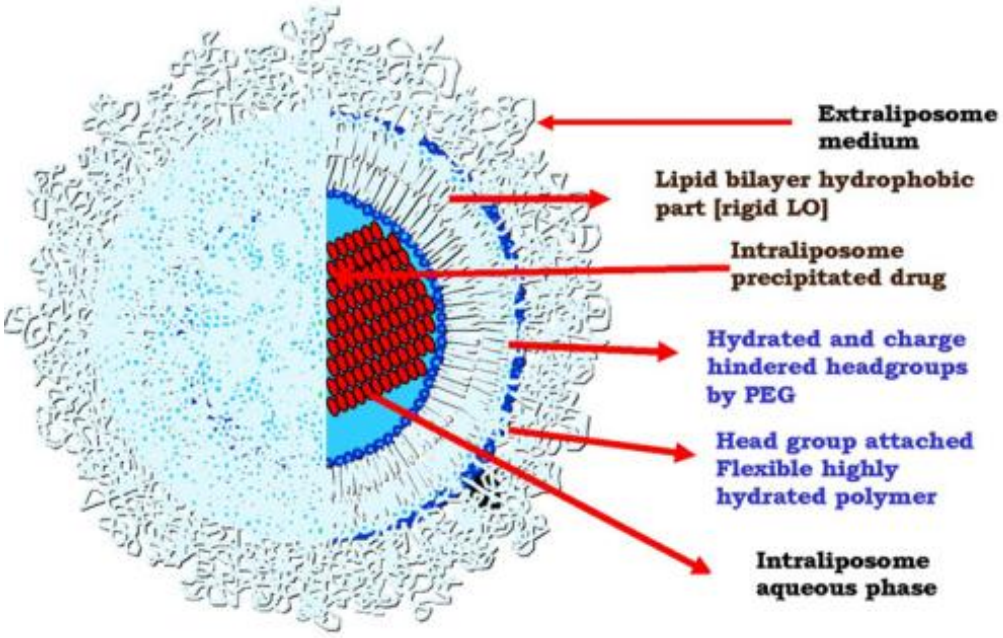

Figure 1-4: Schematic diagram showing Doxil® and its components adapted from Ref [79] with permission.

Myocet® is non –PEgylated liposomal formulation of DOX, approved in Europe and Canada for the treatment of metastatic breast cancer. However, the FDA does not approve it for use in the United States. It is large oligolammelar vesicle (OLV), 180 nm in size. The phospholipid bilayer is composed of egg phosphatidyl choline, cholesterol (1:1). DOX is loaded using hydrogen gradient method in which DOX is precipitated as fiber bundle with citrate [82]. Compared to free DOX, Myocet has lower clearance and volume of distribution[83]. This improved pharmacokinetic profile of Myocet resulted into improved therapeutic index, improved anticancer activity, and less cardiotoxicity in patient with metastatic breast cancer. Although Doxil® and Myocet® are liposomal formulations of DOX, yet they are formulations of different families (different lipid composition, size, loading methods). They are non-bioequivalent formulations with significantly different plasma pharmacokinetic profile, tissue biodistribution, dosing, and safety profile [82].

DaunoXome® is composed of small non-PEgylated unilammellar vesicles (45 nm) of daunorubicin citrate (**Figure 1-5)**. The liposomes composed of a bilayer of DSPC and cholesterol (2:1). It has been approved by the FDA as first line therapy for advanced HIV-associated Kaposi sarcoma. It showed activity and tolerability as single agent or in combination with other medication in refractory or relapsed acute myeloblastic leukemia [84]. It showed promising cardiac tolerability. Noteworthy, phase I dose escalating studies showed that DaunoXome may be effective, and cardiac-safe in metastatic breast cancer[85].

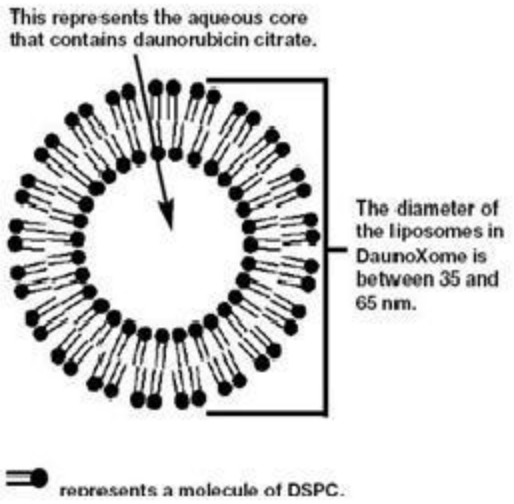

Figure 1-5: Schematic representation of DaunoXome®. Adapted from [86] with permission.

Depocyt ® is multivesicular liposomal formulation of the antimetabolite cytarabine, it utilizes the DepoFoam ® formulation technology for its manufacture. Those liposomes are composed of non-concentric vesicles, each is with an internal chamber encapsulating cytarabine aqueous solution and is surrounded by lipid bilayer made out of cholesterol:triolein:dioleoylphos-phatidylcholine (DOPC): dipalmitoylphosphatidylglycerol (DPPG) (4.4:1.2:5.7:1) (**Figure 1-6**) [87]. It is a sustained release formulation approved by the FDA for the treatment of lymphomatous meningitis. It is designed to release cyatarabine in the cerebrospinal fluid over prolonged period. Compared to free cytarabine, Depocyt shows 24 folds increase in $t_{1/2}$ (82.8 h vs. 3.4) [88, 89].

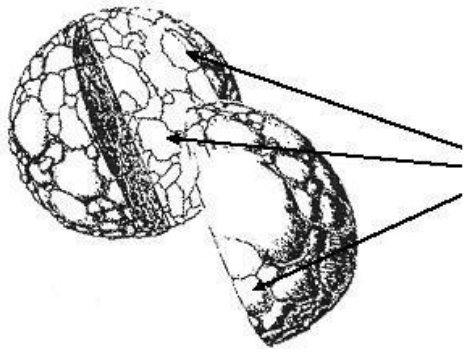

Nonconcentric vesicles, each with an internal, aqueous chamber containing encapsulated cytarabine solution, surrounded by a bilayer lipid membrane.

Figure 1-6: Schematic diagram showing Depocyt ®. Adapted from [87] with permission.

Genexol-PM is a micellar paclitaxel (PTX) formulation made out of PEG-poly(D,L-lactic acid) (PDLLA), (20-50 nm in size) [90]. It gained premarket approval in Korea in 2006, and phase II clinical trial for treatment of pancreatic cancer was completed in US by 2007. Compared to free PTX, Genexol showed three folds increase in MTD and significant increase in antitumor activity [91]. Combination of Genexol –PM and cisplatin exhibited enhanced antitumor activity and permitted the administration of higher doses of PTX in patient with non-small cell lung cancer (NSCLC), no significant toxicity was obvious , however, hypersensitivity reactions was reported [37, 92].

Oncaspar ® is PEGylated L-asparaginase, approved by the FDA in 1994 for the treatment of patient with acute lymphoblastic leukemia (ALL) allergic to the non-PEgylated formulation Elspar (L-asparaginase) [93]. In 2006, the FDA approved Oncaspar® as first line treatment for children diagnosed with (ALL) [58]. The use of Oncspar ® helped to reduce the number of injection given to the patients to three injections over 20 weeks, compared to 21 injections for the

standard course. Due to the popularity of liposomes and polymeric micelles, we will focus mainly onto those two kinds of pharmaceutical nano-carriers.

1.1.2 Polymeric micelles as nano-particulate delivery systems for cancer therapy

Ringsdrof and his research group published the first article on the design of polymeric micelles for anti-cancer drug delivery in 1984 [94]. The first appearance in PEGylated micelles was in late 1980s and early 1990s by Kazunori Kataoka, Teruo Okano and Masayuki Yokoyama in Tokyo. They synthesized diblock copolymers made out of PEG-poly(amino acids) for DOX conjugation and encapsulation [95-97]. Around the same time, Alexander Kabanov in Nebraska developed tri-block copolymers made out of haloperidol-loaded PEGylated micelles based on PEG-poly(propyleneoxide)-PEG (Pluronics®) [98] (**Figure 1-7)**. Polymeric micelles are a unique class of pharmaceutical nano-carriers that can encapsulate water insoluble anticancer medications into their hydrophobic core [99]. They are core and shell colloidal dispersions with a size range from 10-100 nm that are spontaneously formed through assembly of amphiphilic block copolymers at certain concentration and temperature [101]. The size of polymeric micelle makes them appropriate for extravasation and penetration capabilities in tumor tissue. The hydrophobic drug can be incorporated into the core by chemical conjugation through covalent bonding to the polymeric core

block; or physical encapsulation through non-covalent incorporation into the hydrophobic core. The non-covalent interaction can be through hydrophobic, electrostatic interactions, or metal complex formation. Through physical encapsulation a loading capacity ranges between 5-25% wt could be achieved.

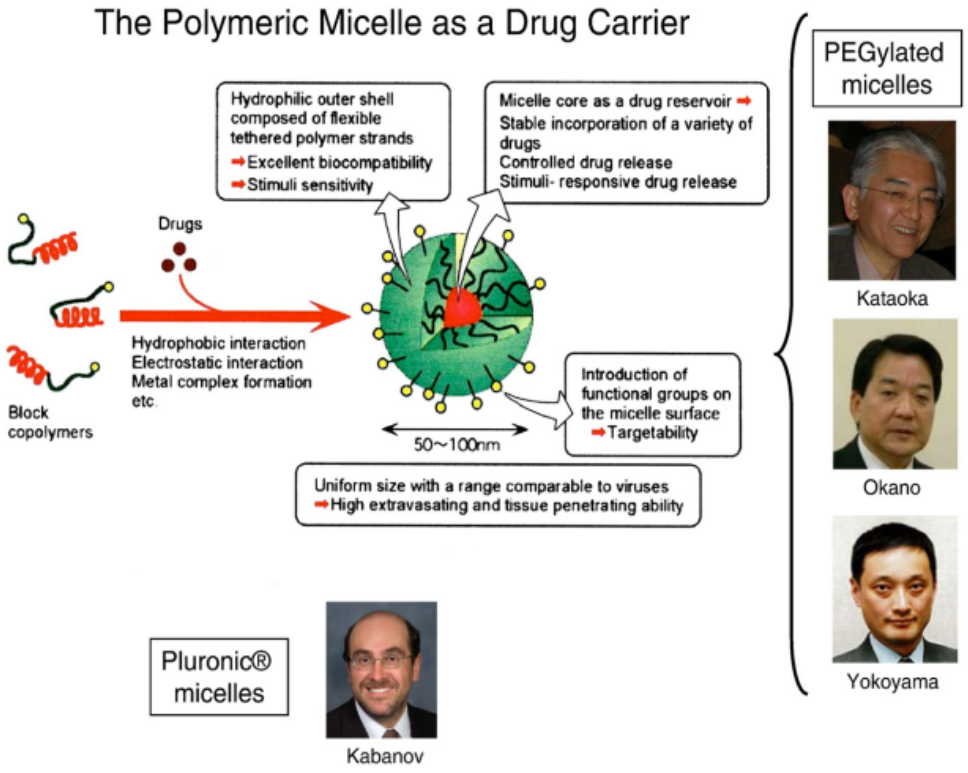

Figure 1-7: The origins and evolution of polymeric micelles as a drug carrier. The stealth polymeric micelles was developed by the Japanese Scientists Kataoka, Okano, Yokoyama in the late 1980s. Alexander Kabanov developed Pluronic® micelles in US at the same time. Adapted from Ref. [81] with permission.

The traditional polymeric micelles usually consist of a hydrophilic block made out of polyethylene glycol (PEG) (MW 1-15 KDa). PEG is water soluble, highly hydrated, efficient steric

protector, and biocompatible [100-102]. This block is usually attached to various hydrophobic polymers such as polyesters, polyethers or polyamino acids. The most commonly used core forming materials are polypropylene oxide (PPO), polycaprolactone (PCL), poly(D,L-lactic acid), poly(L-lysine), Poly(aspartic acid) [97, 103-106] (**Figure 1-13a**). The stability of polymeric micelles depends on the chemical structure and MW of the hydrophobic block, because it will indirectly affect the critical micelle concentration (cmc) of the polymeric micelles. In general, the more hydrophobic the polymer and the higher the MW the lower the cmc and the higher the stability of the polymeric micelles [107, 108].

1.1.2.1 Polymeric micelles for passive drug targeting

The clinical and preclinical application of polymeric micelles is mainly based on the concept of passive targeting. Passive targeting refers to the accumulation of nanocarrier into the tumour site due to patho-phyiological differences between the tumour and normal blood vessels. These differences resulted in phenomena called Enhanced Permeation and Retention Effect (EPR) [109, 110]. This phenomena was first reported by Hiroshi Maeda from Kumamoto University in 1984, while he was carrying an animal study for a dye labeled polymer drug conjugate of poly(styrene-co-maleic anhydride) (SMA) and Neocarcinostatin (NCS) ("SMANCS"), and he found that the dye accumulated into the tumour tissue [111]. He explained this observation by the EPR effect.

The quickly grown tumor cells stimulate the production of blood vessels (angiogenesis), which requires vascular endothelial growth factor (VEGF) and other growth factors involvement. The newly formed blood vessels (neovasculature) carries oxygen and nutritional supply to the tumor cell aggregates. These neovasculature are usually abnormal in form and architecture. They are poorly-aligned defective endothelial cells with wide fenestrations, lacking a smooth muscle layer, or innervation with a wider lumen. **Figure 1-9** shows clearly the anatomical differences between the normal and tumour vascular bed. Moreover, the tumour tissue usually lacks effective lymphatic drainage and this would allow the extravasated nanocarriers to be retained into the tumour tissue (**Figure 1-10**) [112-114].

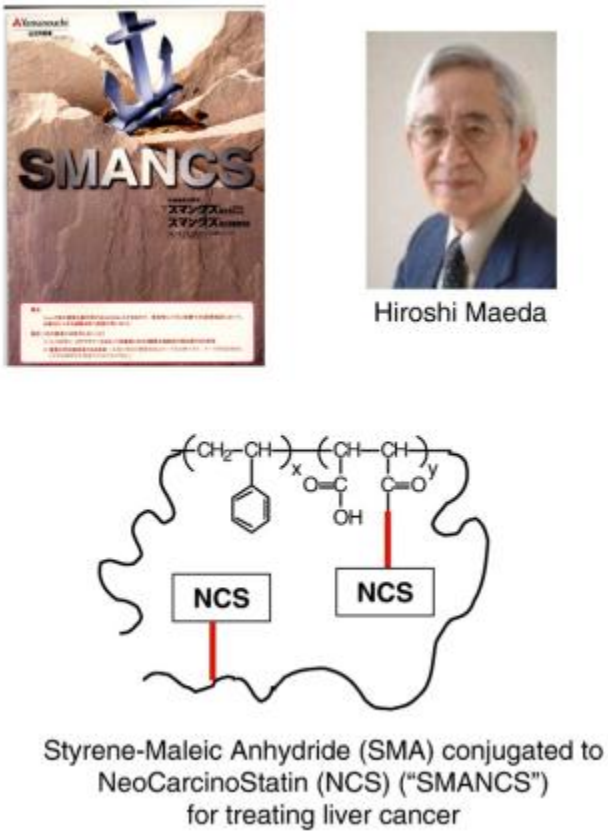

Figure 1-8: The EPR effect was discovered by Horishi Maeda while has was working on the polymer drug conjugate of poly(styrene-co-maleic anhydride) (SMA) and Neocarcinostatin (NCS) ("SMANCS"). Adapted from Ref. [81] with permission.

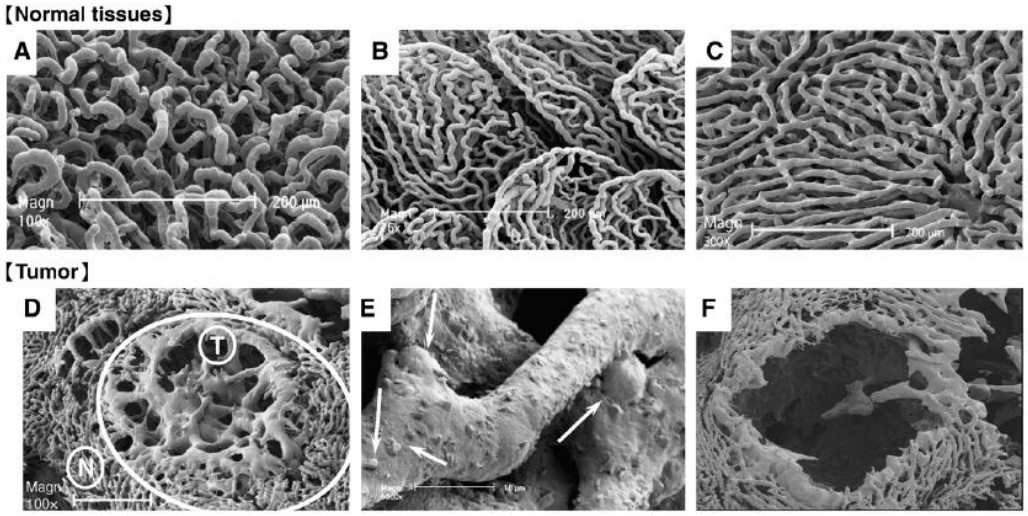

Figure 1-9: SEM image of blood vessels in various normal tissues (A-C), metastatic liver tumours (D-F). Normal capillaries of the pancreas (A), colon in colon (intestinal villi) (B), and liver (sinusoid) (C) are shown. (D) Metastatic tumor nodule (circled area identified with T) in the liver, the normal liver tissue is indicated with "N." (E) Tumor vessels at the capillary level (larger magnification), with a rough surface and an early phase of polymer-extravasating vessels (arrows). Normal tissues show no leakage of polymeric resin (A–C), whereas the tumor nodules clearly demonstrate tumor-selective extravasation of polymer (via the EPR effect) (D, E). After i.v. injection of the macromolecular anticancer drug (SMA-pirarubicin micelles), the tumor vascular bed (visible in D) was completely disintegrated, as shown by an empty void (F). adapted from reference [115] with permission.

To get the maximum benefits from the EPR effect the carrier system should fulfill the following requirements.

i. The carrier should have appropriate size. To avoid the reticuloendothelial system (RES), a size < 200 nm is required [116].

ii. Carrier should avoid strong interaction or uptake by normal tissues (especially RES). This can be achieved by adjusting the hydrophilicity, chemical nature, and surface charge of the carrier. For minimum interaction,

the carrier surface should be hydrophilic, with either neutral or weakly negative charge, or lacking any biologically recognizable chemical structures [117, 118].

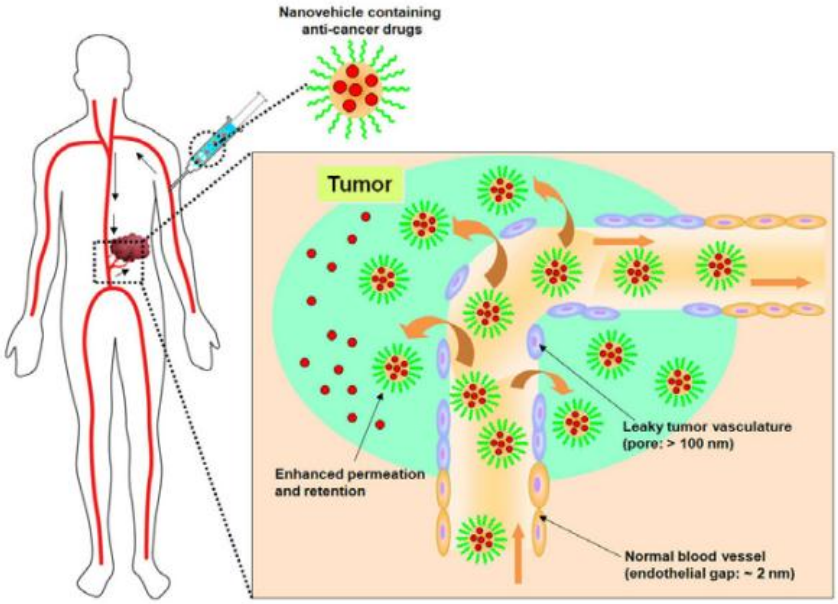

Figure 1-10: Schematic representation showing the accumulation of nano-carriers through the EPR effect. Adapted from reference [119] with permission.

Polymeric micelles have several advantages as carrier for anticancer drug delivery [120]:

i. Polymeric micelles are small in size (diameter 10-100 nm).

ii. High structural stability.

iii. High drug loading.

iv. High water solubility: Many polymer drug conjugates, AB-drug conjugates loses their solubility as a result of hydrophobic drug conjugation. However, polymeric micelles maintain their water

solubility due to the presence of the hydrophilic shell that inhibit the inter-micellar aggregation.

v. Low toxicity : renally excreted if the MW of the unimers is less than the MW threshold for renal filtration.

vi. Possibility of incorporation of different chemical species through either physical of chemical means.

vii. Capacity for chemically tailoring.

However, polymeric micellar carriers possess the following disadvantages [120]:

i. High level of polymer chemistry is needed for preparation (i.e. synthesis of AB block copolymer is more difficult than the synthesis of random copolymer).

ii. No universal drug incorporation methodology.

iii. Slow extravasation compared to low MW drugs. Long circulation time is necessary for delivery of therapeutic amounts.

iv. Slow metabolic processing and possibility of chronic liver toxicity.

Several successful examples of passively targeted polymeric micelles are now in clinical trials **Table 1-1**.

NK105 is a polymeric micelle formulation for PTX (85 nm in size). The micelles consists of PEG-poly(aspartate) modified with 4-phenyl 1- butanolate . It contains 23% w/w physically loaded PTX [95, 121, 122]. In preclinical testing using colon C26 bearing CDF1 mice, NK105 showed 4-6 times increase in the $t_{1/2}$ and 25 times increase in the tumour AUC compared to free PTX formulation

[123]. Phase I clinical studies showed that NK105 generates prolonged systemic exposure of PTX in plasma. The Triweekly 1 h infusion of NK105 was feasible and well tolerated, with antitumor activity in pancreatic cancer patients [124].

NC-6004 is the micellar formulation of cisplatin **(Figure 1-11)**. NC-6004 consist of block copolymer of PEG_{12K}-poly(glutamate)$_{6K}$. The molar ratio of cisplatin to carboxyl groups in the polymer is 0.71 [125]. The size of this micellar formulation is 30 nm . In vitro release studies in distilled water showed that only 19.6% of cisplatin is released after 24 h. Preclinical studies showed 65 fold increase in plasma AUC_{0-t} , and 3.6 folds increase in the tumour AUC compared to animals treated with free cisplatin. Phase I clinical trials is now underway in UK with starting dose of 10 mg/m^2 [126].

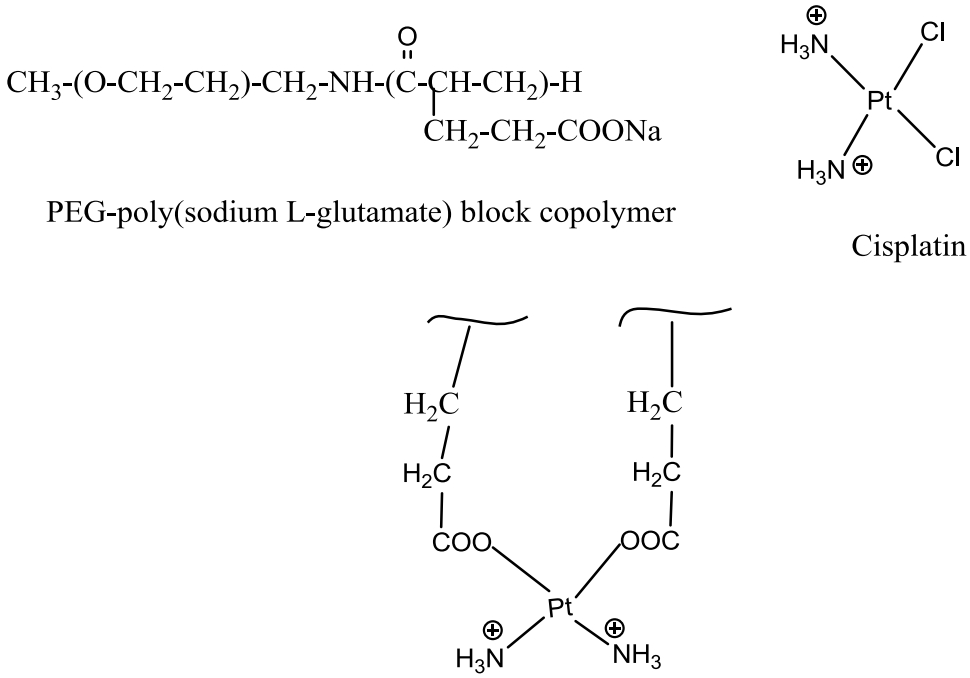

Figure 1-11: Components of cisplatin loaded polymeric micelles NC-6004.

NC-4016 is a polymeric micelle formulation for dichloro-(1, 2-diaminocyclohexane) platinum(II) (DACHPt), an active metabolite of oxaliplatin (**Figure 1-12**). The formulation is composed of PEG-poly(glutamate), and DACHPt is attached to the glutamate block through coordinate complex formation. Phase I clinical trial for NC-4016 started in March 2006, and till now no information about this formulation is available [127].

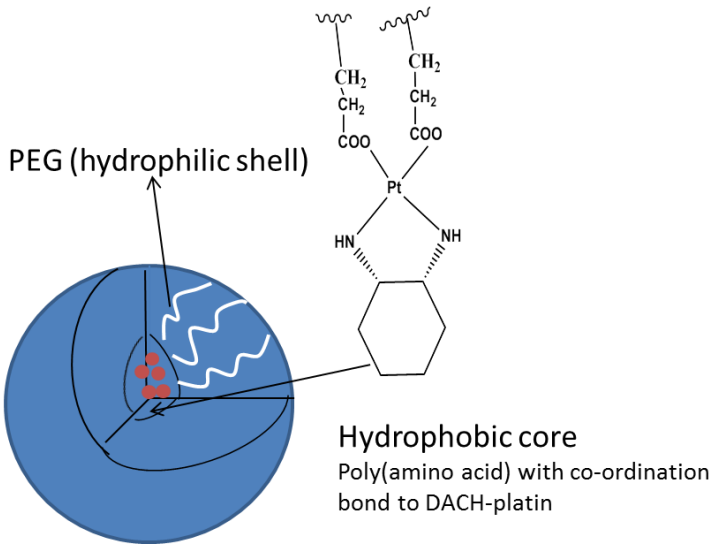

Figure 1-12: Schematic diagram showing NC-4016.

NK012 is a polymeric micelle conjugate of SN-38, a biologically active metabolite of CPT-11. SN-38 is chemically conjugated through an ester bond to a block copolymer of PEG-poly(glutamate**)** [128]. The mean size of NK012 micelles is 20 nm. Preclinical studies showed that NK102 releases SN-38 slowly in phosphate buffered saline, and approximately 57% of the SN-38 content is released after 24 h. Antitumor activity of NK012 in various cancer xenografts showed its superiority in comparison to CPT-11 in all studied models [128-131]. Phase I clinical studies showed that NK012 is well tolerated and exhibit significant antitumor activity in patients with refractory tumours [132, 133].

1.1.2.2 Ligand targeted polymeric micelles

The selectivity of the polymeric micelles for cancer cells can be increased through the development of second generation polymeric micelles (i.e. ligand targeted polymeric micelles) targeting specific receptors located on the tumour cell membrane or tumor vasculature. Ligand targeted micelles are expected to

enhance the intracellular drug delivery selectively in cancer. This active targeting approach is achieved through conjugation of specific ligands like folate, sugars, monoclonal antibodies (mABs) or peptides to the shell forming block of the polymeric micelles (**Figure 1-13**).

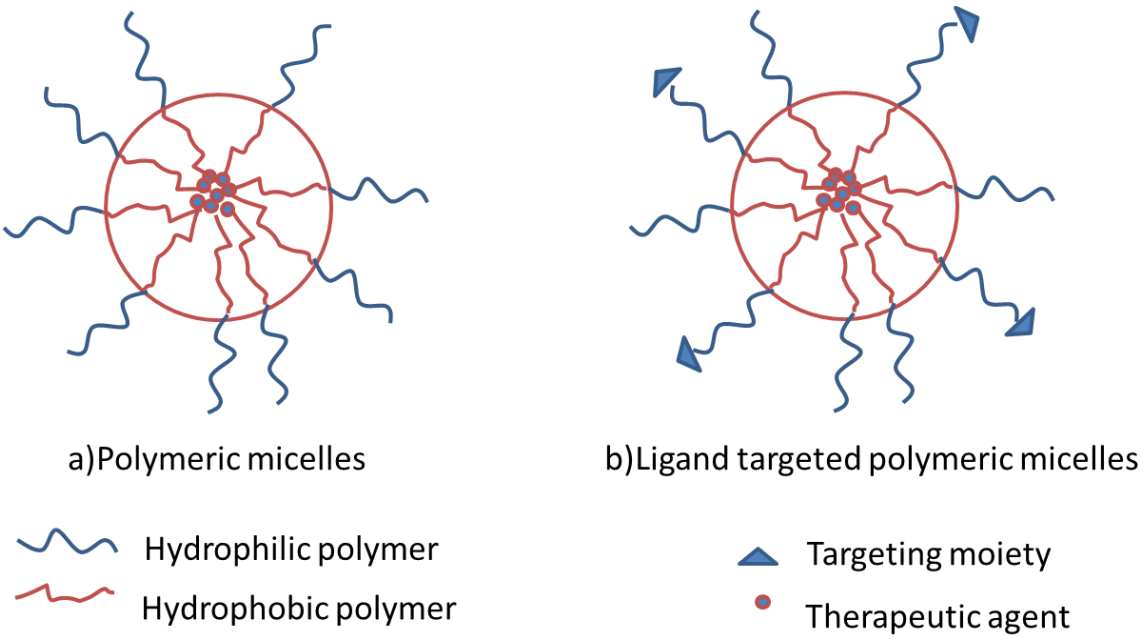

Figure 1-13: Schematic diagram showing a) polymeric micelles b) ligand targeted polymeric micelles

i. Folate: Folic acid or Vitamin B9 specifically binds to folate receptors over-expressed in many human cancers including ovarian, breast, pharyngeal, and liver cancer [134, 135]. Folate-mediated targeting has become one of the most popular cancer targeting approaches due to the low MW (441 Da), good stability, non-immunogenicity, and easy and well-defined conjugation chemistry of folate. Various studies have showed that folate targeting allows rapid internalization and high accumulation into tumour cells [136]. For examples, folate decorated polymeric micelles of poly(ethylene oxide)-poly(lactic co-glycolic acid) PEO-

PLGA increased the cellular accumulation and cellular toxicity of DOX against KB cells, and showed increased DOX tumour accumulation, and significantly lowered the KB tumour size in female athymic nude mice [137]. Similar observation is seen with PTX loaded poly(ethylene oxide)-poly(ε-caprolactone) PEO-PCL micelles, which exhibited increased cellular accumulation and cytotoxicity against MCF-7 and HELa 299 cells compared to non-targeted micelles [138].

ii. Galactose and lactose: The oligosaccharides galactose and lactose are able to mediate targeted delivery to the hepatocytes through asialoglycoprotein receptors mediated endocytosis [139, 140]. Yang et al. [141] prepared galactose decorated core cross-linked polymeric micelles of PEO-PCL for PTX delivery. MTT assay with HepG2 cells showed higher cytotoxicity for galactose decorated polymeric micelles compared to non-targeted micelles. Preliminary in vivo data with human hepatoma (SMMC-7721) bearing nude mice revealed that galactose decorated core cross-linked micelles inhibited the tumour growth more effectively than non-targeted micelles. Wakebayashi et al. prepared lactose conjugated polyion complex micelles for plasmid DNA delivery for the hepatocytes. In vitro results showed enhanced transfection with lactosylated polyion complex micelles compared to non-lactosylated micelles [142].

iii. Monoclonal antibodies mAbs: Antibodies and their genetically engineered fragments have been widely used for active targeting due to the specificity of the antigen antibody-binding, and improved pharmacokinetics and pharmacodynamics of antibody directed anticancer formulations [143, 144].

Examples include anti-HER2 antibody Fab fragment [145, 146], anti-2C5 mAb [147], Bivalent fragment HAb18 F(ab')2 [148], anti-CD22 mAb [149], anti-HIF-1α Ab [150], and anti-EGFR mAb [151]. Vega et al. [152] used C225 Ab against epidermal growth factor receptor to deliver DOX using polymeric micelles of PEO-P(L-Glu)-DOX, and they showed enhanced cytotoxicity of that conjugate against A431 cell in comparison to free DOX. Tumour targeted phospholipid based immunomicelles were developed by Torchilin et al. [153]. They chemically conjugated 2C5 mAbs to the PTX loaded micellar surface. PTX loaded 2C5 immunomicelles showed superior efficacy against human breast cancer cells MCF-7 when compared to plain PTX loaded micelles and free PTX. In vivo studies using ^{111}IN-labeled 2C5 immunomicelles in LCC tumour bearing mice showed significantly higher accumulation of ^{111}IN-labeled 2C5 immunomicelles compared to plain untargeted micelles. In vivo therapeutic efficacy studies in LCC tumour bearing mice showed higher therapeutic efficacy of 2C5 immunomicelles compared to free PTX and PTX loaded untargeted micelles.

iv. Peptides: Peptides are small targeting moieties that were developed to overcome the shortcoming of antibodies (low chemical stability, immunogenicity, low tumour penetration due to their large hydrodynamic diameter (~20 nm) and high tumour interstitial pressure) [154]. Peptides have many advantages as a targeting ligand; they are small molecules; they can be chemically synthesized and engineered and they can achieve high specificity. The successful development of peptide library screening methods (e.g. Phage display technique) resulted into the discovery of many new peptides. Phage display technique is a powerful

biological approach that was first developed by Parmley and Smith in 1985 [155, 156] and the first phage peptide library was reported by Scott and Smith in 1990 [157] . This method relies on a biochemical approach where an expression vector is inserted into a phage to present proteins or peptides on its surface. A phage clones mixture each displaying a single peptide on its surface is used to create a phage display library. This library is then exposed to the peptide target, usually presented on a solid support. The unbound phage is then washed off, and the bound phage is obtained by elution using either non-specific (all phage is removed) or specific (removes only phages bound to the target protein) methods. To obtain enough amount of the desired peptide an amplification procedure of the hit peptides is carried out. The drawback of phage display method is that only natural amino acids will be presented. It is generally difficult to get peptides containing D-isomer and unnatural amino acids, but it is possible to obtain cysteine-cyclized peptide. Nowadays, there are several examples of successful peptides under clinical and preclinical development that will be discussed in later sections. **Table 1-3** shows the in vitro and in vivo behavior of some peptide modified polymeric micelles used for cancer chemotherapy.

1.1.3 Liposomes as nano-particulate delivery system for cancer therapy

Liposomes are phospholipid vesicles that were first described by Alec Bangham and his students in 1965 [158]. They are colloidal bilayer spheres or vesicles with an aqueous interior core composed of phospholipids that spontaneously associate when hydrated with water. Those phospholipids are amphiphilic structures with

hydrophobic fatty acyl chains and hydrophilic head groups that have the tendency to associate in water in a way that shield the hydrophobic tails (**Figure 1-14**).

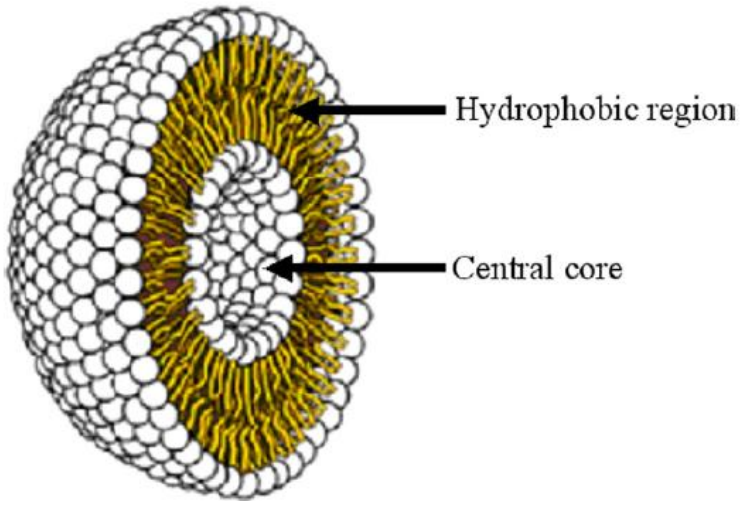

Figure 1-14: Schematic representation of liposomes. Adapted from Ref [159] with permission.

The size and topology of the hydrophobic/hydrophilic chains will determine the association pattern of phospholipids. Cylindrical phospholipids tend to form bilayers and hence liposomes; however, phospholipids with large polar head compared to the acyl chain (i.e. inverted cone shape) tend to form micelles [160]. Phospholipids with small polar head compared to the acyl chain (i.e. cone shape) tend to form reverse micelles. Combination of inverted cone and cone structure will form flat bilayers. This flat bilayer is unstable and tends to undergo phase transition and form micelle and inverse micelles (**Figure 1-15**). The proper choice of phospholipids is essential to control several properties of liposomes including size, charge, stability, and phase transition temperature (T_m). Cholesterol is usually added to liposomes due to its membrane stabilizing effect

which promotes ordered packing of the phospholipid bilayer and prevents drastic changes in the membrane fluidity during the gel-liquid crystal phase transition [161].

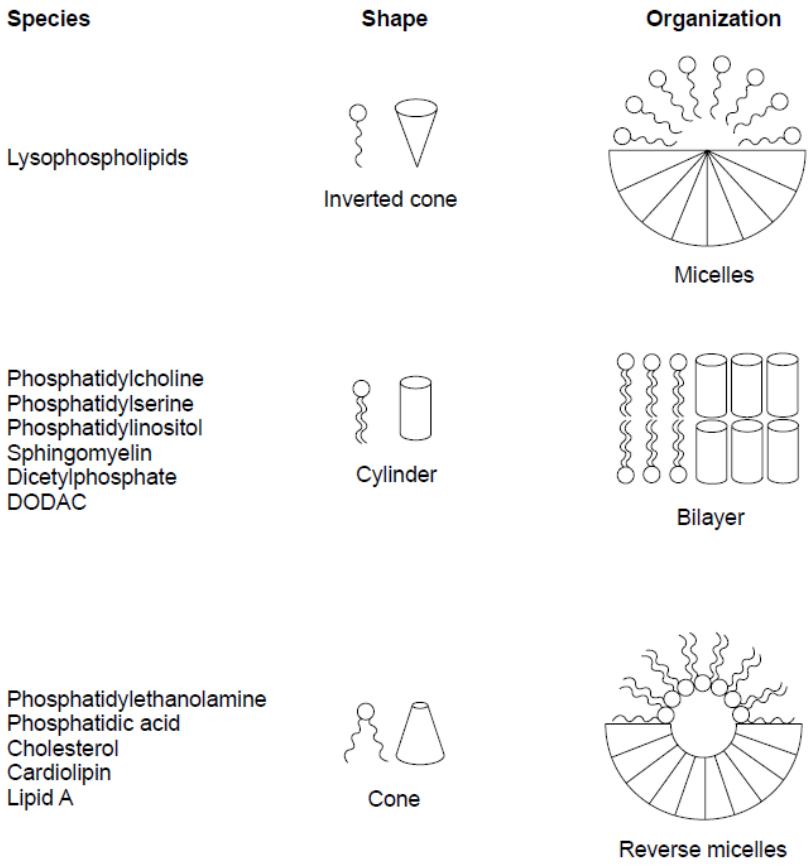

Figure 1-15: Effect of molecular shape of the phospholipids on the formed structure. Adapted from Ref. [160] with permission.

Liposomes can be classified according to their size and lamellarity into small or large unilammelar vesicles (SUV or LUV), or large multilammelar vesicles (MLV) (**Figure 1-16)**. Liposomes prepared by phospholipid film hydration method are MLVs. For drug delivery purposes, unilamellar vesicles are usually preferred due to their large interior aqueous space that permits the encapsulation of larger amount of drug molecules. Various techniques have been developed to

manipulate the size and lamellarity of liposomes including extrusion [162, 163], freeze thawing method [164, 165], sonication[166]. Extrusion is one of the most commonly used approaches for liposome size control, in which the liposomes are subjected to multiple extrusions under moderate pressure (<500 psi) through series of polycarbonate membranes with uniform size (220 -100 nm). This method usually results in formation of unilamellar vesicles with uniform size distribution [162, 163].

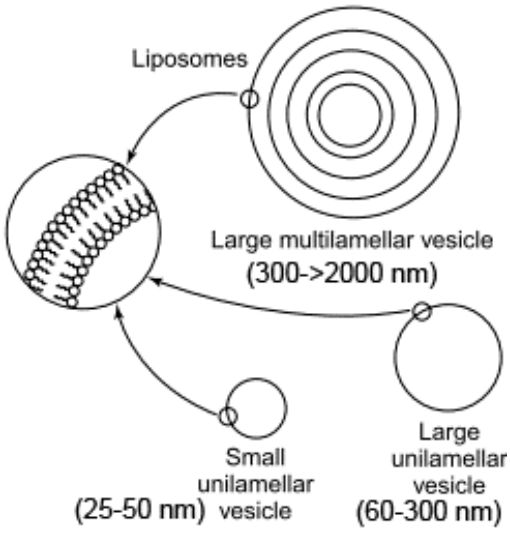

Figure 1-16: liposomes classification according to size and lamellarity. Adapted from Ref [160] with permission.

Liposomes have many potential applications in the field of drug delivery. Some of the potential advantages of using liposomes include:

i. Low toxicity due to their similarity to the biological membranes.

ii. Ease of control of their in vivo fate through manipulation of their phospholipid composition, size, charge, surface functional groups.

iii. Capability for the delivery of both hydrophilic and hydrophobic drugs.

iv. Effective sustained release system.

v. Modulation of the pharmacokinetics of drugs (i.e. increase $t_{1/2}$ of biologically unstable drugs, decrease toxicity to non-target tissues for highly toxic drugs e.g. anticancer medications).

These benefits made the liposomes one of the most widely studied drug delivery systems for the treatment of cancer with almost four formulations approved for clinical use (**Table 1-1**). Liposomes intended for cancer therapy are usually small in size (~100 nm), to allow the extravasation of the carrier out of the leaky vasculature supporting the tumour tissue through EPR effect. Some of the essential development features necessary to obtain an ideal cancer targeted liposome include [167]:

i. Small size (50-100 nm) with homogenous size distribution to ensure extravasation through leaky tumour vasculature.

ii. Efficient drug loading.

iii. Long circulation time (preferably several hours) to ensure enough liposomal drug localization into the tumour tissue.

iv. Capability of drug retention till it reaches the target site.

v. Ability to release the encapsulated drug at reasonable rate once the target site is reached.

Liposomes intended for drug delivery can be classified according to their surface structure into classical liposomes, stealth liposomes and ligand targeted liposomes (**Figure 1-17**).

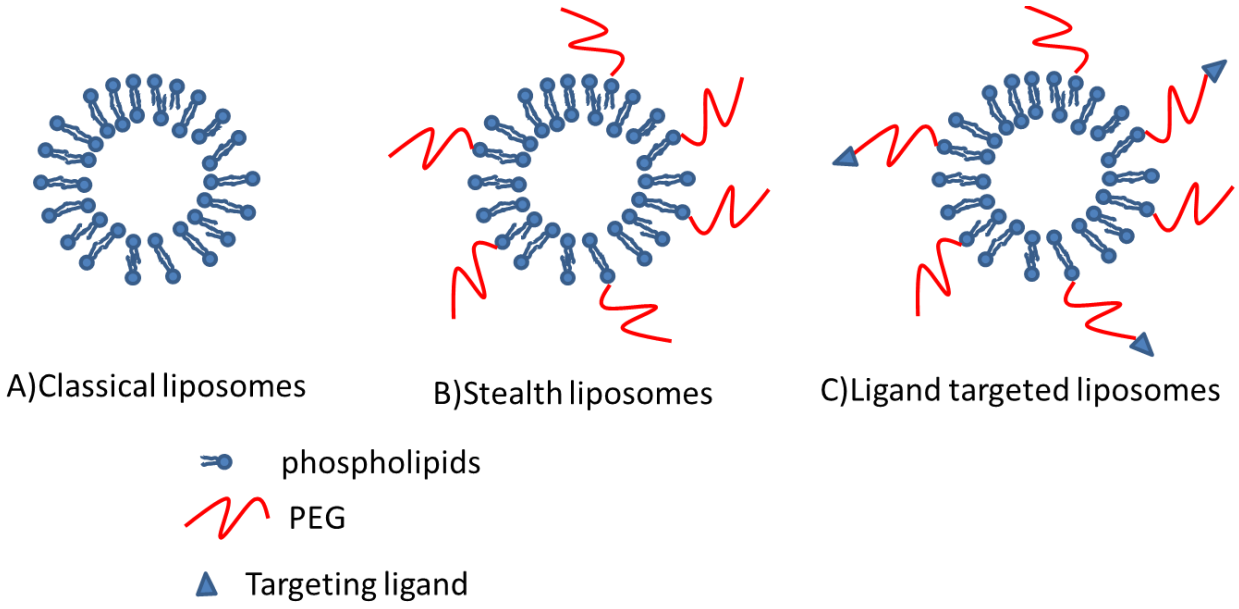

Figure 1-17: Different liposomes types A) classical liposomes B) stealth liposomes C) ligand targeted liposomes.

1.1.3.1. Classical liposomes

The first developed liposomal carrier, containing naked phospholipid bilayer are called classical liposomes. These carriers have shown significant benefit for drug delivery to the reticuloendothelial system (RES) to treat some diseases in the systems like Leishmania [176-178], or to deliver immunomodulators e.g. muramyl tripeptide to macrophages for immune therapy [179-181]. The presence of naked phospholipid attracts the binding of different opsonin and plasma proteins to the liposomal surface [168]. This binding promotes also rapid clearance of the liposomes by the RES [169]. Classical liposomes have dose dependant pharmacokinetics due to their saturable uptake by the RES. This type of liposomal formulation has shown n success in anticancer agent delivery in clinical practice which has been translated to into two clinically approved

anticancer formulations (Myocet®, DanuXome®). The majority of therapeutic application of liposomes requires long circulation time to ensure sufficient exposure of the target site to the encapsulated medication [170]. The rapid clearance of classical liposomes by RES is a drawback in this context.

1.1.3.2 Stealth liposomes

Improvement in liposome research allowed the development of liposomes capable of escaping the recognition by RES. These liposomes are called "stealth liposomes" or "sterically stabilized liposomes" and are built up with the hydrophilic polymer PEG studding out the phospholipid bilayer (**Figure 1-17**). The inert PEG coating is shown to be effective in reducing the uptake of liposomes by the RES through sterically preventing the adsorption of plasma opsonins/proteins [170-172]. In addition, it prolonged the half-life of the radiolabeled liposomes from less than few minutes (classical liposomes) to several hours (stealth liposomes)[173]. Noteworthy that the capability of PEG to increase the liposome circulation time is independent of the phospholipid composition and amount [170, 173, 174]. The effectiveness of PEG required to increase the liposomes circulation time, is related to its density and extension length. The optimal PEG density required to extend the circulation time without affecting the stability of the phospholipid bilayer ranges between 5-10 mol% [170, 174, 175]. The inclusion of PEG on the outer liposomal surface changes the pharmacokinetics of the liposomes from dose dependant, saturable pharmacokinetics to dose independent pharmacokinetics. The advantage of using stealth liposomes in cancer therapy relies on their prolonged circulation time that

permits EPR effect to take place [176, 177]. It is noteworthy to mention that steric stabilization of liposomes does not eliminate uptake by the RES, but it deceases the rate of RES uptake [195]. Therefore, liver and spleen are still the main accumulation sites for sterically stabilized liposomes [196]. Doxil ® is a good example showing the success of PEGylated stealth liposomes in clinic.

Optimization of the rate of drug release is one of the most important factors that should be carefully considered during the development of stealth liposomes. Drug release from liposomal carriers depends on the method of drug encapsulation, the physicochemical properties of the drug and membrane phospholipids [178]. The rate of drug release affects both the therapeutic efficacy and the toxicity of stealth liposome formulations. Liposomal formulations with intermediate DOX release rate showed significant weight loss in mice due to GIT toxicity compared to liposomes with either lower or higher DOX release rate [179, 180]. In other series of studies, liposomes with either high or low rate of drug release showed decreased activity and formulations with optimized drug release rate showed maximum therapeutic activity [181].

To improve liposomal drug accumulation/cell interaction in the target tissue, surface modification of liposomes with ligands capable of recognizing target receptors expressed on the desired tissue has been investigated. It was reported that the toxicity of DOX liposomal formulation with intermediate release rate can be decreased using antibody mediated targeting strategy [193].

1.1.3.3. Ligand targeted liposomes

These liposomes rely on active targeting through targeting ligands on liposomal surface. The targeting ligand can be used on the surface of classical or stealth liposomes. Although ligand targeted conventional liposomes have shown significant improvements in terms of targeting efficiency, still the majority of these liposomes accumulate in the liver due to the insufficient interaction time between target and the liposome. Ligand targeted stealth liposomes have a clear pharmacokinetic benefit over ligand targeted classical liposome for in vivo targeting purposes [182, 183].

Targeting ligands used on liposomes include antibody molecules or engineered fragment [184-188], peptides [189-197], carbohydrates [198-200], folates [201-205]. **Table 1-2** shows examples of ligand targeted liposomes used for anticancer drug delivery. Advantages of ligand targeted liposomes includes:

i. The possibility to deliver large load of drug through receptor mediated endocytosis using relatively few ligand molecules (10-20) per liposome. This is in comparison to immunoconjugats or immunotoxins that deliver few drug molecules (<10) per one ligand molecule [206-208].

ii. The capability to present multiple ligand molecules on the surface of one liposome, this would restore the multivalent binding ability of monovalent antibody fragment and hence increase their binding avidity (i.e. the combined strength of multiple bond interaction) to the target antigen [209].

iii. The use of internalizing ligands would allow the internalization of impermeable molecules (e.g. negatively charged molecules) into the cell.

iv. Synergistic effect could be achieved if the targeting moiety itself have anticancer activity (e.g. antiproliferative or anti-angiogenic activity).

Ligand targeted liposomes have not been successful in reaching the market, so far. One formulation, i.e., MCC-465, is reported to have entered phase I clinical trials [14]. MCC-465 is an immunoliposome of DOX, in which the liposome is decorated with PEG and the (Fab'_2 of human mAb GAH (goat anti-human), targeting cancerous stomach tissue. Pre-clinically, MCC-465 has shown higher cytotoxicity than free DOX or DOX loaded PEGylated liposomes against several human stomach cancer cells. Phase I clinical trials recommended a DOX equivalent dose of 32.5 mg/m^2 for phase II clinical trials [14]. Phase II clinical trials were suggested but no further information is currently available.

Another example of popular active targeting ligand is the use of folate bearing liposomes. The interest in folate targeted delivery increased rapidly [210, 211] after early studies that showed macromolecules [212] and liposomes [213] entering into living cells using folate-mediated endocytosis to bypass cancer cells' multidrug resistance mechanism [214-216].

Table 1-2: Ligand targeted liposomes for delivery of anticancer medications.

Targeting Agent	Target receptors	Model	Drug	Reference
Antibodies or Engineered fragments				
Anti-CD19	CD19	Namalwa Cells (human B-cell lymphoma)	DOX	[217]
Anti-CD19	CD19	ARH 77 cells (Human multiple myloma)	DOX	[218]
Recombinant human anti-HER2-Fab' or scFv C6.5	HER2	HER2-overexpressing breast cancer	DOX	[219]
Anti-HER2	HER2	HER2-overexpressing breast cancer (MDA-435, BT-474, SKBR-3)	Bleomycin	[220]
Anti-Her2 (trastuzumab)	HER2	Human gastric carcinoma (NCI-N87)	Docetaxel	[221]
MRK16	p-glycoprotein	Human myelogenous leukemia, K652	Vincristine	[222]

Targeting Agent	Target receptors	Model	Drug	Reference
Anti-β1-integrin Fab'	Human -β1-integrins	Human non-small cell lung carcinoma	DOX	[223]
CC52	CC531	Rat colon carcinoma	FUdR-dP[1]	[224]
Anti-GD_2 and anti-GD_2 Fab'	GD_2	Human neuroblastoma	DOX	[188]
Anti-GD2	Disialoganglioside, GD2	Human melanoma	Retinoid Feretinide	[225]
Anti-idiotype mAb, S5A8	38C13	Murine B-cell lymphoma	DOX	[223]
Anti-ganglioside G_{M3} (DH2) or Anti-Le^x (SH1)	Carbohydrate, ganglioside (G_{M3}); Lewis X (Le^x)	B16BL6 mouse melanoma and HRT-18 human colorectal adenocarcinoma	DOX	[226]
Anti-ED-B scFv	B-fibronectin (ED-B domain)	Murine F9 teratocarcinoma	FdU-NOAC[2]	[227]
Anti-VEGFR2[3]	VEGFR2	Tumour associated endothelial cells	DOX	[184]

[1] amphiphilic dipalmitoyl derivative of 5-fluorodeoxyuridine (FUdR-dP).
[2] 2'-deoxy-5-fluorouridylyl-N^4-octadecyl-1-βD-arabinofuranosylcytosine (amphiphilic compound with high cytotoxic activity)
[3] VEGFR2: vascular endothelial growth factor receptor 2

Targeting Agent	Target receptors	Model	Drug	Reference
Anti-HB-EGF	HB-EGF[1]	Human breast cancer (MDA-MB-231)	DOX	[185]
mAB-2C5	Murine and human tumour surface-bound nucleosomes	Murine melanoma cells (B16F10), Human adenocarcinoma cells (HeLa)	DOX	[186]
Anti-RON[2]	RON receptor tyrosine kinase	Colon cancer cells (HCT116 and SW620)	DOX	[228]
Anti-CD33 mAb or Fab'	CD33	human myeloid leukemia cell (HL60)	ara-C[3]	[229]
Anti-IGFI-R	IGFI-R[4]	Human neuroendocrine cell (BON cell)	DOX	[187]

[1] HB-EGF: heparin-binding epidermal growth factor
[2] RON: Recepteur d'origine nantais is a receptor tyrosine kinase (RTK) that belongs to the MET proto-oncogene family.
[3] ara-C: 1-beta-d-arabinofuranosylcytosine
[4] IGFI-R: insulin-like growth factor I receptor

Targeting Agent	Target receptors	Model	Drug	Reference
Folic acid	Folate	Human nasopharyngeal carcinoma (KB), Human adenocarcinoma (HeLa)	DOX	[230]
	Folate	Murine ascites tumor (L1210JF cells)	Daunorubicin	[202]
	Folate	Human Epidermoid carcinoma (KB)	Ricin	[203]
	Folate	Human nasopharyngeal carcinoma (KB)	DOX	[231]
	Folate	Human adenocarcinoma (MCF-7), human alveolar adenocarcinoma cell (A-549)	Docetaxel	[204]
	Folate	Human nasopharyngeal carcinoma (KB)	Ara-C[1]	[232]

[1] ara-C: 1-beta-d-arabinofuranosylcytosine

Targeting Agent	Target receptors	Model	Drug	Reference
	Folate	Murine acute myelogenous leukemia	DOX	[233]
	Folate	Human myelogenous leukemia cell (KG1)	Daunorubicin	[214]
Carbohydrates				
Hyaluronic acid	CD44	Murine Melanoma (B16F10)	DOX	[200]
1-amino lactose	lectin	Rat hepatoma cell (AH66)	DOX	[198]

1.1.4 **Peptides as targeting ligands**

The use of antibodies as targeting ligands capable of binding to the tumor-specific antigens have produced little success for solid tumors, which constitute more than 90% of all cancers in humans. This is most likely due to the large MW and poor tumor penetration [234] and the immunogenicity of immunoliposomes as well as their toxicity to liver and bone marrow due to non-specific antibody uptake. These limitations can be avoided by using peptide ligands, which are smaller, less immunogenic, and easier to produce and manipulate. Furthermore, peptide ligands have moderate affinity to antigens, which is beneficial because extremely high affinity of antibody-binding can impair tumor penetration [234]. Furthermore, the small size and moderate affinity of the peptide compared to antibodies may allow the liposomes to move more efficiently against the high interstitial tumour pressure inside the tumour [235-238].

The development of phage display technique has led to the discovery of several peptide targeting ligands that can be used in targeting chemotherapeutic and imaging agent towards the tumour cells. Some of these peptides are listed in **Table 1-3** with their relevant in vitro and in vivo outcomes. Most of these studies showed significant increase in cytotoxicity and therapeutic efficacy and decreased toxicity of peptide bearing nano-carrier formulations compared to untargeted ones. Out of these examples, we will elaborate on some popular examples like RGD, and NGR peptides and the newly discovered p160 peptide and its engineered derivative, which are the focus of this thesis.

Table 1-3: In vitro and vivo behavior of peptide targeted carriers used for cancer therapy.

Peptide	Carrier type	Target cells (receptor)	Cancer type	Payload	In vitro results	In vivo results	Reference
SP94	liposomes	Mahlavue cells	Hepatocarcinoma	Doxorubicin	N/A	In SCID mice, targeted liposomes showed decreased tumour growth ,increased tumour apoptosis and decreased angiogenesis.	[239]
L-peptide	liposomes	NPC-TW01	Nasopharyngeal carcinoma	Doxorubicin	N/A	In tumour bearing SCID mice, peptide decorated liposomes suppress tumor growth by 3.1 times more than untargeted liposomes.	[240]

Peptide	Carrier type	Target cells (receptor)	Cancer type	Payload	In vitro results	In vivo results	Reference
p160	Polymeric micelles	MDA-MB-435	Human Breast cancer	Paclitaxel	Enhanced selective cytotoxicity of paclitaxel against MDA-MB-435 cells over normal non-p160 specific cells. The extent of cell specificity for encapsulated paclitaxel was more for p160-bearing micelles than c(RGDfK)-bearing ones	N/A	[241]
SP5-2	liposomes	CL1-5	Non-small cell lung cancer (NSCLC)	Doxorubicin	N/A	Increase in the survival rate and therapeutic index in liposomal doxorubicin treated mice. Compared to free doxorubicin, targeted liposomes showed 5.7 folds increase in drug accumulation, and enhanced cell apoptosis.	[242]

Peptide	Carrier type	Target cells (receptor)	Cancer type	Payload	In vitro results	In vivo results	Reference
SP5-52	liposomes	CL1-5/SAS	Human non-small cell lung cancer/oral cancer	Doxorubicin	N/A	Decrease in the tumour blood vessels, and high survival rate of human lung and oral bearing xenograft mice.	[237]
PIVO-8	liposomes	H460/BT483 /Mahlavu/PaCa/HCT116	Human lung cancer/breast Cancer/liver cancer/pancreatic cancer/colon Cancer.	Doxorubicin	N/A	Targeted liposomes group showed 4.9- and 1.6-fold increase in intratumoral concentration compared to free doxorubicin and untargeted liposomes groups, respectively.	[238]
PIVO-24	liposomes	H460/BT483 /Mahlavu/PaCa/HCT116	Human lung cancer/breast Cancer/liver cancer/pancreatic cancer/colon Cancer.	Doxorubicin	N/A	Targeted liposomes group showed 4.8- and 1.6-folds increase in mean intratumoral doxorubicin compared to free doxorubicin and untargeted liposomes groups.	[238]
SWKLPPS	liposomes	AZ-P7a ($\alpha_3\beta_1$)	Human gastric carcinoma	Doxorubicin	More anticancer activity against AZ-P7a cells compared to untargeted liposomes	More tumor accumulation in mice.	[243]

Peptide	Carrier type	Target cells (receptor)	Cancer type	Payload	In vitro results	In vivo results	Reference
Truncated basic fibroblast growth factor (tbFGF)	Cationic liposomes	B16F10 (FGFR)	Melanoama	paclitaxel	N/A	Mice treated with tbFGF modified liposomes showed 7.17and 2.0 folds increase in PTX accumulation in tumour compared to free paclitaxel and unmodified liposomes, respectively.	[244]
	Cationic liposomes	B16 cells or TRAMP-C1 cells (FGFR)	Melanoma, prostate carcinoma.	paclitaxel	N/A	In both tumour models, tbFGF modified liposomes showed significant inhibition of tumour growth and improvement in survival rate compared to either free paclitaxel or unmodified liposomes.	[245]

1.1.4.1 RGD peptides

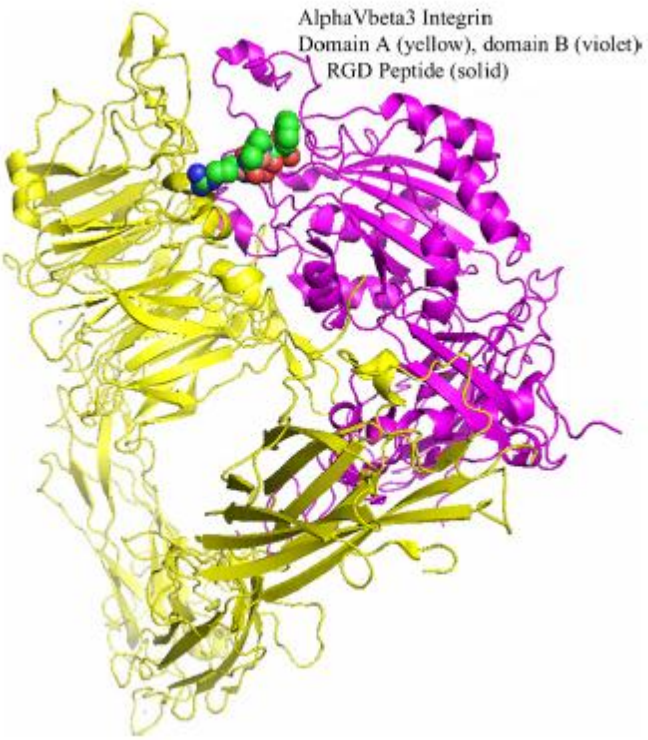

Figure 1-18: The crystal structure of $\alpha_v\beta_3$ integrin cyclic RGD complex. The α_v unit is shown in yellow, while the β_3 is shown in violet. Adapted from Ref [246] with permission.

Cell adhesion molecules (CAMs) [247-249] have a crucial role in many disease including cancer [250, 251], thrombosis [252, 253]. CAMs are glycoproteins over-expressed on the cell surface that acts as receptor for cell to cell adhesion and cell to cell-extra cellular matrix (ECM) adhesion [254-256]. They can be divided into four types: integrins, cadherins, selectin, and the immunoglobulin superfamily. Integrins are family of glycosylated membrane receptors, named for their ability to integrate both intracellular and extracellular membrane scaffolds

allowing them to work together. They are heterodimeric structures composed of non-covalently bound alpha and beta chains that regulates the tumour angiogenesis, cell-cell migration and invasion, and cell-ECM interaction (**Figure 1-18**) [257]. Integrins are considered as an ideal targets for both cancer and anti-angiogenic therapy. This could be due to the capability of integrins to be internalized into the cells on activation with anchoring ligands. This allows the delivery of chemotherapeutic agents attached to integrin ligands into the neoplastic cell expressing integrins on their surface. integrins are over-expressed on angiogenetic endothelial cells, whereas they are absent in pre-existing endothelial cells and normal tissues [258-260].

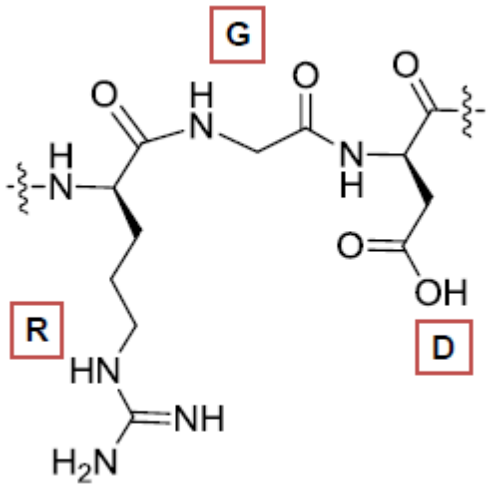

Figure 1-19: Common structure in RGD peptide containing peptides.

Peptides with Arg-Gly-Asp (RGD) sequences (**Figure 1-19**) are one of first peptides discovered through biopanning (affinity selection technique that select the peptides that bind to certain specific target). This sequence was discovered as

cell attachment site for fibronectin almost 30 years ago. It was unexpected that the fundamental recognition site for cells and protein could be abbreviated into three amino acid sequence [261-263]. This peptide sequence was found in many of the naturally occurring proteins shown in (**Table 1-4**). These peptides are known to target integrins that are upregulated during the process of angiogenesis and bind more specifically to the integrins $\alpha_v\beta_3$, $\alpha_v\beta_5$ [264, 265].

Table 1-4: peptide sequence of some of the naturally occurring RGD containing sequence.

Protein	Sequence
Fibronectin	AVTG**RGD**SPASSK
Fibrinogen α-chain	TSYN**RGD**STFESK
λ-receptor on *E.coli*	GSFG**RGD**SDEWTF
Sindbis coat protein	GVGG**RGD**SGRPIM
α-lytic protease	ACMG**RGD**SGGSWI
Testis specific basic protein	KSRK**RGD**SADRNY

Besides the ability of these peptides to bind integrins, RGD peptides are also capable of internalization into the cell causing cell death, and interrupting the development of more tumour vasculature [264, 265]. There are many variants of the RGD peptide, including ACDCRGDCFCG (RGD4C), c(RGDfK), c(RGDf[N-Me]V) (Cilengitide), DGARYCRGDCFDG (RGD10), iRGD (**Figure 1-20**). The specificity and affinity of the RGD peptides to the $\alpha_v\beta_3$ integrin receptors has been controlled by both cyclization and the proper choice of the flaking amino acids that dictate the proper conformation of the arginine and aspartic acid side chains [266]. Linear RGD showed high susceptibility to chemical degradation [267].

Rigidity in the chemical structure conferred through cyclization improved the selectivity of RGD peptide toward integrin subtypes [268]. All selective RGD peptides are cyclic showing at least one or more ring structure. Another way to increase the affinity and specificity of RGD peptides, is through introduction of non-natural D-amino acids or replacement with peptidomimetic structures [268].

The RGD4C and RGD10 peptide were discovered by phage display technology [269, 270]. The RGD4C peptide contains two disulfide bonds and demonstrates at least 20-fold more potency than similar peptide with a single disulfide bond [269, 271]. Although the RGD10 peptide contains only one disulfide bond, the side chains attached to the CRGDC core display similar physicochemical properties as those in RGD4C. Generally, RGD4C and RGD10 exhibit almost the same binding affinity to integrin $\alpha_v\beta_3$ [272]. The main disadvantage of RGD4C is the solution instability of the RGD4C disulphide bond that could lead to significant reduction in the $\alpha_v\beta_3$ binding affinity [273]. To solve this problem, a more stable cyclized RGD structure containing one D-amino acid known as c(RGDfK) is synthesized [274]. This peptide is one of the well-known RGD derivatives used for drug delivery. The main advantages of this peptide are high chemical stability, good water solubility, and ease of chemical conjugation reactions due to the presence of lysine residue (K) in its structure [266]. Another RGD peptide is Cilengitide or EMD121974, which shows a high binding affinity to $\alpha_v\beta_3$ integrins. This high affinity is attributed to the rigid ring structure and the presence of one D-amino acid residue (f) that forces the peptide to form the proper conformation to bind with the $\alpha_v\beta_3$ integrins [275]. This peptide is now in Phase III clinical trials in

combination with Temozolomide and radiation therapy for the treatment of patient with newly diagnosed glioblastoma [276].

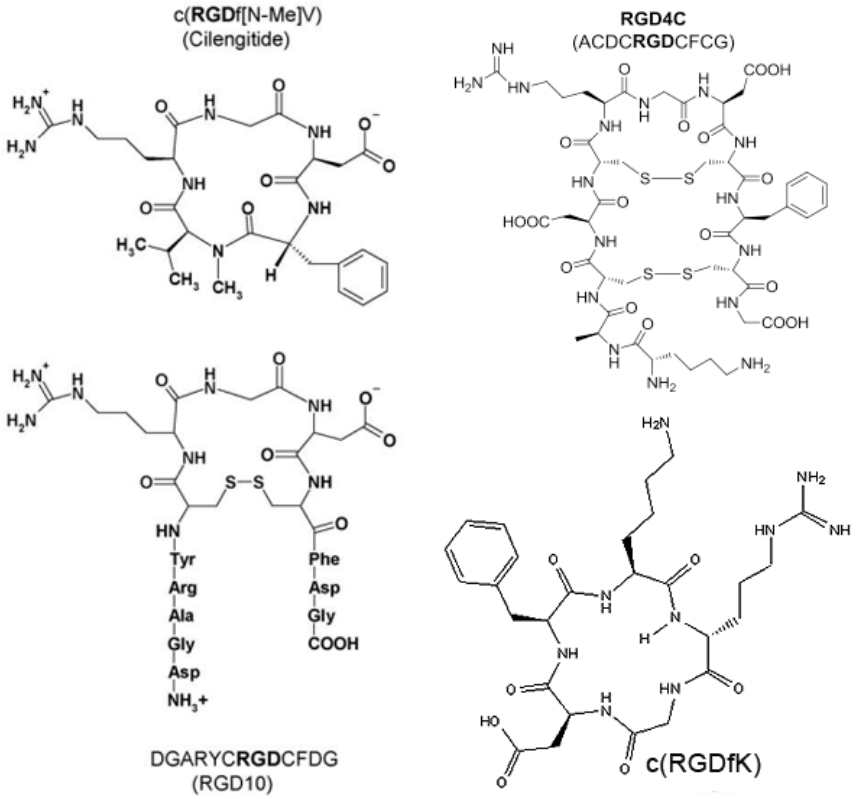

Figure 1-20: Chemical structure of most commonly used RGD peptides. Adapted from Ref [266] with permission.

Another novel unique tumour internalizing RGD peptide that promote the drug penetration into broad range of solid tumours including pancreatic , breast and prostate cancer, is called iRGD. This peptide is a cyclic peptide composed of two components i) the RGD motif that binds to the $\alpha_v\beta_3$/ $\alpha_v\beta_5$ integrin receptors on the tumour blood vessels endothelial cells and tumour cell surface ii) the CendR element (RXXK/R) which is released due to the action of cell associated proteases and is responsible for binding to the neuropilin-1 (NRP-1) , that induces tissue and vascular penetration **(Figure 1-21)** [277]. Physical mixtures of iRGD with

many cytotoxic medications and antibodies was able to increase the accumulation in the extravascular tumour parenynchyma for up to 40 folds [246, 278]. This peptide could help in tumour tissue/cell penetration through chemical attachment of the desired cargo to the N-terminus of the iRGD. This way of attachment is necessary as the disulphide bond in the iRGD structure would break before the peptide is internalized [246].

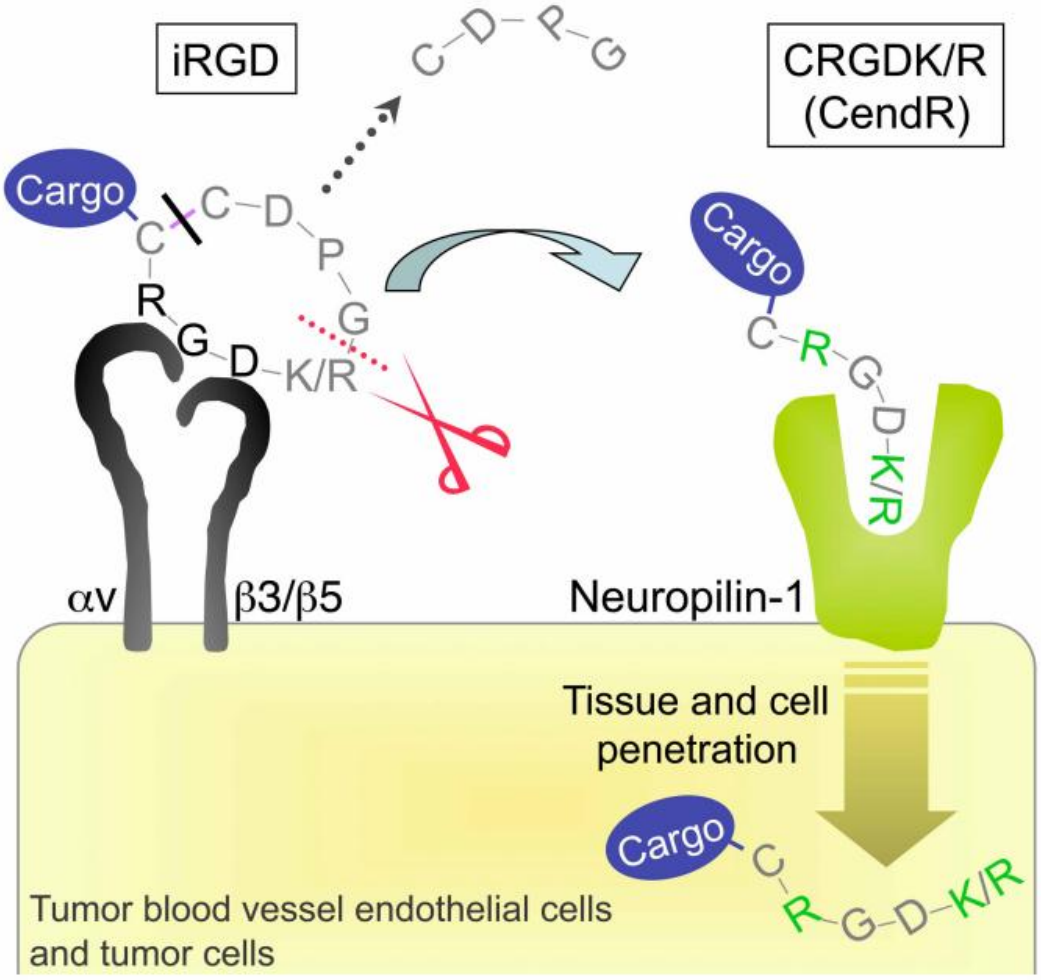

Figure 1-21: Mechanism of binding and internalization of iRGD peptide. Adapted from Ref [246] with permission.

The RGD peptide bearing nano-particulate delivery system has been extensively investigated. Schiffelers et al. [279] developed stable long circulating DOX

containing c(RGDfK)- bearing stealth liposomes that target DOX to integrin expressing murine C26 colon cancer. In vivo intravital microscopy, using fluorescently labeled RGD-liposomes showed difference in the intratumoral distribution of RGD-liposomes compared to untargeted liposomes, with RGD-liposomes showing formation of clustered fluorescence adhering to the vessel wall of the tumour due to specific interaction of these RGD-bearing liposomes with angiogenic endothelium. In vivo study, using DOX containing RGD-liposomes inhibited tumor growth in a DOX-insensitive murine C26 colon carcinoma model, whereas DOX in untargeted stealth liposomes failed to decrease tumor growth. Xiong et al. [280] conjugated the linear RGD peptide sequence to DOX containing stealth liposomes. They showed enhanced cytotoxicity of RGD-liposomes in B16 melanoma cells. In vivo experiment with B16 tumour bearing mice receiving four weekly injections of 5 mg/Kg of DOX liposomes, showed that RGD-liposomes demonstrated significant decrease in both the tumour growth rate and tumour volume compared to untargeted liposomes. `A summary of some of the published in vitro and in vivo results of RGD-modified liposomal formulations is shown in (**Table 1-5**).

Table 1-5: Summary of studies involving RGD targeted liposomes for cancer chemotherapy.

Drug	Targeting moiety	Experimental Model	Results [1]		Ref.
			In vitro	In vivo	
Docetaxel	RGD4C	MDA-231 human breast adenocarcinoma	+	ND	[281]
Combretastatin A-4 and DOX	Linear RGD	B16F10 murine melanoma	+	+	[282]
MDR1-siRNA and DOX	Linear RGD	DOX resistant MCF7/A human breast cancer	+	+	[283]
PTX	Linear RGD	SKOV-3 human ovarian cancer	+	+	[284]
DOX	Linear RGD	B16 melanoma	+	+	[280]
DOX	RGDm[2]	B16 melanoma	+	+	[285]
DOX	RGD10	C26 murine colon carcinoma	ND	+	[270]
5-Fluorouracil	c(RGDfK)	B16F10 murine melanoma	+	+	[286]
DOX	c(RGDfK)	C26 murine colon carcinoma	ND	+	[279]

[1] Compared to untargeted nanocarriers: (+) improved efficacy, (-) less efficacy, (=) comparable efficacy, (ND) not determined.

[2] RGD mimetic: L-arginyl-6-aminohexanoic acid

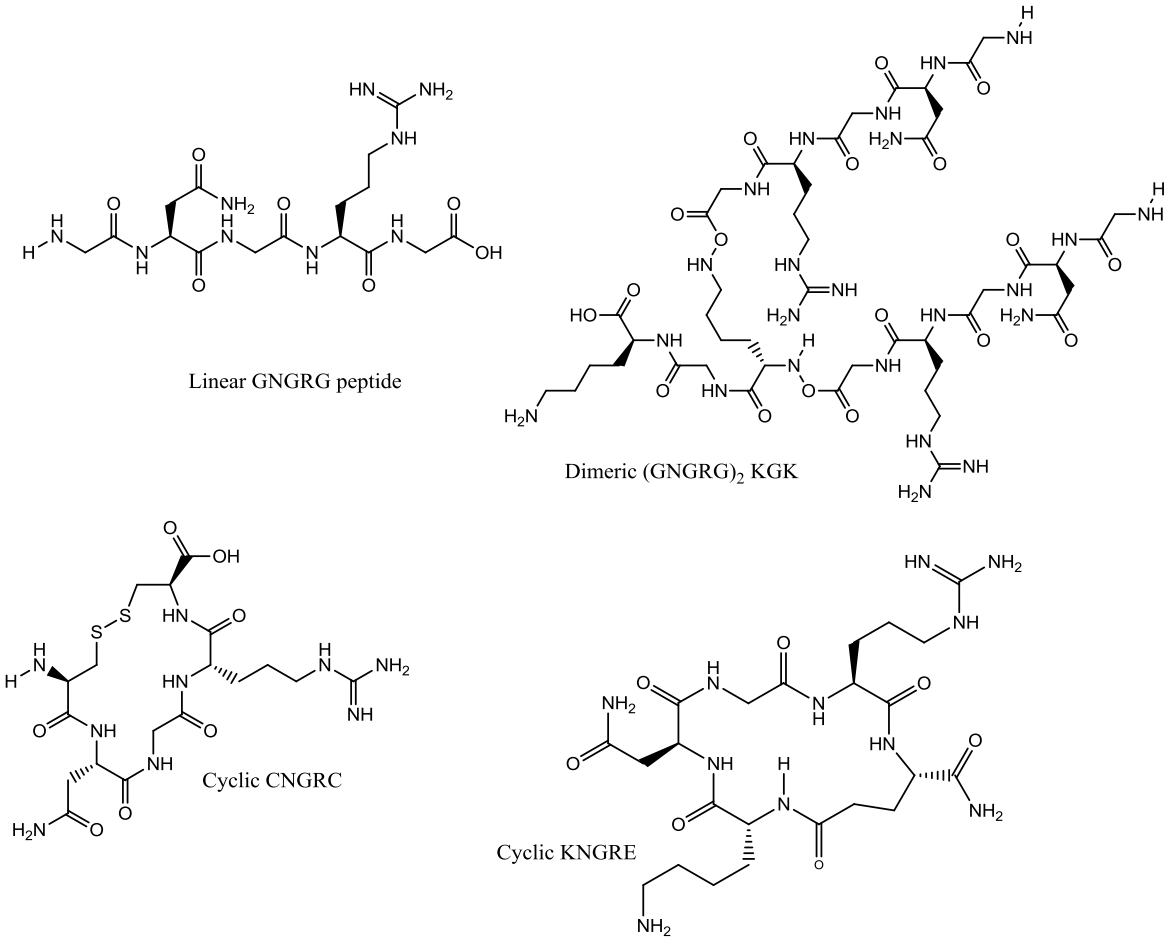

Figure 1-22: Structures of common NGR peptides. Adapted from Ref. [287] .

1.1.4.2 NGR peptides

Another peptide sequence that showed great tumor targeting capability is asparagine-glycine-arginine (NGR) peptide. This peptide is discovered through in vivo panning of peptide phage library in tumour bearing animal models [288]. It can selectively bind aminopeptidase-N/ CD13 (APN/CD13) receptor over-expressed on the surface of many cell lines including epithelial cells, mast cells,

fibroblast and muscle cells, tumour blood vessels [289, 290]. Immunohistochemical analysis proved that the isoform of APN/CD13 expressed in lots of normal tissues, is different from those expressed on cancer tissue [289]. There are similarities between NGR and RGD motif, NGR could bind integrin receptors however the affinity of NGR to the integrin is much less than affinity of RGD [291]. APN/CD13 receptors are membrane bound metallopeptidase that play many functions like regulation of many hormones and cytokines, protein degradation, antigen presentation, cell proliferation, cell migration, and angiogenesis [292-294]. Interestingly, APN/CD13 receptors are upregulated in angiogenic blood vessels but not on the endothelium of normal blood vessels [289, 290]. The highest level of expression of CD13 was identified in human umbilical vein endothelial cells (HUVEC), UC-3, HT-1080, H1299, Hey, and PC33-MM2 cells [295]. Therefore, these cells are commonly used for studies involving NGR peptide. Immunogenic studies of various NGR-conjugates showed that this motif is non-immunogenic. NGR could be converted to isoaspartate-glycine-arginine (isoDGR) which has the capability to bind $\alpha_v\beta_3$ integrins. This binding could inhibit the $\alpha_v\beta_3$ integrins endothelial cells mediated adhesion, proliferation and tumour development [296, 297].

GNGRG is a linear pentapeptide with one amino acid G flanked at both ends of the NGR motif. It shows the minimum requirements for binding activity [288] (**Figure 1-22**). Several linear and cyclic forms of the NGR peptides have been reported, among which the c(NGR) that forms a cyclized structure through the formation of disulphide bond between two cysteines [288] showed high affinity

and specificity toward CD13 receptors [298]. The disulphide bond in the c(NGR) structure could be unstable to biodegradation and chemical modification. Therefore, a more robust chemical structure could be obtained through cyclization of the KNGRE peptide through the attachments of the lysine and glutamic acid terminals. Studies involving conjugates of the linear or cyclic NGR with tumor necrosis factor alpha (TNF-α) showed 10 folds enhanced antitumor activity of conjugate involving c(NGR) compared to conjugate of the linear NGR [299]. This enhanced activity could be due to enhanced bend geometry of glycine and arginine in c(NGR), also due to the non-specific interaction of linear NGR with integrins due to isoDGR formation [296]. Linear or cyclic NGR were used to target tumor necrosis factor alpha (TNF-α) [300, 301], interferon gamma [302, 303], and liposomal DOX [304, 305] to the tumour neovasculature. Recently, Dunne et al [306] studied the biodistribution and pharmacokinetics of different iohexol containing NGR- liposomes in mice bearing H520 tumor xenografts using micro-CT. They evaluated the effect of both the NGR-peptide density and the length of PEG chain on the biodistribution and pharmacokinetic profiles. They showed that increasing the peptide density from 0.64 mol% to 2.56 mol% significantly reduced the tumour accumulation in mice. However, changing the NGR density for the actively targeted liposomes did not change the blood pharmacokinetics of the carrier and did not result in increased accumulation of carrier in the spleen or other normal tissues. The decreased tumour accumulation with high density NGR-liposomes has been attributed to possible instability at the tumour site, lower binding affinity, or slower convection through the tumor.

Meanwhile, the inclusion of longer PEG chain ($PEG_{3.4K}$ vs. PEG_{2k}) changed the shape of tumour accumulation vs. time profile, resulting into a shift of the time to reach maximum concentration from 48 h to 72h. This could be due to slower clearance of liposomes with longer PEG from the tumour. Takara et al. [307] developed a DOX containing dual ligand targeted liposomes. The liposomes are functionalized with NGR (CD13 targeting ligand) and R4 (Cell-penetrating peptide) on the top of PEG chain and on the surface of the liposomes, respectively. In the blood circulation, the CPP should not be functional due to the steric hindrance of the PEG chains. While, after arriving the target tumour endothelial cells, cellular association occur due to the interaction of the NGR with the CD13 receptors and this would allow the CPP (R4) to exert their ability to internalize the liposomes into the cells due to close proximity of the liposomes to the endothelial cell surface. The dual targeted liposomes supressed tumor growth mostly because of efficient disruption of tumor blood vessels.

1.1.4.3 p160 and its derivatives

The peptide p160 (VPWMEPAYQRFL) (**Figure 1-23**) is a linear dodeca peptide with specificity and high binding affinity to the breast cancer cells (MDA-MB-435) and neuroblastoma cells (WAC-2). This peptide was first discovered through phage display technique using neuroblastoma cell lines (WAC-2) [308]. The binding of bacteriophage displaying p160 peptide (t160) to the WAC-2 cells was competitively inhibited by pre-treatment with free chemically synthesized p160 peptide. Immunofluorescence analysis through confocal microscopy showed that the major fraction of p160 is internalized into the WAC-2 cells. This

internalization is reduced to 20% by K+ depletion, which indicates that the internalization is through receptor-mediated endocytosis. The p160 peptide was able to bind with high affinity to several neuroblastoma cell lines (WAC-2, SH-EP, Tet21N), and breast cancer cell line (MDA-435, MCF-7). Later, it was shown that p160 does not bind to the normal primary endothelial cell lines (HUVEC) and normal cell lines. This observation provided the first basis for the possibility of p160 peptide utilization as a targeting ligand for drug delivery purposes [308].

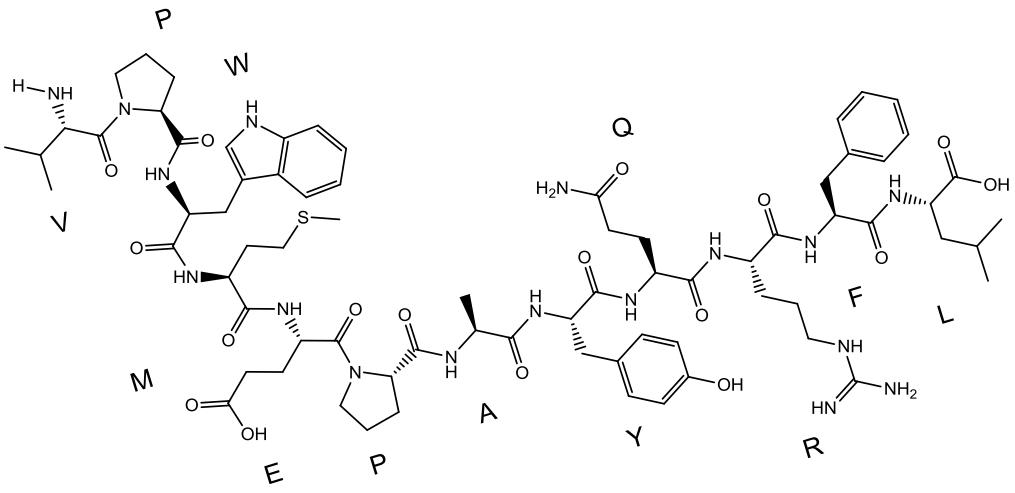

Figure 1-23: Structure of p160 peptide.

Further investigation by Askoxylakis and co-worker [309, 310] on the kinetics of radiolabeled p160 uptake by the WAC-2, MC7 , MDA-435 cells showed initial time dependant increase followed by time dependant decrease in the cellular uptake with almost complete decrease in the bound activity to the background level after 3 h with the MDA-435 cells. The biodistribution studies of ^{131}I labeled p160 before and after perfusion in MDA-435 tumour bearing mice showed high

tumour accumulation of ^{131}I labeled p160 compared to other organs (heart, lung, spleen, liver, kidney, muscle, brain). A high tumour to organ ratio was shown with the ^{131}I labeled p160 compared to ^{131}I labeled RGD-4C peptide in similar animal model. This observation could be due to higher affinity of the p160 peptide to the MDA-435 cells in comparison to RGD-4C. The in vitro stability of p160 in human serum showed complete degradation of p160 peptide by serum protease within 4 hours. The main products of serum degradation appeared after 2 h incubation had a MW of 1276, 1120 and 1022 g/mol, respectively. The first fragment (VPWMEPAYQR) is obtained by removal of the two C-terminal amino acids Phe, Leu. The second fragment is (VPWMEPAYQ) which is obtained through further loss of the C-terminal (Arg). The third fragment is (EPAYQRFL), which is obtained by cleavage of the N-terminal VPWM fragment. Some of the obtained degradation products do not share the same high binding affinity to the target cells as naïve p160 peptide [309, 310]. The in vivo metabolic stability after i.v injection of ^{131}I labeled p160 peptide in serum was also investigated by HPLC. The in vivo stability studies showed fast degradation of p160 by serum protease resulting into the formation of more hydrophilic fragments that appear within 2-5 minutes after circulation into the blood stream. These results show the importance of further work towards stabilization of the p160 peptide sequence [309, 310].

The results of studies aiming towards optimizing the binding and serum stability of the p160 peptide showed that the sequence EPAYQR is essential for the binding of the p160 peptide to the target cells [309]. Several p160 peptide analogues have been prepared (**Table 1-6**). Among those peptides the β-Ala-

p160-8-2 peptide showed more than two folds increase in the binding capacity of the p160 toward WAC-2 cells. Biodistribution studies of β-Ala-p160-8-2 showed decrease in the uptake in healthy tissue but not in the tumour. Stability of β-Ala-p160-8-2 peptide in serum showed only one metabolic product after 5 minutes in incubation, and this metabolite remained stable for more than 6 h.

Table 1-6: Relative binding of different synthesized fragment of p160 to WAC-2 cells. Adapted from Ref [309] with permission.

Peptide name	Amino acid sequence	Relative binding to naïve p160
p160	VPWMEPAYQRFL	1
p160-8-1	EPAYQRFL	1.2
p160-8-2	WMEPAYQRFL	1.04
p160-8-3	VPWMEPAY	0.12
Nle-p160-8-2	WXEPAYQRFL	1.73
βAla-p160-8-2	WMEPβAYQRFL	2.56

Further trials have been made by Kaur and coworkers to improve the binding affinity and stability of the p160 peptide [311, 312]. First, they prepared peptide arrays based on the p160 peptide and screened the peptides for their recognition by MDA-435 as well as MCF-7 human cancer cells. Three peptides were identified, namely p11, p18, p40, which showed highest binding affinity to the MDA-435, MCF-7 and low affinity towards the normal HUVEC cells. The amino acid sequence of these peptides with their relative binding adhesion compared to naïve p160 is shown in (**Table 1-7).** Flow cytometry experiment using FITC labeled-p11, p18, p40, p160 peptides after 30 minute incubation with the MDA-435 cells showed higher increase in FITC fluoresce with p18-peptide, and p11 in comparison to the FITC labeled p160-peptide. These results confirmed the results

obtained with the peptide array-cell binding assay with p18 and p11. Furthermore, these results showed the superiority of p18 peptide with almost 3 folds increasing the cellular uptake by the MDA-435 compared to p160. Flow cytometry experiment with HUVEC cells showed almost negligible change in the FITC fluorescence in comparison to p160 peptide [311]. Further in vitro stability studies of the p18 peptide in serum using HPLC showed that p18 peptide completely degrade with 30 minutes, giving two main degradation products that appear 10 minutes after incubation with serum. The first degradation product is obtained by cleavage of the first two N-terminal amino acids (W,X) to get (EAAYQRFL, MW 977 Da), the second fragment is obtained by loss of the C-three terminal amino acids to get (WXEAAYQ, MW 878 Da) [312].

Table 1-7: Amino acid sequence and relative cell binding affinity of different p160 analogues. Adapted from [311] with permission.

Peptide name	Sequence	Relative cell adhesion in compare to naïve p160	
		MDA-435	MCF-7
p160	VPWMEPAYQRFL	1	1
p11	RGDPAYQGRFL	1.7	1.8
p18	WXE**A**AYQRFL	2.2	2.7
p40	WXEPAYQR**K**L	2.7	2.7

Soudy et al. [312] developed three novel analogues of the p18 peptide with high affinity to the breast cancer cell lines MDA-435, MCF-7 and MDA-231 namely,

p18-4, p18-9, and p18-10 (**Table 1-8**). P18-9, and p18-10 are mixed α/β peptides, whereas p18-4 is an α peptide (**Figure 1-24**). Flow cytometry experiments showing the cellular uptake of different FITC labeled peptide analogues by MDA-435, MCF-7, MDA-231 breast cancer cells evidenced the superiority of the p18-4 peptide in comparison to other peptide analogues. p18-4 showed 3.5, 3.1, 2.8 folds increase in the cellular uptake when compared to p18 peptide by MDA-435, MCF-7 and MDA-231 cells, respectively. With the non-cancerous cells HUVEC and MCF 10A , minimal cellular uptake was seen. Interestingly, p18-4, p18-9, p18-9 showed stability in human serum, and liver homogenate for more than 24 h [312]. Due to the high specific binding of the p18-4 peptide along with the inherent resistance to proteolytic degradation by proteases, it is considered as an ideal candidate as a short peptide ligand for cancer therapeutic application. The potential of p18-4 peptide as a peptide ligand to target DOX liposomes toward breast cancer cells was assessed in this thesis.

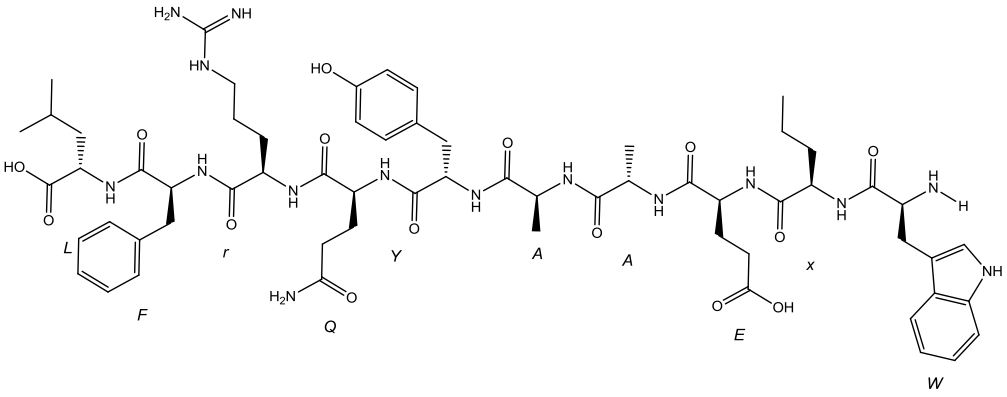

Figure 1-24: Structure of p18-4 peptide.

Table 1-8: The amino acid sequence of engineered p160 analogues developed by Soudy et al. [312].

Peptide name	Amino acid sequence[1]
P18	WXEAAYQRFL
P18-4	W**x**EAAYQ**r**FL
P18-9	ZXEAAYQKFL
P18-10	ZXEAAYQKFL

[1] Lowe case letters denote D-amino acid, underlined letters denote β- amino acid derived from L-Asp. X(is Nle) , and Z is a β^3 residue with N-naphthyl chain.

1.1.4.4 Other peptides

Peptide sequence derived from the protein transduction domains (PTDs), named cell-penetrating peptides (CPPs) are another class of peptides used in drug/gene delivery. PTDs are short peptide sequence that promote internalization through the cell membrane [313]. Examples of PTDs includes Antennapedia (Antp), poly arginine peptides, penetratin, and the HIV-TAT (Transactivator of transcription) [314]. The mechanism by which CPPs mediate the cellular uptake is still not clear despite the presence of many theories that explain it. CPPs appears to be capable of bypassing the endocytic pathway [313]. TAT peptide is one of the most frequently used CPP [313] that has been attached to liposomal surface to deliver several therapeutic payloads [315-319]. Kale and Torchilin [315] developed a liposomal formulation bearing TAT peptide on theirs surface. In this structure TAT is shielded with PEG coating at high pHs, and once these liposomes is delivered to the tumour site through the EPR effect, the TAT peptide is de-shielded due to the low pH of the tumour micro-environment in a way that allow the TAT-mediated transport into the tumour cells.

Another class of cancer targeting peptide are “collagen mimetic peptides”. These peptides target the CD44 receptors that are over-expressed on the surface of many tumour cells. The CD44 receptors in the metastatic melanoma are the chondrointin sulfate proteoglycan (CSPG) modified form of the CD44 receptors [320]. These CD44/CSPG receptors binds to a specific amino acid sequence from collagen called IV-H1 (GVKGDKGNPGWPGAP). This IV-H1 peptide was modified with several dialkyl tails to create collagen like peptide amphiphiles.

Several studies showed that the peptide-amphiphile [$(GP\text{-}Hyd)_4$-GVKGDKGNPGWPGAP- $(GP\text{-}Hyd)_4$] could bind specifically the CD44/CSPG receptors. Rezler et al. [321] showed that stealth liposomes decorated with the peptide-amphiphile [$(GP\text{-}Hyd)_4$- GVKGDKGNPGWPGAP- $(GP\text{-}Hyd)_4$] exhibited specific ligand receptor interaction.

The PR_b peptides are also used for targeting purposes. This peptide sequence is a synergy segment (Pro-His-Ser-Arg-Asn) (PHSRN) that is localized in the 9^{th} type III repeat of fibronectin. Fibronectin is a high MW glycoprotein of the ECM that binds to integrin receptors. The PHSRN segment has shown to enhance the binding affinity and a crucial part for the specificity of fibronectin to the $\alpha_5\beta_1$ [322]. Mardilovich and Kokkoli [323] suggested that a neutral linker having a distance of 37 ^{o}A between the RGD and PHSRN sequences is required for a single peptide molecule to mimic the binding site of naïve fibronectin. The effort of Mardilovich and Kokkoli resulted into the formation of a novel peptide sequence called PR_b which bind effectively and specifically to the $\alpha_5\beta_1$ integrins [324]. Stealth liposomal formulation bearing PR_b peptide were used to deliver therapeutics to colon [195] and prostate cancer cells [325]. Those studies showed clearly enhanced cell adhesion, internalization and cytotoxicity for the PR_B functionalized liposomes compared to RGD-bearing liposomes or non-targeted liposomes.

1.1.5. **Anticancer drugs under this study**

In this thesis, two chemotherapeutic agents were selected (paclitaxel and doxorubicin). They are among the first line single therapy used to treat metastatic breast cancer[326, 327]. They belong to different families of chemotherapeutic agent (taxane vs. anthracycline) that have different mechanism of action, toxicity profile, water solubility. However, both have high individual activities and are generally prescribed after failure of endocrine therapy as a first line for treatment of patient with receptor negative breast cancer or with life threatening metastasis [328, 329]. Phase III randomized trial of combination therapy of both paclitaxel and doxorubicin showed a significant advantage in term of improving the response rate, time to progression, and overall survival compared to standard combination that include fluorouracil, doxorubicin and cyclophosphamide in women with metastatic breast cancer [330].

1.1.5.1. ***Paclitaxel***

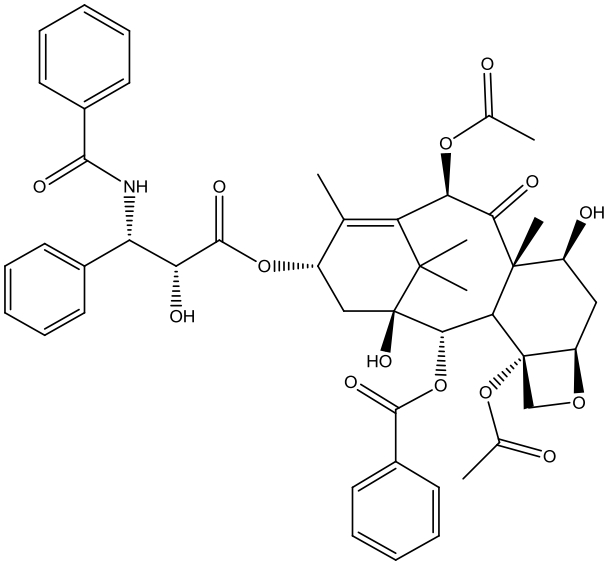

Figure 1-25: Chemical structure of Paclitaxel.

Paclitaxel (PTX) is a polyoxygenated diterpene with a MW of 853.5 Da, one of the 300 molecules of the class of taxane diterpenoids (**Figure 1-25**). The history of PTX development is summarized in (**Table 1-9**). The discovery of the antitumor activity of PTX is considered one of the most important milestones in the chemotherapy of breast cancer [331]. Since the approval of PTX by the FDA 1992, it represents the main treatment for breast and ovarian cancer. Its discovery is attributed to drug screening program initiated by the national cancer institute in early 1960s. In 1971, pure PTX was isolated with a very low yield (0.02%) from *Taxus brevifolia*. The development of PTX was suspended for around 10 years (1971-1983) due to problems with the drug formulation. After extensive studies, the most feasible choice to improve PTX water solubility was found to be a vehicle composed of polyethoxylated castor oil (Cremophor® EL) and ethanol (Taxol®;CrEL-paclitaxel). PTX is a lipophilic compound with compound with a reported aqueous solubility of 1 µg /mL [332]. Solid state characterization of PTX confirm that PTX exist as dihydrate. Currently PTX is semi-synthesized from 10-deacetylbuccatin III, which is found in the leaves of *Taxus baccata* in large quantities. This method is currently used by Bristol Mayer Squibb in the commercial production of PTX [333].

The main mechanism of action of PTX involves inhibition of the microtubules depolymerisation leading to stable microtubules formation and inhibition of spindle formation during late G2 phase and M phase of the cell cycle [334]. This will result in mitotic arrest and apoptosis. Microtubules are formed by the self-

association of α, and β tubulin heterodimers. The binding site of PTX is the 31 amino acid region at the N-terminal of β tubulin [334]. Microtubule assembly require the β tubulin to be charged with the GTP that is hydrolyzed to GDP after addition of the dimer to the growing end of the microtubules. While the microtubules is stabilized by the GTP at the growing end, its hydrolysis to GDP renders the microtubules unstable and prone to depolymerisation. Binding of PTX to the β tubulin compensate the instability induced by GDP and results in a conformational change of the protofilament. The exact nature of PTX induced conformational changes is unknown, crystallography studies established that PTX binds to the microtubules in a 1:1 ratio indicating that binding occur at only one site [335]. In addition to stabilizing effect of PTX on the microtubules, PTX activates cdc-2 kinase, IL-β, TNF-α and facilitate phosphorylation of BCL-2, which contribute in cell apoptosis [336].

Table 1-9 : History of PTX discovery and development. Adapted from Ref. [337] with permission.

Date	
Early 1960s	Discovery and detection of the antitumor activity of Pacific Yew tree bark Extract
1971	Characterization of the active ingredient of the bark extract (Paclitaxel)
1979	Tubulin stabilization as the mechanism of action was established
1983	NCI started Phase I investigation on wide range of cancers
1985	Start of Phase II clinical trials
1991	Start of commercialization, activity in breast cancer was noticed
1992	FDA Approval of PTX for refractory metastatic breast cancer
1994	Approval of PTX for refractory, relapsed breast cancer
1995	FDA approved the semisynthetic PTX
1997-1999	Additional indication for semisynthetic PTX in Kaposi Sarcoma, ovarian , and non-small cell lung cancer

The major challenges related to successful chemotherapy with PTX are drug resistance and low aqueous solubility. The main molecular mechanism of PTX resistance include [336]:

i. Overexpression of p-glycoprotein.

ii. Alteration of β-tubulin isotype.

iii. Alteration in cytokine level.

iv. Mutation in BCL-2, p-53, and other genes involved in apoptosis.

P-glycoprotein is ATP-dependant transmembrane efflux pump that is expressed in a variety of tumours. PTX is a substrate of the p-glycoprotein and is actively effluxed out of the tumour cells. Overexpression of this protein on the surface of the tumour cells is a result of mutation in the multidrug resistance gene (MDR-1) [338]. The low oral bioavailability of PTX is attributed to the rapid efflux of the drug by the p-glycoprotein expressing intestinal cells [339].

The main adverse effects related to PTX chemotherapy are: dose dependant neutropenia, thrombocytopenia, mucositis, neurotoxicity, hypersensitivity, toxic effects on the cardiovascular system that include: bradycardia, AV conduction blocks, and arrhythmia. Furthermore, hepatotoxicity, and gastrointestinal disturbances are common [331].

The C_{max} , AUC, and total clearance of PTX are dose dependant. About 89-98% of PTX is bound to serum proteins. Urinary clearance of PTX is minimal and its hepatic metabolism and biliary excretion is extensive. PTX is metabolized by cytochrome p450 isoenzyme CYP2C to 6α-hydroxypaclitaxel. A total of five metabolite of PTX have been identified, of which four are monohydroxylated and one is dihydroxylated by-products [340].

Taxol® was the first commercialized formulation of PTX, in which PTX is dissolved in a 50:50 v/v co-solvent of the non-ionic surfactant Cremophor EL and ethanol. Clinical studies with Taxol® showed high response rate in patients with

ovarian carcinoma, breast carcinoma, and AIDS- related Kaposi sarcoma. Cremophor EL has been reported to cause severe adverse effects, most importantly, anaphylactic hypersensitivity reactions, which is characterized by dyspnoea, flushing, rash, tachycardia, hypotension, and angioedema. In addition, hyperlipidemia, neurotoxicity, non-linear pharmacokinetic profile of Taxol® have been attributed to the presence of Cremophor EL [341]. However, in the absence of clinical viable alternative, Taxol® has been co-administered with immunosuppressant such as corticosteroids, and antihistamine to mitigate the hypersensitivity reaction toward Cremophor EL [342, 343]. Development of alternative delivery system for i.v administration of PTX that eliminate the need for Cremophor EL has been the focus of much attention.

In 2006, the FDA approved albumin-bound formulation of PTX called Abraxane® for the treatment of metastatic breast cancer. The solubility of PTX in this formulation was increased using nab™ technology, that involves the non-co-solvent combination of PTX with biocompatible protein (albumin) to get a nanoparticle that is 130 nm in size. The main advantages of Abraxane® over Taxol® include the shorter infusion time (30 min vs. > 3 h for single administration of Taxol ®), and absence of hypersensitivity reactions [344]. The main adverse effects of Abraxane® are neutropenia, anemia, thrombocytopenia, hypotension, dose dependant neuropathy, arthralgia, myalgia, weakness, and fatigue [345].

Other formulations of PTX currently in clinical trials include PTX-polyglumex (xyotax®, or opaxio®), and Tocosol®. Xyotax® is a polymeric conjugate of PTX

with poly(L-glutamic acid). Xyotax® is currently in phase III clinical trial in combination with carboplatin for the treatment of recurrent non-small cell lung cancer [346, 347]. Tocosol® is vitamin E containing o/w emulsion of PTX that have demonstrated excellent tolerability and efficacy in preclinical trials [348]. It is currently in phase III clinical trials for the treatment of metastatic breast cancer.

1.1.5.2. ***Doxorubicin***

In 1962, a powerful glycosidic antibiotic named daunomycin (**Figure 1-26**) was isolated from a strain of Streptomyces caeroleorubididus in France and from strains of Streptomyces peucetius in Italy [349]. Then, a more potent hydroxylated derivative of daunomycin with more efficacy against solid tumours, doxorubicin (Adriamycin) (**Figure 1-26**), was isolated from a mutant strain of Streptomyces peucetius [350] .

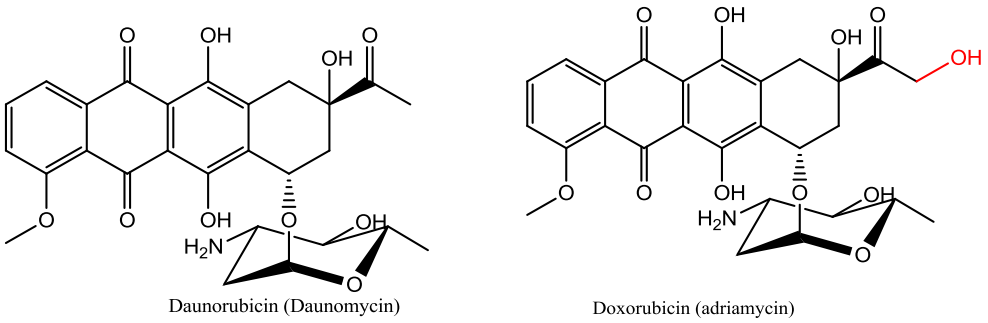

Figure 1-26: Structures of the anthracyclines Doxorubicin and its parent compound daunorubicin.

Doxorubicin ($C_{27}H_{29}NO_{11}$) has a MW 543.52 Da. The reported aqueous solubility for its base and the HCl salt are 92.8 µg/mL and 10 mg/mL, respectively [351, 352]. Doxorubicin has been successfully used in clinical practice for more than 20 years. Several human tumours are shown to be responsive to DOX include

acute leukemia [353-358], resistant Hodgkin and non-Hodgkin lymphoma [359-365], sarcoma [366-372], neuroblastoma [373-375], ovarian and endometrial carcinoma [376-381] and breast carcinoma[382-385]. The dose limiting toxicity, including stomatitis [386], mucositis [387], nausea, vomiting [388], bone marrow suppression, cardiomyopathy [389-393]. Doxorubicin itself has a characteristics fluorescence (excitation wavelength = 488nm, emission wavelength = 595 nm). This would allow DOX to be easily identified using flow cytometry and fluorescence spectroscopy for studying the cellular uptake of several DOX containing carriers [394-396].

The most obvious drawback of DOX treatment is the fatal cardiotoxicity that is characterized by dilated cardiomyopathy and congestive heart failure [397]. This increased cardiotoxicity is mainly due to cumulative doses of DOX received, therefore several studies have been made to reduce the cumulative dosing of DOX while maintaining the therapeutic efficacy [397-400].

The concentration of DOX in the blood stream play a major role in the manner by which DOX will mediate cell death [401, 402]. Free DOX diffuses through the cell membrane, and in the cytoplasm it binds to proteasome to form a complex passes through the nuclear pores to the intranuclear milieu through ATP-mediated nuclear pore mechanism [403, 404]. Once, inside the nucleus, DOX interchalate with DNA and by this way it will stop the action of topoisomerase II (TopoII) through stabilizing an intermediate step. TopoII normally functions through cleaving both stands of the DNA to allow the passage of another DNA stand through. By this way, it will relieve the mechanical stress and lead to chromosome

entanglement. It then re-ligate the stands together. DOX stabilizes the step in which the two strands are separated, and TopoII will be unable to re-ligate them together again [405]. This would activate apoptotic signals, resulting into activation of p53 and it downstream mediators, which includes p21, XRCC1, Bcl-2, and caspases. It was found that DOX treatment affected also several genes involving cell cycle regulation, signal transduction, metabolism, and protein degradation and transcription factors [406-409]. More recent work pointed to the possibility of formation of reactive oxygen species that interact with several components in the intracellular milieu as the main mediator of cellular death [397, 410]. Also, other effects have been reported as a result of DOX treatment at high concentrations (>5 μM) which includes free radical generation, lipid peroxidation, DNA cross linking, inhibition of helicase II, and inhibition of telomeric DNA. DOX also triggers the mitochondria to release cytochrome c, initiating caspase activation and apoptosis [397, 411].

Resistance to DOX is most commonly due to the up regulation of membrane associated efflux transporters [412]. The best characterized of these multidrug resistance transporters is p-glycoprotein (pgp, ABCB1), a product of mdr1 gene transcription [412-415]. The mdr1 gene is normally expressed in different organs systems, including the adrenal gland, kidney, lung, and GIT [416]. Number of other non-pgp transporters have been identified, including the MDR associated protein (MRP) and breast cancer related protein (BCRP, ABCG2). All these transporters are members of the ATP binding cassette (ABC) family [417].

Doxorubicin is available commercially as traditional formulations or liposomal formulations. The traditional formulation includes Adriamycin® and Rubex® which are i.v preparation that contains DOX.HCL. The liposomal formulations include Doxil® and Myocet®.

1.1.6. **Research Proposal**

1.1.7. **Rational**

The available cancer therapies have low specificity for the tumour cell and have serious side effects. The utilization of targeted drug delivery systems have shown great potential to provide enhanced efficacy and reduced side effects for the incorporated anti-cancer agent. This is mainly due to a change in the normal biodistribution of the drug away from normal tissues and towards tumor site as imposed by its carrier. The target for most anti-cancer agents resides within the tumor cells, however. Development of means that can improve either the homing of the nanocarriers on tumor cells or increase the access of encapsulated drug to intracellular space are expected to enhance the therapeutic benefit of nano-delivery systems in cancer therapy even further. Cancer targeting ligands decorating the surface of nanocarriers can be used to achieve the mentioned objective. Despite the promising clinical results obtained with the long circulation liposomes Doxil ® in several tumour models in compare to free DOX, the non-specific mucocutaneous reactions (e.g. hand and foot syndrome) still unresolved problem, and further optimization is ongoing concern. Several attempts have been made to improve the anticancer activity of Doxil ® by targeting it through several molecules specific to receptors typical for cancer cells including folate

[230, 418], and monoclonal antibodies [419]. Those studies showed substantial increase in the cytotoxicity and improved anticancer activity towards the target cells both in vitro and in vivo compared to non-targeted DOX liposomes. Naturally occurring ligands e.g. folate have low MW, non-immunogenic, easy to handle and store. Receptors for these ligands are usually overexpressed on the tumour cell surface, however. This means that the receptor expression is not specific for the cancer cells and the normal cells might be affected and suffer toxicities. On the other hand, the utilization of mABs is limited by their large size, poor tumour penetration, immunogenicity, and difficulty of chemical manipulation. Nowadays, peptides have emerged as ideal ligands for cancer cells targeting due to their high specificity towards tumour cells, low immunogenicity, improved pharmacokinetic profile and ease of chemical manipulation. Lately, several peptides have been recognized that has the capability to target tumour cell surface e.g. p160 and its engineered analogue p18-4. Previous studies have demonstrated the usefulness of these peptides to target breast cancer cells (MDA-435, MCF-7 and MDA-231) compared with traditional anti-angiogenic peptides (e.g. RGD4C). In addition to the efficient and specific homing capacity to different tumour tissue, p160-peptide and its analogues are suggested to be internalized into breast cancer tumour cells through receptor mediated endocytosis [310]. The homing of p160 and its analogues is tumour type specific; it could accumulate in some tumour (MDA-435, MCF-7 and MDA-231) but not in others. The motivation for this work is to investigate the efficacy of p160 and p18-4 peptides –mediated drug delivery systems (i.e. polymeric micelles nano-

containers, polymeric conjugate, and liposomes) for the treatment of breast cancer in vitro and in vivo.

1.1.8. **Hypothesis**

Breast cancer cell targeting peptides (p160, or p18-4) can increase the specificity and therapeutic efficacy of polymer and lipid based nano-carriers containing PTX or DOX against breast cancer.

1.1.9. **Objective**

Development of novel polymer and lipid based nano-carriers of conventional anticancer agents, i.e., PTX and DOX, modified on their surface with engineered breast cancer cell targeting peptides and assess the effect of peptide modifications on the specificity and anti-cancer activity of developed formulation making comparisons with free drugs and unmodified nano-delivery systems of related anti-cancer agents.

1.1.10. **Specific aims**

1- Development of novel self-associating poly(ethylene oxide)-b-poly(ε-caprolactone) based drug conjugates and nano-containers for paclitaxel delivery.

2- Development of p160 decorated polymeric micellar drug nano-containers and conjugates for active targeting of PTX.

3- Development p18-4 peptide DOX loaded liposomal nano-carriers for active drug targeting.

4- Assessment of the effect of p18-4 peptide decoration on the liposomal surface on selective cytotoxicity and in vivo therapeutic efficacy of liposomal DOX formulations.

Chapter 2
Novel self-associating poly(ethylene oxide)-b-poly(ε-caprolactone) based drug conjugates and nano-containers for paclitaxel delivery[17]

[17] The content of this chapter has been previously published in : Shahin M, Lavasanifar A. Novel self-associating poly(ethylene oxide)-b-poly(ε-caprolactone) based drug conjugates and nano-containers for paclitaxel delivery. International Journal of Pharmaceutics, 2010, 389(1-2): p. 213-22

2.1 Introduction

Paclitaxel (PTX), is an antineoplastic drug successfully used against a variety of tumors including ovarian, breast and non-small cell lung tumors in clinic [420-422]. However, the main difficulty in its clinical use is its limited solubility in water 1 μg/mL) and many other acceptable pharmaceutical solvents [423, 424]. The commercial injectable formulation of PTX, Taxol®, utilizes a mixture of Cremophor EL and ethanol (1:1, v/v) [425]. This formulation requires in-line filtration and should not be allowed to contact with plasticized polyvinyl chloride (PVC) devices as Cremophor EL is known to leach phthalate plasticizer [426, 427]. Also, the high amount of Cremophor EL in Taxol® results in hypersensitivity reactions, nephrotoxcicity, and neurotoxcicity [428]. It has been reported that Cremophor EL can modify the pharmacokinetics of PTX [429]. To overcome these problems, several alternative pharmaceutical carriers have been developed for PTX delivery [425, 430].

We report on the development of new self -associating block copolymer-PTX conjugates and nano-containers based on functionalized poly(ethylene oxide)-*block*-poly(ε-caprolactone) (PEO-*b*-PCL) for the solubilization and delivery of PTX. Conjugation of small molecule drugs to macromolecular carriers to produce polymer-drug conjugates has proven to be a valuable formulation strategy for anticancer agents [110]. To date, two PTX polymeric conjugates, i.e., PNU166945 and Xyotax ™ (CT-2103) have entered clinical trials [431]. In PNU166945, PTX is linked to hydroxypropyl methacrylamide polymer through formation of an ester bond with a short peptide linker (Gly-Phe-Leu-Gly). PNU166945 has shown poor pharmacokinetics in phase I clinical trials due to

instability of ester linkage conjugating PTX [432]. Xyotax ^{TM}, polyglutamic acid (PGA) conjugated to PTX through an ester linkage, is the only PTX polymeric conjugate in phase III clinical trials for the treatment of non-small cell lung cancer in combination with carboplatin [433-435]. In general polymer-drug conjugates offer potential advantages over Taxol®, first they eliminate the need for toxic solubilizing agent (Cremophor EL) and enhance the tumor tissue uptake through Enhanced Permeation and Retention (EPR) effect, as well as they show better pharmacokinetic profile and less toxicity due to limited normal tissue exposure to free drug [347].

In this study, the block copolymer-PTX conjugate was synthesized through formation of an ester bond between a hydroxyl group in PTX and free side carboxyl groups on poly(ethylene oxide)-*block*-poly(α-carboxyl-ε-caprolactone) (PEO-*b*-PCCL) producing PEO-*b*-P(CL-PTX). This block copolymer-PTX conjugate contains several side PTX molecules on the hydrophobic block of one polymer chain and readily assembles to polymeric nanoparticles. The ester bond between PTX and polymeric backbone was expected to be protected within the hydrophobic core of nano-carriers preventing premature drug release within the systemic circulation. A similar approach has been used to form block copolymer conjugates of doxorubicin (DOX) through formation of amide bonds between free amino group of DOX and PEO-*b*-PCCL in our previous publication [436]. As an alternative to chemical conjugation of PTX to self-associating block copolymers, PEO-*b*-PCL, PEO-*b*-poly(α-benzyl carboxylate-ε-caprolactone) (PEO-*b*-PBCL) and PEO-*b*-P(CL-PTX) were self-

assembled to polymeric nano-carriers and used for physical encapsulation of PTX, as well.

2.2 Materials and methods

2.2.1 Materials

Methoxy polyethylene oxide (average molecular weight of 5000 gmol-1), diisopropyl amine (99%), benzyl chloroformate (tech. 95%), sodium (in Kerosin), butyl lithium (Bu-Li) in hexane (2.5 M solution), palladium coated charcoal, N, N dicylcohexyl carbodiimide (DCC), dimethylamino pyridine (DMAP), and pyrene were purchased from Sigma chemicals (St. Louis, MO, USA). Paclitaxel (purity> 99.5) was purchased from LC Laboratories (Woburn, MA, USA). ε-caprolactone was purchased from Lancaster Synthesis, UK. Stannous octoate was purchased from MP Biomedicals Inc., Germany. Fluorescent probes, pyrene and 1,3-(1,1′-dipyrenyl)propane were purchased from Molecular Probes, USA. Cell culture media RPMI 1640, penicillin-streptomycin, fetal bovine serum, and L-glutamine were purchased from GIBCO, Invitrogen Corp. (Burlington, ON, Canada). All other chemicals were reagent grade.

2.2.2 Methods

2.2.2.1 Synthesis of PEO-b-PCL and PEO-b-PBCL block copolymers

PEO-*b*-PCL block copolymer was synthesized by ring opening polymerization of ε-caprolactone using methoxy polyethylene oxide as initiator and stannous octoate as catalyst. Methoxy PEO (MW: 5000 g mole^{-1}) (0.5 g), ε-caprolactone (0.5 g) and stannous octoate (0.002 eq of monomer, 35 mg) were added to dry 10 mL ampoule nitrogen purged and sealed under vacuum. The reaction was carried out by placing the ampoule at 140 ^{0}C for 4 hours in oven and

terminated by cooling the product to room temperature [437]. For the synthesis of PEO-*b*-PBCL, methoxy PEO (MW: 5000 g mol^{-1}) (3.5 g), α-benzylcarboxylate-ε-caprolactone (3.5 g) and stannous octoate (0.002 eq. of monomer, 35 mg) were used as initiator, monomer and catalyst under identical reaction condition. The synthesis of functionalized monomer, i.e., α-benzyl carboxylate-ε-caprolactone is reported in a previous paper [437]. Briefly, to a solution of (8.4 mL, 60.0 mmol) of dry diisopropylamine in of dry THF, (24 mL, 60.0 mmol) of butyl lithium in hexane were slowly added at −30°C under vigorous stirring with continuous argon supply. The solution was cooled to −78°C and kept stirring for additional 20 min. Freshly distilled ε-caprolactone (3.42 g, 30 mmol) was dissolved in dry THF and added to the above mentioned mixture slowly, followed by the addition of benzyl chloroformate (5.1 g, 30 mmol). The temperature was allowed to rise to 0°C after 1.5 h and the reaction was quenched with 5 mL of saturated ammonium chloride solution. The reaction mixture was diluted with water and extracted with ethyl acetate. The combined extracts were dried over Na_2SO_4 and purified by column chromatography using an eluant of 25% ethyl acetate in hexane.

2.2.2.2 Synthesis of PEO-b-P(CL-PTX)

The synthesis of PEO-*b*-P(CL-PTX) was accomplished in two steps (**Scheme 2-1**). In the first step, PEO-*b*-PCCL was synthesized through catalytic debenzylation of PEO-*b*-PBCL in the presence of hydrogen gas as reducing agent and palladium coated charcoal as catalyst according to a procedure described before [437]. In the second step, PTX was chemically conjugated to PEO-*b*-PCCL through formation of an ester bond by a DCC and DMAP mediated coupling reaction [438]. Briefly, DMAP (17.7 mg, 0.145 mmol) and DCC (29.9 mg, 0.145

mmol) were added to a stirred solution of PEO-*b*-PCCL (MW: 6900 g mol^{-1}) (100 mg, 0.0145 mmol) in anhydrous dichloromethane (DCM) (20 mL). Subsequently, after stirring for 30 min PTX (37.1 mg, 0.0435 mmol) in 1 mL of dried DCM was added. The reaction was carried out under argon gas while protected from light for 4 days at room temperature. Thin layer chromatography (TLC) in the presence of THF: DCM (1:4) as the mobile phase was used to monitor the reaction progress and spots were detected by a UV lamp at 254 nm [439]. The by-product dicyclohexyl urea was filtered out. The product was condensed by bubbling of nitrogen gas. The purification of the polymer from free PTX was carried out by dialysis against 1 L of dimethlyl sulphoxide (DMSO) for one day, then against double distilled water for another day using cellulose membrane (Spectrapore, cutoff MW: 3500 g mol^{-1}). The PTX conjugated block copolymer, i.e., PEO-*b*-P(CL-PTX), was then lyophilized to a white powder. The prepared copolymer was characterized for its average molecular weights and polydispersity by ^{1}H NMR and Gel permeation chromatography (GPC). ^{1}H NMR was carried out by Bruker Unity-300 spectrometer at room temperature, using deuterated chloroform ($CDCl_3$) as solvent and tetramethyl silane as internal reference standard. The GPC was carried out at 25 ^{0}C with an HP instrument equipped with Waters Styragel HT_4 column (Waters Inc., Milford, MA). The elution pattern was detected at 35 ^{0}C by refractive index (PD 2000, precision detector, Inc.)/light scattering (model 410, Waters Inc.) detectors. THF (1 mL/min) was used as eluent. Samples of 20 µL from 10 mg/mL polymer solution in THF were injected. The column was calibrated with a series of standard polystyrenes. The PTX content in the

conjugate was calculated from the ^{1}H NMR spectrum using the peak integration of phenyl protons signal at (7.3-8.4 ppm) and the ethylene proton signal (3.7 ppm).

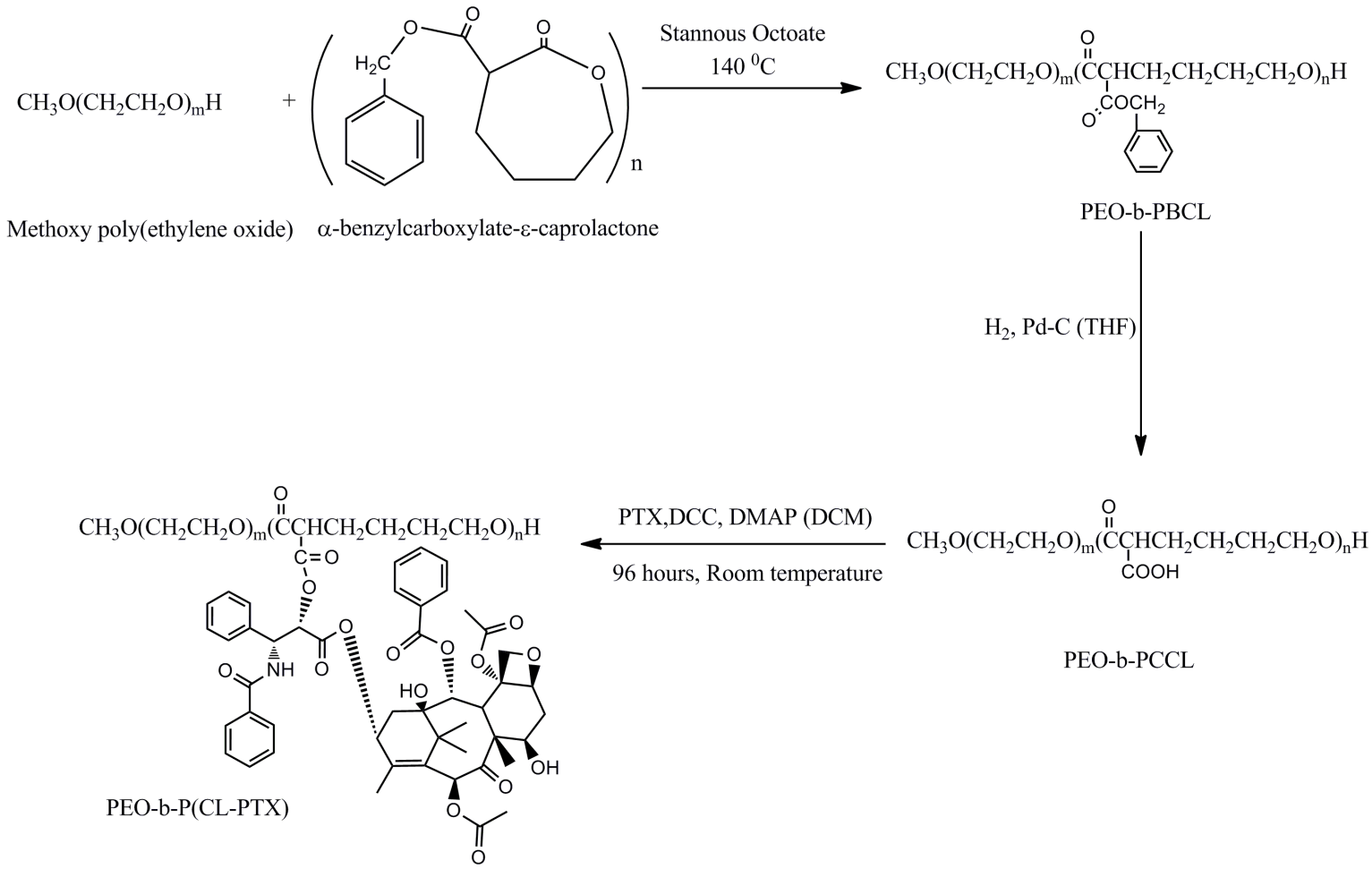

Scheme 2-1: Synthesis of PEO-b-P(CL-PTX) block copolymer.

2.2.2.3 Self-assembly of block copolymers and physical encapsulation of PTX in the assembled structures

Self-assembly of PEO-*b*-P(CL-PTX) was accomplished through dialysis method. The block copolymer (3 mg) was dissolved in DMSO (0.5 mL). This solution was added to doubly distilled water (3 mL) in a drop-wise manner under moderate stirring for 1 day followed by organic solvent removal by dialysis against double distilled water for another day (Spectrapor, M_W cutoff 3,500 $g.mol^{-1}$). This solution was then centrifuged 11,600 × g for 5 min to remove any free unimers.

Encapsulation of PTX in PEO-*b*-PCL, PEO-*b*-PBCL and PEO-*b*-P(CL-PTX) micelles was carried out by an identical procedure with the exception that the polymer and PTX were dissolved in N-N, dimethyl formamide (DMF) as an organic solvent and the final polymer concentration was adjusted to 0.36 mM [440]. To determine the maximum loading of PTX in micelles, several micellar formulations were prepared with increasing amounts of PTX in DMF/copolymer solution. After dialysis, the solution was centrifuged at 11,600 × g for 5 min to remove any precipitate, and an aliquot (100 µL) of the micellar solution was diluted with acetonitrile. The solution was analysed for PTX content using HPLC. Varian prostar 210 HPLC system at a flow rate of 1.0 mL/min at room temperature was used. The detection was performed at 227 nm using a Varian 335 Photodiode Array HPLC detector (Varian Inc., Australia). Reversed phase chromatography was carried out with a Microsorb-MV 5 µm C18-100 Å column (4.6 mm × 250 mm) with 20 µL of sample injected in a gradient elution using

0.1% trifluroacetic acid aqueous solution and acetonitrile. The percent of acetonitrile was 40% at time and increased with elution time up to 100% within 15 minutes [441]. The level of PTX loading (w/w%), (mol/mol%) and encapsulation efficiency were calculated using the following equations (1-3):

$$\text{PTX loading (w/w\%)} = \frac{\text{amount of physically loaded PTX in mg}}{\text{amount of copolymer in mg}} \text{X } 100 \quad (1)$$

$$\text{PTX loading (mole/mole \%)} = \frac{\text{amount of physically loaded PTX in moles}}{\text{amount of copolymer in moles}} \text{X } 100 \quad (2)$$

$$\text{Encapsulation efficiency (\%)} = \frac{\text{amount of physically loaded PTX in mg}}{\text{amount of PTX added in mg}} \text{X } 100 \quad (3)$$

2.2.2.4 Characterization of polymeric micelles

2.2.2.4.1 Critical micellar concentration

A change in the fluorescence excitation spectra of pyrene in the presence of varied concentration of PEO-*b*-P(CL-PTX) block copolymer was used to measure its CMC according to the method described previously [442]. Briefly, pyrene was dissolved in acetone and added to 5 mL volumetric flasks to provide a concentration of 6×10^{-7} M in the final solutions. Acetone was then evaporated and replaced with aqueous polymeric micellar solutions with concentrations ranging from 0.061 to 1000 μg/mL. Samples were heated at 65 °C for an hour, cooled to room temperature overnight, and deoxygenated with nitrogen gas prior to fluorescence measurements. The excitation spectrum of pyrene for each sample was obtained at room temperature using a Varian Cary Eclipse fluorescence spectrophotometer (Victoria, Australia). The scans was performed at medium speed (600 nm/min) and at a PMT detector voltage of 575 V. Emission wavelength and excitation/emission slit were set at 390 nm and 5 nm,

respectively. The intensity ratio of peak at 338 nm to that at 333 nm was plotted against the logarithm of copolymer concentration. CMC was measured from a sharp rise in intensity ratios (I_{338}/I_{333}) at the onset of micellization.

2.2.2.4.2 Core viscosity

The viscosity of hydrophobic domain in the self-assembled structures was estimated by measuring excimer to monomer intensity ratio (I_e/I_m) from the emission spectra of 1,3-(1,1′-dipyrenyl)propane at 480 and 373 nm, respectively, in the presence of polymer solutions at 1 mg/mL concentration. The details of the method are described in a previous publication [443].

2.2.2.4.3 Micellar shape and size

The average diameter and size distribution of the prepared nano-carriers were estimated by dynamic light scattering (DLS) using Malvern Zetasizer 3000 after centrifugation at 11,600 × g for 5 minutes.

The morphology of PEO-*b*-P(CL-PTX) nano-carriers was determined by both transmission electron microscopy (TEM) and atomic force microscopy (AFM). The TEM experiment was carried out by placing an aqueous droplet (20 µL) of the micellar solution with a polymer concentration of 1 mg/mL on a copper coated grid. The grid was held horizontally for 20 s to allow the colloidal aggregate to settle. Then, a drop of 2% solution of phosphotungstic acid in PBS was added to provide the negative stain. After 1 min, the excess fluid was removed by filter paper. The sample was then air dried and loaded into transmission electron microscope (Hitachi H 7000, Tokyo, Japan) [443].

The AFM experiment was carried out by placing an aliquot (2 µL) of the micellar solution (0.1 mg/mL) on a freshly cleaved mica surface (flogopite,

$KMg_3AlSi_3O_{10}(OH)_2$) and air dried at room temperature. Samples were imaged in air at room temperature and humidity with MFP-3D inverted optical AFM (Digital Instruments, Santa Barbara, CA), equipped with a 120 µm xy and 6 µm z scanner for accurate length, height and force measurements. An integral silicon tip cantilever (OMCL-AC160TS-W2, Olympus Cantilevers) with a spring constant of 10 pN/nm was used. AFM tapping mode imaging was done at scan rates of 1-1.5 Hz/line and set point of 600 mV. All images were processed with a second-order flattening routine for background correction.

2.2.2.5 Evaluation of the physical stability of prepared nano-carriers

The PEO-*b*-P(CL-PTX) micellar solution (1 mg/mL) was prepared as described previously in phosphate buffer (0.01 M, pH 7.4) and left for 7 days at room temperature. At different time points, the hydrodynamic diameter as well as the polydispersity of the micellar solution was assessed using Malvern Zetasizer 3000 as described above. For physically encapsulated PTX nano-carriers, solutions in double distilled water were prepared at 0.36 mM polymer concentration. The possibility for the formation of secondary aggregates was then investigated by measuring the size of nano-carriers right after preparation.

2.2.2.6 Assessing the hydrolysis of poly(ester) backbone in PEO-b-P(CL-PTX)

PEO-*b*-P(CL-PTX) micellar solutions (1 mg/mL) in 0.01 M phosphate buffer (pH 7.4) and 0.01 M citrate buffer (pH 5.0) were prepared, and incubated in a closed vial at 37 ^{0}C in a Julabo SW 22 shaking water bath (Germany). After 72 h, the micellar solution was freeze dried and dissolved in THF. Aliquot of 20 µL from this solution was injected into the GPC system as described above.

2.2.2.7 Release of PTX from polymeric micelles

Release of PTX from the PEO-*b*-P(CL-PTX) conjugate was determined in 0.01 M phosphate buffer (pH 7.4) and 0.01 M citrate buffer (pH 5.0) containing 2 M sodium salicylate at 37 ^{0}C [444, 445]. The experiment was initiated by the addition of free or micellar PTX solution to the buffer to give a final PTX concentration of 25µg/mL. At fixed time intervals, a sample of 1 mL was withdrawn, freeze dried and dissolved in acetonitrile, then 20 µL aliquot was injected into HPLC to determine the amount of released PTX.

The PTX loaded micelles were prepared at 20 µg/mL PTX concentration from PEO-*b*-PCL, PEO-*b*-PBCL and PEO-*b*-P(CL-PTX) block copolymers according to the previously mentioned method. Then, 10 mL of the micellar solutions were transferred into a dialysis bag (Spectrapor, MW cutoff 3,500 g mol^{-1}). The dialysis bags were placed into 500 mL of 0.01 M phosphate buffer (pH 7.4) or 0.01 M citrate buffer (pH 5.0). The release study was performed at 37 ^{0}C in a Julabo SW 22 shaking water bath (Germany). At selected time intervals the whole release media has been replaced with fresh one and aliquots of 200 µL were withdrawn from the inside of the dialysis bag for HPLC analysis. The amount of PTX released was calculated by subtracting the amount of PTX remained in the dialysis bag from the initially added PTX. The release profiles were compared using similarity factor, f_2, and the profiles were considered significantly different if $f_2 < 50$ [446] .

$$f_2 = 50 \text{ x } \log\left(\left[1 + \left(\frac{1}{n}\right)\sum_{j=1}^{n} |R_j - T_j|^2\right]^{-0.5} \text{ x } 100\right) \quad (4)$$

Where n is the sampling number, Rj and Tj are the percent released of the reference and test formulations at each time point j.

2.2.2.8 In vitro cytotoxicity of physically encapsulated and chemically conjugated PTX against MDA-MB-435 cancer cell

The cytotoxicity of PEO-*b*-P(CL-PTX), PEO-*b*-PCCL and PTX loaded in PEO-*b*-PCL, PEO-*b*-PBCL and PEO-*b*-P(CL-PTX) block copolymer micelles against human MDA-MB-435 cancer cells was investigated using 3-(4,5-dimethylthiazol-2-yl)-2,5-diphenyltetrazolium bromide MTT assay. Cells were grown in RPMI 1640 complete growth media supplemented with 10 % fetal bovine serum, 1% (w/v %) L-glutamine, 100 units/mL penicillin and 100 µg/mL streptomycin and maintained at 37 °C with 5% CO_2 in a tissue culture incubator. Growth medium RPMI containing 4000 cells was placed in each well in 96-well plate and incubated overnight to allow cell attachment. After 48 h (50% confluency), micellar solutions and free PTX at different concentrations were incubated with the cells for 24, 48 and 72 h. For conjugated PTX, a 96h incubation period was also tried. After this time, MTT solution (20 µL; 5mg/mL in sterile-filtered PBS) was added to each well and the plates were re-incubated for another 4 h. The formazan crystals were dissolved in DMSO, and the cell viability was determined by measuring the optical absorbance differences between 570 and 650 nm using a Power Wave X 340 microplate reader (Bio-Tek Instruments, Inc., USA). The mean and the standard deviation of cell viability for each treatment was determined, converted to the percentage of viable cells relative

to the control. The concentration required for 50% growth inhibition (IC_{50}) was estimated from the plot of the % viable cells versus log PTX concentration using Graphpad prism for Windows, Version 5.0 (Graphpad Software Inc.).

2.2.2.9 Statistical analysis

Values are presented as mean ± standard deviation (SD) of triple measurements. Statistical significance of difference was tested either using Students't-test or one-way ANOVA test (Sigma plot for windows, Version 11.0, Systat software Inc.). The level of significance was set at $\alpha = 0.05$.

2.3 Results

2.3.1 Preparation and characterization of PEO-b-P(CL-PTX) nano-conjugates

Synthetic scheme for the preparation of PEO-*b*-P(CL-PTX) through conjugation of PTX to PEO-*b*-PCCL in the presence of DCC and DMAP is illustrated in (**Scheme 2-1)**. The 2' and 7 hydroxyl groups of PTX are suitable sites for conjugation [447]. The reaction is more likely to occur at the 2' hydroxyl group since steric hindrances reduce the reactivity of the 7-hydroxyl group [448]. The successful conjugation of PTX to PEO-*b*-PCCL was confirmed by thin layer chromatography (TLC), where no spot for free PTX has been visualized in the TLC for the polymeric conjugate solution. Further evidence for conjugation was provided by comparing the ^{1}H NMR spectra of PEO-*b*-PCCL (**Figure 2-1**A) to that of PTX and PEO-*b*-P(CL-PTX) (**Figure 2-1**B & C, respectively), where characteristic peaks of PEO-*b*-PCCL and PTX were observed in the ^{1}H NMR spectrum of PEO-*b*-P(CL-PTX). Importantly, in the spectrum of PEO-*b*-P(CL-PTX) the disappearance of the resonance at $\delta = 4.8$ ppm (s, 1H) which is observed

in the spectrum of PTX and corresponds to the proton of the 2' -OH confirmed the completion of the conjugation reaction at this position (enlarged windows **Figure 2-1** B & C). Furthermore, the GPC chromatogram of the PEO-*b*-P(CL-PTX) exhibited a single peak, which is left shifted compared to that of PEO-*b*-PCCL indicating the increase of molecular weight due to PTX conjugation. Also, the HPLC chromatogram of PEO-*b*-P(CL-PTX) block copolymer did not show free PTX peak (data not shown). Together, the results of TLC, ^{1}H NMR, HPLC along with GPC provided strong evidence for the conjugation of PTX to the PEO-*b*-PCCL and efficient removal of free PTX after the purification process. The PTX content in the conjugate calculated from comparing the peak integration of the phenyl protons signal (δ=7.3-8.4 ppm) and ethylene protons (δ=3.7) of the poly(ethylene oxide) in the ^{1}H NMR (**Figure 2-1**C) was ~20% by weight. The substitution level of PTX on the polymer on molar basis was ~22% (moles PTX/moles monomer). This corresponds to 1.79 PTX molecules per PEO_{114}-*b*-$P(CL\text{-}PTX)_8$ chain on average.

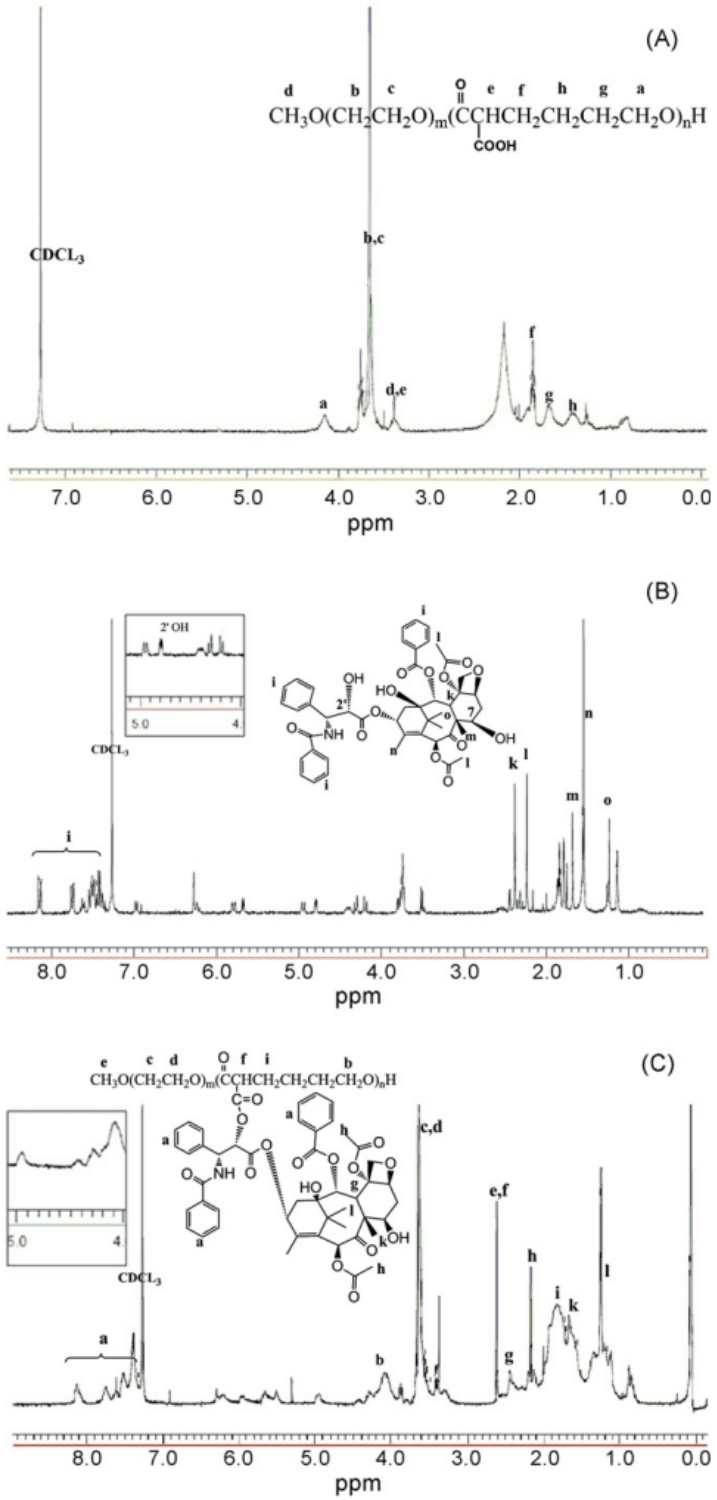

Figure 2-1:[1] H NMR spectra of (A) PEO-b-PCCL, (B) PTX and (C) PEO-b-P(CL-PTX) in $CDCl_3$.

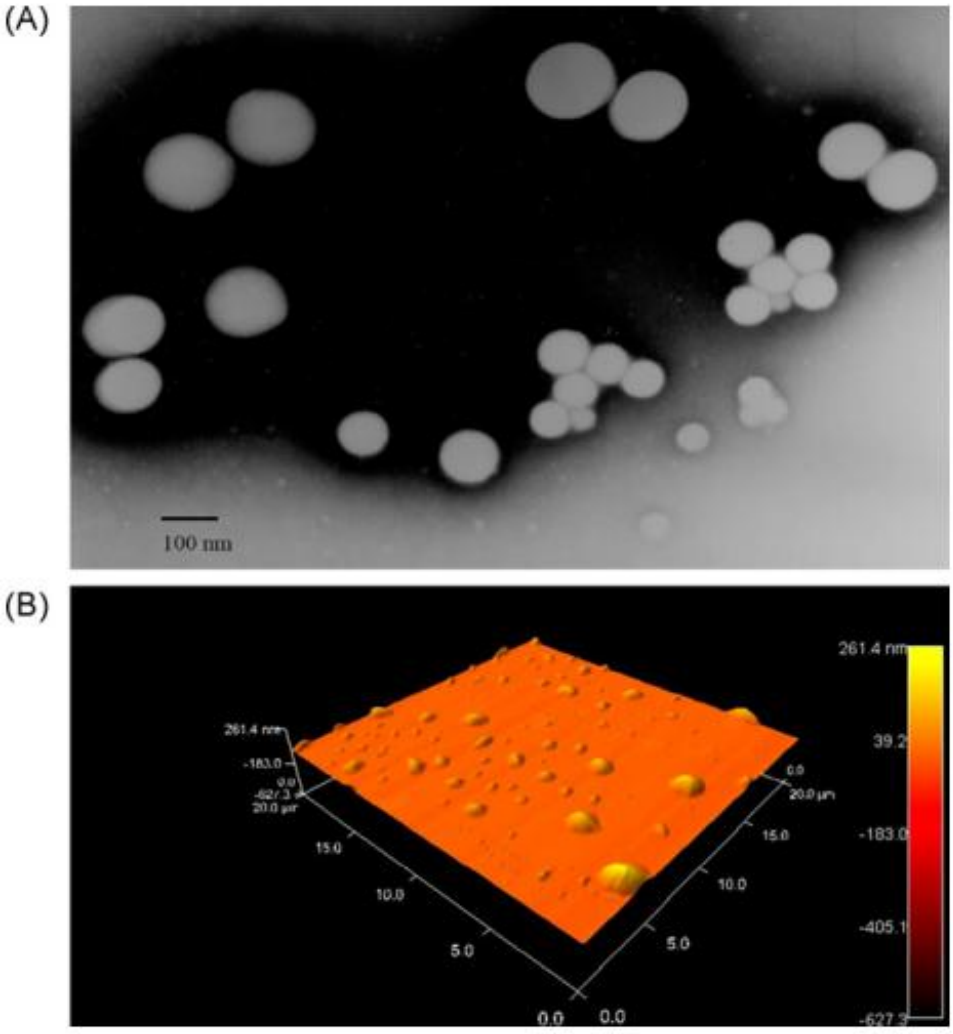

Figure 2-2: (A) TEM and (B) AFM images of empty PEO-b-P(CL-PTX) nanoparticles.

The results of characterization studies on prepared polymeric micelles are summarized in **Table 2-1**. The average hydrodynamic diameter of the unloaded PEO-*b*-P(CL-PTX) particles and their polydispersity were 123.0 ±0.6 nm and 0.14 as determined by DLS technique, respectively. This was larger than the size of PEO-*b*-PCL, PEO-*b*-PBCL, PEO-*b*-PCCL micelles formed through a similar assembly process. To visualize the shape of the formed particles TEM and AFM images were obtained (**Figure 2-2** A& B, respectively). From the TEM, spherical

particles were observed with an average diameter of (105.0±28.3 nm). AFM provided another evidence for the spherical morphology of particles with an average diameter of 87 nm. The CMC of PEO-*b*-P(CL-PTX) conjugate in aqueous media as estimated by pyrene partition study was 60.6 x 10^{-2} µM (**Table 2-1**). The PTX conjugated polymer showed significantly higher CMC in comparison to PEO-*b*-PCL ($P<0.05$, unpaired student's t- test) (**Table 2-1**). The higher CMC of PEO-*b*-P(CL-PTX) in comparison to that of PEO-*b*-PCL under this study, is attributed to the presence of free carboxyl groups and shorter chain length of the core forming block both leading to a decreased hydrophobicity of P(CL-PTX) in comparison to PCL. The lower CMC of PEO-*b*-P(CL-PTX) compared to that of PEO-*b*-PCCL is due to PTX conjugation on PCCL that makes the core forming block more hydrophobic.

Table 2-1 : Characteristics of prepared block copolymers and empty polymeric micelles (n=3)

Block copolymer[a]	M_n (g mol^{-1})[b]	Polydispersity (M_w/M_n)[c]	Average micellar size[d] ± SD (nm)	PDI[e]	CMC[f] ± SD (µM)	I_e/I_m ±SD[g]
PEO_{114}-*b*-PCL_{42}	9790	1.097	62.5 ± 1.80	0.24	0.18 ± 0.010[h]	*0.055* ± *0.007*[h]
PEO_{114}-*b*-$PBCL_{18}$	9470	1.175	64.3 ± 3.50	0.34	N/D	*N/D*
PEO_{114}-*b*-$PCCL_{12}$	6900	1.321	89.5 ± 3.60	0.44	N/D	*N/D*
PEO_{114}-*b*-P(CL-PTX)$_8$	7770	1.285	123.0 ± 0.60	0.14	0.61 ± *0.014* *	*0.173* ± *0.004* *

N/D not determined
[a] The number showed as subscript indicates the polymerization degree of each block determined from ^{1}H NMR spectroscopy.
[b] Number average molecular weight measured by ^{1}H NMR.
[c] Polydispersity = M_w/M_n measured by GPC
[d] Hydrodynamic diameter estimated by DLS.
[e] Polydispersity index estimated by DLS.
[f] Critical micelle concentration measured from the rise in the intensity ratio of peaks at 338 nm to the peaks at 333 nm in the fluorescence excitation spectra of pyrene plotted versus logarithm of polymer concentration.
[g] Intensity ratio (excimer/monomer) from emission spectrum of 1,3-(1,1′-dipyrenyl)propane in the presence of polymeric micelle.
[h] The data is reproduced from [436] for comparison.
* Statistically different from PEO-*b*-PCL ($P<0.001$).

Studying the core viscosity of both PEO-*b*-P(CL-PTX) and PEO-*b*-PCL using the fluorescence emission spectrum of 1,3-(1,1′-dipyrenyl)propane at a polymer concentration above CMC (1 mg/mL) revealed a lower core viscosity for PEO-*b*-P(CL-PTX) (**Table 2-1**). This is evidenced by the significantly higher I_e/I_m ratio for PEO-*b*-P(CL-PTX) (0.173) in comparison to PEO-*b*-PCL micelles (0.055) ($P<0.001$, unpaired student's t- test).

PEO-*b*-P(CL-PTX) micelles retained their average size and polydispersity over the 7 days incubation period ($P>0.05$) indicating good stability of the plain PEO-*b*-P(CL-PTX) particles at room temperature (**Figure 2-3**).

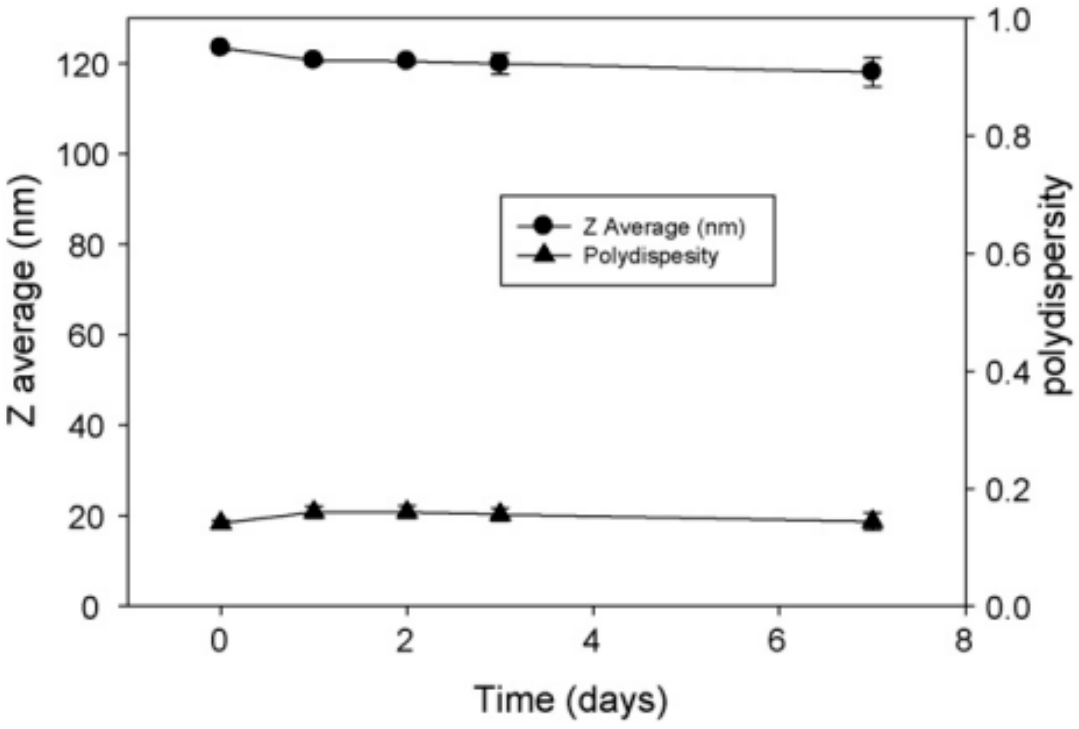

Figure 2-3: The average diameter and polydispersity of PEO-b-P(CL-PTX) nanoparticles during storage at room temperature as measured by dynamic light scattering (DLS).

As shown in **Figure 2-4 A**, the release of intact PTX from the polymeric conjugate was very slow within 3 days at both pHs. After 72 h incubation, only

6.7% of total PTX were detected in media as intact PTX at pH 5.0 compared to 5.0 % at PH 7.4. The lower level of free PTX at pH 7.4 may be attributed to the lower stability of PTX at this pH rather than a slower drug release from the conjugate. Similar reduction in the level of solubilized PTX has been seen at this pH for free drug. It has been reported that free PTX is susceptible to mild basic hydrolysis [449].

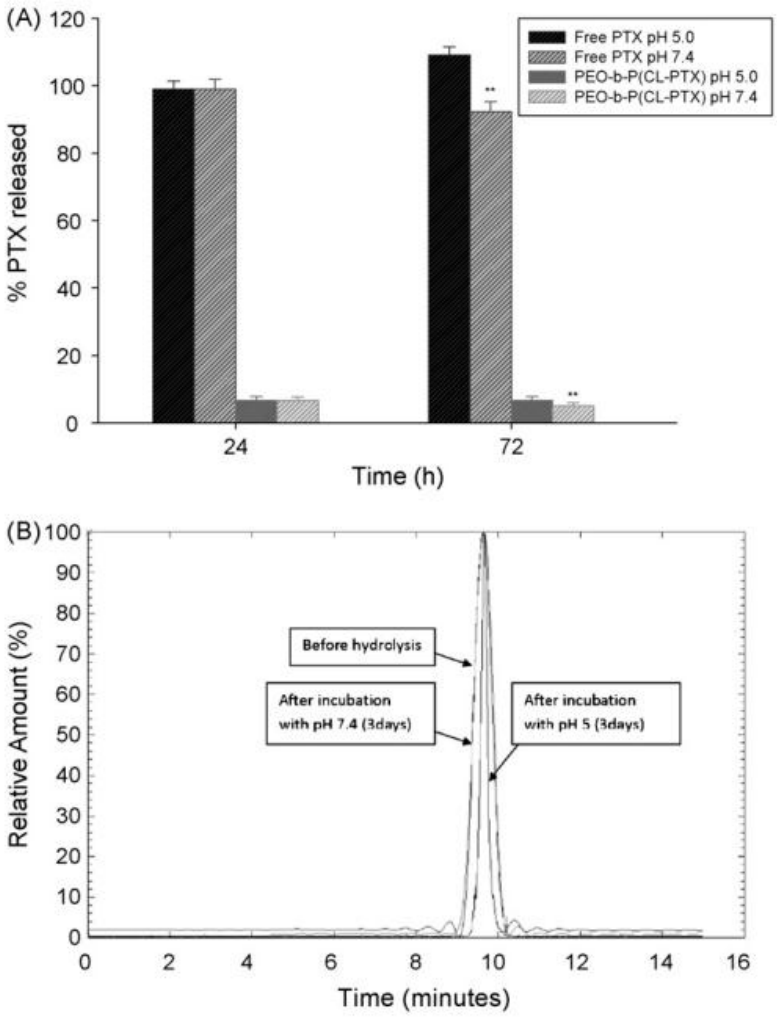

Figure 2-4: (A) Percentage of intact PTX regenerated from PEO-b-P(CL-PTX) in buffer solutions (pH 7.4 and pH 5) containing 2 M sodium salicylate at 37 ^{0}C in comparison to free PTX. (B) Gel permeation chromatogram of PEO-b-P(CL-PTX) before and after incubation at pHs 7.4 and 5 for 72 h. Significantly different from pH 5 (** P < 0.05).

Figure 2-4 B shows the GPC chromatogram of chemically conjugated PTX after incubation at pH 7.4 and 5.0 for 72 h. No significant change in the elution time of polymer-PTX conjugate after incubation at both pHs was seen indicating no change in its number average molecular weight. However, a change in its polydispersity upon incubation at pH 5.0 was observed implicating a decrease in the weight average molecular weight of the polymer-drug conjugate at this pH.

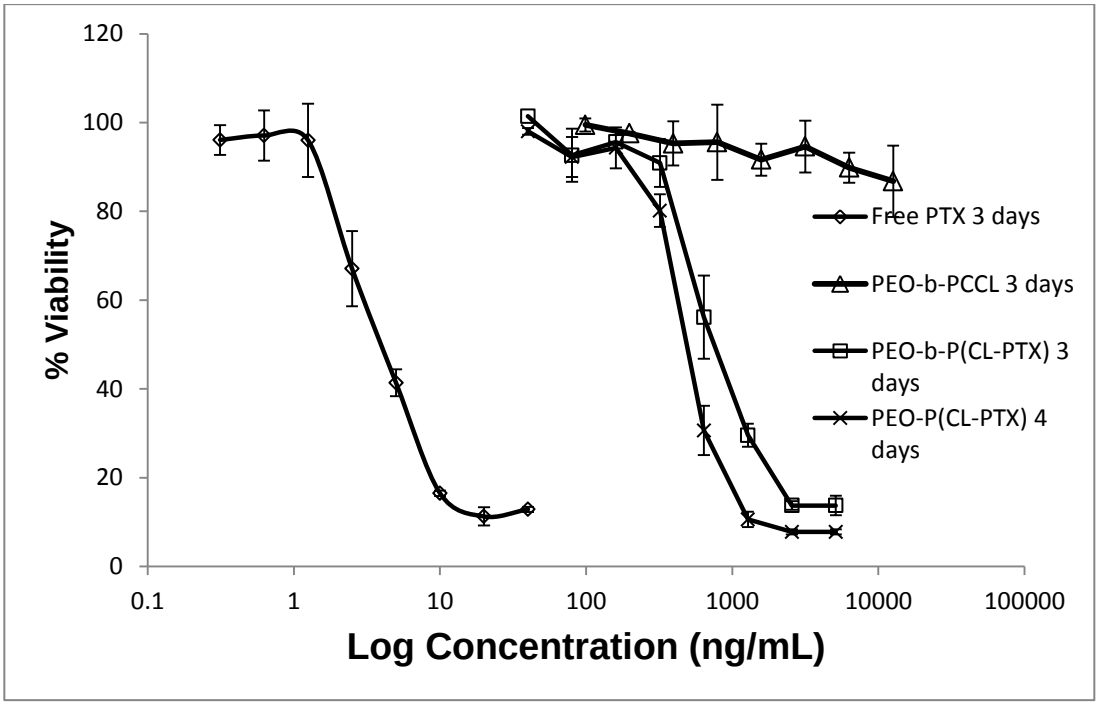

Figure 2-5: In vitro cytotoxicity of PEO-b-P(CL-PTX), PEO-b-PCCL block copolymers and free PTX against MDA-435 cells at defined incubation times.

The cytotoxicity of free PTX, PEO-*b*-P(CL-PTX), PEO-*b*-PCCL against human MDA-MB-435 cancer cells using MTT assay is shown in **Figure 2-5**. A change in cell viability with a change in the concentration of both free PTX and the PTX polymeric conjugate was observed. The conjugate showed lower cytotoxicity than free PTX (IC_{50} of 680 ng/mL for conjugate versus 3.5 ng/mL for

free PTX) after 72 h incubation. The polymer without conjugated PTX, i.e., PEO-*b*-PCCL, did not show noticeable cytotoxicity at concentrations equivalent to what used in this study. When the incubation time increased to 96h, the cytotoxicity of PTX polymeric conjugate increased (i.e. the IC_{50} decreased significantly from 680 to 475 ng/mL) ($P<0.05$, unpaired student's t- test).

2.3.2 Preparation and characterization of polymeric micelles containing physically encapsulated PTX

The capability of PEO-*b*-PCL, PEO-*b*-PBCL, and PEO-*b*-P(CL-PTX) micelles for the solubilization of PTX in aqueous media was investigated at different drug to polymer weight ratios (**Figure 2-6**). Except for PEO-*b*-P(CL-PTX), all the prepared solutions were clear, up to a certain ratio, after which precipitation was evident by visual inspection. The amount of the drug solubilized increased to a maximum concentration for PEO-*b*-PCL and PEO-*b*-PBCL as the drug to polymer ratio was raised from 2 to 5 and 2 to 2.5 wt%, respectively, above which solubility decreased. This ratio coincided with the formation of precipitates. In contrast, PTX solubilization by PEO-*b*-P(CL-PTX) kept increasing as the drug to polymer ratio was raised from 1.34 to 6.67 wt % (the latter was the maximum PTX/polymer wt % examined). Overall, a maximum PTX solubility of 44.5, 32.7, 62.1 µg/mL has been achieved with PEO-*b*-PCL, PEO-*b*-PBCL and PEO-*b*-P(CL-PTX) block copolymers, respectively, at polymer concentrations under study. The calculated loading content of PTX (mole of

PTX/mole of polymer) in PEO-*b*-PCL micelles was 14.5. Compared to PEO-*b*-PCL, PTX loading content was increased in PEO-*b*-P(CL-PTX) micelles (by 1.4 folds), but this value decreased in PEO-*b*-PBCL (**Table 2-2**). PTX loading did not cause any significant change in the average diameter of PEO-*b*-PCL and PEO-*b*-PBCL ($P>0.05$, unpaired student's t-test) while PTX loading led to a significant increase in the average diameter of PEO-*b*-P(CL-PTX) particles ($P<0.01$, unpaired student's t-test) (**Table 2-2**). The PTX loaded PEO-b-PCL or PEO-b-PBCL micelles did not show any secondary aggregation. However, physical encapsulation of PTX into PEO-b-P(CL-PTX) resulted in the production of particles which showed signs of secondary aggregation.

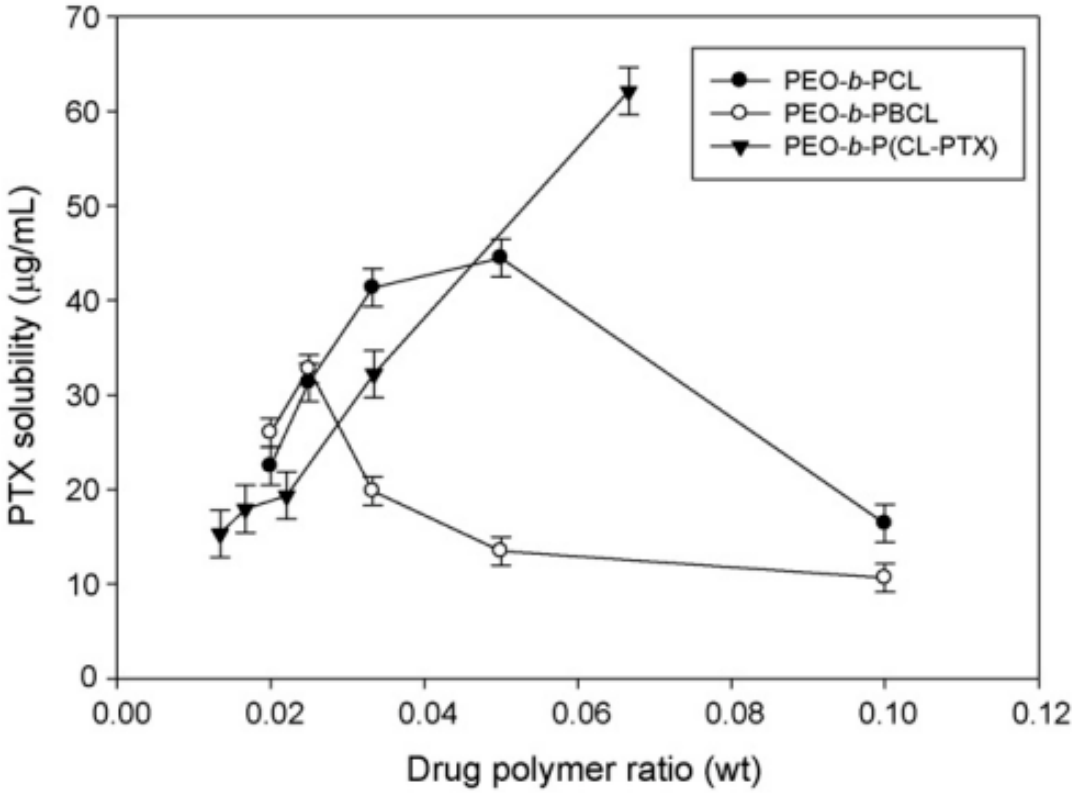

Figure 2-6: Solubilization of PTX by block copolymers at different PTX: block copolymers weight ratios.

The results of assessments on the *in vitro* release of PTX from three different polymeric nano-carriers and free PTX in phosphate (pH 7.4, 0.01 M) and citrate buffer (pH 5.0, 0.01 M) at 37 ºC is illustrated in **Figure 2-7**A & B, respectively. Free PTX was released from the dialysis bag at a rapid rate, which means that the transfer of PTX through dialysis membrane to buffer solution is not a restricting factor and the release of PTX from the micellar formulation is the rate limiting step in this process. Comparison of the release profiles of free PTX revealed similar release profiles at pH 7.4 and 5.0 (f_2 >50). The release of PTX from polymeric micelles at both pHs was strongly affected by the micellar core composition, with PEO-*b*-PCL showing the minimum rate of drug release at both

pHs. At pH 5.0, changing the core composition significantly affected the % of PTX released after 6 h incubation (one-way ANOVA, $P < 0.05$). At 6 h incubation at this pH, 6.80, 20.2 and 15.6% of physically loaded PTX was released from PCL, PBCL and P(CL-PTX) containing particles, respectively. Before 6h, release rates were similar between different carriers. At pH 7.4; however, differences between release of PTX from nano-carriers was only obvious after 24 h incubation (one-way ANOVA, $P < 0.05$). At pH 7.4 at 24 h incubation, 21.1, 38.6 and 62.9% of physically loaded PTX were released from PCL, PBCL and P(CL-PTX) containing particles, respectively. At the same time point, 12.1, 31.1 and 48.5 % of encapsulated PTX were released from PEO-*b*-PCL, PEO-*b*-PBCL and PEO-*b*-P(CL-PTX) particles at pH 5.0, respectively. Similar to what has been observed for free PTX, comparing the release profiles of physically loaded PTX from polymeric micelles at different pHs using the similarity factor (f_2) showed that the release of PTX from different nano-carriers is not affected by pH ($f_2 > 50$).

Table 2-2: Characteristics of PTX loaded copolymer micelles (n=3)

Block copolymer micelles	PTX loading content (%) ± SD		Encapsulation efficiency% ± SD	Average diameter ± SD	PDI[a]	PTX release after 72 h (%)[b]	
	PTX/polymer (mole%)	PTX/polymer (w%)				pH 5.0	pH 7.4
PEO_{114}-*b*-PCL_{42}	14.5 ± 1.0	1.26 ± 0.09	24.7% ± 3.10	69.2 ± 15.98	0.51	50.6±4.98	47.6 ±8.68
PEO_{114}-*b*-$PBCL_{18}$	10.7 ± 3.2*	0.96 ±0.29 *	36.4% ± 1.20*	61.0 ± 1.2	0.45	58.8±1.13*	57.4 ±6.71
PEO_{114}-*b*-$P(CL\text{-}PTX)_8$	20.2 ± 2.8 [c]*	2.22 ± 0.31[c]*	34.0% ± 3.40*	159.3 ± 8.7[d*]	0.54	79.3±3.23*	81.8 ±3.81 *

[a] Polydispesity index of micellar size distribution.
[b] Release study was performed in citrate buffer (pH 5.0) and in phosphate buffer (pH 7.4).
[c] The level is estimated for physically encapsulated PTX only.
[d] Secondary aggregation was evident.
* Significantly different from PEO-*b*-PCL ($P<0.05$)

The results of *in vitro* cytotoxicity of physically loaded PTX in PEO-*b*-PCL, PEO-*b*-PBCL and PEO-*b*-P(CL-PTX) after 24 and 72h of incubation are shown in **Figure 2-8**. At all studied incubation times, the physically loaded PTX formulations had similar cytotoxicity against MDA-435 cancer cells to that of free PTX, reflected by similar IC_{50} values ($P<0.05$, one-way ANOVA test). This observation is attributed to the low equivalent polymer concentrations, which were below the CMC values, under conditions of the cytotoxicity study and rapid release of free PTX from formulations below CMC.

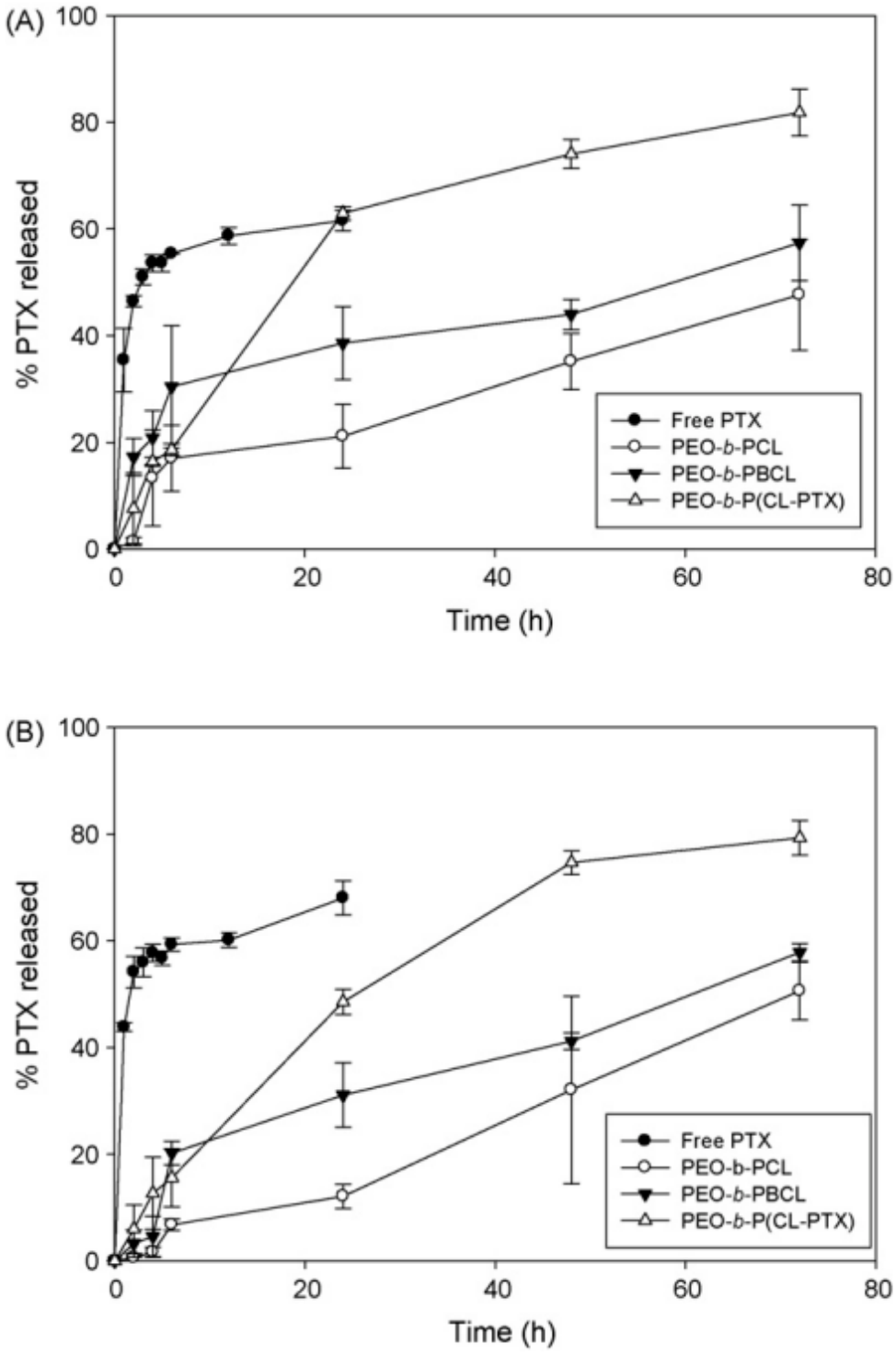

Figure 2-7: In vitro release profile of physically loaded PTX from different micellar formulations at (A) pH 7.4 and (B) pH 5.0 at 37 ◦C. Each point represents mean ± SD (n = 3).

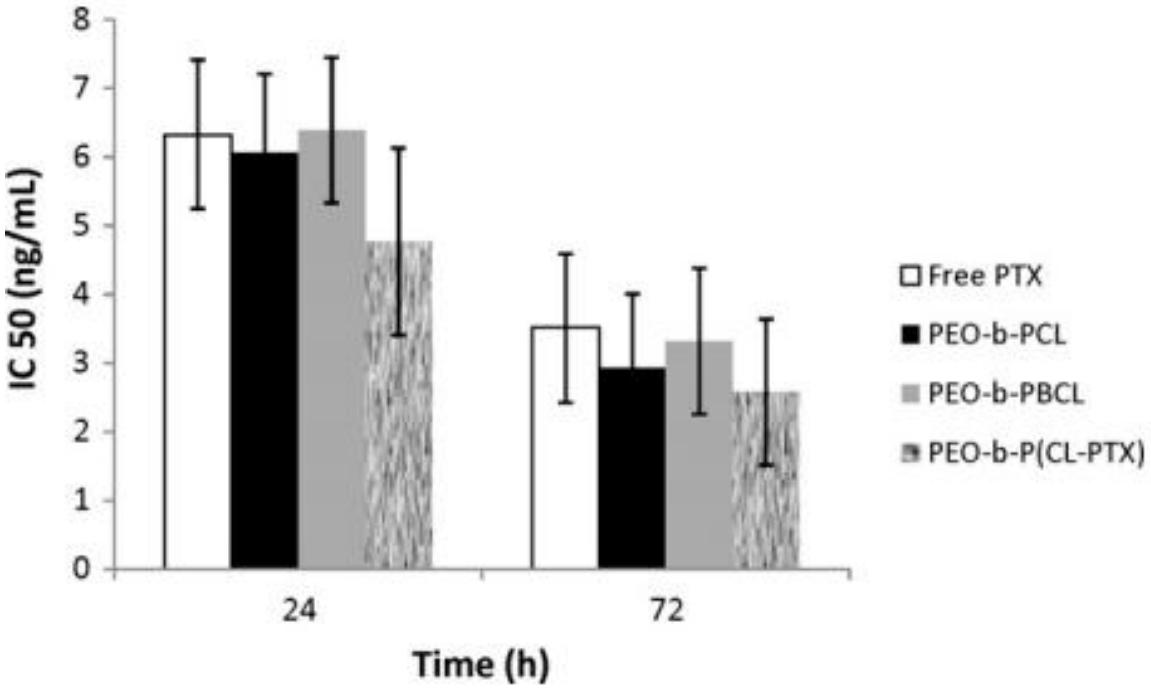

Figure 2-8: In vitro cytotoxicity of free and physically loaded PTX micellar formulations against MDA-435 after 24 h and 72 h of incubation. Each point represent mean IC_{50} ± SE (n = 3).

2.4 Discussion

The long term objective of this research is to develop a biodegradable and biocompatible polymeric carrier in nanometer size range for efficient solubilization and tumor targeted delivery of PTX. An optimized PTX delivery system is expected to act as an efficient and safe solubilizing agent for PTX, be able to prevent early elimination of drug from systemic circulation, reduce PTX exposure and toxicity in non-target sites, but enhance the access of PTX to its cellular and molecular targets. To fulfill these characteristics, two PTX polymeric conjugates, through esterification of PTX with PGA (in Xyotax ^{TM}) or attachments of PTX to hydroxypropyl methacrylamide polymer through peptide linkers (in PNU166945), have been developed and entered clinical trials. PNU166945 have shown poor pharmacokinetics due to premature drug release as

a result of the instability of ester linkage between PTX and polymer in phase I clinical trials. In contrast, Xyotax ^{TM} has shown low drug release *in vitro* (< 14% after 24 h incubation in buffered saline and plasma) and reduced PTX side effects *in vivo* [347]. This formulation showed better efficacy compared to that of Taxol® when administered at its maximum tolerable dose which was significantly higher than that of Taxol®, in preclinical and clinical trials.

The PEO-*b*-P(CL-PTX) nano-conjugate developed here is expected to provide several advantages over clinical PTX polymer conjugates. First, the self-association of PEO-*b*-P(CL-PTX) to nanoparticles is expected to stabilize the conjugated PTX within its carrier. Because unlike previous formulations, the ester bond conjugating PTX to polymeric backbone is hidden in the hydrophobic domain of nanoparticles and is not easily accessible for cleavage. Furthermore, the hydrophobicity of PCL structure is anticipated to cause further delay in the dissociation of carrier and/or release of PTX from PEO-*b*-P(CL-PTX) nano-conjugates in comparison to previous clinical PTX polymer conjugates. Owing to the larger size of particles compared to single polymer-PTX chains, the elimination of PEO-*b*-P(CL-PTX) nanoparticles through glomerular filtration will be postponed. Meanwhile, the "stealth" properties induced by the PEO shell is expected to prevent opsonisation and early removal of PEO-*b*-P(CL-PTX) carrier by mononuclear phagocytic system. To achieve similar benefits, direct conjugation of PTX to PEO (at different molecular weights) producing PEO-PTX conjugates has also been pursued previously [450, 451]. Overall, compared to clinical conjugates of PTX, a better pharmacokinetic profile for PEO-*b*-P(CL-

PTX) leading to improved tumor accumulation is anticipated. On the other hand, unlike poly(methacrylamide) and PGA, which are the building blocks of PNU166945 and Xyotax ^{TM}, respectively, the PCL backbone is readily degradable in extra-cellular or endosomal environment. Degradability of the polymer backbone in addition to the acid liable linkages between PTX and PCL was hypothesized to provide sufficient release of PTX from the polymeric conjugate in the tumor micro-environment as well as endosomes of tumor cells that have acidic pHs and contain esterase.

In our observations, the PEO-b-P(CL-PTX) has illustrated a high tendency for self-assembly reflected by a relatively low CMC (**Table 2-1**). Meanwhile, the introduction of PTX substituent on the PCL chain lowered the viscosity of the hydrophobic domains in PEO-b-P(CL-PTX) particles (**Table 2-1**), possibly due to the increased space between chain entanglements and reduced packing of the hydrophobic chains leading to more freedom of movement in the micellar core. The presence of bulky PTX substituent in the inner core also resulted in the formation of micelles with a larger average diameter (**Table 2-2**). Similar effect has been observed in PEO-b-poly(α-cholesteryl carboxylate ε-caprolactone) micelles [452]. Despite this, the size of PEO-b-P(CL-PTX) particles was still in the appropriate range for tumor targeting by EPR effect (< 150 nm)

Table 2-2). Besides, the particles did not show any sign of aggregation or dissociation during storage at room temperature (**Figure 2-3**). The average micelle size measured by DLS technique was larger than that obtained by TEM or AFM (**Figure 2-2**). This observation has been attributed to the acquirement of the TEM, AFM images under a dry state as opposed to DLS that measures particle size in a hydrated state in aqueous solutions [453, 454]. Besides, in TEM and AFM only the dense core of the micelle is visualized without any contribution from the hydrated hydrophilic PEO shell. The difference between AFM and TEM measurements may be attributed to the difference in the interfacial interaction between the nanoparticles and different surfaces and/or different concentration of polymeric nanoparticles used for the two methods (1 mg/mL for TEM vs. 0.1 mg/mL for AFM).

The results of our in vitro studies on PTX release revealed the efficient protection of PTX by its PEO-b-P(CL-PTX) nano-conjugate preventing the premature release of PTX and its stabilization within the nano-carrier in physiological conditions mimicking that of systemic circulation (pH 7.4 and temperature of 37 °C) **(Figure 2-4**A). Despite degradability of the PCL backbone in acidic pHs mimicking that of tumor tissue or endosomal pH (pH 5.0) (**Figure 2-4**B), release of free PTX from this carrier was found to be too low (**Figure 2-4**A) to provide efficient cytotoxicity in cancer cells even upon prolonged exposure **(Figure 2-5**). The latter was characterized by a high IC_{50} for PEO-b-P(CL-PTX) in comparison to free PTX at 72 h incubation (**Figure 5**). Although IC_{50} of polymer-PTX conjugate dropped significantly after 96 h incubation, it was still significantly

higher than that of free PTX. The low extent of PTX release from the PEO-b-P(CL-PTX) nano-conjugate is perhaps due to high hydrophobicity of the micellar core, which retards the diffusion of water into the core and subsequent cleavage of the hydrolysable ester bonds between polymer and PTX. The slow uptake of PEO-b-P(CL-PTX) nano-conjugate by cancer cells because of the protective effect of PEO, may contribute to the reduced and time dependent cytotoxicity of PEO-b-P(CL-PTX) nano-conjugate, as well. In this regard, further optimization of this carrier, which is currently underway in our research group, will focus on the modification of the surface PEO-b-P(CL-PTX) with cancer targeting ligands to improve the cancer cell selective uptake, release and cytotoxic effects of this formulation. Nevertheless, final verdict on the promise of this formulation for successful PTX delivery in cancer can only be made after completion of in vivo pharmacokinetics, toxicity and efficacy studies. In fact, Xyotax ™ has also shown low PTX release in vitro but was found to enhance the therapeutic index of PTX in vivo. This is because the in vitro condition of the experiment does not provide a precise mimic of the in vivo situation where enhanced accumulation of the carriers in tumor site as a result of EPR effect and the presence of additional physiological degradation mechanisms such as metabolizing enzymes, may play a role in modifying the therapeutic index of PTX by its nano-formulation. Such studies are currently under way.

In an effort to find the best structure for the delivery of PTX, PEO-*b*-PCL micelles as well as micelles with modified PCL cores, i.e., PEO-*b*-PBCL and PEO-*b*-P(CL-PTX), were used to physically encapsulate PTX. For PEO-*b*-PCL

and PEO-*b*-PBCL block copolymers, the amount of drug solubilized increased up to a maximum concentration, above which drug as well as polymer precipitated (**Figure 2-6**). The solubility profile did not take an exponential curve with a plateau after certain drug: polymer ratio possibly because of polymer/drug precipitation after the point of maximum drug solubility. Micelles containing chemically conjugated PTX demonstrated the highest capacity for physical entrapment of free PTX among structures under study. This observation was similar to observation by Yokoyama et al. [455] who reported a significant increase in DOX loading by micelles of PEO-b-poly(aspartic acid-DOX). The low solubility of PTX in PCL block copolymer has been ascribed to the low compatibility between PTX and PCL, as determined by the calculated Flory Huggin interaction parameter [456]. Micelles of PEO-*b*-PBCL even showed lower PTX encapsulation to that obtained by PEO-*b*-PCL micelles, which may be ascribed to the higher rigidity of the core in PEO-*b*-PBCL micelles.

In contrast to chemically conjugated PTX, more rapid loss of physically loaded PTX from its carriers was detected during the release study. The release profile of free and physically encapsulated PTX was not affected by the pH of the release medium. In general, the release of physically encapsulated PTX from its carrier is dependent on both the rate of drug diffusion from micellar core and core degradation; whereas for conjugated PTX, core degradation plays a major role. The nature of core structure significantly affected the rate of PTX release from its carriers. The high rate of PTX release from P(CL-PTX) core in comparison to

PCL core may be a reflection of the lower core rigidity for PEO-*b*-P(CL-PTX) micelles.

A comparable cytotoxicity for the physically loaded and free PTX against MDA-MB-435 cells was observed after 24 h incubation. At the reported IC_{50} values for physically encapsulated PTX, the block copolymers' concentrations were below CMC. Therefore, PTX is likely present in its free form. The similar IC_{50} values, only reflects dissociation of all micellar formulations under study within 24-72 h rather than a similarity in PTX release and cell penetration between encapsulated PTX in different micellar structures. Pharmacokinetics studies on these formulations are underway to define the stability of formulations and their potential of targeted PTX delivery in a biological system.

2.5 Conclusions

In this study, a novel self-associating PTX polymeric conjugate has been successfully prepared with a high loading of PTX. This polymeric conjugate showed sign of PCL chain cleavage only at pH 5.0 (not pH of 7.4). However, cleavage of the ester bond between PTX and PCL leading to the release of intact PTX was very slow and insufficient at both pHs of 7.4 and 5.0. The *in vitro* cytotoxicity of this polymeric conjugate was lower than that of free PTX even after 4 days of incubation with MDA-MB-435 human cancer cells. From the polymeric micellar systems used for the physical encapsulation of PTX, PEO-*b*-P(CL-PTX) micelles significantly improved the solubilization of PTX, while maximum control over the rate of PTX release was achieved with PEO-*b*-PCL micelles. The results point to the potential of self-associating PEO-*b*-PCL based conjugates and containers as nano-carriers for the solubilization and controlled

delivery of PTX. *In vivo* studies are needed to determine whether these formulations can in fact improve the therapeutic efficacy of PTX in cancer models. In the next chapter, we will develop actively targeted nanocarriers of PTX based on both PEO-b-PCL and PEO-b-PBCL block copolymers as a way to improve the selectivity of PTX toward the breast cancer tumours.

Chapter 3
Modification of polymeric micelles with cancer-specific peptide ligands for active targeting of paclitaxel[18]

[18] A version of this chapter has been previously published in: Shahin M, Ahmed A, Kaur K, Lavasanifar A. Decoration of polymeric micelles with cancer-specific peptide ligands for active targeting of paclitaxel. Biomaterials, 2011, 32 (22): p. 5123-33

3.1 Introduction

In an attempt to provide selective targeting to cancer cells, we have chosen to develop p160 decorated poly(ethylene oxide)-*b*-poly(ε-caprolactone) (PEO-*b*-PCL) or poly(ethylene oxide)-*b*-poly(α-benzyl carboxylate-ε-caprolactone) (PEO-*b*-PBCL)polymeric micellar carriers and compare the efficiency of those to micelles decorated with c(RGDfK) peptide in cancer cell binding and uptake, as well as selective PTX delivery. Previously, we developed a physically loaded PTX nano-container using PEO-*b*-PCL or PEO-*b*-PBCL which showed *in vitro* cytotoxicity close to free PTX [457]. Here, we decorated the shell of these polymeric micelles with cancer-specific peptides as means to improve the cytotoxicity and/or specificity of loaded PTX for cancer cells.

3.2 Materials and methods

3.2.1 Materials

Wang resin (1.1mmol/g), benzotriazol-1-yloxy-tris(dimethylamino)-phosphonium hexafluorophosphate (BOP), 1-hydroxybenzotriazole (HOBt), 2-chlorotrityl chloride resin (1.4 mmol/g) and the Fmoc-amino acids were purchased from NovaBiochem (San Diego, CA, USA). The side chains of the amino acids used in the synthesis were protected as follows: Boc (Lys, Trp), PbF (Arg), t-Bu (Thr), OtBut (Asp, Glu), and Trt (Asn, Cys, Gln, His). Dichloromethane (DCM), methanol, isopropyl alcohol (IPA), acetonitrile (ACN), diethyl ether, pyridine, and piperidine were purchased from Caledon Laboratories Ltd. (Canada). N,N-Disopropylcarbodiimide (DIC), DMF, N-methyl morpholine (NMM), N-methyl-2-pyrrolidone (NMP), [3-(4,5-dimethylthiazol-2-yl)-2,5-diphenyl] tetrazolium

bromide (MTT), tetrahydrofuran (THF), dichlorobenzoyl chloride (DCB), trifluoroacetic acid (TFA), triisopropyl silane (TIPS), ethylene oxide, diisopropyl amine (99%), benzyl chloroformate (tech. 95%), sodium (in Kerosin), butyl lithium (Bu-Li) in hexane (2.5 M Solution), 3,3 diethoxy 1-propanol (DEP) , naphthalene and potassium were purchased from Sigma-Aldrich (St. Louis, MO, USA). Paclitaxel (purity> 99.5) was purchased from LC Laboratories (MA, USA). ε-caprolactone was purchased from Lancaster Synthesis (MA, USA). Stannous octoate was purchased from MP Biomedical Inc. (OH, USA). The fluorescent probe DiI was purchased from Molecular Probes (Carlsbad, CA, USA). p160 and c(RGDfK) peptides are kindly provided by Dr. K.Kaur.

3.2.2 Cell lines

All cell lines were cultivated at 37 ºC in a 5% CO_2 incubator. The human cancer cell line MDA-MB-435 was received as a gift from the laboratory of Dr. R. Clarke (Georgetown University, USA). These cells were cultured in RPMI 1640 with 1% L-glutamine, and 10% FCS (Invitrogen, Karlsruhe, Germany), 100 IU/mL penicillin, and 100 IU/mL streptomycin. The human umbilical vein endothelial cells (HUVEC) was a kind gift from the laboratory of Dr. Sandra Davidge, University of Alberta. These cells were cultivated using Endothelial Cell Growth medium EBM-2 (Lonza, USA) supplemented with EGM-2 Single Quots growth supplements and 20% FCS (Invitrogen, USA). The human non-tumorigenic epithelial cell line MCF 10A was obtained from ATCC (Manassas, USA) and cultured in MEGM media kit (Lonza, USA) supplemented with 100 ng/mL cholera toxin (Sigma chemicals, USA).

3.2.3 Synthesis of block copolymers with functionalized PEO

Synthesis of acetal-PEO-*b*-PCL and acetal-PEO-*b*-PBCL block copolymers has been described in our previous publications in detail [458]. Briefly, in a triple neck flask rounded bottom flask, 0.15 mL (1 mmol) of initiator 3,3 diethoxy1-propanol (DEP) and 3.5 mL (1 mmol) of catalyst potassium naphthalene were added to 20 mL of dry THF. After 10 minutes of stirring, 5.7 mL (114 mmol) of condensed ethylene oxide was added. The reaction was left for 2 days till a light brown highly viscous solution was formed. At this point, the reaction was stopped by the addition of 1-2 mL of acidified ethanol to neutralize excess potassium, and the polymer precipitated by the addition of the reaction mixture to a large amount of cold diethyl ether. Acetal-PEO was then centrifuged for 15 minutes at 1800 × g. For the synthesis of acetal-PEO-*b*-PBCL, acetal-PEO (0.5g), α-benzylcarboxylate-ε-caprolactone (0.5 g) and stannous octoate (0.002 eq. of monomer, 35 mg) were added to a 10 mL previously flamed ampoule, nitrogen purged and sealed under vacuum. The polymerization reaction was allowed to proceed for 4 h at 140º C in an oven [459]. The reaction was terminated by cooling the product to room temperature. PEO-*b*-PCL is prepared in a similar way but using the non-functionalized monomer (ε-caprolactone) (0.5 g).

3.2.4 Synthesis of peptides and preparation of peptide decorated micelles

The p160 peptide was obtained by solid phase peptide synthesis using Fmoc coupling protocol. The peptide synthesis was performed manually in a polyethylene peptide synthesis vessel with a frit at the bottom and screw cap with a septum at the top for the addition of reagents. Solvents and soluble reagents

were removed by suction. Washing between deprotection and coupling was carried out with DMF (4 x 1min), DCM (4 x 1min) and IPA (4 X 1min). The Fmoc group was removed by treatment with 20% piperidine/DMF (2 x 7min). In a solid phase reactor, Wang resin (90 mg, 0.1 mmol) was weighed and washed with DMF, DCM and IPA and swelled for 1 h in DCM. Next, the first amino acid, N- α-Fmoc-Leu (234 mg, 4 eq.), DCB (57 μL, 4 eq.), pyridine (54 μL, 6 eq.) was activated for 5 min and then added to the swelled resin. The reaction was mixed for overnight. The Fmoc protecting group of the first amino acid was removed with a solution of piperidine–DMF (1:4) and the linear peptide was assembled using standard Fmoc procedures by consecutive addition of the protected amino acid (2 eq.), BOP (86 mg, 1.95 eq.), HOBt (27 mg, 2 eq.), and NMM (50 uL, 4.5 eq.) in DMF for 1 to 2 h. After addition of the last amino acid, the N-terminal Fmoc group was then removed with 20% piperidine in DMF (2 X 10 min). The resin was washed using DMF and IPA. The peptide was cleaved from the resin by TFA-TIPS-H_2O (95:2.5:2.5, 7.5 mL). The resulting mixture was agitated for 2 h before washing with TFA:CH_2Cl_2 (1:9, 7 mL). The acid washings were concentrated to approximately 1 mL and precipitated by cooled diethyl ether. The precipitate was collected by centrifugation and washed with ice-cooled dry diethyl ether (4× 30 mL). The precipitate was isolated and dried in a stream of nitrogen and freeze dried. The crude product was purified by preparative HPLC. The mass of the products was confirmed by MALDI-TOF mass spectrometry.

The cyclized RGD peptide was synthesized using similar procedures. Briefly, a solution of Fmoc-Asp-OAll (119 mg, 3 eq.) and DIPEA (210 μL, 12

eq.) in dry CH_2Cl_2 were added to 2-chlorotrityl resin (0.1 mmol, 70 mg). The resin was capped, and the Fmoc protecting group was removed, and the linear pentapeptide was assembled using standard Fmoc procedures. After addition of the last amino acid, the C-terminal allyl ester was removed by treatment with $Pd(PPh_3)_4$ (0.16 eq.) and PhSiH3 (16 eq.) in DCM/DMF for 2 h. The reaction mixture was washed with diethyldithiocarbamic acid sodium salt. The N-terminal Fmoc group was then removed with piperidine–DMF (1:4) before addition of BOP (1.95 eq., 86 mg), HOBt (27 mg, 2 eq.), and NMM (50 uL, 4.5 eq.) in DMF for 2 h to allow on-resin cyclization and give cyclized peptide. It was treated with TFA:CH_2Cl_2 (1:1, 8 mL) for 2 h and washed with TFA:CH_2Cl_2 (1:9). The acid washings were concentrated to approximately 1 mL and precipitated by cooled diethyl ether to obtain c(RGDfK) in 70% yield and more than 95% purity as confirmed by HPLC and mass spectrometry.

The p160 or c(RGDfK) peptide was conjugated to the micellar surface through reaction with the functional acetal groups on the micellar shell as reported previously [458]. Briefly, acetal-PEO-*b*-PCL or acetal-PEO-*b*-PBCL was assembled into polymeric micelles by dissolving (30 mg) of the polymer in DMSO (1 mL). This solution was added to doubly distilled water (6 mL) in a drop-wise manner under moderate stirring for 1 day, then the organic solvent removed by dialysis against double distilled water for another day (Spectrapor, MW cut-off 3,500). The micellar solution was then centrifuged 11,600 × g for 5 min to remove any free unimers. The aqueous solution of polymeric micelles was then acidified to pH 2 with 0.5 M HCl and stirred for 2 h at room temperature to

produce aldehyde polymeric micelles. The resulting solution was then neutralized with 0.5 M NaOH. For conjugation of the peptide, the pH of the micellar solution was adjusted by the addition of an appropriate volume of concentrated sodium phosphate buffer solution (pH 7.4, 0.1 M) to obtain a 4 mg/mL polymer concentration. An aqueous solution of the peptide (1% DMSO for p160 peptide) was added and incubated with the aldehyde bearing micelles at room temperature for 2 h under moderate stirring. Subsequently, $NaBH_3CN$ (10 eq.) was added to the polymer to reduce the Schiff's base. After 96 hours of reaction, the unreacted peptide and reducing agent were removed by extensive dialysis against distilled water. The final product was obtained by freeze drying of the resulting aqueous solution. The conjugation efficiency of the peptide to polymeric micelle was assessed by gradient reversed phase HPLC method. A μ Bondpack (Waters Corp., United States) C_{18} analytical column (10 μm 3.9 X 300 mm) was used. Gradient elution was performed at a flow rate of 1 mL/min using a Varian Prostar 210 HPLC System. Detection was performed at 214 nm using a Varian 335 detector (Varian Inc., Australia). The mobile phase consisted of 0.1% Trifluoroacetic acid (TFA) in H_2O (solution A) and 0.1% TFA in 90/10 Acetonitrile/ H_2O. The mobile phase was programmed as follow: (1) 100% A for 1 min (2) linear gradient from 100% A to 60 % A in 20 min (3) linear gradient from 60% A to 0 % A in 4 min (4) 0% A for 2 min (5) linear gradient from 0% A to 100 % A in 4 min (6) 100% A for 5 min. The concentration of unreacted peptide was calculated based on a calibration curve for the peak height of known concentrations of peptide in double distilled water or 1% DMSO (p160). The

amount of conjugated peptide was calculated by subtracting the amount of unreacted peptide from the initial peptide added to the reaction, and was expressed as number of peptide molecules conjugated per 100 polymer chains. The conjugation level of the peptide has been confirmed using the micro bicinchoninic acid (BCA) protein assay kit (Thermo scientific, USA) on the freeze dried product.

3.2.5 Characterization of the prepared block copolymers and polymeric micelles

The prepared block copolymers (acetal-PEO-*b*-PCL, acetal-PEO-*b*-PBCL, p160-PEO-*b*-PCL, p160-PEO-*b*-PBCL, c(RGDfK)-PEO-*b*-PCL and c(RGDfK)-PEO-*b*-PBCL) were characterized for their average molecular weights by ^{1}H-NMR (Bruker Unity-300 MHz) using deuterated chloroform ($CDCl_3$) as solvent and tetramethyl silan as an internal reference standard. The average diameter and size distribution of the prepared micelles were estimated by dynamic light scattering (DLS) using Malvern Zetasizer 3000 after centrifugation at 11,600 × g for 5 min at a polymer concentration of 1 mg/mL in double distilled water at 25 ^{0}C.

3.2.6 Cell uptake studies

Physical entrapment of the hydrophobic fluorescent probe DiI was used to prepare fluorescent labeled polymeric micelles for cellular uptake investigation. Briefly, 30 ug DiI and 30 mg of the block copolymer were dissolved in acetone (0.5 mL). This solution was added to 3 mL of water in a drop-wise manner followed by evaporation of the organic solvent under vacuum. The micellar solution was then centrifuged at 11600 × g to remove the unencapsulated DiI. An aliquot of the

micellar solution was diluted with an equal volume of DMSO and was used to quantify the level of encapsulated DiI by Varian Cary Eclipse fluorescence spectrophotometer (Victoria, Australia), with an excitation wavelength 550 nm and emission wavelength of 565 nm. The release of DiI from micelles was investigated in PBS containing lipid vesicles as the receiver phase as described previously [460]. Cell uptake was measured using either fluorescent spectroscopy or flow cytometry.

Human MDA-MB-435 cells were seeded into a 24-well plate (10^5 cells/well) containing 1 mL of media to grow to ~70% confluence after 24 h incubation. DiI loaded polymeric micelles were added and incubated with MDA-MB-435 cells for 3 h at 37°C. The final DiI and polymer concentration in each well was 0.5 µg/mL and 0.5 mg/mL, respectively. Cells incubated with the medium were used as negative controls. For the competition experiments, MDA-MB-435 cells were pre-incubated with excess free peptide (1 mg/mL) for 30 min to saturate receptors and to inhibit the binding and internalization of peptide conjugated micelles. Following the incubation period, medium was removed and cells were washed with cold PBS three times. Then, 1 mL of DMSO was added to each well to lyse the cells. The fluorescence emission intensity of DiI at 565 nm (fluorescence concentration analyzer, Baxter, United States) provided means for the measurement of internalized DiI levels. Percent uptake was calculated using the following equation:

Cell uptake (%)= (Concentration of internalized DiI/ Concentration of encapsulated DiI added to each well) × 100

In a separate set of experiments, DiI loaded micellar formulations c(RGDfk)-PEO-*b*-PBCL and p160-PEO-*b*-PBCL micelles with different p160 densities (0%, 14%, 20%, 27 and 34%) were incubated with MDA-MB-435 cells in six-well plates for 3 h at 37°C at a final concentration of 0.5 µg/mL DiI. Cells incubated with medium were used as negative controls. Then the cells were trypsinized, washed twice with cold PBS, centrifuged at 500 × g for 5 min and re-suspended in 500 µL FACs buffer (5% FBS in PBS). The resulting cell suspension was finally examined on a FACsort™ flow cytometer (Becton-Dickinson Instruments, Franklin Lakes, NJ, US). Ten thousand cells were counted with logarithmic settings. The cell-associated with DiI was excited with an argon laser (488 nm) and fluorescence was detected at 560 nm.

3.2.7 Encapsulation of PTX in polymeric micelles and their characterization

Paclitaxel (PTX) loaded polymeric micelles were prepared by the dialysis method [457]. Briefly, the block copolymer and PTX were dissolved in DMF (0.5 mL). This solution was added to double distilled water (3 mL) in a drop-wise manner under moderate stirring for 1 day, followed by organic solvent removal by dialysis against double distilled water for another day (Spectrapor, MW cut-off 3,500). The micellar solution was then centrifuged 11,600 × g for 5 min to remove any free unimers and unencapsulated PTX. The solution was analyzed for PTX content using HPLC Varian Prostar 210 system at a flow rate of 1.0 mL/min at room temperature. The detection was performed at 227 nm using a Varian 335 Photodiode Array HPLC detector (Varian Inc., Australia). Reversed phase

chromatography was carried out with a Microsorb-MV 5µ C18-100Å column (4.6mm×250mm) with 20µL of sample injected in a gradient elution using 0.1% trifluroacetic acid aqueous solution and acetonitrile. The percent of acetonitrile was 40% at time zero and increased to 100% in 15 min [441].

3.2.8 In vitro cytotoxicity study

The cytotoxicity of free PTX and PTX encapsulated in acetal-PEO-*b*-PCL, acetal-PEO-*b*-PBCL, p160-PEO-*b*-PCL, p160-PEO-*b*-PBCL, c(RGDfK)-PEO-*b*-PCL and c(RGDfK)-PEO-*b*-PBCL block copolymer micelles against different cell lines (MDA-MB-435, HUVEC, and MCF 10A) was investigated using 3-(4,5-dimethylthiazol-2-yl)-2,5-diphenyltetrazolium bromide (MTT) assay. The cells were grown in the corresponding complete growth media and maintained at 37 °C with 5% CO_2 in a tissue culture incubator. Growth medium containing 8000 cells (4000 cells in case of the MDA-MB-435 cells) was placed in each well of a 96 well plate and incubated overnight to allow cell attachment. After 48 h when the cells had adhered (50% confluency), micellar solutions and free PTX at different concentrations were incubated with the cells for 16 hours. For the competition experiments, the cells were pre-incubated with excess free p160 (1 mg/mL) for 30 min. MTT solution (20 µL; 5mg/mL in double distilled water) was added to each well and the plates were incubated for a further 4 h. The media was aspirated and the formazan crystals were dissolved in DMSO. Cell viability was determined by measuring the optical absorbance differences between 570 and 650 nm using a Power Wave X 340 microplate reader (Bio-Tek Instruments Inc., USA). The mean and the standard deviation of cell viability for each treatment was

determined, converted to the percentage of viable cells relative to the control and plotted versus log PTX concentration [459]. The IC_{50} was calculated based on fitting into the sigmoid dose-response equation: Y= bottom + (top-bottom)/(1+10^(Log IC_{50} –X)*Hill slope), where X is the logarithm of PTX concentration, Y is the %Activity and start at the top and goes to the bottom. The Hill slope is the slope of the linear region dropping in the sigmoid curve. The selectivity index (SI) was defined as the ratio of the measured IC_{50} in either HUVEC or MCF10A cells to the IC_{50} in the cancer cells MDA-MB-435.

3.2.9 Statistical analysis

Data are presented as mean ± standard deviation (SD) of triplicate measurements throughout the manuscript. Statistical significance of difference was tested either using students' t-test or one way ANOVA test with Tukey post-test analysis. The significance level (α) was set at 0.05. All data that required non-linear regression analysis were processed using (Graphpad prism, version 5.00, Graphpad Software Inc., La Jolla, CA, USA).

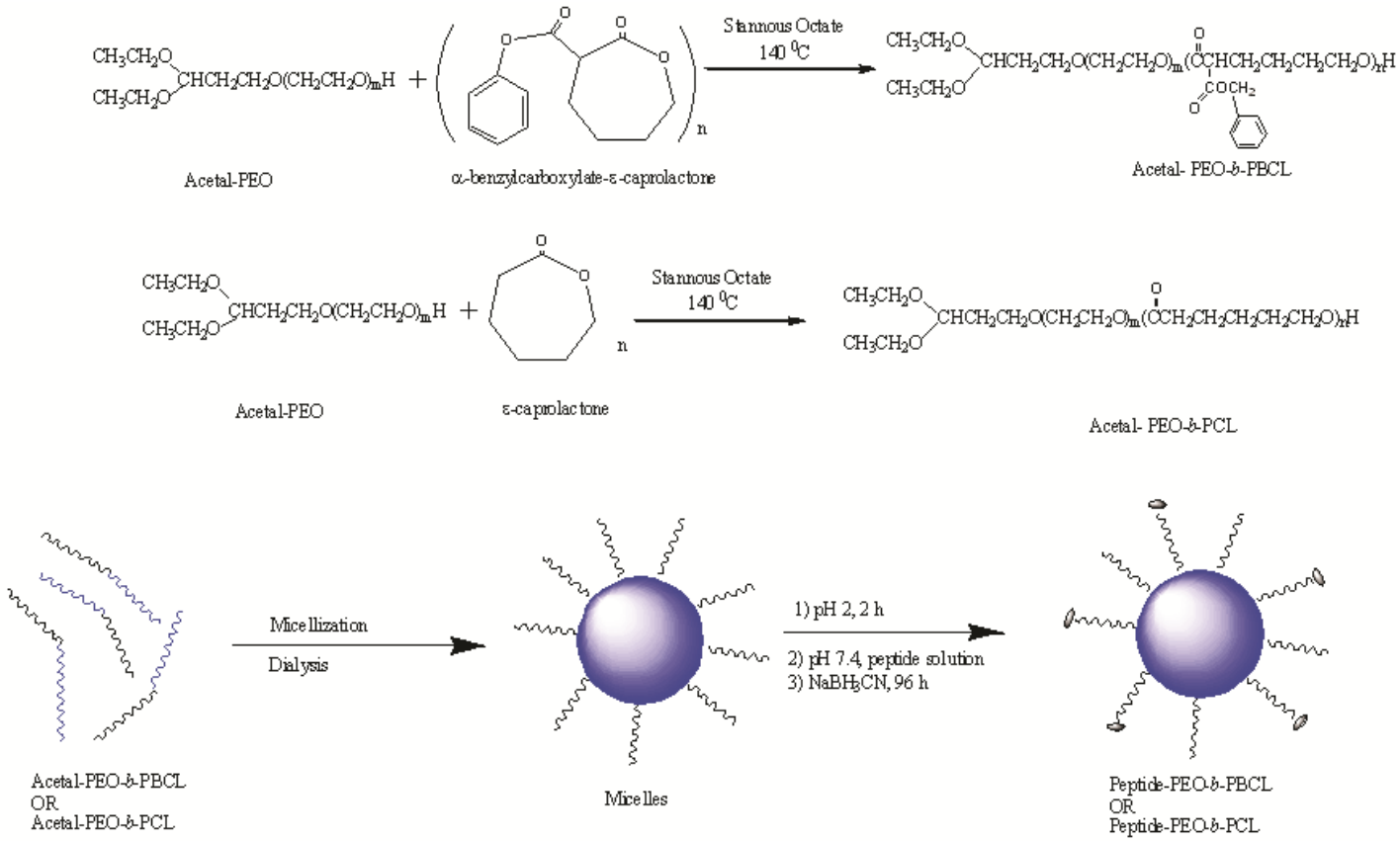

Scheme 3-1: Synthesis scheme and models for the preparation of p160- and c(RGDfK)- decorated PEO-b-PBCL and PEO-b-PCL micelles

3.3 Results and discussion

Micelles decorated with p160 or cyclic pentapeptide c(RGDfK) were prepared using either acetal-PEO-*b*-PCL or acetal-PEO-*b*-PBCL block copolymers (**Scheme 3-1**). The utilized coupling method is advantageous since it does not require any chemical modification in the peptide structure [458]. The conjugation efficiency was quantified by reversed phase HPLC. The standard free c(RGDfk) eluted at retention time 13.8 min while the free p160 eluted at 25.7 min without any interference from the polymer peak (**Figure 3-1, Figure 3-2**). Under the reaction conditions described, the reaction mixture showed no significant peaks of free peptides implying a conjugation efficiency reaching 100% after 96 h reaction. The molar conjugation % for c(RGDfk) and p160-decorated polymers were 17 and 21%, respectively (**Table 3-1**). This means there is around one peptide molecule per five polymer chains. This conjugation level was confirmed by the micro BCA protein assay, which gave similar results to those obtained by HPLC.

Table 3-1: Characteristics of prepared block copolymers and DiI encapsulated micelles.

Block copolymer	M_n (g mol^{-1})	PEO end group Conjugation level (mol %)	DiI/Polymer loading content (w/w)%	*Encapsulation efficiency of DiI in micelles (%) ± SD*
Acetal-PEO-b-PCL	7693[a]	100%[c]	N/D	*N/D*
Acetal-PEO-b-PBCL	7775[a]	100%[c]	0.087	*87.2% ±1.9*
p160-PEO-b-PCL	7983[b]	21.3%[d]	N/D	*N/D*
p160-PEO-b-PBCL	8068[b]	21.3% [d]	0.085	*85.1% ± 2.1*
c(RGDfK)-PEO-b-PCL	7782[b]	17.3% [d]	N/D	*N/D*
c(RGDfK)-PEO-b-PBCL	*7864*[b]	*17.3%* [d]	*0.085*	*85.1% ± 2.3*

[a] Number average molecular weight measured by ^{1}H NMR.

[b] Number average molecular weight measured using a combination of ^{1}H NMR and RP-HPLC.

[c] determined by ^{1}HNMR.

[d] determined by RP-HPLC

N/D: not determined.

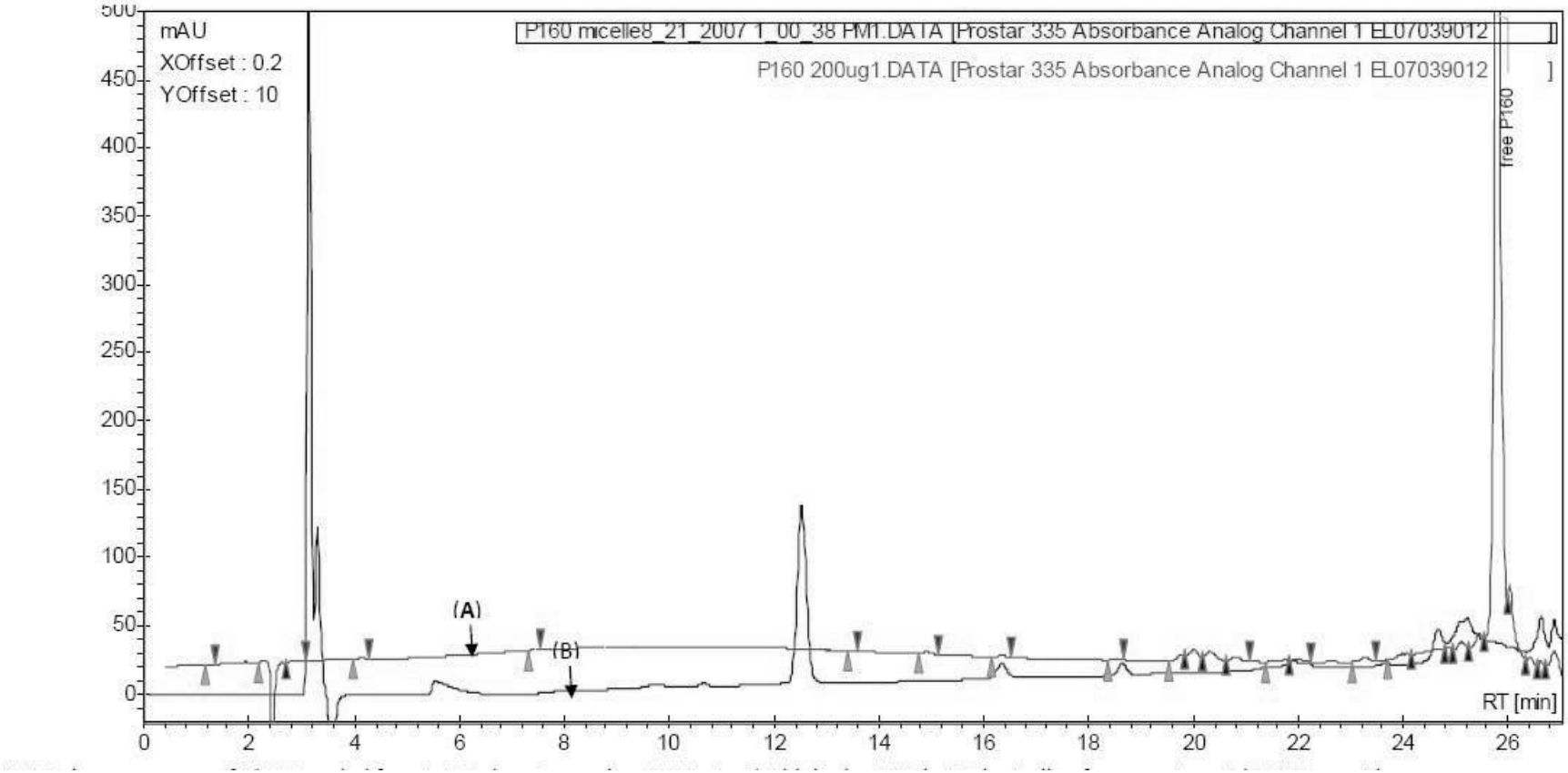

Figure 3-1: Assessment of p160 conjugation to polymeric micelles by RP-HPLC. A) chromatogram of 200 µg/mL free p160 showing peak at 25.7 min , B) aldehyde micelles after reaction with free p160 showing no peaks at 25.7 min.

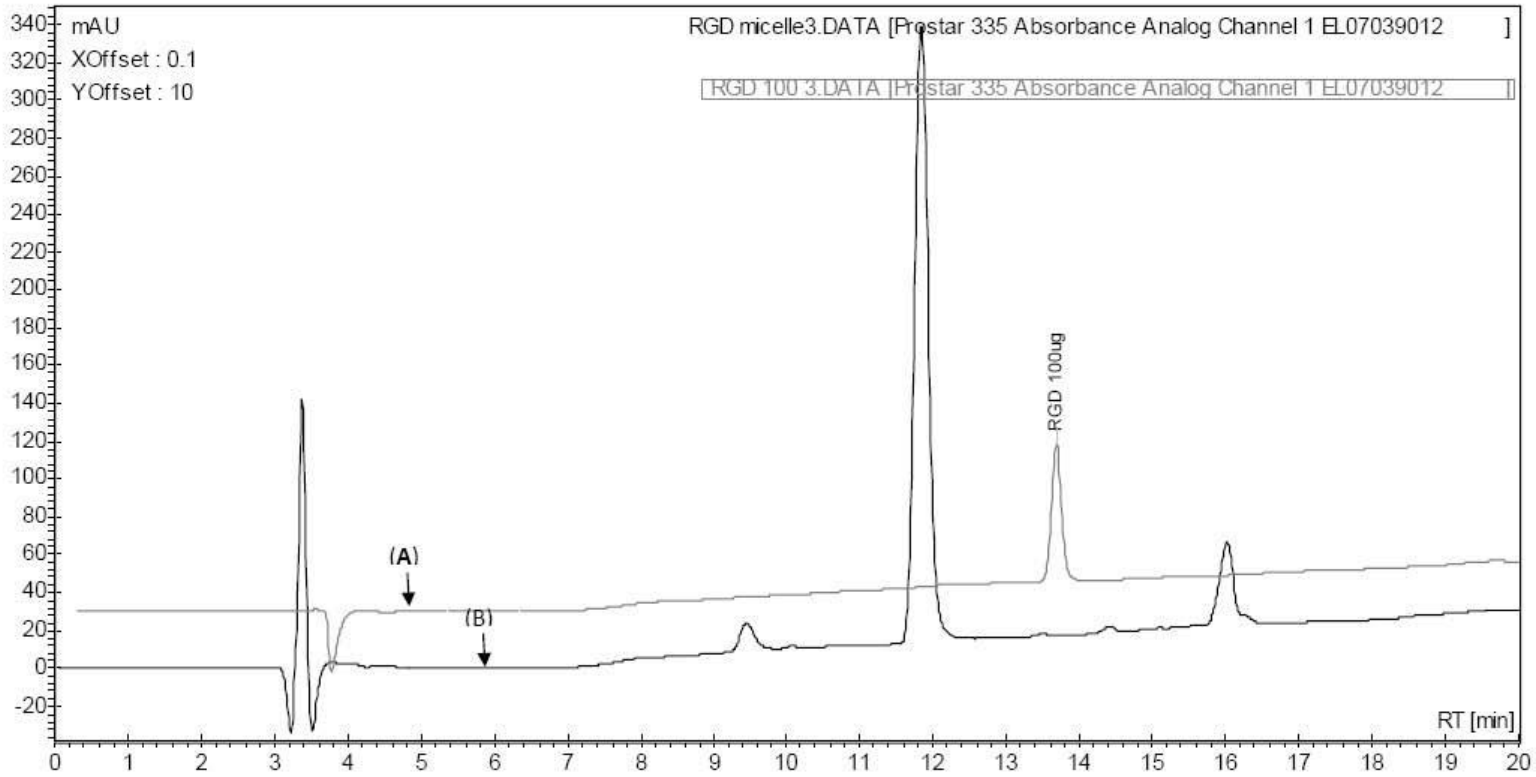

Figure 3-2: Assessment of c(RGDfK) conjugation to polymeric micelles by RP-HPLC. A) chromatogram of 100 µg/mL free c(RGDfK) showing peak at 13.8 min , B) aldehyde micelles after reaction with free c(RGDfK) showing no peaks at 13.8 min.

DiI was used as a hydrophobic fluorescent probe to study the effect of p160 modification on the uptake of PEO-*b*-PBCL micelles by MDA-MB-435 cells compared with c(RGDfK)-modified micelles or unmodified micelles. As reported in **Table 3-1**, DiI has been successfully loaded into PEO-*b*-PBCL micelles with an encapsulation efficiency of > 85%. The rate of hydrophobic DiI transfer from micelles to lipid vesicles was used to evaluate its retention into the used micellar carrier. The acetal-PEO-*b*-PBCL micelles showed slow release of DiI into lipid vesicles, retaining > 74% of the encapsulated DiI after 24 h. This implies that most of the DiI could remain with the micellar carrier during the time frame of the cell uptake experiment. On the other hand, free DiI was rapidly released under the same experimental conditions within 5h (**Figure 3-3**). These results are similar to what already reported for micelles bearing PCL core structure [460].

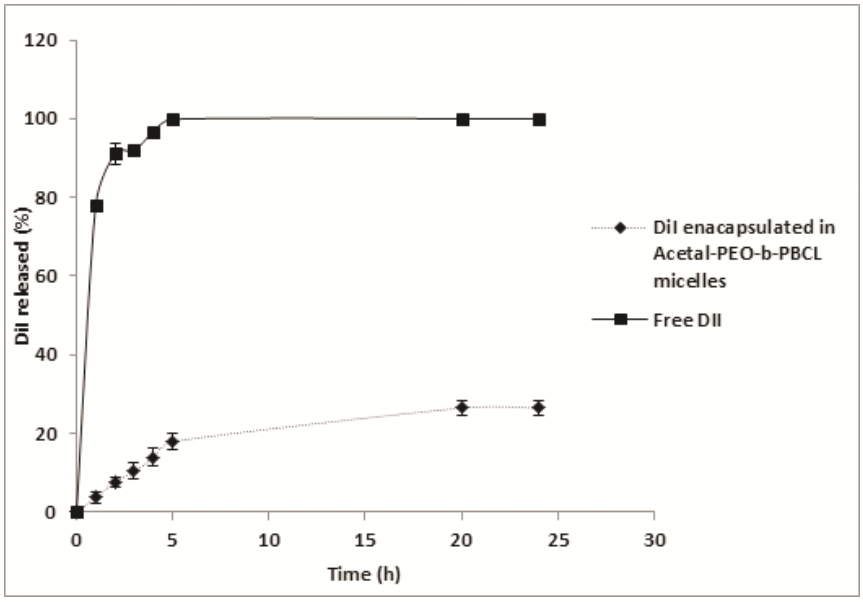

Figure 3-3: Transfer of free DiI and DiI encapsulated in PEO-*b*-PBCL micelles to lipid vesicles.

Coupling of peptide ligands (either p160 or c(RGDfK) to polymeric micelles facilitated their uptake by MDA-MB-435 cells (**Figure 3-4**). The flow cytometry histogram showed a greater cellular uptake for p160-decorated micelles compared to c(RGDfK)-modified PEO-*b*-PBCL micelles. This observation suggests the superiority of p160 as targeting ligand in comparison to c(RGDfK) in terms of improving the cellular uptake. This *in vitro* observation is in line with the *in vivo* results reported by Askoxylakis et al. [310] showed better tumor-homing of [^{131}I]p160 than [^{131}I]FITC RGD-4C in BALB/c nu/nu mice with MDA-MB-435 tumors. The increase in the cell-associated fluorescence could be due to better uptake of p160-decorated micelles through endocytosis and/or improved binding of those micelles on the cell surface followed by release of the incorporated DiI and its diffusion into the cells.

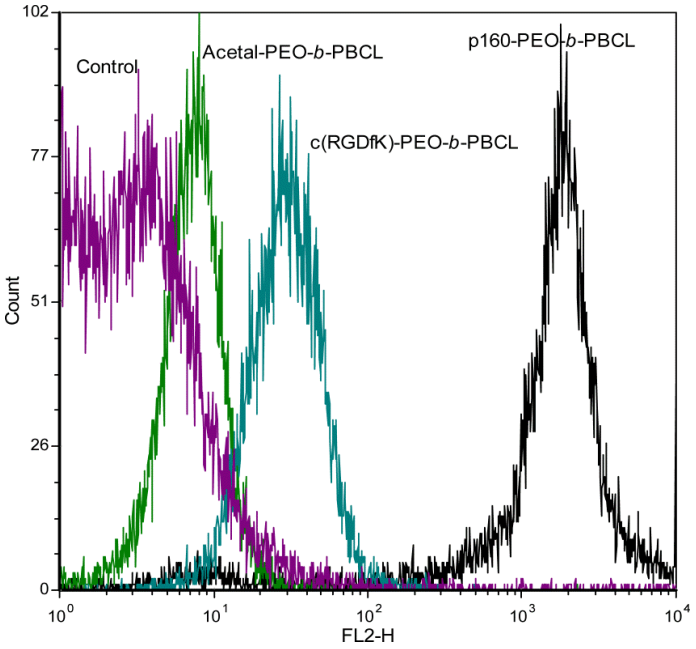

Figure 3-4: Flow cytometry histograms of the uptake of DiI loaded acetal-PEO-b-PBCL, c(RGDfK)-PEO-b-PBCL and p160-PEO-b-PBCL micelles after incubation with MDA-MB-435 cells for 3 h at 37 ^{0}C.

To investigate the possible role of receptor mediated cell binding/uptake of p160-modified polymeric micelles, DiI loaded acetal-PEO-*b*-PBCL and p160-PEO-*b*-PBCL were incubated with MDA-MB-435 cells at 37 ^{0}C in the presence or absence of free p160. Cell uptake of micelles was then evaluated using fluorescence spectroscopy, as reported in our previous publications [460]. As illustrated in **Figure 3-5**a, p160-decorated micelles demonstrated higher cellular uptake compared to acetal decorated micelles after 3 h. Pretreatment of cells with free p160 significantly reduced the cellular uptake of p160-PEO-*b*-PBCL micelles. The uptake of p160-PEO-*b*-PBCL micelles by cells pretreated with free p160 was comparable to that of unmodified micelles pointing to the involvement of receptors in micellar binding and/or uptake. Although the specific cellular receptors for p160 are still unknown, these results clearly show that internalization of p160 into the cell could be through a receptor mediated process and the presence of these receptors is essential for the uptake of p160-functionalized micelles into the MDA-MB-435 cells. These results are in agreement with the results obtained by Askoxylakis et al. [310] who reported that the binding and internalization of [^{125}I]p160 in MDA-MB-435 cells is possibly through receptor mediated endocytosis.

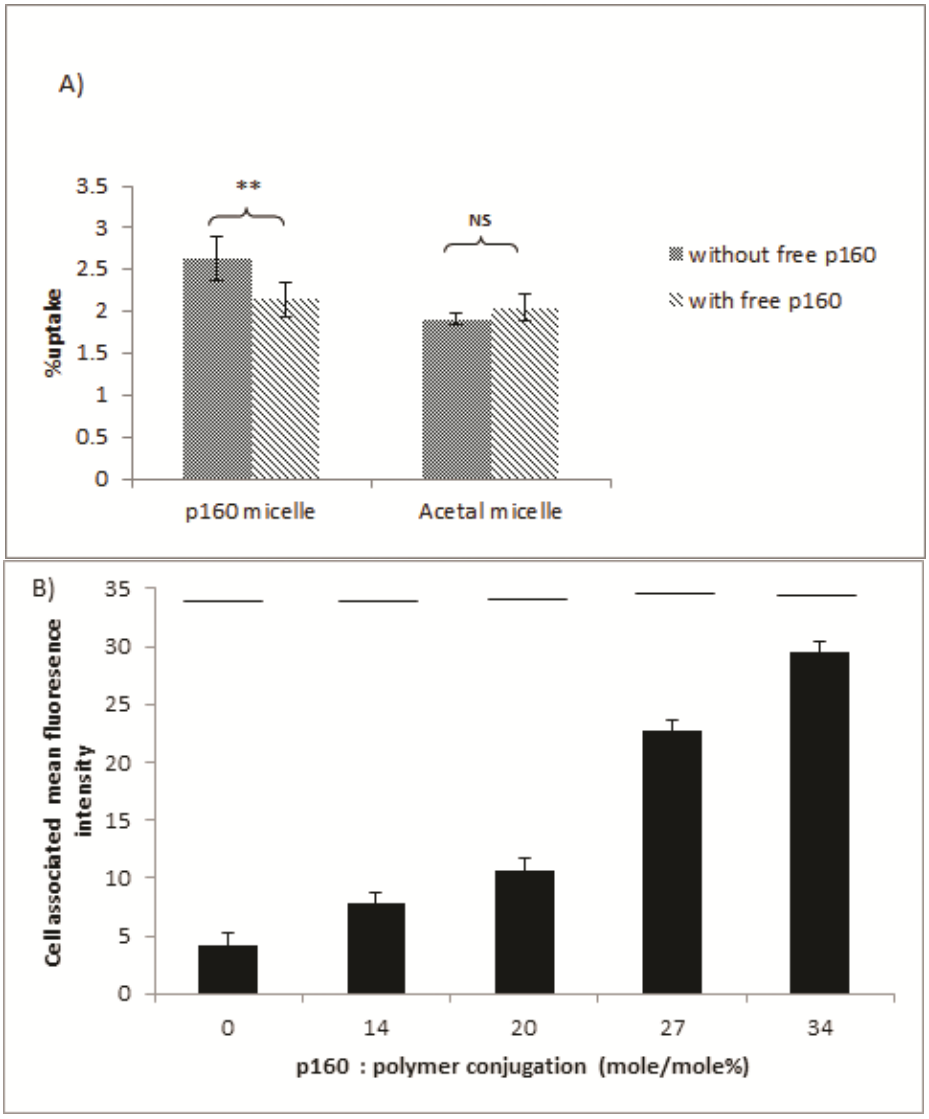

Figure 3-5: A) Cellular uptake of DiI loaded p160-micelles and acetal-micelles after 3 h of incubation at 37 °C with or without pretreatment with free p160. Each bar represents average uptake (%) ± SD (n=3). NS denotes statistically non-significant difference (P>0.05), ** denotes statistically significant from the undecorated micelles (P < 0.05). B) The uptake of DiI loaded p160-PEO-b-PBCL micelles by MDA-MB-435 cells as a function of p160 density after incubation for 3 h at 37 ^{0}C. Each bar represent mean fluorescence intensity ± SD (n=3). Discontinuation of the line above the bars indicates statistically significant difference among different formulations (P<0.05).

Figure 3-5b shows the cellular uptake of DiI loaded p160-PEO-*b*-PBCL micelles by MDA-MB-435 cells at 37 ^{0}C after 3 h incubation, as a function of the conjugated peptide density. It is clearly shown that the higher the attached density of p160 peptide the higher the cellular uptake. The cellular uptake of DiI loaded p160-PEO-*b*-PBCL micelles increases significantly as the density of the surface bound p160 peptide increase ($p<0.05$). At 3h incubation with p160-PEO-*b*-PBCL micelles, a conjugation level as low as 14% was sufficient to observe an increase in the MDA-MB-435 cell-associated fluorescence. A 7 fold increase in the mean fluorescence intensity of cells was seen with a 34% p160 peptide conjugation, compared to the undecorated acetal-PEO-*b*-PBCL micelles. Similar results have been previously reported by many investigators [319, 461, 462].

Table 3-2: Characteristics of PTX loaded copolymer micelles (n=3)

Block copolymer	PTX loading content (%) ± SD			Encapsulation efficiency ± SD (%)	Average diameter ± SD(nm)	*PDI*[a] ± *SD*
	PTX/polymer (mole%)	PTX/monomer (mole%)	PTX/polymer (wt%)			
Acetal-PEO-*b*-PCL	8.0 ± 0.4	0.25 ± 0.01	0.89 ± 0.04	17.69 ± 0.81	111.1 ± 3.5	*0.37± 0.00*
p160-PEO-*b*-PCL	9.2 ± 0.2	0.29 ± 0.01	0.99 ± 0.02	19.73 ± 0.39	76.2 ± 0.9	*0.15 ± 0.01*
c(RGDfK)-PEO-*b*-PCL	8.0 ± 0.1	0.25 ± 0.01	0.88 ± 0.02	17.61 ± 0.32	92.9 ± 2.1	*0.22 ± 0.01*
Acetal-PEO-*b*-PBCL	7.4 ± 0.4	0.49 ± 0.03	0.81 ± 0.02	32.24 ± 0.30	119.5 ± 2.6	*0.14 ± 0.02*
p160-PEO-*b*-PBCL	7.8 ± 0.3	0.52 ± 0.02	0.83 ± 0.03	33.00 ± 1.18	95.3 ± 0.6	*0.12 ± 0.02*
c(RGDfK)-PEO-b-PBCL	*5.6 ± 0.2*	*0.37 ± 0.01*	*0.61 ± 0.02*	*24.33 ± 0.96*	*122.9 ± 1.3*	*0.20± 0.01*

[a] Polydispersity index of micellar size distribution measured by DLS.

In further studies, PTX was loaded into polymeric micelles by the dialysis technique as previously reported [457]. The characteristics of PTX loaded micelles are shown in **Table 3-2**. The calculated loading content of PTX (mole of PTX/mole of polymer) in PEO-*b*-PCL based micelles ranged from 8-9.2 %. The PEO-*b*-PBCL based micelles showed a lower loading content that ranged from 5.6-7.8%. To account for the difference in the degree of polymerization of PCL and PBCL (PCL was longer than PBCL), and to study the effect of different core forming blocks on the loading level of PTX , the mole% of PTX to monomer was calculated. The loading ratios based on moles of PTX/moles of monomers in the core forming block for PTX in acetal-PEO-*b*-PCL and acetal-PEO-*b*-PBCL were 0.25 and 0.49, respectively. This observation could be explained by the better compatibility and improved interaction between the PBCL core and PTX. Further elongation of the hydrophobic chain length of PBCL may improve the overall solubility of PTX into these polymeric micelles. The resulting nanocarriers had a diameter between 76 and 123 nm, with a good acceptable polydispersity ranging between 0.37 and 0.12.

Assessment of cytotoxicity against MDA-MB-435 cancer cells showed the safety of the empty micelles as well as the free peptides at concentrations used in cytotoxicity studies implying no effect from the carrier (data not shown). The cytotoxicity of free PTX versus PTX encapsulated in different polymeric micellar formulations was evaluated at an equivalent PTX concentration (300 ng/mL), where PTX encapsulated in acetal-PEO-*b*-PBCL micelles showed reduced cytotoxicity compared to free PTX (**Figure 3-6** A). This observation can reflect

the slow release of PTX from the micellar carrier and/or slow uptake of the micellar formulation by the cancer cells. Conjugation of either p160 or c(RGDfk) to PEO-*b*-PBCL micelles resulted in an enhanced cytotoxicity for encapsulated PTX reaching levels comparable to that of free PTX (**Figure 3-6** A and 4B). For both p160- and c(RGDfK)-decorated micelles, in the presence of excess free peptide pre-incubated with the cells, the cytotoxicity of encapsulated PTX was reduced and reached that of PTX encapsulated in acetal-PEO-*b*-PBCL micelles pointing to the involvement of receptors in micellar cell binding/uptake. This is consistent with our earlier observation on the uptake of these micelles by MDA-MB-435 cells (**Figure 3-5** a).

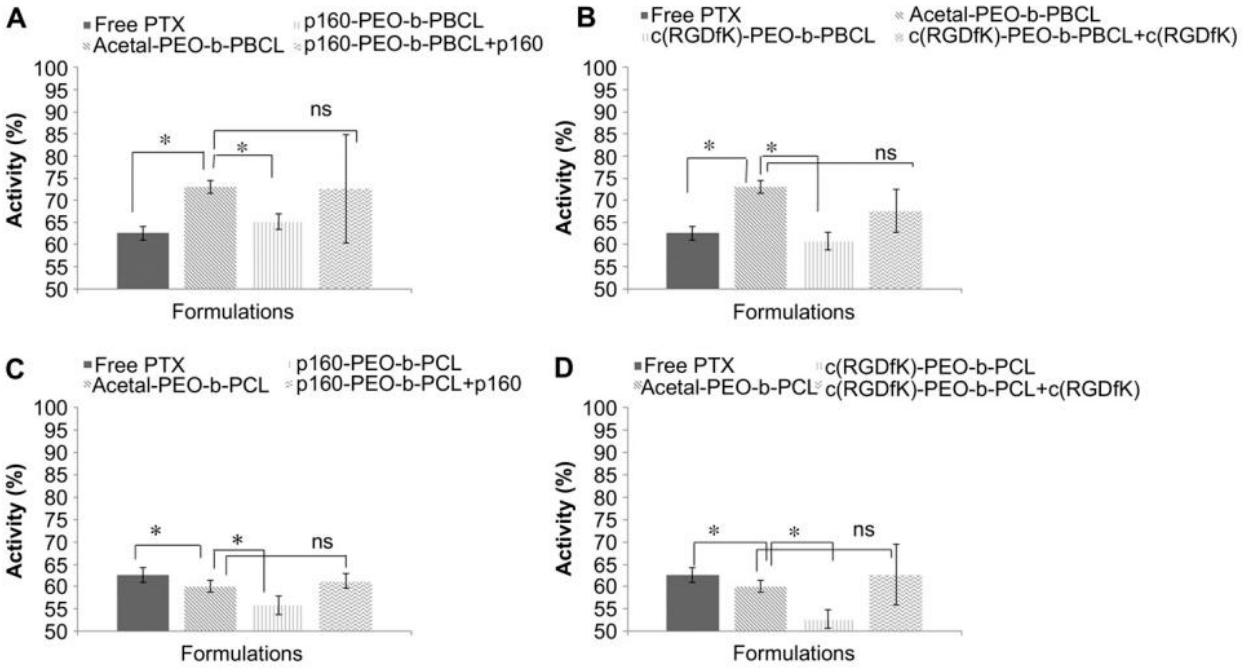

Figure 3-6: *In-vitro* cytotoxicity of PTX encapsulated in A) p160-PEO-*b*-PBCL, B) c(RGDfK)-PEO-*b*-PBCL, C) p160-PEO-*b*-PCL; and D) c(RGDfK)-PEO-b-PCL micelles in comparison to PTX encapsulated in plain micelles, free PTX and after pre-incubation with free peptide against MDA-MB-435 cells after 16 h. * denotes statistically significant difference (P< 0.05).

Decoration of PEO-*b*-PCL micelles with either p160 or c(RGDfK) enhanced the cytotoxicity of encapsulated PTX (**Figure 3-6** C and 4D) over what was achieved by free PTX. Consistent with our observation on free peptide competition studies reported earlier, the presence of free peptide reduced the cytotoxicity of PTX in both p160- and c(RGDfK)-decorated PEO-*b*-PCL micelles to that of PTX containing acetal-polymeric micelles (**Figure 3-6** C and 4D).

A comparison between the cytotoxicity of PTX encapsulated in PEO-*b*-PCL and that in PEO-*b*-PBCL micelles revealed a better effect for PTX in PEO-*b*-PCL carriers (**Figure 3-7**). The trend was similar for acetal-, p160-, and c(RGDfK)-decorated micelles. The cytotoxicity of encapsulated PTX may result from the cellular uptake of the carrier followed by intracellular and/or extracellular release of PTX and diffusion of released drug into the cells. Therefore, better effect of encapsulated PTX in PCL containing micelles may be due to better protection of PTX by these micelles, better interaction of PEO-*b*-PCL micelles with cancer cells, or improved release of PTX from PCL containing micelles and its subsequent diffusion to cells. It is not clear which of these mechanisms is playing a more significant role at this stage.

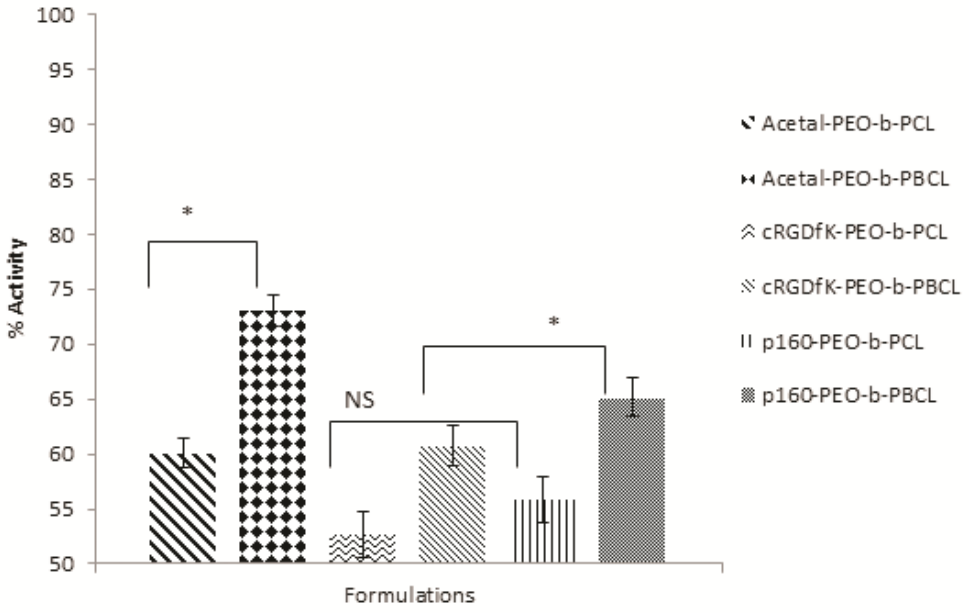

Figure 3-7: Comparing the *in vitro* cytotoxicity of acetal and peptide decorated micelles containing physically encapsulated PTX against MDA-MB-435 cells after 16 h incubation. NS denotes statistically non-significant difference (P>0.05). * denotes statistically significant difference (P< 0.05).

A comparison between the cytotoxicity of encapsulated PTX in p160- and c(RGDfK)-decorated PEO-*b*-PBCL micelles showed higher cytotoxicity of PTX in c(RGDfK)-PEO-*b*-PBCL micelles than PTX in p160-PEO-*b*-PBCL ($p<0.05$). The cytotoxicity of encapsulated PTX in p160- and c(RGDfK)-decorated PEO-*b*-PCL micelles showed a similar trend, although in this case the difference was not statistically significant ($P>0.05$) (**Figure 3-7**). This was unexpected, since the uptake study has shown a better uptake of p160- micelles compared to c(RGDfK)-micelles by MDA-MB-435 cancer cells. The observation may be due to additive effects of c(RGDfK) and PTX on this cell line. Further studies are needed to test the validity of this hypothesis.

Other research groups have attempted to study the RGD directed PTX delivery using polymeric carriers. Danhier et al. [463] physically loaded PTX into PEO-b-PLGA nanoparticles (NP) grafted with RGD linear peptide. They evaluated the *in vivo* antitumor efficacy of PTX-NP, PTX-RGD-NP in TLT tumor-bearing mice. They showed that PTX-RGD-NP effectively delay the tumor growth when compared to PTX-NP. Similarly, Yin et al. [464] incorporated PTX into polymeric micelles (PM) of PEO-PLGA decorated with cyclic RGDyK on their corona. Compared to the undecorated micelles, the RGDyK-PTX-PM gave 1.74 and 2.77 time decrease in the IC_{50} values against the B16-F10 and HUVEC cells, respectively. In another study, PTX loaded RGD-PEO-PLA micelles gave a dramatic reduction in tumor size in MDA-MB-435 tumor-bearing nude mice compared to those treated with PTX loaded PEO-PLA [465]. Decoration of polymeric micelles with the more cancer-specific p160 ligand was expected to introduce higher specificity to the encapsulated PTX for cancer cells than normal cells compared to specificity afforded by RGD decoration of micelles.

To test this hypothesis, we examined the specificity of formulated PTX for cancer cells by comparing the IC_{50} of free and micelle encapsulated PTX against the MDA-MB-435 cell versus the non-tumorigenic cell lines (HUVEC and MCF 10A) using the MTT assay (**Figure 3-8**, **3-9**). Although free PTX showed low IC_{50} against cancer cell line MDA-MB-435 (IC_{50} 21.25 ng/mL), it was still relatively toxic towards normal cells (IC_{50} of 15.81 and 48.09 ng/mL against HUVEC and MCF 10A cell lines, respectively). The selectivity index (SI) of free PTX for cancer over HUVEC or MCF 10A was calculated at 0.74 and 2.26,

respectively. SI of <1 implies even a higher selectivity of free PTX for HUVEC over MDA-MB-435 cells. Encapsulating PTX into non-targeted polymeric micelles, i.e. acetal-PEO-*b*-PCL, increased its cytotoxic effect against all cell lines under study (**Figure 3-8**, **3-9**). As a result, the SI of PTX encapsulated in plain micelles was either reduced significantly (0.26 for HUVEC) ($P<0.05$) or did not significantly change (2.53 for MCF10A cells) ($P<0.05$). This lack of specificity against the tumorigenic cell line makes these carriers a non-ideal carrier for PTX. On the other hand, installment of a tumor specific peptide on the micellar surface, e.g. p160, increased the cytotoxicity of encapsulated PTX significantly against the MDA-MB-435 cells ($P<0.05$), but reduced its cytotoxicity significantly against normal cell lines ($P<0.05$) (MCF-10A, HUVEC) (**Figure 3-9**). p160-PEO-*b*-PCL showed an average IC_{50} of 3.60, 17.31 and 46.68 ng/mL against MDA-MB-435, HUVEC and MCF10A, respectively. This reflects a 5.9 fold increase of cytotoxicity against MDA-MB-435 cells in comparison to free PTX. The lower cytotoxicity of p160 decorated micelles against HUVEC cells is in line with the findings of Askoxylakis et al. [310] who reported the low specific binding capacity of radiolabelled p160 for that cell line.

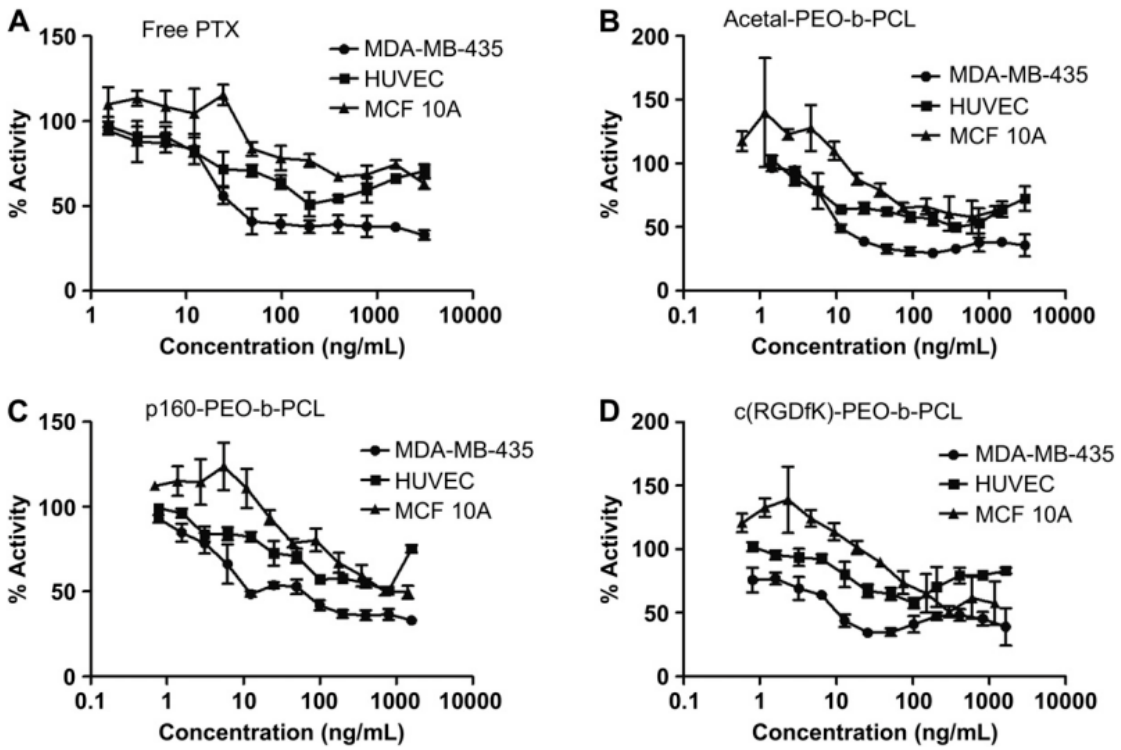

Figure 3-8: *In vitro* cytotoxicity of A) Free PTX B) acetal-PEO-*b*-PCL C) p160-PEO-*b*-PCL D) c(RGDfK)-PEO-*b*-PCL micelles containing physically encapsulated PTX against different cell lines MDA-MB-435, HUVEC and MCF 10A cells after 16 h incubation.

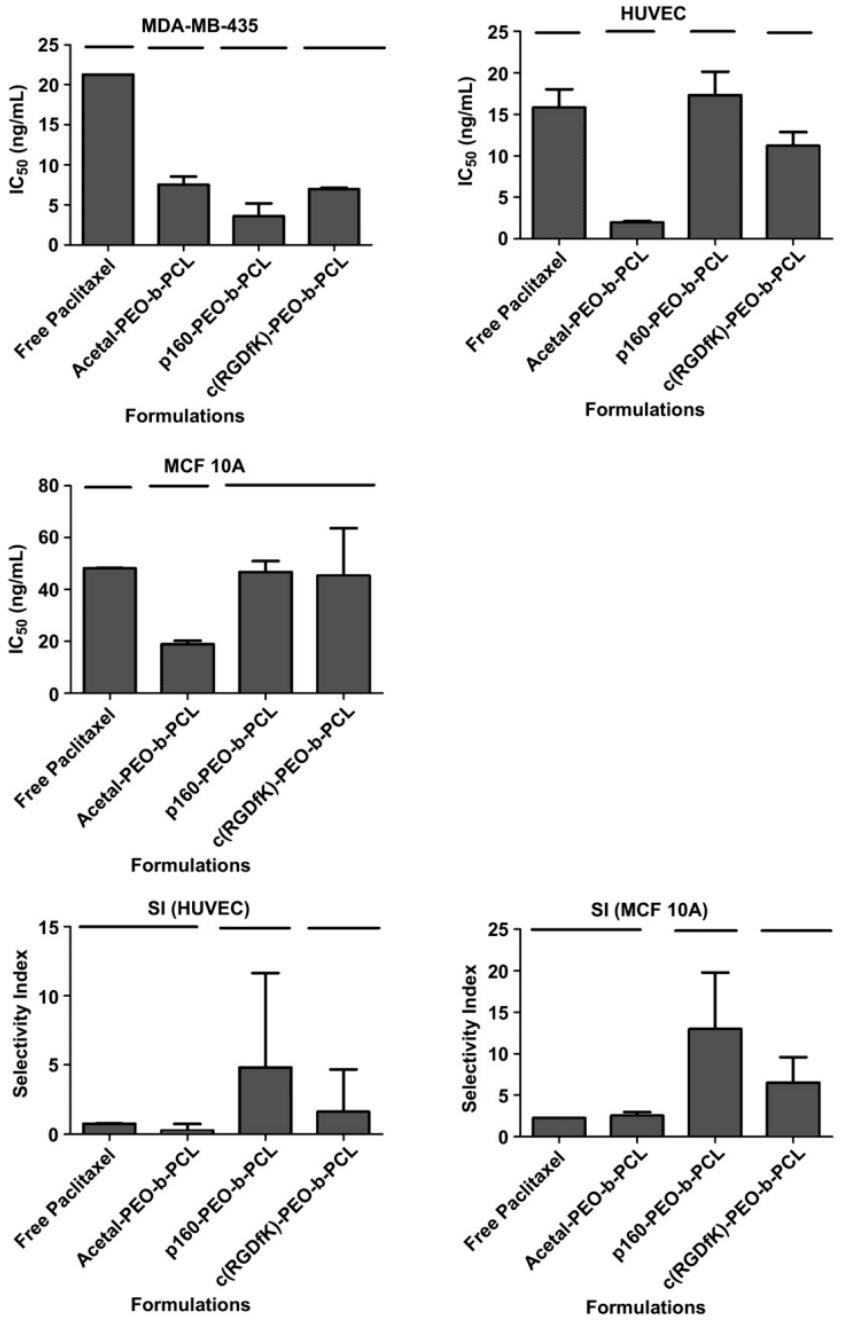

Figure 3-9: IC_{50} and Selectivity index (SI) of different formulations against studied cell lines. Selectivity index (SI) = IC_{50} against non-tumorigenic cell line (HUVEC or MCF10A)/ IC_{50} against tumorigenic cell line (MDA-MB-435). Each bar represents mean IC_{50} or SI ± SE (n=3). Discontinuation of the line above the bars indicates statistically significant difference among different formulations (P<0.05). Differences between means were assessed using one-way ANOVA followed by post hoc analysis using Tukey's multiple comparison test (Graphpad prism, version 5.00, Graphpad software. Inc, La Jolla, CA, USA). The level of significance was set at α = 0.05.

On the other hand, decorating micelles of PEO-*b*-PCL with $\alpha_v\beta_3$ integrin targeting ligand (i.e. c(RGDfK)) decreased the IC_{50} of encapsulated PTX by 3.0 fold against the MDA- MB-435, compared to free PTX. Against HUVEC and MCF-10A cells, IC_{50} values of 11.20 and 45.43 ng/mL were observed for PTX encapsulated in c(RGDfK)-PEO-*b*-PCL micelles. This corresponds to 1.4 fold decrease in IC_{50} against HUVEC ($P<0.05$) and a non-significant change in IC_{50} against MCF10A cells ($P>0.05$) in comparison to free PTX. The SI of PTX encapsulated in c(RGDfK)-PEO-*b*-PCL micelles for MDA-MB-435 cells against HUVEC and MCF10A cells was 1.6 and 6.52, respectively. Installment of p160 on the micellar shell of PEO-*b*-PCL increased the SI of PTX for MDA-MB-435 cells against HUVEC and MCF10A cells by 6.48 and 5.73 folds, respectively, in comparison to free PTX. However, micelles decorated with c(RGDfK) showed 2.17 and 2.88 fold increase in the SI of PTX for MDA-MB-435 against HUVEC and MCF10A cells, respectively.

3.4 Conclusion

Our results point to the potential of p160 and c(RGDfK) modified polymeric micelles for active and selective drug targeting to human cancers. Better selectivity for cancer cell targeting and cytotoxicity may be achieved through delivery of PTX by p160-decorated PEO-b-PCL micelles over c(RGDfK)-micelles. The better interaction of nanocarriers of PTX with cancer over normal cells achieved through p160 targeting ligand is expected to improve the bio-distribution redirecting the drug towards malignant cells and away from the normal tissues leading to better in vivo therapeutic index for the encapsulated

PTX, in turn. It may also lead to a better penetration of the targeted drug carrier into the tumor mass. Further in vivo studies are warranted to verify the validity of this assumption. In the next chapter, the potential of the p160 peptide to improve the activity of polymeric conjugate of PTX will be studied.

Chapter 4

Development of actively targeted polymeric conjugate of paclitaxel with breast cancer specific peptide ligand

4.1 Introduction

Drug-polymer conjugates can be designed as nanosized hybrid molecules that contain several copies of active drug molecules with a single polymer chain through covalent chemical bonding [110, 466]. The existence of several clinically approved PEGylated enzymes/cytokines and numerous polymer bound chemotherapy drugs (including polymer conjugates of paclitaxel, PTX, and doxorubicin, DOX) that are currently in clinical trials, have established a potential for polymer-drug conjugates in improving the therapeutic performance of conjugated active agents [467-470]. Cell therapeutics Inc has developed a PTX/polymer conjugate using biodegradable polymer poly(glutamic acid) (PGA). In this construct, PTX was conjugated to the polymer backbone through an ester bond using a polypeptide spacer producing Xytotax® [347]. Xyotax®, has shown clinical benefit and superior safety compared to free PTX, either alone or in combination with radiotherapy or other chemotherapeutic agents (i.e. cisplatin) [435, 471-473].

Drug polymer conjugates made out of amphiphilic block copolymers can self-assemble to micellar structures of 10-100 nm. Polymeric micelles are expected to show an improved pharmacokinetic profile leading to preferential tumor accumulation by the EPR effect compared to polymer-drug conjugates. Chemical conjugation of drugs to polymeric micelles can prevent the early and premature leakage of incorporated drug from the micellar carrier [474, 475]. However, the restricted release of drug from the polymeric carrier within the target tissue may endanger the therapeutic efficacy of the polymeric micellar drug conjugate.

Second generation polymeric micellar drug conjugates utilizing tumour targeting ligands on their surface are developed to enhance the intracellular delivery of the polymeric through receptor mediated endocytosis by cancer cells. This strategy may enhance the chance of triggered drug release from the carrier upon localization of polymeric micellar drug conjugate within the endosomes of cancer cells which has acidic pH and is rich in metabolizing enzymes.

In an attempt to improve the therapeutic efficacy and cytotoxicity of PTX, a novel multifunctional polymeric construct namely p160-poly(ethylene oxide)-*b*-poly(ε-caprolactone-paclitaxel) (p160-PEO-P(CL-PTX)) was developed. This polymeric conjugate consist of the amphiphilic block copolymer PEO-*b*-poly(ε-caprolactone) (PEO-b-PCL) bearing i) several copies of PTX covalently attached to the hydrophobic block PCL through a hydrolysable ester and ii) a breast tumour internalizing peptide, p160, linked to the hydrophilic PEO block. In theory, this polymeric micellar PTX conjugate can target the tumour both passively through the EPR effect (because of its surface properties and size of around 100 nm) and actively (because of the presence of tumour homing peptide p160) and at the same time, provide an endosomally triggered drug release within the cancer cells. The potential of this breast tumor targeted polymeric micellar PTX conjugate for such functional properties was investigated here.

4.2 Materials and methods

4.2.1 Materials

Ethylene oxide, diisopropyl amine (99%), benzyl chloroformate (tech. 95%), sodium (in Kerosin), butyl lithium (Bu-Li) in hexane (2.5 M Solution), 3,3 diethoxy 1-propanol (DEP) , naphthalene, potassium, palladium coated charcoal, N, N dicylcohexyl carbodiimide (DCC), Dimethylamino pyridine (DMAP),and pyrene were purchased from Sigma chemicals (St. Louis, MO, USA). Paclitaxel (purity> 99.5) was purchased from LC Laboratories. ε-caprolactone was purchased from Lancaster Synthesis, UK. Stannous octoate was purchased from MP biomedicals Inc, Germany. Fluorescent probe 1,3-(1,1′-dipyrenyl)propane were purchased from Molecular Probes, USA. p160 was kindly provided by Dr. K.Kaur's lab. Cell culture media RPMI 1640, penicillin-streptomycin, fetal bovine serum, and L-glutamine were purchased from GIBCO, Invitrogen Corp. All other chemicals were reagent grade.

4.2.2 Methods

4.2.2.1 Synthesis of acetal-PEO

In a triple neck flask rounded bottom flask, 0.15 mL (1 m.mol) of initiator 3,3 diethoxy1-propanol (DEP) and 3.5 mL (1 m.mol) of catalyst potassium naphthalene were added to 20 mL of dry THF. After 10 minutes of stirring, 5.7 mL (114 m.mol) of condensed ethylene oxide were added. The reaction is left for 2 days till a light brown highly viscous solution is formed. The reaction stopped by addition of 1-2 mL of acidified ethanol to neutralize excess potassium, and the

polymer precipitated by addition of the reaction mixture to large amount of cold diethyl ether. The polymer is left for 1 hour in the freezer then centrifuged for 15 minutes at 4000 rpm. The dry polymer is obtained by placing the polymer in the vacuum oven overnight.

4.2.2.2 Synthesis of Acetal-PEO-b-PBCL

The synthesis of functionalized monomer, i.e., α-benzyl carboxylate-ε-caprolactone, and functional group bearing block copolymer, i.e., acetal-poly(ethylene oxide)-*block*-poly(α-benzylcarboxylate-ε-caprolactone) (acetal-PEO-*b*-PBCL) have been reported in a previous paper [437]. Briefly, acetal-PEO (3.5g), α-benzylcarboxylate-ε-caprolactone (3.5 g) and stannous octoate (0.002 eq of monomer, 3.5 mg) were added to a 10 mL previously flamed ampoule, nitrogen purged and sealed under vacuum. The polymerization reaction was allowed to proceed for 4 h at 140º C in oven. The reaction was terminated by cooling the product to room temperature.

4.2.2.3 Synthesis of acetal-PEO-b-P(CL-PTX)

The synthesis of acetal-PEO-b-P(CL-PTX) has been accomplished in two steps. In the first step, acetal-poly(ethylene oxide)-*block*-poly(α-carboxyl-ε-caprolactone) acetal-PEO-b-PCCL has been synthesized through catalytic debenzylation of acetal-PEO-*b*-PBCL in the presence of hydrogen gas as reducing agent and palladium coated charcoal as catalyst according to the procedure described in a previous publication [476]. Briefly, one gram of acetal-PEO-b-PBCL was dissolved in 25 mL of dry THF in a 100 mL rounded bottom flask. Then, 300 mg of charcoal coated palladium is added to the reaction mixture. After

stirring the reaction mixture in presence of hydrogen for 24 h, the reaction mixture is condensed under vacuum and charcoal has been removed by centrifugation for 15 minutes at 3000 rpm. The polymer is obtained by precipitation in 250 mL of cold diethyl ether and washed out repeatedly to remove any impurities. The final polymer is dried in the vacuum oven for 24 h at room temperature.

In the second step, PTX was chemically conjugated by ester bond to acetal-PEO-b-PCCL through DCC and DMAP mediated coupling reaction. Briefly, DMAP (10.1 mg, 0.083 mmol) and DCC (17.7 mg, 0.083 mmol) were added to a stirred solution of acetal-PEO-*b*-PCCL (MW: 6050 g mol^{-1}) (50 mg, 0.0083 mmol) block copolymer in anhydrous dichloromethane (DCM) (20 mL). Subsequently, after stirring for 30 min, PTX (21.1 mg, 0.025 mmol) in 1mL of dried DCM has been added. The reaction was carried out under argon gas and protected from light for 4 days at room temperature. Thin layer chromatography in the presence of THF: CM (1:4) as the mobile phase was used to monitor the reaction progress. The by-product dicyclohexyl urea was filtered out. The product was condensed by bubbling of nitrogen gas. The purification of the polymer from free PTX was carried out by dialysis against 1 L of dimethlyl sulphoxide (DMSO) for 1 day, then against double distilled water for another day using cellulose membrane (spectrapore, cutoff MW: 3500). Then the PTX conjugated block copolymer, i.e., acetal-PEO-*b*-P(CL-PTX), was lyophilized to a white powder.

4.2.2.4 Synthesis of p160-PEO-b-P(CL-PTX)

The p160 peptide was conjugated to the micellar surface by the functional acetal groups on the micellar shell. The prepared block co-polymers, i.e. acetal- PEO-b-P(CL-PTX) were assembled to polymeric micelles by dissolving (30 mg) was dissolved in DMSO (1 mL). This solutions was added to doubly distilled water (6 mL) in a drop-wise manner under moderate stirring for 1 day followed by organic solvent removal by dialysis against double distilled water for another day (spectrapor, MW cut off 3,500). The micellar solution was then centrifuged 11,600 g for 5 min to remove any free unimers. The aqueous solution of polymeric micelles was then acidified to pH 2 with 0.5 M HCl and kept stirring for 2 hrs at room temperature to produce aldehyde polymeric micelles. The resulted solution was then neutralized with 0.5 M NaOH. For conjugation of p160, the pH of the micellar solution was adjusted by addition of appropriate volume of concentrated sodium phosphate buffer solution (pH 7.4, 0.1 M) to obtain a 4 mg/mL polymer concentration. p160 was added and incubated with the aldehyde bearing micelles at p160: polymer ratio of 1:4.8 at room temperature for 2 hrs under moderate stirring. Subsequently, $NaBH_3CN$ (10 eq.) was added to the polymer to reduce the Schiff ‘s base. After 96 hours of reaction, the un-reacted peptide and reducing agent were removed by extensive dialysis. The conjugation efficiency of p160 to polymeric micelle was assessed by gradient reversed phase HPLC method. The concentration of unreacted peptide was calculated based on a calibration curve for the peak area of known concentrations of peptide in double distilled water. The amount of conjugated peptide was calculated by subtracting the amount of unreacted peptide from the initial peptide added to the reaction and

was expressed as number of peptide molecules conjugated per 100 polymer chains.

4.2.2.5 High performance liquid chromatography analysis

A gradient reversed high performance liquid chromatography was developed to quantify the conjugation efficiency of p160 on the polymeric micelles. A μ Bondpack (Waters Corp., United States) C-18 analytical column (10 μm 3.9 X 300 mm) was used. Gradient elution was performed at a flow rate of 1 mL/min using Varian Prostar 210 HPLC System. The detection was performed by at 214 nm using a Varian 335 Photodiode Array HPLC detector (Varian Inc, Australia). The mobile phase consisted of 0.1% Tri-flouroacetic acid (TFA) in H_2O (solution A) and 0.1% TFA in 90/10 acetonitrile/ H_2O. The mobile phase was programmed as follows: (1) 100% A for 1 min (2) linear gradient from 100% A to 60 % A in 20 min (3) linear gradient from 60% A to 0 % A in 4 min (4) 0% A for 2 min (5) linear gradient from 0% A to 100 % A in 4 min (6) 100% A for 5 min.

4.2.2.6 Characterization of the prepared block copolymers and polymeric micelles

The prepared block co-polymers were characterized for their average molecular weights and polydispersity by ^{1}H-NMR and Gel permeation chromatography (GPC). ^{1}H-NMR was carried out by Bruker Unity-300 spectrometer at room temperature, using deuterated chloroform ($CDCl_3$) as solvent and tetramethyl silan as internal reference standard. GPC was carried out at 25 ^{0}C with an HP instrument equipped with Waters Styragel HT4 column (Waters Inc, Milford, MA). The elution pattern was detected at 35 ^{0}C by refractive index (PD 2000,

precision detector, Inc)/ light scattering (model 410, Waters Inc.) detectors. THF (1 mL/min) was used as eluent. Samples of 20 uL from 10 mg/mL polymer solution in THF were injected. The column was calibrated with a series of standard polystyrene. The PTX content in the conjugate calculated from the ^{1}H-NMR spectrum using the peak integration of phenyl protons signal at (7.3-8.4 ppm) and the ethylene proton signal (3.7 ppm).

Polymeric micelles were prepared by dialysis method. The block copolymer (3 mg) was dissolved in DMSO (0.5 mL). This solutions was added to doubly distilled water (3 mL) in a drop-wise manner under moderate stirring for 1 day followed by organic solvent removal by dialysis against double distilled water for another day (spectrapor, MW cut off 3,500). The micellar solution was then centrifuged 11,600 × g for 5 min to remove any free unimers.

The average diameter and size distribution of the prepared micelles were estimated by dynamic light scattering (DLS) using Malvern Zetasizer 3000 after centrifugation at 11,600 g for 5 min at a polymer concentration of 1 mg/mL in double distilled water at 25 ^{0}C.

4.2.2.7 In vitro cytotoxicity study against breast cancer cells MDA-MB-435

The cytotoxicity of free PTX, free p160 , PEO-b-P(CL-PTX), and p160-PEO-b-P(CL-PTX) block copolymer micelles against MDA-MB-435 breast cancer cells was investigated using 3-(4,5- dimethylthiazol-2-yl)-2,5-diphenyltetrazolium bromide MTT assay. The cells were grown in RPMI 1640 complete growth media supplemented with 10 % fetal bovine serum, 1% w/v % L-glutamine, 100

units/mL penicillin and 100µg/mL streptomycin and maintained at 37 °C with 5% CO_2 in a tissue culture incubator. Growth medium RPMI containing 4000 cells was placed in each well in 96 well plate and incubated overnight to allow cell attachment. After 48 h when the cells had adhered (50% confluency), micellar solutions and free PTX at different concentrations were incubated with the cells for 72 hours. After 72 h, MTT solution (20 µL; 5 mg/mL in sterile-filtered PBS) was added to each well and the plates were reincubated for further 4 h. The formazan crystals were dissolved in DMSO, and the cell viability was determined by measuring the optical absorbance differences between 570 and 650 nm using a Power Wave X 340 microplate reader (Bio-Tek Instruments, Inc. USA). The mean and the standard deviation of cell viability for each treatment was determined, and converted to the percentage of viable cells relative to the control. The concentration required for 50% growth inhibition (IC_{50}) was estimated from the plot of the % viable cells versus log PTX concentration using Graphpad prism for Windows, Version 5.0 (Graphpad Software Inc.).

4.2.2.8 Statistical analysis

Values are presented as mean ± standard deviation (SD) of triple measurements. Statistical significance of difference was tested either using students' t test or one way ANOVA test (Sigma plot for windows, version 11.0, Systat software Inc.). Differences between means of IC_{50} were assessed using one way ANOVA (Sigma plot for windows, version 11.0, Systat software Inc.). The level of significance was set at $\alpha = 0.05$.

4.3 Results and discussion

4.3.1 Preparation and characterization of p160-P(CL-PTX)

The ^{1}H-NMR spectra of starting and intermediate polymers utilized in the synthetic process of p160-P(CL-PTX) are shown in **Figure 4-1 (A-D) .** The ^{1}H NMR spectra of acetal-PEO-b-PBCL in $CDCL_3$ (**Figure 4-1 A)** shows peaks at δ 1.2 (t), 1.25-2 (m), 3.65 (s) , 4.05 (t) , 4,65 (t), 5.15 (s), 7.35 (s). On the other hand, ^{1}H-NMR of the reduced polymer PEO-b-PCCL in $CDCL_3$ (**Figure 4-1 B)** shows the disappearance of the characteristic phenyl peak at δ 7.35. Synthetic scheme for the preparation of p160-b-P(CL-PTX) through conjugation of PTX to the acetal-PEO-b-PCCL in the presence of DCC and DMAP is illustrated in **Scheme 4-1.** The completeness of the esterification reaction is confirmed through TLC, where almost no visible spot is seen for free PTX under the UV lamp. Further confirmation of the success of the conjugation reaction is provided through the comparison of the ^{1}H NMR spectra of acetal-PEO-PCCL (**Figure 4-1 B)** to that of PTX (**Figure 4-1 C)** and acetal-PEO-b-P(CL-PTX) (**Figure 4-1 D)**. The results of the TLC and ^{1}H NMR provided a clear evidence of the success of the conjugation reaction and the efficient removal of any free PTX during the purification step through DMSO dialysis. The PTX content of the conjugate calculated by comparing the peak intensity of the phenyl protons signals (δ=7.3-8.4 ppm) and ethylene protons (δ=3.7) of the PEO in the ^{1}H NMR (**Figure 4-1 D)**, was ~ 16% by weight. The substitution level of PTX on the polymer on molar basis was ~19.8 % (moles PTX/moles monomer). This corresponds to 1.39 PTX molecules per acetal-PEO_{114}-b-$P(CL)_7$ chain on average.

Micelles decorated with p160 were prepared using acetal-PEO-b-P(CL-PTX) polymeric conjugate **Scheme 4-1**. The peptide conjugation reaction proceeded through Schiff's base formation between the acetal and N-terminal amino group of the p160 peptide. This coupling method did not require any chemical modification in the structure of the peptide. The conjugation efficiency of the peptide was measured through RP-HPLC. The standard free p160 eluted at 25.7 min with any interference of the polymeric conjugate peak. The reaction mixture chromatogram did not show any characteristics peak for the unreacted p160 implying 100% conjugation efficiency of the peptide. The molar conjugation % for p160 was 8.41%. This means there is one p160 molecule per approximately 13 polymeric conjugate molecules.

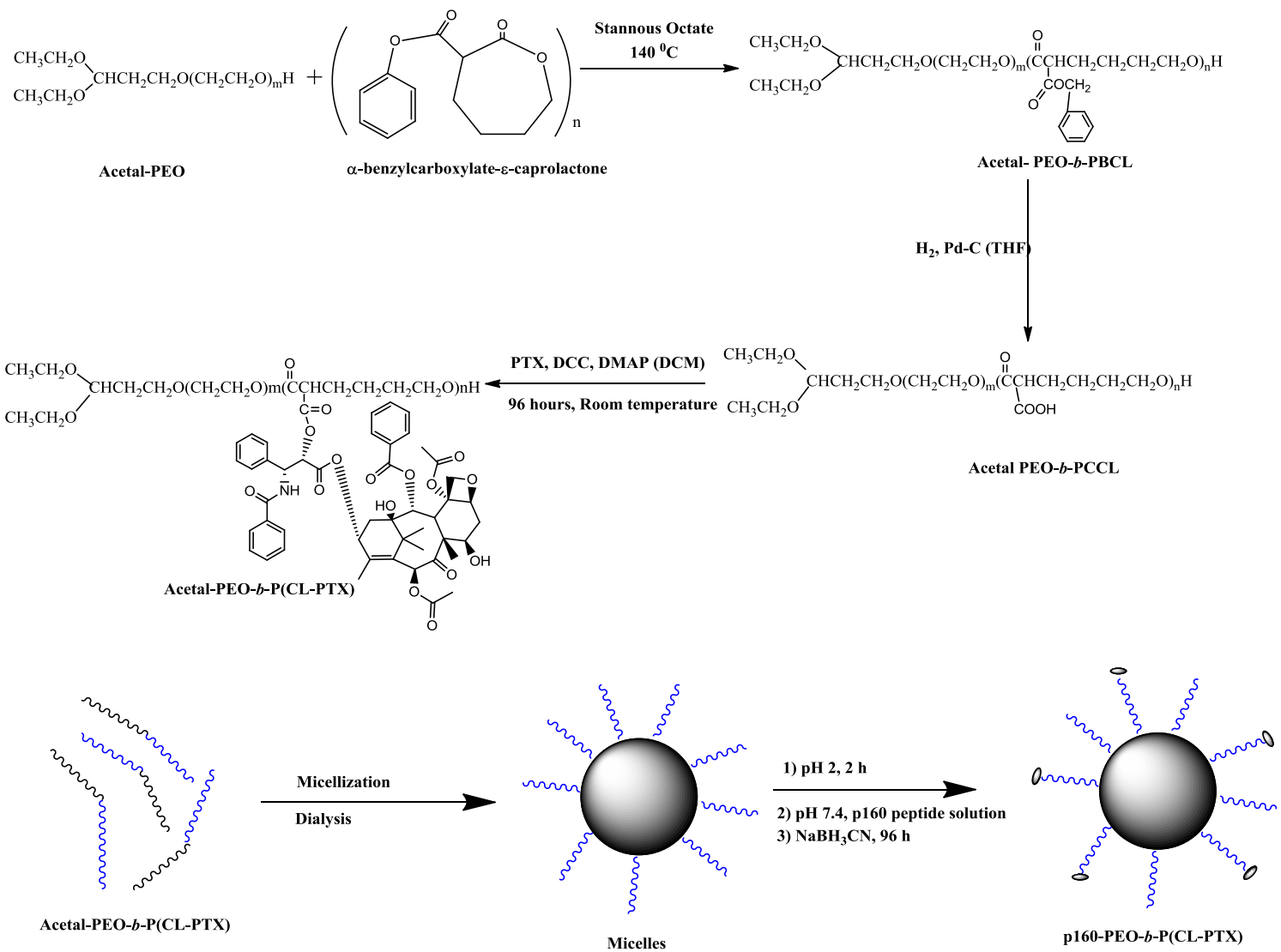

Scheme 4-1: Scheme showing the preparation method of p160-PEO-b-P(CL-PTX).

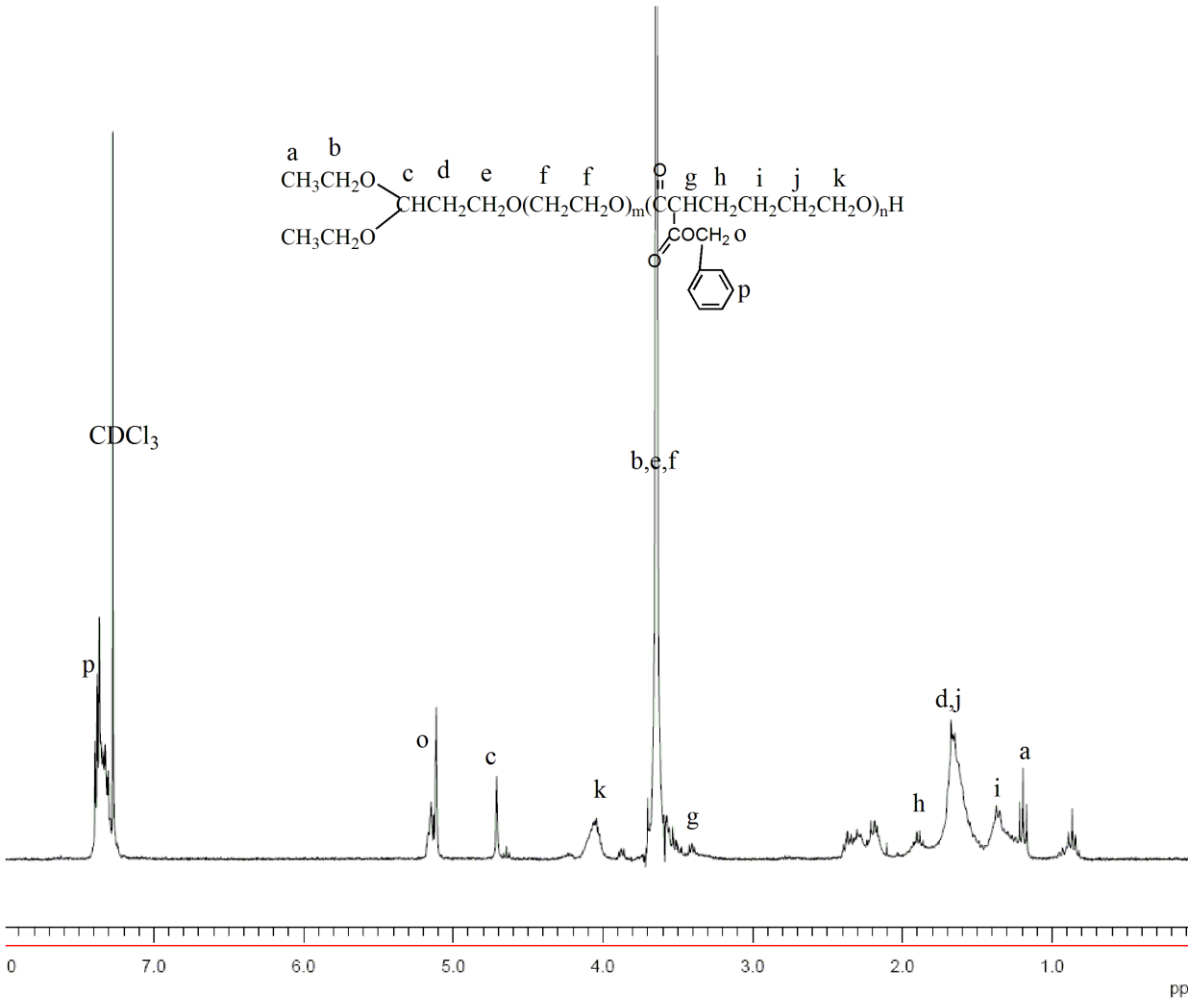

Figure 4-1 A: ^{1}H NMR and peak assignments of acetal-PEO-b-PBCL

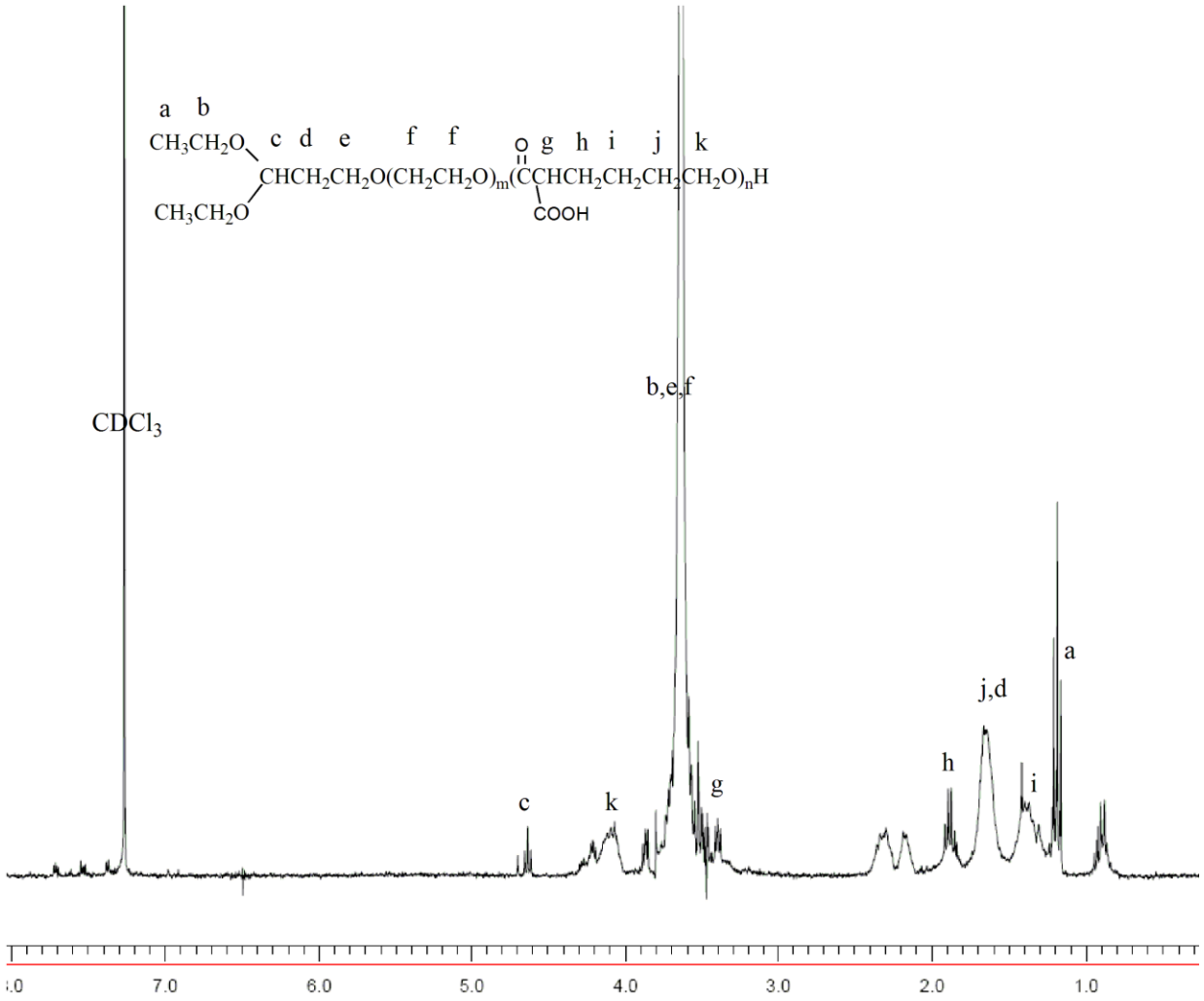

Figure 4-1 B: ^{1}H NMR and peak assignments of acetal-PEO-b-PCCL

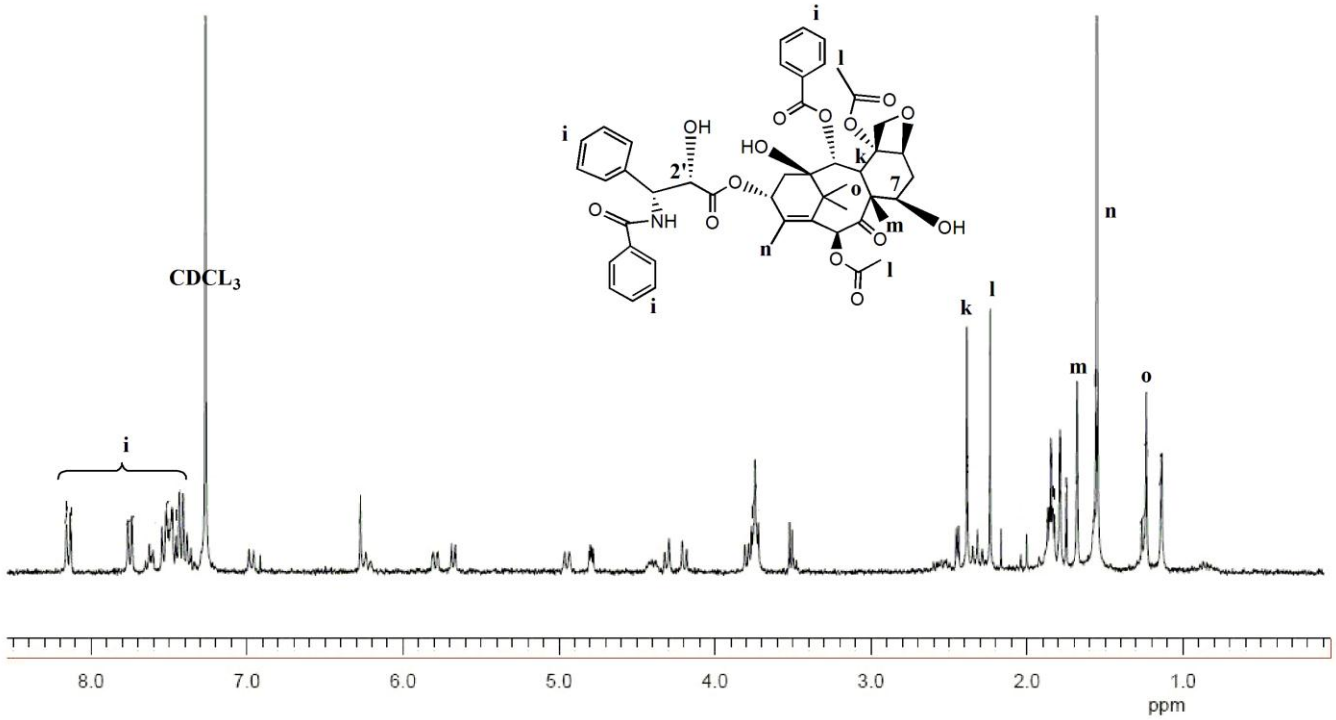

Figure 4-1 C: ^{1}H NMR and peak assignments of PTX

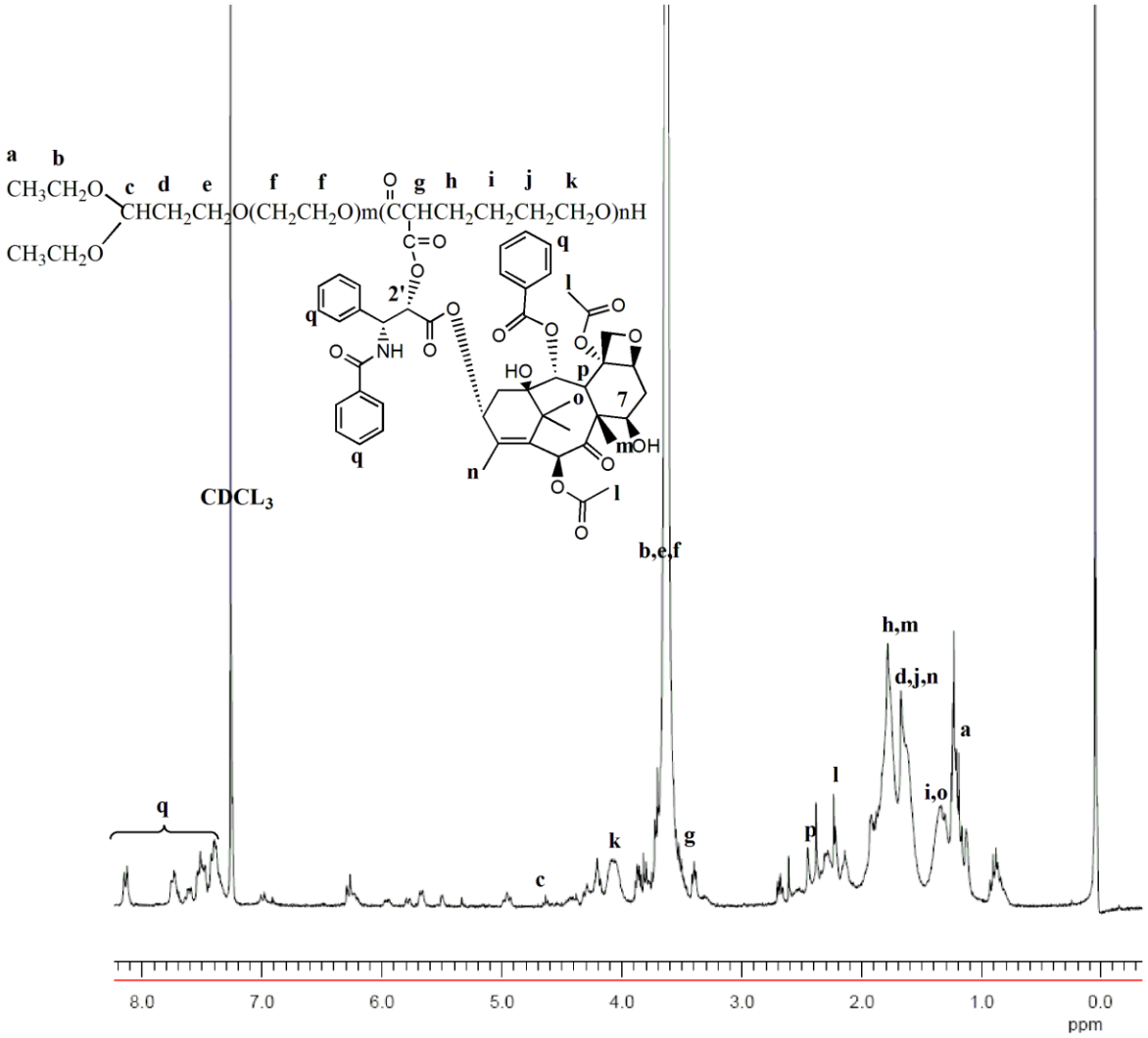

Figure 4-1 D: ^{1}H NMR and peak assignments of acetal-PEO-b-P(CL-PTX).

The results of the characterization studies on the prepared block co-polymers and polymeric micelles are summarized in (**Table 4-1).** The average hydrodynamic diameter of polymeric conjugates acetal-PEO-b-P(CL-PTX) and p160-PEO-b-P(CL-PTX) determined by DLS, was 78.2 and 101.4 nm, respectively. Micelles of acetal-PEO-b-P(CL-PTX), and p160-PEO-b-P(CL-PTX) showed secondary peaks at larger diameters (358.8 and 280.6 nm, respectively). Polymeric conjugates of PTX showed also high polydispersity values ranging from (0.62-0.77) compared to micelles prepared by acetal-PEO-PBCL (0.2).

4.3.2 In vitro cytotoxicity studies

The cytotoxicity of free PTX, free p160, PEO-*b*-P(CL-PTX), and p160-PEO-*b*-P(CL-PTX) against human MDA-MB-435 cancer cells using MTT assay is shown in **Figure 4-2** and **Figure 4-3.** Free p160 showed almost negligible cytotoxicity against the MDA-MB-435 after 72 h incubation in the studied concentration range (12.5 – 0.006 µg/mL). p160 bearing PEO-*b*-P(CL-PTX) showed enhanced cytotoxicity against MDA-MB-435 cells compared to unmodified PTX polymeric conjugate (IC_{50} of 154.9 ng/mL for the p160-PEO-b-P(CL-PTX) versus 674.6 for the PEO-b-P(CL-PTX)). This corresponds to 3.5 folds increase in the cytotoxicity of the conjugated PTX. On the other hand, the p160-PEO-b-P(CL-

PTX) still showing reduced cytotoxicity in comparison to free PTX (IC_{50} of 3.5 ng/mL).

Table 4-1: Characteristics of prepared block copolymers and empty polymeric micelles.

Block copolymer[a]	M_n ($g.mol^{-1}$)[b]	Polydispersity (M_w/M_n)[c]	Average micellar size [d] ± SD (nm)	Average size of secondary peak (nm)	PDI[h]
Acetal-PEO_{114}-*b*-$PBCL_{12}$	7930	1.343	100.2 ± 3.8	N/A	0.202 ± 0.078
Acetal-PEO_{114}-*b*-$P(PTX\text{-}CL)_7$	7350	1.318	78.2 ± 0.2	358.8 (52%)[m]	0.620 ± 0.003
p160-PEO_{114}-b-$P(PTX\text{-}CL)_7$	7400	1.09	101.4 ± 8.3	280.6 (33.2%) [m]	0.770 ± 0.075

[a] The number showed as subscript indicates the polymerization degree of each block determined from ^{1}HNMR spectroscopy.

[b] Number average molecular weight measured by ^{1}H NMR.

[c] Polydispersity = M_w/M_n measured by GPC

[d] hydrodynamic diameter estimated by DLS.

[h] Polydispersity index estimated by DLS

[m] Numbers in the parenthesis indicate the frequency of secondary peak in micellar population in percentage.

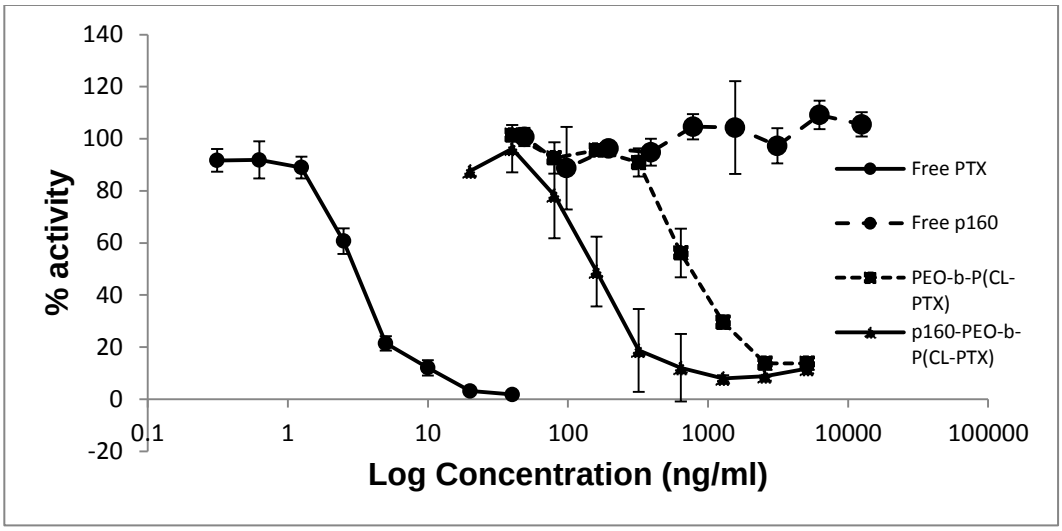

Figure 4-2: Cytotoxicity profile of p160-PEO-P(CL-PTX) in comparison to PEO-b-P(CL-PTX), free PTX, free p160 against MDA-MB-435 cells after 3 days incubation .

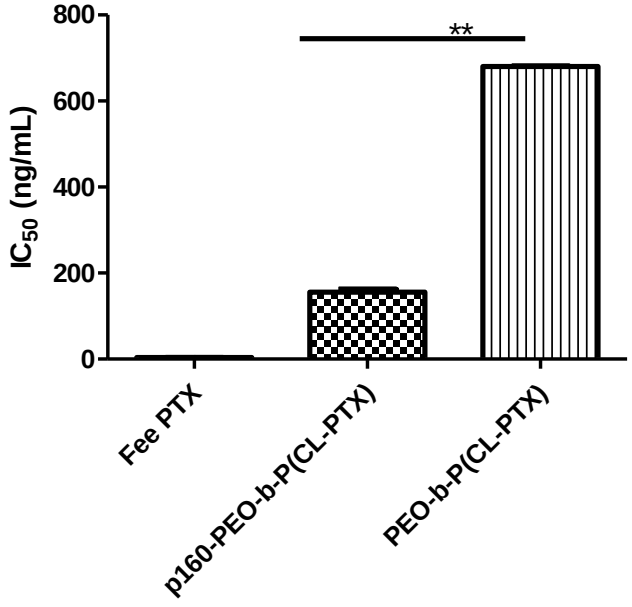

Figure 4-3: IC_{50} values of p160-PEO-b-P(CL-PTX) , PEO-P(CL-PTX), and free PTX against MDA-MB-435 cells after 3 days incubation. ** denotes statistically significant difference (P<0.05).

4.4 Discussion

The main objective of this study is to assess the feasibility of self-assembled multifunctional polymeric conjugate of PTX with hydrolysable polyester core and modified at the same time with breast cancer targeting peptide, p160, for tumor targeted delivery of conjugated PTX. The potential of this architecture to improve the cytotoxicity of chemically conjugated PTX to breast cancer cells MDA-MB-435 was investigated. Our research group similarly developed GRGDS-PEO-b-P(CL-DOX) through covalent attachment of DOX by an amide bond using DCC and NHS chemistry to the hydrophobic PCL block, and GRGDS to the hydrophilic PEO block through Schiff's base formation [459]. The acetal-PEO-b-P(CL-DOX) polymeric conjugate showed signs of core degradation at low pH values (i.e. pH 5) with formation of 2-DOX-6-hydroxy hexanoic acid (DOX-HA) and 2-(4-hydroxybutyl)malonic acid (HBMA) as possible degradation products. In vitro cytotoxicity studies involving the metastatic melanoma cells B16F10 showed superior cytotoxicity of GRGDS modified polymeric conjugate compared to unmodified conjugate with almost 1.8 and 2.7 folds decrease the IC_{50} values against B16F10 cells after 24 and 48 h incubation, respectively.

In this study the reaction between the PEO-PCCL and the PTX probably proceeded through ester bond formation between the pendent carboxyl groups of

the PCCL block and the 2' hydroxyl group of PTX since steric hindrance decreases the possibility of the reaction with 7' hydroxyl group of PTX [448]. Compared to Xytotax ® that contains 36% by weight PTX which correspond to one PTX molecule per 11 glutamic acid units, our conjugate contains ~16% by weight PTX that represent one PTX molecule per 5 units of caprolactone. The majority of micelles prepared from this polymer-PTX conjugate showed small hydrodynamic diameters on average (<100 nm) that is necessary to promote the carriers extravasation by EPR effect. The high degree of the polydispersity (0.62-0.77) of these structures may be a reflection of the secondary association of these PTX bearing polymeric conjugates. A possible reason for this aggregation is through the association of free un-esterified COOH groups in the poly(caprolactone) block. Similar observation has been reported by Mahmud et al. with micelles prepared by block copolymer of PEO-PCCL using co-solvent evaporation method [476].

The MDA-MB-435 cells are chosen for this study as a model for untreated breast cancer patient with no prior exposure to systemic chemotherapy due their few endogenous drug resistance mechanisms [477]. The enhanced cytotoxicity of p160-PEO-P(CL-PTX) in comparison to PEO-P(CL-PTX) could be due to

increased cellular uptake of p160 modified PTX polymeric conjugate through receptor mediated endocytosis.

On the other hand, the reduced cytotoxicity of p160-PEO-P(CL-PTX) in compare to free PTX could be attributed to the different cellular uptake pathways between the polymeric conjugate and free PTX (receptor mediated endocytosis vs. simple diffusion, respectively), slow release of PTX derivatives from the polymeric conjugate through the hydrolytic cleavage of the ester bonding in the PCL backbone as pointed out in our previous study with PEO-b-P(CL-PTX); or slow cleavage of free PTX from PCL backbone [457]. The latter two mechanisms can be accelerated upon internalization of p160-decorated polymeric micellar conjugate into the endosomal compartments of the cells as a result of accelerated uptake of those micelles by cancer cells expressing p160 receptors.

Better results in terms of the cytotoxicity and specificity against breast cancer tumour cells could be achieved through increasing the PTX conjugation level to the PCL backbone and through attachment of peptide analogues with more affinity to target breast cells.

4.5 Conclusion

Actively targeted, self-assembled polymeric conjugate of PTX containing PTX attached to PEO-b-PCL polymer chain has been successfully developed. This conjugate demonstrated significantly higher cytotoxicity in human breast cancer cell line MDA-MB-435 compared to unmodified PEO-b-P(CL-PTX) polymer conjugate. This study clearly shows the potential of p160 peptide as a targeting

ligand to improve the cytotoxicity of polymer drug conjugates. Further studies involving conjugate development with higher PTX conjugation level and higher affinity peptide (i.e.p18-4) is recommended. Also, additional experiments for better understanding the in vivo pharmacokinetics and therapeutic efficacy of this conjugate in several tumour models is warranted. Although, we were successful to show the in vitro benefits of several peptide decorated polymeric carriers, unfortunately we could not concentrate these carriers to a therapeutically effective concentration that we could inject into suitable animal model. Therefore, we decided to shift our research toward investigating doxorubicin liposomal formulations bearing analogue of the p160 peptide (i.e. p18-4) on their surface as a better approach to show the potential of peptide decoration on the efficacy of nanocarriers in vivo. In the next chapter, we studied the development of actively targeted DOX liposomal formulations modified with p18-4 peptide on their surface.

Chapter 5
Engineered peptides for the development of actively tumor targeted liposomal carriers of Doxorubicin[19]

[19] A version of this chapter has appeared in: Shahin M, Soudy R, Kaur K, Lavasanifar A. Engineered peptides for the development of actively targeted liposomal carriers of Doxorubicin. Cancer Letters, accepted with minor revisions.

5.1 Introduction

Conventional chemotherapy is the treatment of choice for many cancers, but its effectiveness has been limited. Severe side effects by chemotherapeutics, resulting from non-selective action and distribution of anticancer drugs, are one of the major reasons for this shortcoming [478-482]. Evidence from preclinical and clinical investigations, have shown a benefit for the use of properly designed drug carriers in reducing the side effects and toxicity of incorporated anticancer drugs against healthy tissues.

The use of liposomes is recognized as a promising strategy for improving the selective delivery of anticancer drugs to tumors, leading to reductions in drug toxicity and improvements in therapeutic outcomes [180, 483]. Liposomal carriers of appropriate size range (70-150 nm) can avoid extravasation through continues capillaries of healthy tissues and provide a physical barrier for exposure of encapsulated drug to healthy cells, if the drug can be retained within the carriers. Carriers of this size range and hydrophilic surface characteristics can also avoid early filtration by kidneys and escape removal by mononuclear phagocytes (i.e., show stealth property). This will lead to the circulation of stealth liposomes for prolonged periods in blood leading to a better probability for liposomal carrier for permeation through newly-induced leaky vasculature of solid tumors. Owing to the impairment of the lymphatic drainage, the permeated nano-carrier can retain in tumor site and provide a high and steady level of anticancer drug to tumor cells. This phenomenon known as Enhanced Permeation and Retention (EPR) effect is believed to be the reason for passive accumulation of nanocarriers in solid tumors

and their therapeutic benefit over conventional formulations in cancer therapy. Most anticancer agents; however, act on intracellular targets and their effectiveness can be further improved by facilitating cellular drug uptake. This is possible by decorating the drug carrier with tumor cell binding molecules, which may result in improved retention of the carriers at tumor sites (i.e. by reducing passive transport away from tumor), and/or enhanced uptake of the drugs by tumor cells. Antibodies have been used as tumor-binding ligands [484-487]. Compared to monoclonal antibodies, targeting through small peptides is preferred due to the smaller size and flexibility for chemical modifications of peptide structure [3, 310]. Engineered peptide sequences containing (Arginine-Glycine-Aspartic acid) RGD or (Asparagine-Glycine-Arginine) NGR have been widely used as tumor targeting ligands [282, 488-491]. The NGR and RGD peptides target the isoform of aminopeptidase N (APN), and $\alpha_v\beta_3$ integrin receptors, respectively [289, 492-495]. These receptors are overexpressed on the endothelial cells of angiogenic vessels and also on some tumor cells. Cancer therapy using liposomes modified with either NGR or RGD [279, 496], where liposomes were loaded with different chemotherapeutic agents, e.g. doxorubicin [279, 496], 5-fluorouracil (5-FU), has been reported. [286]. Although RGD and NGR peptides are promising reagents for some tumors, their target also include non-tumorigenic tissues. Moreover, the target of RGD and NGR peptides is highly expressed on the endothelial cells of angiogenic blood vessels in tumor. As a result, RGD and NGR modified carrier can be sequestered by tumor endothelium. This can restrict their access and interaction with tumor cells.

Our research team is investigating the use of cancer targeting peptides that are more cancer selective than RGD and NGR sequences, for active drug targeting to breast tumor cells. In this context, a linear dodecapeptide, p160 (VPWMEPAYQRFL), has been used as a targeting ligand to decorate polymer based nanocarriers providing active anticancer drug delivery to breast tumor cells [309, 310]. p160 was first separated from a peptide library developed by phage display for its high affinity for neuroblastoma cells [308]. Later, it was found to strongly attach and get internalized by several breast cancer cells (MDA-MB-435, and MCF-7), but not by healthy human umbilical vein endothelial cells (HUVEC). Radio-labelled p160 achieved better tumor targeting *in vivo* compared to RGD4C [310]. We have also reported on the engineering of p160 peptide leading to the development of analogue, namely p18-4 (WxEAAYQrFL), with better selectivity for cancer over normal cells and improved stability in biological fluids [312]. The aim of this paper was to assess the potential of the engineered p18-4 peptide as ligands for breast tumor targeting by liposomal nanocarriers. Three different coupling methods, namely: conventional, post conjugation, and post insertion, were used to prepare p18-4 decorated liposomal DOX, and the effect of peptide coupling method on the cytotoxicity and cellular uptake of liposomal formulations of DOX was evaluated.

5.2 Material and methods

5.2.1 Materials

Hydrogenated soy phosphatidylcholine (HSPC) and methoxypoly(ethylene glycol) (MW 2000 Da), covalently linked to 1,2-

distearoylphosphadidylethanoloamine ($mPEG_{2000}$-DSPE), were generous gifts from ALZA Corporation, Inc. (Mountain View, CA). DSPE-PEG_{3400}-NHS was purchased from Nanocs. (New York, NY). Cholesterol (CHOL) was purchased from Avanti Polar Lipids (Alabaster, AL). Doxorubicin hydrochloride (purity > 98%) was purchased from Ontario Chemicals, INC. (Guelph, ON). [3-(4,5-dimethylthiazol-2-yl)-2,5-diphenyl] tetrazolium bromide (MTT) was purchased from Sigma-Aldrich (St. Louis, MO, USA). 2-Chlorotrityl chloride resin (1 mmol/g), (2-(6-chloro-1H-benzotriazole-1-yl)-1,1,3,3-tetramethylaminium hexafluorophosphate) (HCTU), 1-hydroxybenzo triazole (HOBt), and the Fmoc-amino acids were purchased from Nova Biochem (San Diego, CA). Piperidine, N, N diisopropyl ethylamine (DIPEA), N-methyl morpholine (NMM), trifluoroacetic acid (TFA), Triisopropylnaphthalenesulfonic acid sodium salt (TIPS), N-(3-dimethylaminopropyl)-N-ethylcarbodiimide hydrochloride (EDC) and (Sulpho-N-hydroxysuccinimide) (S-NHS) were purchased from Sigma-Aldrich. The p-18-4 peptide is kindly provided by Dr. K.Kaur ‘s lab. All solvents used in purification were HPLC grade. All other chemicals are reagent grade and are purchased from Caledon Laboratories Ltd. (Canada).

5.2.2 Cell lines

The human cancer cell lines MDA-MB-435 were cultivated at 37 ^{0}C in a 5% CO_2 incubator. They were received as a gift from the laboratory of Dr. R. Clarke (Georgetown University, USA). These cells were cultured in RPMI 1640 with 1% L-glutamine, and 10% FCS (Invitrogen, Karlsruhe, Germany), 100 IU/mL penicillin, and 100 IU/mL streptomycin.

5.2.3 Peptide synthesis

Mrs. Rania Soudy developed and synthesized the p18-4 peptide (WxEAAYQrFL) (**Figure 5-1**). It is synthesized manually using solid phase peptide synthesis on 2-chlorotrityl chloride resin as described previously [312]. Briefly, the first Fmoc-amino acid was coupled using DIPEA. Further amino acids were coupled at two-fold excess using HCTU/HOBt/NMM in DMF. After completion of the synthesis, peptides were cleaved from resin and all protecting groups were removed. The cleaved peptide combined with TFA washes was concentrated by rotary evaporation. Crude peptides were dissolved in water and purified using reversed-phase HPLC to obtain pure peptides in 45 to 70% yield.

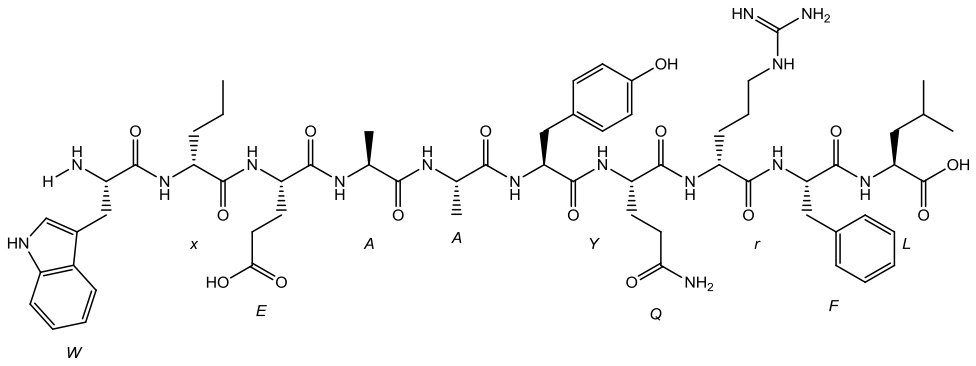

Figure 5-1: Chemical structure of p18-4.

5.2.4 Synthesis of p18-4-PEG-DSPE

The activated DSPE-PEG-NHS was used to conjugate p18-4 peptide to DSPE-PEG. In brief, the peptides and DSPE-PEG-NHS (peptide:DSPE-PEG-NHS 1:3 moles) were dissolved in PBS 7.4 and stirred for 24 h at room temperature (**Figure 5-2A**). The conjugation of peptide with the PEG was confirmed by RP-

HPLC method [241]. Briefly, A µ Bondpack (Waters Corp., United States) C18 analytical column (10 mm 3.9 x 300 mm) was used. Gradient elution was performed at a flow rate of 1 mL/min using a Varian Prostar 210 HPLC System. Detection was performed at 214 nm using a Varian 335 detector (Varian Inc., Australia). The mobile phase consisted of 0.1% Trifluoroacetic acid (TFA) in H2O (solution A) and 0.1% TFA in 90/10 Acetonitrile/H_2O. The mobile phase was programmed as follows: (1) 100% A for 1 min (2) linear gradient from 100% A to 60% A in 20 min (3) linear gradient from 60% A to 0% A in 4 min (4) 0% A for 2 min (5) linear gradient from 0% A to 100% A in 4 min (6) 100% A for 5 min. The concentration of unreacted peptide was calculated based on a calibration curve for the peak height of known concentrations of peptide in double distilled water. Finally the reaction mixture was dialyzed extensively (MW cut off 3500 Da) against distilled water for 24 h to remove all impurities and then lyophilized.

5.2.5 Preparation of p18-4 decorated Liposomes

The p18-4 targeted liposomes were prepared using three different methods: conventional (Con), post insertion (PI), and post conjugation (PC) methods.

a. Conventional (Con) method A mixture of HSPC: CHOL: $mPEG_{2000}$ DSPE: p18-4-PEG_{3400}- DSPE (1.5:1: 0.125: 0.015) in chloroform: methanol (2:1), was used to prepare the lipid film by rota-evaporation for 1 h (Rotavapor RE 111, Switzerland). The film was then placed in a desiccator overnight. The lipid film was hydrated at a concentration of 10–30 mM phospholipid (PL) with 250 mM ammonium sulfate. Hydrated liposomes were extruded at 65 °C using a Lipex

extruder (Northern Lipids, Vancouver, Canada) through a series of polycarbonate filters, with pore sizes from 0.22 μm to 0.1 μm (**Figure 5-2B**).

b. Post insertion (PI) method Peptide-PEG_{3400}-DSPE micelles were prepared using mPEG-DSPE:p18-4-PEG-DSPE (4:1) (**Figure 5-2C**). The micellar dispersion was then co-incubated with preformed plain DOX liposomes at 60 °C for 30 min. Uncoupled peptide were separated from the liposomes by passing the mixture through a Sepharose CL-4B column in PBS (pH 7.4). The efficiency of coupling was determined by estimating the amount of free unreacted peptide by RP-HPLC [241].

c. Post conjugation (PC) method A mixture of HSPC:CHOL:DSPE–PEG_{3400}–COOH (1.5:1:0.14) was used to prepare empty liposomes by film hydration method as previously mentioned. Then, DOX was encapsulated into the liposomes using the ammonium sulfate gradient method (described below). Conjugation of p18-4 to the liposomal surfaces was achieved by adding 360 μL of both 0.5M EDC and 0.5 M S-NHS per 10 μmol of lipid for 10 min, at pH 5.2 adjusted by citric acid (**Figure 5-2D**). The pH was then adjusted to 7.4 with 0.1M NaOH. p18-4 (125 μg/μmol phospholipid) was added and gently stirred for 8 h at 4 ^{o}C. The level of peptide on the liposomal surface was estimated by RP-HPLC [241]. Unbound peptide was removed by passing the liposome suspension through a Sephadex G-50 gel column.

Untargeted liposomes were prepared by Con method using HSPC:CHOL:DSPE-PEG3400 (1.5:1: 0.14) micelles . The size of liposomes was determined using dynamic light scattering.

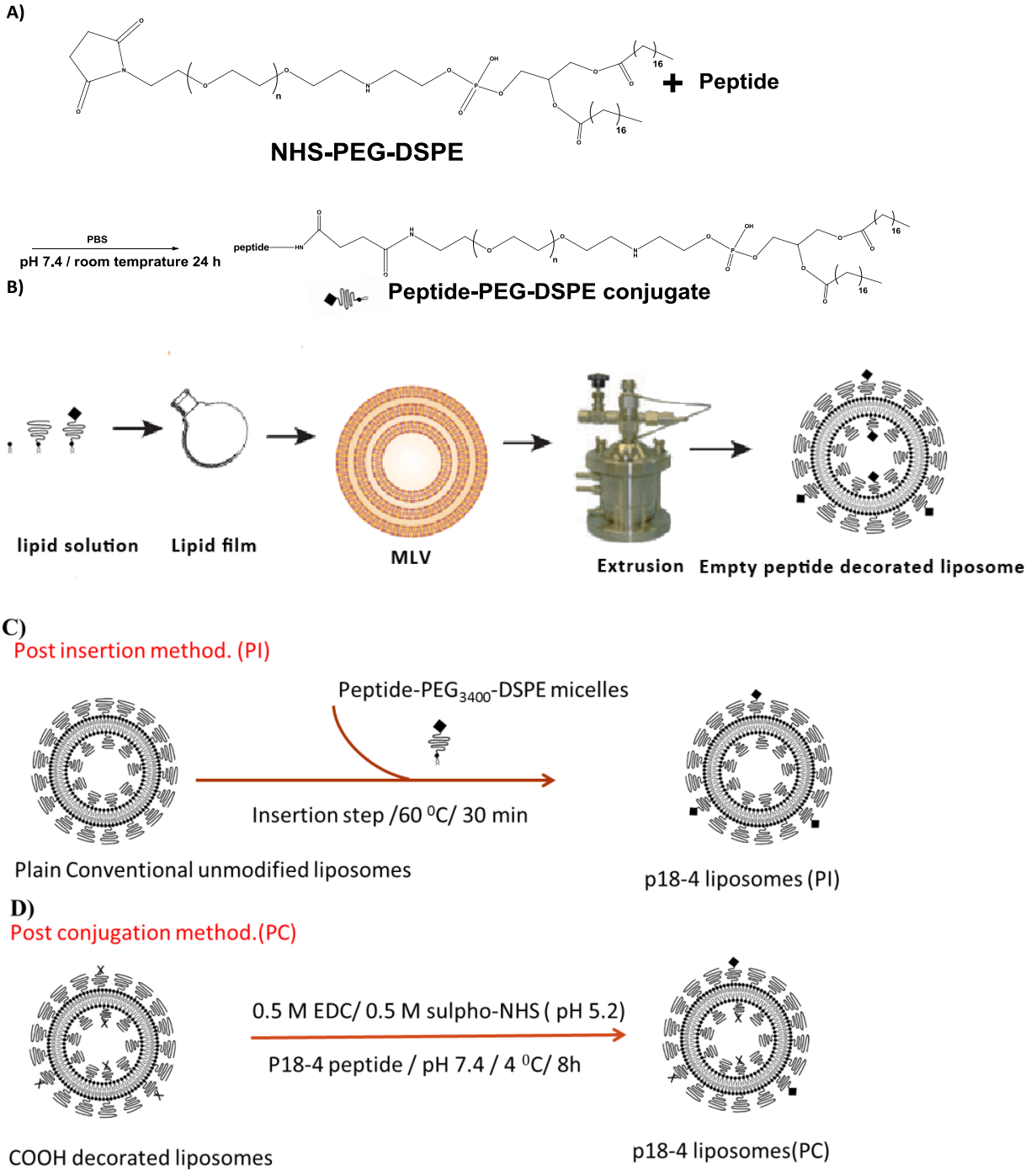

Figure 5-2: Models for the A) synthesis of peptide-PEG-DSPE conjugate, and preparation of peptide decorated liposomal DOX through B) conventional, C) post insertion and D) post conjugation methods.

5.2.6 DOX encapsulation in liposomes

DOX was encapsulated into the liposomes using an ammonium sulfate gradient. After removing the extra-liposomal salt by a Sephadex G-50 column in 10% sucrose, DOX solution (2 mg/mL) was added immediately into this solution at a concentration of 0.2 mg DOX/ mg HSPC phospholipid. The mixture of liposome and DOX was incubated in 60 °C water bath for 30 min with agitation. After loading, un-trapped DOX was removed by Sephadex G-50 gel filtration in PBS pH 7.4. The amount of DOX trapped inside the liposomes was determined spectrophotometry at 485 nm, after diluting aliquot of the liposomes with methanol. Liposome size after DOX loading was measured by dynamic laser scattering (Zetasizer Nano ZS, MA, US).

5.2.7 In vitro DOX release

The *in vitro* release of DOX from p18-4 modified liposomes prepared by different peptide coupling procedures was studied using a dialysis method. Free DOX, unmodified liposomal DOX, or p18-4 liposomal DOX (Con, PI or PC) at equivalent DOX concentration of 400 µg/mL were placed in a dialysis bag (MW cut-off of 3500 Da). Each dialysis bag which contained 3 mL of the formulation was placed into a 500 mL of phosphate buffer pH 7.4 (10 mM). Release study was performed at 37 ^{0}C in a shaking water bath at 100 rpm (Julabo SW 22 shaking water bath, Germany). At selected time intervals, aliquots of 200 µL from the inside of the dialysis bag were diluted with methanol for UV/visible spectroscopy analysis based on absorbance intensity at 485 nm (Beckman Coulter DU 73 UV/Vis spectrophotometer, ON, Canada). The amount of DOX released was

calculated by subtracting the amount of DOX remained in the dialysis bag from the initially added DOX.

5.2.8 In vitro cell uptake studies

The effect of peptide conjugation method on the cellular uptake of encapsulated DOX was assessed using flow cytometry (Beckman Coulter Cell Quanta SC, ON, Canada). MDA-MB-435 cells were seeded into 24-well plates at densities of $1x10^5$cells/well, and incubated at 37 ^{0}C for 24 h till 70% confluence reached. Unmodified liposomal DOX, p18-4 liposomal DOX (Con, PI, and PC), and free DOX at a concentration of 5 µg/mL equivalent DOX were incubated with the cells at 37 ^{0}C for 24 h. For the competition experiments, MDA-MB-435 cells were pre-incubated with excess free p18-4 peptide (1 mg/mL) for 30 min to assess the receptor mediated endocytosis by inhibiting the binding and internalization of peptide conjugated liposomes by free peptide interacting with the receptors. The medium was aspirated and cells were rinsed with cold PBS three times. Then the cells were detached using trypsin EDTA and suspended into PBS solution containing 4% formalin. Five thousand cells were counted with logarithmic settings. The cell-associated DOX was excited with an argon laser (488 nm) and the fluorescence was detected at 560 nm. All data are expressed in mean fluorescence intensity ± standard deviation (SD) (n=4).

5.2.9 In vitro fluorescence microscopy studies

Fluorescence microscopy was used to compare the intracellular distribution and cellular uptake of DOX loaded unmodified liposomes, p18-4

liposomes (PI, and PC). In this regard, 1x 10^4 MDA-MB-435 cells were cultured on the top of sterile cover slip at 37 ºC for 24 h till 50% confluent. Then, the media was removed and replaced with 1 mL containing DOX loaded formulations at a concentration of 5 µg/mL. The cells were incubated with the formulations for 24 h at 37 ºC. After incubation, the media was removed and the cells were washed with serum free media (3 x 2 mL). The cells were fixed on ice with 2% formaldehyde for 20 min. The formaldehyde was removed by washing with media (3 x 2 mL). The cover slips were put on slides containing one drop of DAPI-antifade (Molecular Probes, Invitrogen Co., OR, USA) to stain the nucleus. The cells were imaged under the fluorescence microscope (Carl Zeiss microscope system ,Jena, Germany) with 40x magnification using oil immersion lens.

5.2.10 In vitro cytotoxicity studies

MTT assay was used to study the cytotoxicity of DOX as part of unmodified and p18-4 modified liposomes against MDA-MB-435 cells. Briefly, 10000 cells were seeded in each well of 96 well plates. After 24 h, the cells were exposed to serial dilutions of free DOX, unmodified liposomal DOX and p18-4 decorated liposomal DOX prepared by different methods (Con, PI, PC). After 24 h, the cell monolayer was washed with PBS. Then, 20 µL of MTT solution (5 mg/mL) was added to each well, followed by incubation for another 4 h at 37 ^{0}C. Finally, the medium was replaced by 200 µL of dimethyl sulphoxide (DMSO), and the absorbance was read on Power Wave x 340 Microplate Reader (Bio-tek instruments Inc., USA) at wavelength of 570 nm. The data reported represent the

means of triplicate measurement. The IC_{50} was calculated from the plot of the % of viable cells vs. log DOX concentration.

5.2.11 Statistical analysis

Data are presented as mean ± SD of triplicate measurements unless mentioned otherwise. Statistical significance of difference was tested either using unpaired students' t-test or one-way ANOVA test with Tukey post-test analysis. The significance level (α) was set at 0.05. All data that required non-linear regression analysis were processed using (Graphpad prism, version 5.00, Graphpad Software Inc., La Jolla, CA, USA).

5.3 Results

5.3.1 Preparation and physicochemical characterization of p18-4 decorated liposomal DOX

The conjugation of the p18-4 peptide to NHS-PEG-DSPE was confirmed by RP-HPLC by measuring the level of unreacted peptide in the unpurified sample. The standard free p18-4 peptide eluted at retention time 27.5 min. The peptide conjugation efficiency was ~ 35% for p18-4. This corresponds to a p18-4 density of 0.3 mole% on liposomal carrier prepared either by Con or PI methods assuming the incorporation of 100% of p18-4-PEG-DSPE to the liposomal carrier. For the liposomes prepared by the PC method the level of unreacted peptide measured by HPLC was 65%. This corresponds to a peptide conjugation efficiency and density of 35% and, 0.3 mole% , respectively. Characteristics of prepared liposomes are summarized in **Table 5-1**.

Before conduction of further studies, liposomes were extensively dialysed against distilled water to separate any impurity. DOX was successfully loaded in to liposomes using a gradient technique. The particle size of prepared liposomes was around 130 nm and the polydispersity index (PDI was < 0.048. Method of liposome preparation did not affect the size of liposomes and their PDI (**Table 5-1**). Peptide incorporation in the liposomal structure also did not affect the average diameter and PDI of liposomes. Except for the p18-4 liposomes (PI), the encapsulation efficiency of DOX was > 95% for all liposomal formulations under study. However, the PI method gave liposomes with DOX encapsulation efficiency of less than 30%.

Table 5-1: Characteristics of DOX loaded liposomes prepared by different peptide coupling techniques

Sample	Z average ± SD (nm)[i]	Polydispersity index ± SD [i]	Peptide density (mole %)	Encapsulation Efficiency (%)
Unmodified liposomes	128.5 ± 1.9	0.048 ± 0.01	0	98.5% ± 2.1
p18-4 liposomes (Con)	124.2 ± 4.5	0.034 ± 0.01	0.3	97.1% ± 1.3
p18-4 liposomes (PC)	125.8 ± 1.4	0.047 ± 0.01	0.3	97.4% ± 1.9
p18-4 liposomes (PI)	129.4 ± 0.6	0.019 ± 0.01	0.3	28.4% ± 1.7

[i] Determined by DLS

The results of the *in vitro* release of DOX from different liposomal formulations and free DOX in phosphate buffer pH 7.4 at 37 ^{0}C are presented in **Figure 5-3.** Free DOX was released from the dialysis bag at a rapid rate (88% within 8h), which means that the transfer of DOX through dialysis membrane to buffer solution is not the restricting factor and the release of DOX from the liposomes is the rate limiting step. p18-4 conjugation to the liposomal shell using either the conventional or post conjugation methods did not significantly affect the release profile of DOX compared to untargeted liposomes. After 3h, p18-4 (Con) and p18-4 (PC) released 15 % and 10 % of DOX content, respectively, which was not different from unmodified liposomes ($P>0.05$). DOX release from p18-4 (Con) and p18-4 (PC) liposomes reached 22 and 17 % within 72 h, respectively, which was again comparable to DOX release from unmodified liposomes ($P>0.05$). p18-4 (PI) released only 6 and 13 % of its DOX content within 3 and 72h, respectively, which was significantly lower than that for unmodified liposomes ($P<0.05$).

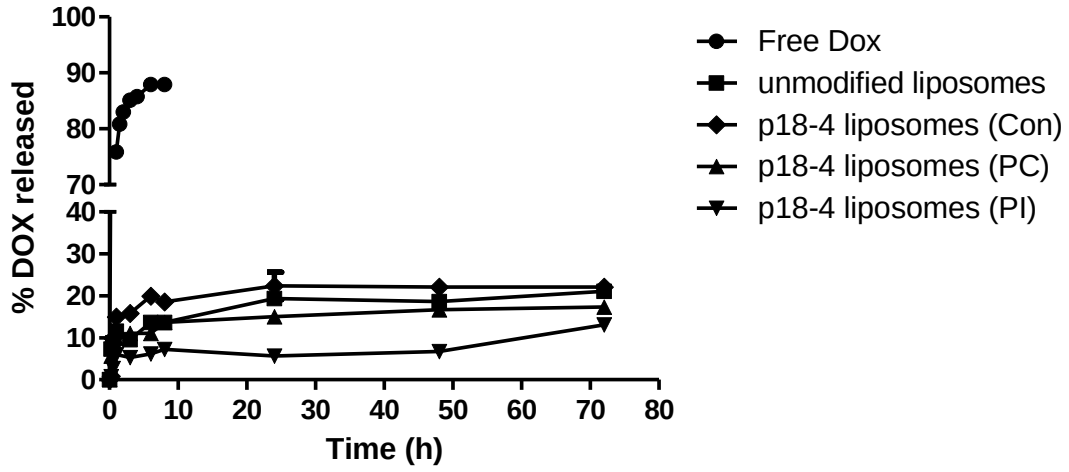

Figure 5-3: The release profile of DOX from various p18-4 modified liposomal formulations prepared by different peptide conjugation methods in phosphate buffer pH 7.4 at 37 ^{0}C in comparison to unmodified liposomal DOX formulation. Each point represents mean ± SD (n=3).

5.3.2 In vitro cell uptake studies

The cellular uptake of different peptide modified liposomal formulations prepared by various peptide conjugation techniques is shown in **Figure 5-4**. After 24 h incubation, flow cytometry showed enhanced cellular uptake of p18-4 (Con) and p18-4 (PC) liposomes by MDA-MB-435 cells in comparison to unmodified liposomes (1.8 and 1.6 folds increase in mean fluorescence intensity, respectively). However, after similar incubation time with p18-4 (PI) liposomes, the mean fluorescence intensity decreased significantly by 1.6 folds compared to cells incubated with unmodified liposomal DOX. To investigate the possible role of receptor mediated cell binding/uptake of p18-4 modified liposomes, we pretreated the MDA-MB-435 cells with 1 mg/mL free p18-4. As shown in

Figure 5-4, 1 mg/mL free p18-4 reduced the cellular uptake of both p18-4 (Con) and p18-4 (PC) liposomes by MDA-MB-435 significantly (44.94 vs. 27.89 and 39.05 vs. 24.63 for p18-4 Con and PC liposomes, respectively; $p<0.05$, Unpaired student's t test). Whereas the uptake of p18-4 (PI) liposomes by MDA-MB-435 cells did not change significantly by pre-treatment with free p18-4 (15.14 vs. 14.2, $p>0.05$; unpaired student's t-test).

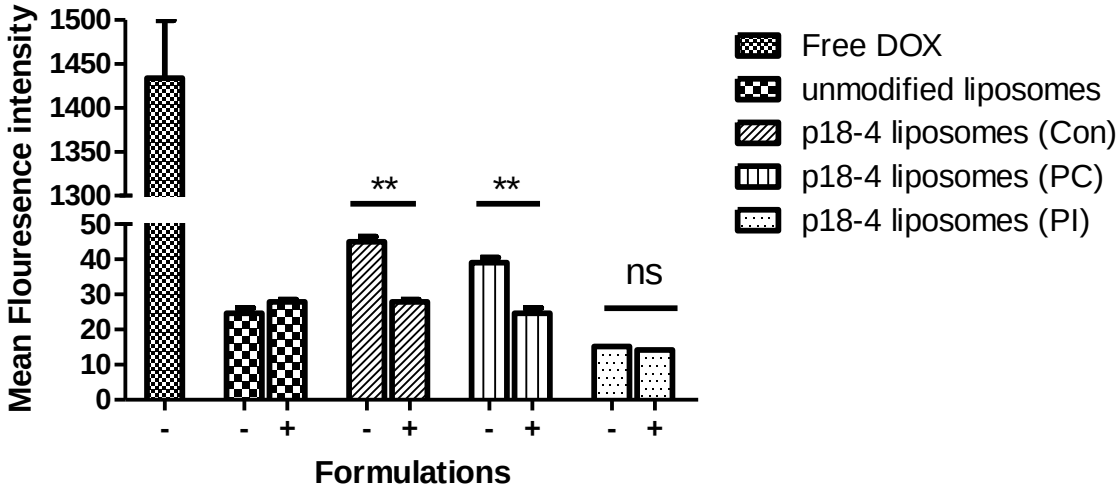

Figure 5-4: *In vitro* cell uptake of free DOX, unmodified liposomal DOX, p18-4 (Con), p18-4 (PC), p18-4 (PI) liposomal DOX by MDA-MB-435 cells with (+) or without (-) pre-treatment with excess of free p18-4 peptide after 24 h incubation. Each bar represents mean fluorescence intensity ± SD (n=4). ** denotes statistically significant difference (P<0.05). ns denotes statistically non-significant difference (P>0.05).

5.3.3 In vitro fluorescence microscopy

Fluorescence microscopy images displaying MDA-MB-434 cells treated with DOX loaded unmodified liposomes, p18-4 liposomal formulations (PI, PC) are shown in **Figure 5-5**. After 24 h incubation, the MDA-MB-435 cells treated with unmodified liposomes and p18-4 liposomes (PI) showed that the majority of

visible DOX fluorescence is mainly localized in the cytoplasmic compartment. However, after similar incubation time cells treated with p18-4 liposomes (PC) showed more intense DOX fluorescence which was mainly localized into the nuclear compartment indicating increased cellular uptake of DOX. Comparison of DOX fluorescence in cells treated with p18-4 liposomes (PI) and p18-4 liposomes (PC) reveals higher cellular DOX accumulation with p18-4 liposomes (PC). Intensity quantification of nuclear DOX fluorescence of unprocessed, raw image data confirmed a statistically significant ($P<0.05$) increase in DOX uptake by MDA-MB-435 cells of approximately 1.3 folds between p18-4 liposomes (PC) and unmodified liposomes (data not shown).

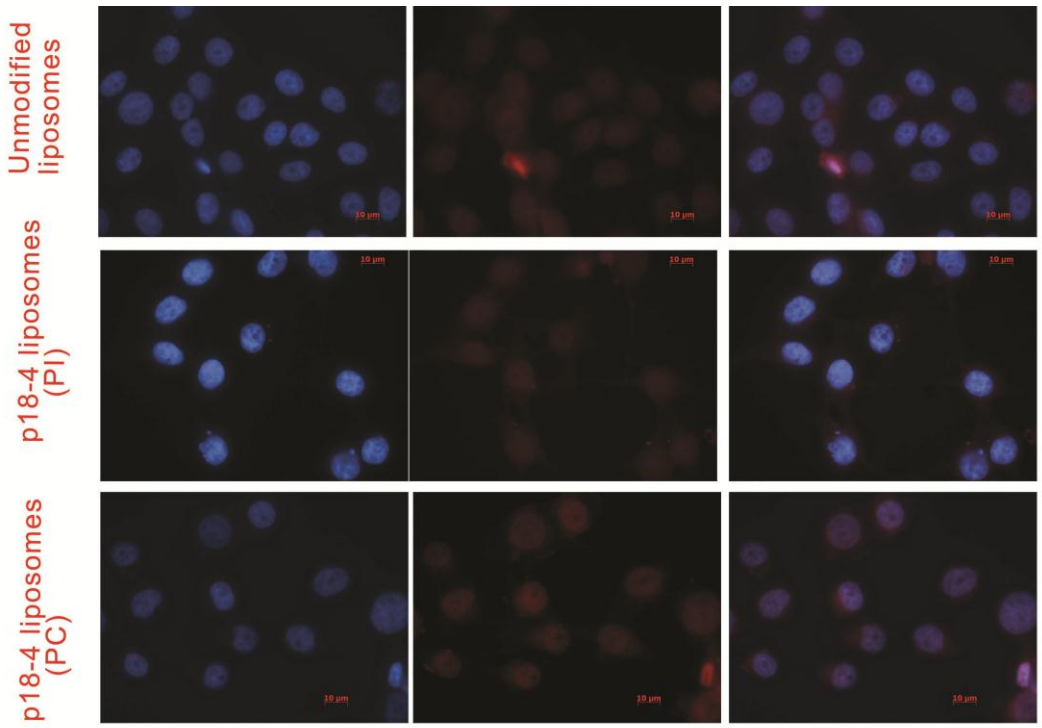

Figure 5-5: In vitro fluorescence microscopy images of DOX accumulation in MDA-MB-43 cells after 24 h incubation with different liposomal formulations. All the three DOX formulations have DOX concentrations of 5 µg/ml. Cells were fixed in 2% paraformaldehyde and treated with DAPI (blue) for nuclei staining. Red: fluorescence of DOX. Blue: fluorescence of DAPI. Co-localization of DAPI and DOX is also represented (the merged fluorescence of blue and red showing pink colour).

5.3.4 In vitro cytotoxicity study

The MTT assay showed that the proliferation of MDA-MB-435 cell was inhibited in a concentration dependant manner for free and liposomal DOX preparations under this study. Free DOX, unmodified DOX liposomes, p18-4 (Con), p18-4 (PC), and p18-4 (PI) DOX liposomes showed IC_{50}s of 0.77, 42.92, 29.85, 33.68, and 124.0 µg/mL against MDA-MB-435 cells, respectively (**Figure 5-6**). Compared to untargeted liposomes, p18-4 modification using either the conventional or post conjugation methods increased the cytotoxicity of incorporated DOX by 1.4 and 1.3 folds, respectively. However, p18-4

modification using the post insertion method showed significant decrease of the cytotoxicity of DOX by 2.9 folds as compared to unmodified liposomes.

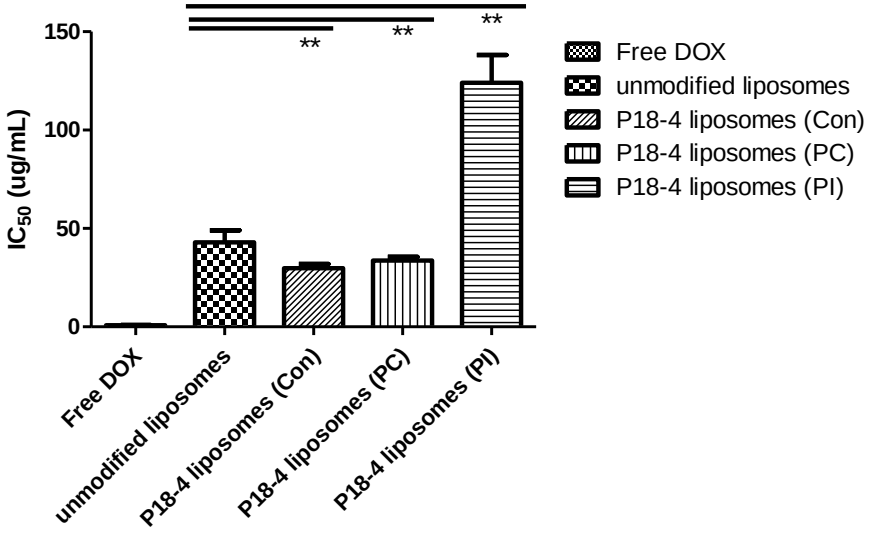

Figure 5-6: *In vitro* cytotoxicity of different formulations against MDA-MB-435 cells after 24 h incubation. Each bar represents mean $IC_{50} \pm$ SD (n=3). ** denotes statistically significant difference (P<0.05). Differences between means were assessed using one-way ANOVA followed by post hoc analysis using Tukey's multiple comparison test (Graphpad prism, version 5.00, Graphpad software. Inc., La Jolla, CA, USA). The level of significance was set at α= 0.05.

5.4 Discussion

Conventional chemotherapy is the treatment of choice in many cancers, but its effectiveness is limited due to intolerable toxicities that emerge after intensive therapy. This is inevitable since conventional chemotherapeutic agents are systemically administered without any means of restricting drug exposure to tumor cells. As a result, healthy tissues get equally exposed to the powerful chemotherapeutic agents, leading to detrimental effects on these tissues. This will not only reduce the quality of life in cancer patients, but also force the clinicians to use suboptimal doses of the drug to prevent acute and chronic toxicities. To reduce the intolerable toxicities of current chemotherapy, anticancer drug can be formulated in drug carriers designed at nanoscopic dimensions and hydrophilic surface properties so that they can direct the encapsulated drug to tumor and take it away from healthy tissues. Doxil® or Caelyx® are commercially available PEGylated liposomal nano-formulations of a conventional chemotherapeutic agent, DOX, designed to accomplish this purpose. The liposomal formulations of DOX were developed for the treatment of Kaposi's sarcoma and are now approved for use in ovarian cancer and multiple myeloma by US Food and Drug Administration (FDA) [497]. PEGylated liposomal DOX has been shown to significantly improve the therapeutic index of DOX both in preclinical [498-502] and clinical studies [503-505]. Modification of the surface of PEGylated liposomes with tumor targeting ligands (e.g., monoclonal antibodies and peptides) is expected to improve the therapeutic benefit of DOX in the treatment of several solid and hematological tumors even further. Peptide sequences based on RGD

and NGR that can target tumor cells and tumor associated endothelium has been tried extensively for this purpose [237-240, 242, 243].

The aim of this study was to assess the potential of a novel stable breast cancer targeting peptide, p18-4 (**Figure 5-1**) [312], that has been prepared by our research team, for the development of tumor targeted liposomal DOX formulations. The p18-4 peptide is a proteolytically stable analogue of p160 peptide, that has shown high degree of specific binding to breast cancer cell lines MDA-MB-435 and MCF-7 [310]. The development process of the p18-4 ligand modified liposomes involved investigation of the possible effect of the peptide coupling technique on the cytotoxicity and uptake of the carrier by cancer cells. The peptide coupling technique could significantly affect the way the peptide is presented on the liposomal surface and how it interacts with its target receptors on the tumor cells. In an attempt to find out the best conjugation method, herein, we studied three different techniques to incorporate the p18-4 peptide to attach our peptide to the liposomal bilayer: the conventional, post conjugation, and post insertion methods (**Figure 5-2**).

In the conventional method, the synthesized p18-4-PEG-DSPE lipid conjugate was mixed with PEG-DSPE for the formation of liposomes and DOX was loaded in the liposomes afterwards. The conventional method is easy and convenient, but it may lead to the production of liposomes that do not fully express the peptide ligand on their surface as the peptide can be embedded within the vesicular structure during preparation process. The post conjugation method involves a reaction between reactive groups on the liposomal bilayer (i.e. –

COOH) with the N-terminal of the peptide. This method ensures that all the conjugated peptide will be fully expressed on the liposomal bilayer. However, the presence of unreacted reactive groups on the outer and/or inner liposomal bilayer could result into possible side reactions. The post insertion method relies on the spontaneous exchange of PEG-DSPE peptide conjugate from micellar structures with the liposomal phospholipid membrane at temperature exceeding the phase transition temperature of the phospholipid [506-508]. This method has been successfully tried to prepare several ligand modified liposomes [487, 506, 509, 510].

p18-4 modified liposomes prepared with all three techniques showed similar average with diameters of ~ 130 nm (**Table 5-1**), which is appropriate for both extravasation into the tumor interstitial space and retention into the tumor tissue. Modification of liposomes with p18-4 did not seem to affect the liposomal size perhaps because of the small dimensions of p18-4. Liposomal formulations were able to encapsulate DOX effectively and restrict its release as a results utilization of the ammonium sulfate gradient **(Figure 5-3)** [285]. This procedure results in the precipitation of DOX in a slowly dissolving aggregated gel like state at the inner phase of the liposome. The solubility of DOX sulfate in the pH range of 4.0-7.5 is 1.7-2.3 mg/mL. This decreased solubility leads to efficient DOX encapsulation, slow DOX dissolution and release [511]. The peptide incorporation by conventional and post conjugation techniques did not affect DOX encapsulation and release rate significantly compared to untargeted liposomes. However, liposomes prepared by the PI techniques have shown a lower

encapsulation and release of DOX from the carrier. Liposomal membrane may be perturbed during the post insertion process leading to the loss of loaded DOX. Moreira et al. [506] reported 60 % of DOX leakage when they incubated untargeted liposomes containing 9 mole% mPEG-DSPE with antagonist G-PEG-DSPE micelle at 60 ^{0}C. Similarly, Ishida et al. [512] reported little DOX leakage when DOX loaded liposomes were heated up at 60 ^{0}C for 6 h in the presence or absence of IgG-PEG-DSPE. The author explained this behaviour by permanent or transient membrane perturbation caused by hydrophobic antagonist G interaction with the phospholipid bilayer at elevated temperatures. The low extent and rate of DOX release by liposomes prepared by PI technique could be explained by the low encapsulation level of DOX in these liposomes which resulted into lower drug/lipid ratio compared to liposomes prepared by other methods.

A higher uptake for free DOX by the MDA-MB-435 cells compared to ligand modified liposomal DOX was observed. This could be explained by different mechanisms of DOX uptake. Free DOX is a small molecule that could pass rapidly through the cell membrane by diffusion, whereas the ligand modified liposomal DOX delivers its content in a slower rate either by i) slow release of encapsulated DOX in the tumor cells lieu that gradually diffuses through the cell membrane, and/or ii) interaction of the whole liposome with its target receptor expressed on the cell surface and subsequent uptake through receptor mediated endocytosis [39-41]. Moreover, the flow cytometry showed that the uptake of p18-4 modified liposomes prepared by either conventional or post conjugation method by MDA-MB-435 cells to be comparable with each other, but higher than

that of unmodified liposomal DOX formulations. This enhancement in the cellular uptake is the result of specific interaction between the p18-4 peptide with target receptors on the MDA-MB-435 cells. This was confirmed by competition studies where free peptide competed with peptide modified liposomes for cell interaction in case of liposomes prepared by conventional and post conjugation method **(Figure 5-4)** which points to the involvement of receptor mediated endocytosis in the uptake of p18-4 liposomes. This observation is also in line with what reported for the parent peptide, p160 [10]. p18-4 decoration of liposomes by the PI method; however, did not lead to any enhancement in the uptake of liposomal DOX by MDA-MB-435 cells. Besides, pre-treatment of cells with free peptide did not affect the uptake of p18-4 liposomal DOX prepared by the PI method. This might be attributed to a change in the conformation of p18-4 during the PI process upon exposure to 60 °C leading to reduced p18-4 affinity to its target receptors.

In agreement with the results obtained with flow cytometry, fluorescence microscopy images of MDA-MB-435 cells treated with p18-4 liposomes (PC) showed enhanced cellular uptake compared to cells treated with either p18-4 liposomes (PI) and non-specific control unmodified liposomes. This would provide conclusive evidence that support the results obtained by flow cytometry. This study revealed the marked nuclear localization of DOX in case of p18-4 liposomes (PC), which contributes to the enhanced activity (i.e. cytotoxicity) of p18-4 liposomes (PC), since nuclear localization is essential for the activity of

DOX, which acts through DNA intercalation and topoisomerase poisoning [513-515].

The results of cytotoxicity study was in line with that of cell uptake results, where p18-4 modified liposomal DOX prepared by the conventional and post conjugation techniques have increased the cytotoxicity of encapsulated DOX compared to unmodified liposomes. DOX encapsulated in p18-4 modified liposomes prepared by PI method; however, showed lower cytotoxic effects compared to that of unmodified liposomes. This can be credited to the lower rate and extent of DOX release from the liposomes prepared by PI method or their lower uptake by the cells. Overall, the conventional and post conjugation methods led to the production of comparable DOX liposomal formulation with similar characteristics and behaviour in terms of liposomal size, DOX release, cell uptake and cytotoxicity in MDA-MB-435 cells. The p18-4 decorated liposomal DOX formulations were superior to their unmodified counterparts in terms of DOX uptake and cytotoxicity in breast tumor cells.

In conclusion, we report on the successful development of stealth liposomes bearing an engineered ligand, p18-4 peptide that can target the breast cancer MDA-MB-435 cells on its surface using conventional or post conjugation methods. The developed ligand guided nanocarriers may be used to enhance the therapeutic index of encapsulated DOX through enhancement in the delivery of DOX to tumor cells. The validity of this assumption is under study in preclinical animal models of breast tumor in our laboratory. In next chapter, the in vitro and

in vivo therapeutic efficacy of p18-4 decorated DOX liposomal formulation bearing different p18-4 peptide density is studied.

Chapter 6
Modification of stealth liposomal Doxorubicin formulations with engineered peptides targeting breast tumors: evaluation of in vitro and in vivo anticancer activity

6.1 Introduction

The majority of chemotherapy drugs currently in use for cancer treatment rely on the utilization of non-specific small cytotoxic molecules that can inhibit the growth and proliferation of rapidly dividing cancer cells. Most anticancer agents can induce toxic side effects in normal tissues, because of their non-specific action on other cellular/molecular drug targets. Besides, the non-selective action of anticancer drugs on cancer cells can results in substantial toxicity to many normal rapidly dividing cells in the human body (e.g. bone marrow cells, hair follicles) [516, 517]. Drug delivery systems are expected to reduce the toxic side effects of such anticancer agents by providing a physical barrier between the anti-cancer agents and normal tissue and changing the biodistribution of anti-cancer agents away from sites of drug toxicity towards the site of drug action, i.e., tumors.

Among several drug delivery systems that have been developed to improve the therapeutic benefit of chemotherapeutics, liposomal formulations are in the front line of development. In 1995, Doxil ®, a stealth liposomal formulation of anthracycline drug doxorubicin (DOX), received accelerated approval by FDA for the treatment of AIDS related Kaposi sarcoma [518]. Nowadays, Doxil® is indicated for treatment of recurrent ovarian cancer after failure of platinum based chemotherapy, and for treatment of relapsed/refractory multiple myeloma in combination with bortezomib [519, 520]. A new generation of liposomal formulations bearing cancer targeting ligands on their surface have been under investigation to improve the selective delivery of drugs to diseased tissues even

further. This approach can be employed to improve therapeutic outcome by increasing the homing of anti-cancer agents in the vicinity of their molecular targets [521-523]. In some cases, synergistic anti-cancer activity by the targeting ligand and the encapsulated anti-cancer drug may also be achieved.

In the previous Chapter we have reported on the development of liposomal formulations of doxorubicin (DOX) decorated on their surface with p18-4 peptide. Several methods of peptide incorporation into the liposomal carrier has been tried to achieve optimum properties for active targeting of DOX to breast cancer cells by its p18-4 decorated liposomal carriers. The aim of this study was to evaluate the selective *in vitro* and *in vivo* anti-cancer activity of the optimized p18-4 decorated liposomal DOX in detail. In this context, special attention was paid to the effect of p18-4 peptide density on the carrier surface on the specific interaction of the carrier with cancer cells and the final therapeutic outcome in *in vitro* and *in vivo* models of breast cancer. The choice of the proper peptide density is one of the critical liposomal design considerations that determine the targeting efficiency and the success of the whole delivery system *in vivo*. Different ligand densities have been reported in the literature to promote binding of the liposomes to their cellular targets [524-526], but the optimal peptide ligand density is still controversial [527]. The reported differences in optimum peptide ligand density may be related to the difference in the accessibility of the ligand to its target receptors, or difference in the way of chemical attachment, or the variation in ligand affinity to their targets. A minimum threshold concentration should be attained to achieve minimal binding to the targeting receptors [528]. In general,

high concentration of the targeting ligand often increases the binding cellular uptake of nanocarriers [195, 529]. However, high targeting ligand density could promote non-specific interaction with the endothelial cells and non-cancerous cells leading to increased immunogenicity as well as opsonization mediated clearance [530]. Therefore, the density of targeting ligand should be carefully investigated to reduce the non-specific interaction and to enhance the activity in a way that promote the selective delivery of encapsulated cargo to target cells.

6.2 Materials and methods

6.2.1 Materials

Hydrogenated soy phosphatidylcholine (HSPC) and methoxypoly(ethylene glycol) (MW 2000 Da), covalently linked to 1,2-distearoylphosphadidylethanoloamine ($mPEG_{2000}$-DSPE), were generous gifts from ALZA Corporation, Inc. (Mountain View, CA). DSPE-PEG_{3400}-NHS was purchased from Nanocs. (New York, NY). Cholesterol (CHOL) was purchased from Avanti Polar Lipids (Alabaster, AL). Doxorubicin hydrochloride (purity > 98%) was purchased from Ontario Chemicals, INC. (Guelph, ON). [3-(4,5-dimethylthiazol-2-yl)-2,5-diphenyl] tetrazolium bromide (MTT) was purchased from Sigma-Aldrich (St. Louis, MO, USA). 2-Chlorotrityl chloride resin (1 mmol/g), (2-(6-chloro-1H-benzotriazole-1-yl)-1,1,3,3-tetramethylaminium hexafluorophosphate) (HCTU), 1-hydroxybenzo triazole (HOBt), and the Fmoc-amino acids were purchased from NovaBiochem (San Diego, CA). The side chains of amino acids used in the synthesis were protected as follows: tert-butyl (tBu) for tyrosine, tert-butoxy (OtBu) for glutamic acid, trityl (Trt) for glutamine,

t-butoxycarbonyl (Boc) for tryptophan, 2,2,4,6,7-pentamethyldihydrobenzofuran-5-sulfonyl (PbF) for arginine. Piperidine, N, N diisopropyl ethylamine (DIPEA), N-methyl morpholine (NMM), trifluoroacetic acid (TFA), Triisopropylnaphthalenesulfonic acid sodium salt (TIPS) were purchased from Sigma-Aldrich. All solvents used in purification were HPLC grade. All other chemicals are reagent grade and are purchased from Caledon Laboratories Ltd. (Canada).

6.2.2 Cell lines

All cell lines were cultivated at 37 ºC in a 5% CO2 incubator. The human cancer cell line MDA-MB-435 was received as a gift from the laboratory of Dr. R. Clarke (Georgetown University, USA). These cells were cultured in RPMI 1640 with 1% L-glutamine, and 10% FCS (Invitrogen, Karlsruhe, Germany), 100 IU/mL penicillin, and 100 IU/mL streptomycin. The human cancer cell lines MCF-7 cells was obtained from ATCC (Manassas, USA) and cultured in DMEM media with 1% L-glutamine, and 10% FCS (Invitrogen, Karlsruhe, Germany), 100 IU/mL penicillin, and 100 IU/mL streptomycin. The human non-tumorigenic epithelial cell line MCF 10A was obtained from ATCC (Manassas, USA) and cultured in MEGM media kit (Lonza, USA) supplemented with 100 ng/mL cholera toxin (Sigma chemicals, USA).

6.2.3 p18-4 peptide synthesis

As described in Chapter 5 section 5.2.3

6.2.4 Synthesis of p18-4-PEG-DSPE

As described in Chapter 5 section 5.2.4

6.2.5 Preparation of liposomes

Targeted liposomes bearing different p18-4 peptide density were prepared in identical procedures as described in Chapter 5 (section 5.2.5 A), replacing part of the DSPE-PEG_{2000} with DSPE-PEG-p18-4 according to the required peptide density. Briefly, The high density liposomes (HD) and low density (LD) liposomes were synthesized from HSPC:CHOL: mPEG-DSPE: DSPE-PEG_{3400}-p18-4 with (1.5:1: 0.07:0.07) and (1.5:1: 0.125 :0.015) ratios, respectively. For the preparation of DOX loaded liposomes, DOX was encapsulated into liposome using an ammonium sulfate gradient. After removing the extra-liposomal salt by a Sephadex G-50 column in 10% sucrose, DOX solution (2 mg/mL) was added immediately into the above solution at a concentration of 0.2 mg DOX/1 mg HSPC phospholipid. The mixture of liposome and DOX were incubated in 60°C water bath for 30 min with agitation. After loading, un-trapped DOX was removed by Sephadex G-50 gel filtration in PBS pH 7.4.

The amount of DOX trapped inside the liposomes was determined spectrophotometry, after diluting aliquot of the liposomes with methanol, and then DOX concentration was determined using UV measurement at 485 nm (Beckman Coulter DU 73 UV/Vis spectrophotometer, ON, Canada). Liposomes sizes after DOX loading were measured by dynamic laser scattering.

6.2.6 In vitro release study

The *in vitro* release of DOX from p18-4 modified liposomes having different peptide densities was studied using a dialysis method. Free DOX, unmodified liposomes, p18-4 liposomes (LD), p18-4 liposomes (HD) at equivalent DOX concentration 400 µg/mL were prepared and placed in dialysis bag (MW cut off, 3500 Da). Each dialysis bag contained 3 mL of the formulation were placed into a 500 mL of phosphate buffer pH 7.4 (10 mM). Release study was performed at 37 ^{0}C in a shaking water bath at 100 rpm (Julabo SW 22 shaking water bath, Germany). At selected time intervals, aliquots of 200 µL from the inside of the dialysis bag were diluted with methanol for UV/visible spectroscopy analysis based on absorbance intensity at 485 nm. The amount of DOX released was calculated by subtracting the amount of DOX remained in the dialysis bag from the initially added DOX.

6.2.7 In vitro cell uptake study

To study the effect peptide density on the cellular uptake of encapsulated DOX, cellular DOX uptake was quantified using flow cytometry (Beckman Coulter Cell Quanta SC, ON, Canada). Different cell lines (MDA-MB-435, MCF-7, MCF-10 A) were seeded into 24-well plates at densities of $1x10^{5}$ cells/well, and incubated at 37 ^{O}C for 24 h till 70% confluence reached. Unmodified liposomes, p18-4 liposomes (LD), p18-4 liposomes (HD), and free DOX at a concentration of 5 mg/mL equivalent DOX were added and incubated for 24 h at 37 ^{O}C. For the competition experiments, MDA-MB-435 cells were pre-incubated with excess free p18-4 peptide (1 mg/mL) for 30 min to saturate receptors and to inhibit the

binding and internalization of peptide conjugated liposomes. The medium was aspirated and cells were rinsed with cold PBS three times. All the cells were detached using trypsin EDTA and suspended into PBS solution containing 4% formalin. Five thousand cells were counted with logarithmic settings. The cell-associated DOX was excited with an argon laser (488 nm) and the fluorescence was detected at 560 nm. All data are expressed in mean fluorescence intensity ± SD (standard deviation) (n=4).

6.2.8 In vitro cytotoxicity assay

Cytotoxicities of various liposomes were tested against different cell lines (MDA-MB-435, MCF-7, MCF-10 A). Briefly, each well of 96-well plates was seed with 10,000 cells and incubated for 24 h. The cells were then exposed to serial concentrations of free DOX, unmodified liposomes, and targeted DOX liposomes (i.e. LD, HD) diluted in culture medium. After cultured for 24 h at 37 ^{0}C, the cell monolayer was washed with PBS. Then, 20 µL of MTT solution (5 mg/mL) was added to each well, followed by incubating for another 4 h at 37 ^{0}C. Finally, the medium was replaced by 200 µL of (Dimethyl Sulfoxide) DMSO, and the absorbance was read on power wave x 340 Microplate Reader (Bio-tek instruments Inc., USA) at wavelength of 570 nm. The experiment was carried out in triplicate. The data reported represent the means of triplicate measurement. The IC_{50} was calculated from the plot of the % of viable cells vs. log DOX concentration. The selectivity index (SI) was defined as the ratio of the measured IC_{50} in MCF10A cells to the IC_{50} in the cancer cells MDA-MB-435 or MCF-7

6.2.9 *In vivo* therapeutic efficacy study

Therapeutic efficacy experiment was carried out in female NOD-SCID mice bearing MDA-MB-435 tumors, randomly assigned into four groups of 6 mice per group. Mice were inoculated with 2 X 10^6 of MDA-MB-435 cells in a volume of 100 µL PBS injected into the right flank. Treatments were commenced on day ten post-inoculation when tumor size was approximately 0.1 cm^3. They were treated with 25 µg/week of DOX equivalent (2.5 mg DOX/kg) by tail vein injection every 7th day for six doses (days 10, 17, 24, 31, 38, and 45). For SCID mice bearing tumors, treatments consisted of saline, untargeted DOX liposomes, p18-4 liposomes (HD), p18-4 liposomes (LD) liposomes. Mice were observed daily, and mouse body weights as well as signs of stress (e.g. lethargy, ruffled coat, ataxia, etc.) were detected as possible signs of toxicity. In each experiment, the mice were monitored for up to 45 days after tumor inoculation or until one of the following conditions for euthanasia was met: (1) the mouse's body weight dropped below 15% of its initial weight, (2) the mouse's tumor was >2.0 cm across in any dimension, (3) the mouse became lethargic or sick and unable to feed, (4) the mouse developed ulcerated tumor. Tumor size (cm^3) was measured twice weekly with a caliper in two dimensions and calculated using the formula: volume= 0.4 LW^2 (L is the long diameter and W is the short diameter of a tumor). The tumor volumes of individual mouse at different times were normalized with the tumor volume at the study onset to obtain a relative volume change for each tumor. Mean ± standard deviation (SD) of relative tumor volumes in each group were calculated and plotted as a function of time. All animal studies are according

to the Health Sciences Laboratory Animal Services (HSLAS) guidelines and experimental protocols were approved by the University of Alberta Health Sciences Animal Policy and Welfare Committee.

6.2.10 Statistical analysis

Data are presented as mean ± SD of triplicate measurements throughout the chapter. Statistical significance of difference was tested either using students' t-test or one way ANOVA test with Tukey post-test analysis. The significance level (α) was set at 0.05. All data that required non-linear regression analysis were processed using (Graphpad prism, version 5.00, Graphpad Software Inc., La Jolla, CA, USA).

6.3 Results and discussion.

6.3.1 Synthesis p18-4-PEG-DSPE

p18-4-PEG-DSPE was synthesized after conjugation of p18-4 peptide (calculated MW 1296 Da) with NHS-PEG-DSPE (calculated MW 4396 Da) in PBS pH 7.4. The conjugation of p18-4 to NHS-PEG-DSPE was confirmed by RP-HPLC. The standard free p18-4 peptide eluted at retention time 27.5 min. Free peptide after the completion of the reaction is removed by extensive dialysis against distilled water. The p18-4 peptide conjugation efficiency was ~ 35%. The low conjugation efficiency of the peptide to the NHS-PEG-DSPE could be due to the short half-life of NHS esters in aqueous environment.

6.3.2 Preparation of DOX loaded liposomes

DOX loaded stealth liposomes bearing p18-4 peptide were successfully prepared. Two p p18-4 modified DOX liposomal formulations bearing different peptide density, namely p18-4 liposomes LD and p18-4 liposomes HD were synthesized. The particle size of various liposomes was around 130 nm, (PDI < 0.076), and all types of liposomes have similar particle size and polydispersity index (**Table 6-1**). Liposomes with diameter ~ 100 nm are the optimal size for both optimum extravasation into the tumor interstitial space and retention into the tumor tissue. The molar peptide density of p18-4 liposomes (HD) and p18-4 liposomes (LD) were 1.5, and 0.3 mole %, respectively. This corresponds to 638 and 136 peptide molecules per liposome, assuming the liposomes are 100 nm in size [531]. The

encapsulation efficiency of DOX was > 95%. The level of peptide conjugation did not affect the conjugation efficiency of DOX into the liposomes.

Table 6-1.Characteristics of the prepared DOX loaded liposomes (n=3).

	Peptide density (mole%)	Z average (nm)	Polydispersity index[a]
Unmodified liposomes	0	128.5 ± 1.9	0.048 ± 0.01
p18-4 liposomes (HD)	1.5	133.3 ± 1.3	0.076 ± 0.01
p18-4 liposomes (LD)	0.3	124.2 ± 4.5	0.034 ± 0.01

[a] determined by DLS.

6.3.3 In vitro DOX release study

The release profile of DOX from different p18-4 peptide modified liposomes in phosphate buffer pH 7.4 is shown in **Figure 6-1.** It demonstrates clearly that free DOX is rapidly released from the dialysis bag showing almost 88% of DOX released within 8 h, this means that the release of DOX from the liposomes is the rate limiting step and the dialysis membrane does not form any barrier against DOX release. Neither p18-4 peptide conjugation nor its density affected the rate or extent of DOX from prepared liposomes. After 72 h p18-4 liposomes (HD), and p18-4 liposomes (LD) released 29.7, and 32.4 % of their DOX content into phosphate buffer pH 7.4, respectively. This was not significantly different from unmodified liposomes ($P>0.05$) which released 30.7 % of its DOX content under similar conditions. The low release rate of DOX from prepared liposomes is due to the utilization of the ammonium sulfate gradient method [285]. This method

results in precipitation of DOX in a slowly dissolving aggregated gel like state at the inner phase of the liposome. The solubility of DOX sulfate in the pH range 4.0-7.5 is (1.7-2.3 mg/mL), this decreased solubility leads to efficient DOX encapsulation, slow DOX dissolution and release[511].

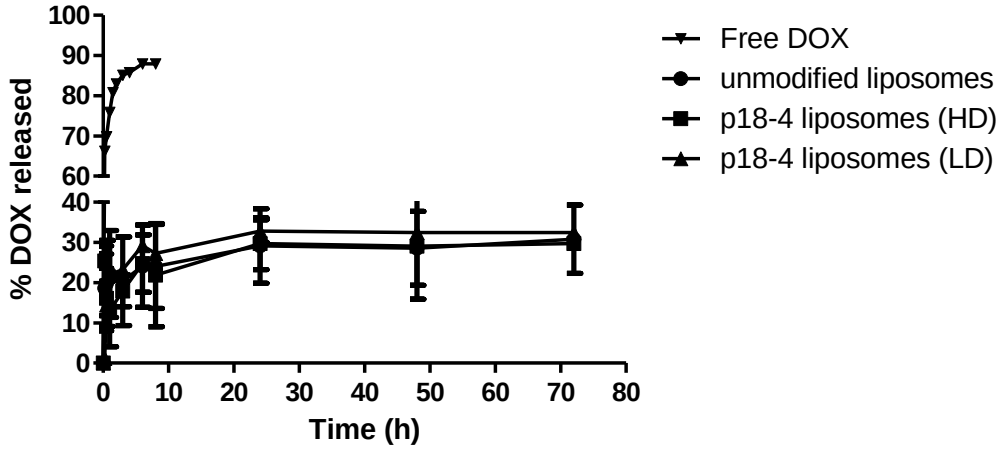

Figure 6-1. The release profiles of DOX from various p18-4 modified liposomal formulations having different peptide density in phosphate buffer pH 7.4 at 37 ^{0}C. Each point represents mean ± SD (n=3).

6.3.4 In vitro DOX uptake study

The density of the conjugated peptide is an important determinant of the liposome uptake by the cells. **Figure 6-2** A presents data from an *in vitro* study with free DOX, unmodified liposomes, p18-4 liposomes (LD), p18-4 liposomes (HD) investigating the cellular association of DOX as part of these formulations with the MDA-MB-435 cells after 24 h incubation. The data reveals that increasing the peptide density significantly increases the cellular association and/or uptake of encapsulated DOX ($P<0.05$) in the MDA-MB-435 cells after 24 h incubation. The cellular association of the liposomes presenting 1.5 mole % of the p18.4 peptide

was 4.43 times compared to the cellular association of the untargeted liposomes. The liposomes presenting 0.3 mole % of p18-4 peptide demonstrated ~1.82 folds ($P < 0.05$) greater cellular association than did the untargeted liposomes To explore whether this increased cellular association could be attributed to the presence of receptor for the p18-4 peptide, a competition experiment was carried out, in which the cellular uptake of liposomal DOX by MDA-MB-435 cells pretreated with excess free p18-4 peptide was evaluated. In another experiment, the cellular uptake study was completed with a negative cell line (e.g. the MCF-10A). The results presented in **Figure 6-2 A** reveal that the presence of excess free p18-4 peptide significantly reduced ($P<0.05$) the cellular association of p18-4 liposomes by the MDA-MB-435 cells. This points to the involvement of receptor mediated endocytosis process in the uptake of p18-4 decorated liposomes. Similarly Soudy etal. [312] reported 50 % decrease in the cellular uptake of FITC labeled p18-4 peptide in presence of excess free unlabeled peptide by MDA-MB-435 cells after 30 min incubation. Also, Askoxylakis and coworkers [310] studied the competitive binding of radiolabelled [^{125}I]p160 by MDA-MB-435 in presence of different concentrations of free unlabeled p160 peptide after 60 min. They found that a concentration of 0.6 µM unlabeled p160 could cause 50% reduction in the binding of radiolabelled [^{125}I]p160. The same cellular uptake experiment with the breast cancer cell lines MCF-7 (**Figure 6-2B**) showed enhanced cellular uptake of p18-4 liposomes in comparison to unmodified liposomes. The cell uptake proportionally increased with an increase in the ligand density. **Figure 6-2 C** show the cellular uptake results with negative cell MDA-10A. The graph

reveals that the degree of cellular association was not significantly ($P>0.05$) affected by the ligand density. Guofeng [532] suggested that the binding affinity of c(RGD) modified liposomes to activated platelets increased as the c(RGD) peptide density increased up to 1 mole %. Ligand density > 1 mole % showed almost no beneficial effects in terms of binding affinity, which means that the binding affinity reaches a plateau when the ligand density is above a threshold (1 mole %). Accordingly, they suggested a c(RGD) peptide density approximately ~ 1 mole % is required for the greatest liposome binding affinity. The presence of threshold has been also reported for anti –HER2-immunoliposomes targeted to SK-BR-3 human breast cancer cells [533], in which a plateau in the cellular binding at about 35-40 Fab' per liposome in the outer leaflet of the liposomal bilayer was reported.

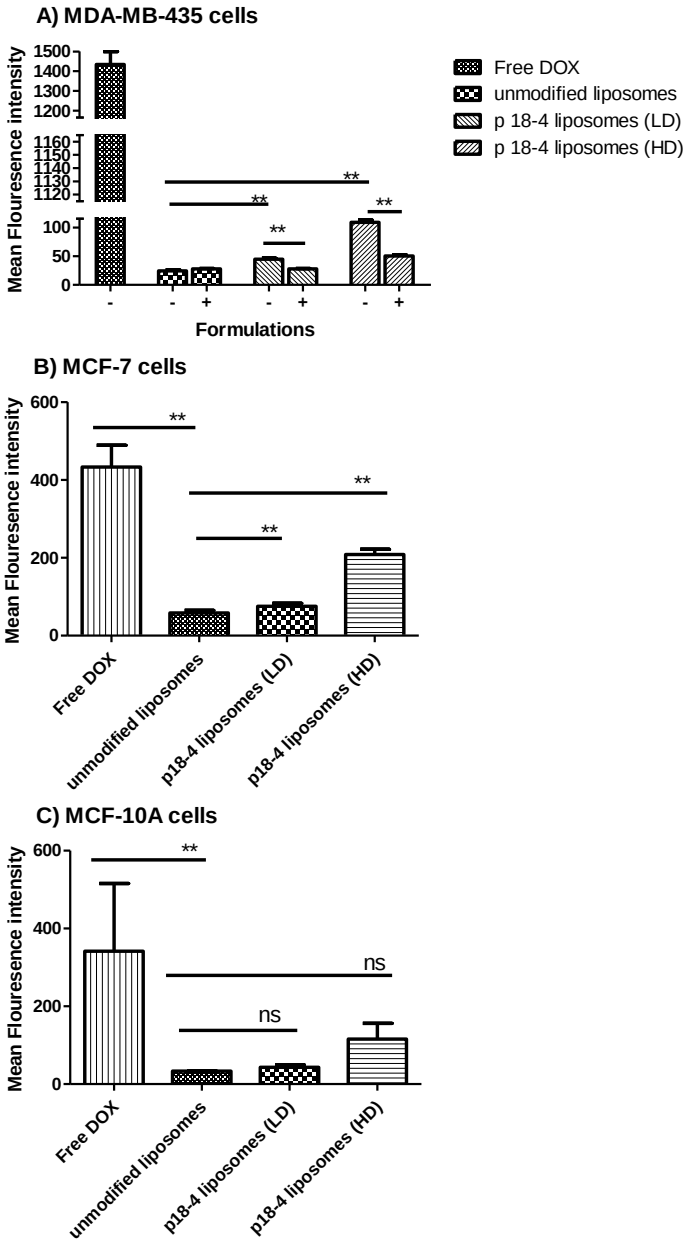

Figure 6-2. *In vitro* cell uptake of free DOX, Unmodified liposomes, p18-4 Liposomes (LD), and p18-4 Liposomes (HD) by A) MDA-MB-435 cells with (+) or without (-) pre-treatment with excess of free p18-4 peptide after 24 h incubation B) MCF-7 cells after 24 h incubation C) MCF-10 A cells after 24 h incubation. Each bar represent mean fluorescence intensity ± SD (n=4) . ** denotes statistically significant difference (P<0.05). ns denotes statistically non-significant difference (P>0.05).

6.3.5 In vitro cytotoxicity study

The effect of the p18-4 peptide level on cytotoxicity of DOX in both MDA-MB-435 cells and MCF-7 cells after 24 h incubation was evaluated using the MTT assay (**Figure 6-3**). Cell viability was compared with untreated control. All p18-4-modified liposomes showed higher cytotoxicity (i.e. lower IC_{50}) than untargeted liposomes. Compared to unmodified liposomes, 1.5 mole% p18-4 peptide modified liposomal DOX showed 2.4 and 5 folds decrease in IC_{50} in MDA-MB-435 and MCF-7 cells, respectively. On the other hand, modification of liposomal DOX at 0.3 mole% p18-4 peptide, led to 1.6 and 2.2 folds decrease in IC_{50} of DOX in MDA-MB-435 and MCF-7 cells, respectively. This improved cytotoxicity for the (HD) p18-4 liposomes compared to (LD) p18-4 liposomes may be attributed to the better binding avidity of the liposome for target receptors. Some cancer targeted formulations utilizes biologically active targeting ligands (e.g. trastuzumab, rituximab mAbs) that have intrinsic cytotoxicity due to their ability to interfere with cancer cell signalling pathways. p18-4, perhaps has improved the anticancer activity of DOX merely through active targeting; since our in vitro results showed negligible anticancer activity against tumour cells for this peptide in MDA-MB-435 cells.

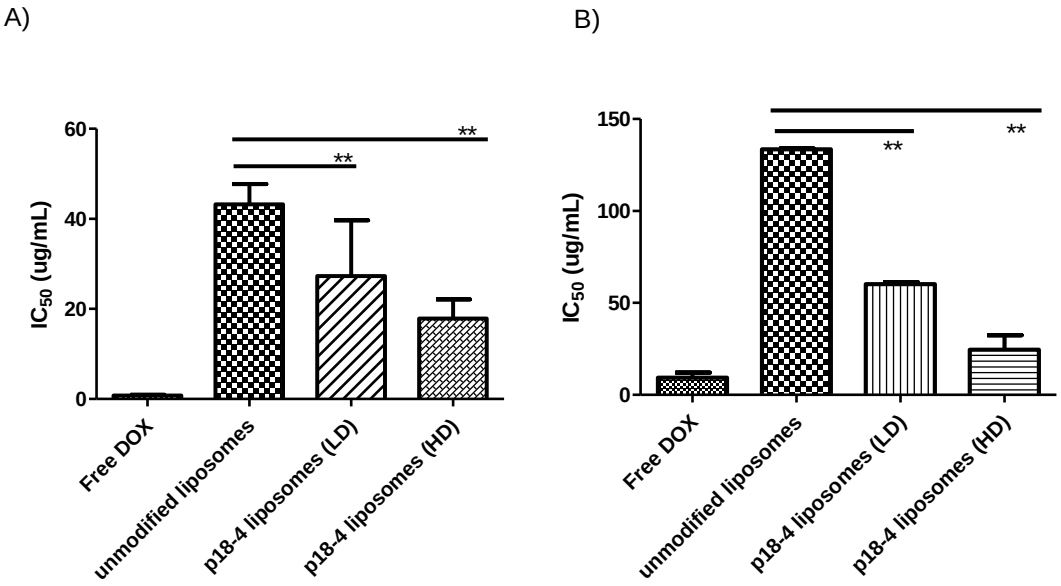

Figure 6-3. In-vitro cell cytotoxicity of unmodified liposomes, p18-4 Liposomes (LD), p18-4 (HD) and free DOX against A) MDA-MB-435; and B) MCF-7 after 24 h incubation. ** means statistically different ($P < 0.05$), ns means statistically not different ($P > 0.05$). Each bar represent mean IC_{50} ± SD (n=3).

Evaluation of the SI of different formulations against different cancerous cell lines (MDA-MB-435 and MCF-7) vs. MCF-10A non-cancerous cell line revealed that modification of the p18-4 liposomes with 0.3 mole % of the peptide (LD) showed better selective cytotoxicity against the studied cancer cell lines compared to liposomes modified with 1.5 mole % p18-4 peptide (HD) **(Figure 6-4**). Compared to untargeted liposomes, the SI of p18-4 liposomes (LD) for the MDA-MB-435 cells over MCF-10A cells increased by 15 folds. Although the p18-4 peptide liposomes (HD) showed higher cytotoxicity against the MDA-MB-435 cell compared to p18-4 liposomes (LD), they showed lower selective cytotoxicity. In comparison to unmodified liposomes, the SI of p18-4 liposomes (HD) for MDA-MB-435 cells over MCF-10A cells was reduced by 8 folds. Similarly, the p18-4

liposomes (LD) showed better selective cytotoxicity in MCF-7 cells compared to the p18-4 liposomes (HD). In comparison to unmodified liposomes, the SI of p18-4 liposomes (HD) against MCF-7 cells vs. MCF 10A was reduced by 5 folds. Decoration of peptides on liposomal surface at high density might have increased the chance of non-specific interactions with cell membranes compensating for the effect of receptor mediated endocytosis.

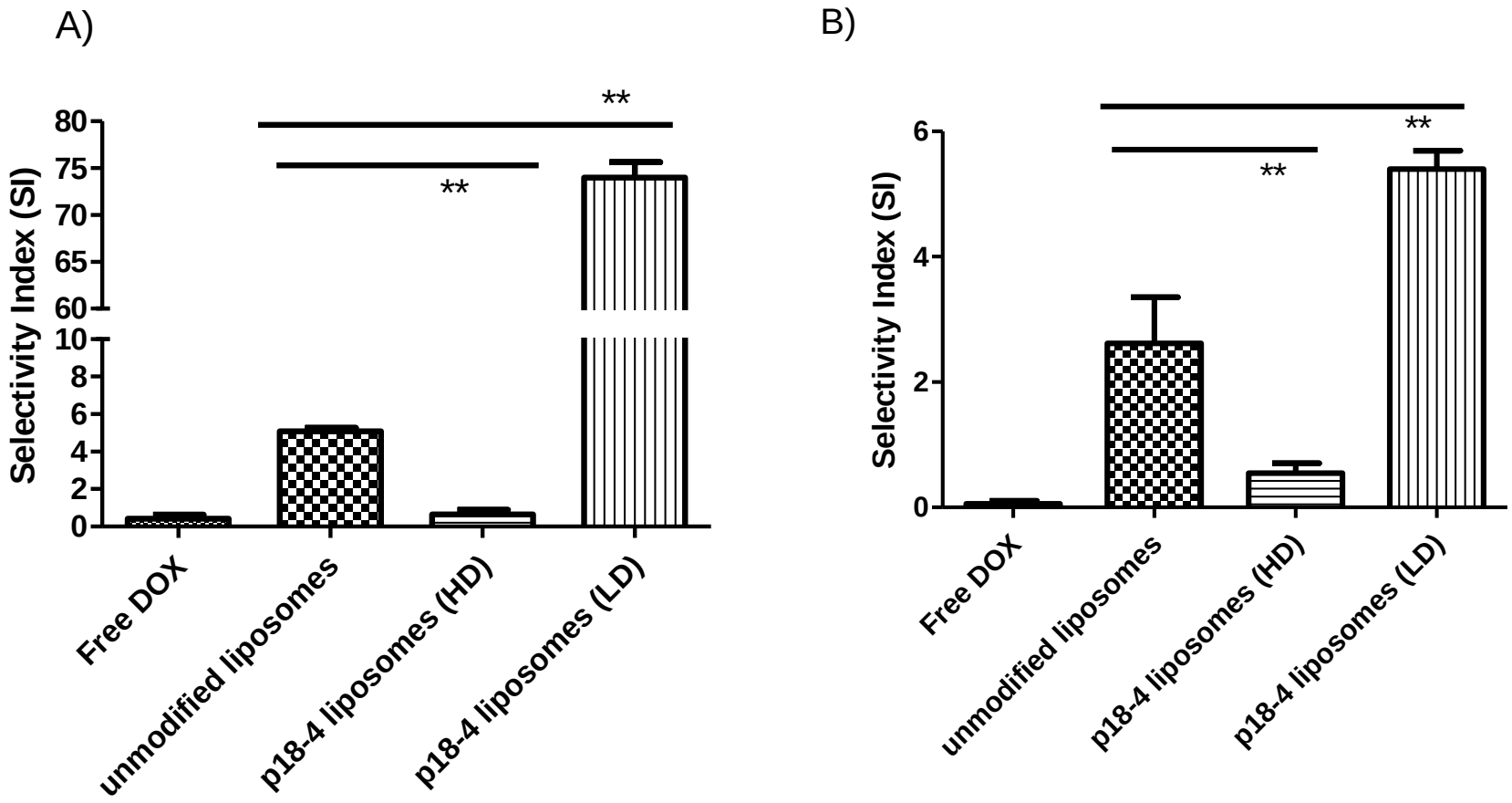

Figure 6-4. Selectivity index (SI) of unmodified liposomes, p18-4 Liposomes (LD), p18-4 (HD) and free DOX by (A) MDA-MB-435 cells vs. MCF-10A (B) MCF-7 vs. MCF 10 A. ** means statistically different ($P < 0.05$), ns means statistically not different ($P > 0.05$). Each bar represent mean SI ± SD (n=3). SI is the ratio of the calculated IC_{50} in non-cancerous cells (MCF10A) to the IC_{50} in the cancer cells (MDA-MB-435 or MCF-7).

6.3.6 In vivo therapeutic efficacy study

The *in vivo* anti-cancer activity of developed formulations following intravenous multiple dosing was assessed using MDA-MB-435 s.c. xenograft in NOD-SCID mice. The general safety of formulations was also assessed by observing the animal behaviour and body weight monitoring during the study. Mice injected with liposomal doxorubicin formulations, except for p18-4 liposomes (HD), did not show changes in their overall activity during the period of study. However, mice treated with p18-4 HD liposomes showed bigger tumors, which affected the movement of some animals. In general, mice that received unmodified liposomes and p18-4 liposomes (LD) tolerated the regimen well. The treatments did not seem to have any adverse obvious impact on the activity level and mean body weight of those animals **(Figure 6-5**). As shown in

Figure 6-6, both unmodified liposomes and p18-4 LD liposomes significantly decreased the relative tumor volume compared with control group (i.e. saline treatment) ($P<0.5$). However, the p18-4 liposomes (LD) exhibited better relative tumor volume inhibition compared to unmodified liposomes. Mice treated with LD liposomal DOX showed 4.8 folds reduction in the mean relative tumor volume compared to non-targeted DOX liposomes. This enhanced therapeutic efficacy of p18-4 liposomes (LD) is attributed to the capability of the p18-4 peptide to facilitate the uptake of DOX into the breast cancer cells MDA-MB-435, thus increasing the intracellular DOX concentration. On the other hand, mice treated with p18-4 HD liposomes showed significantly bigger relative tumor volume compared to mice treated with saline ($P<0.05$). The reason for this

observation is not clear but it could be attributed to the poor bio-distribution profile and/or possible uptake of this formulation by phagocytic cells leading to the generation of inflammatory response in tumor [534-536] as tumors dissected from animals treated with p18-4 liposomes (HD) at the end of study were inflamed and ascetic.

These results are in line with the *in vitro* cytotoxicity results that showed better selectivity of p18-4 (LD) liposomes over p18-4 liposomes (HD). Ligand bearing liposomes have shown greater *in vivo* efficacy in different tumor models than their corresponding non-targeted liposomal formulation in several tumor models, and sometimes resulted into a complete cure [206, 217, 219]. Our results are in agreement with those obtained by Gabizon and co-worker who studied the effect of ligand density in DOX loaded Her2-targeted stealth liposome (HT-PLD) *in vivo* for ligand density of 7.5, 15, or 30 per liposome [537]. Liposomes with ligand density of 15 showed the best safety margin and *in vivo* performance. However, ligand density of 30 exhibited accelerated plasma clearance in the tumor-bearing mice, and the 7.5 ligand density reduced cytotoxicity after *in vivo* passage. Gu et al. [538] prepared nanoparticles with different compositions of diblock copolymers and aptamers to determine the optimal aptamer density on the nanoparticle surface *in vitro*. They reported that increasing the ligand density up to 5% significantly improved the uptake by the target LNCaP cells, but further increase in aptamer density modestly increased the nanoparticle uptake. Mouse model bearing LNCaP xenograft injected with the targeted nanoparticles showed that increasing the aptamer density from 0% to 5% significantly increased

nanoparticle retention in tumors, however the retention decreased significantly for aptamer densities beyond 10%. The authors attributed this reduction with higher aptamer densities to the reduced nanoparticle stealth properties, which resulted into rapid clearance by the liver.

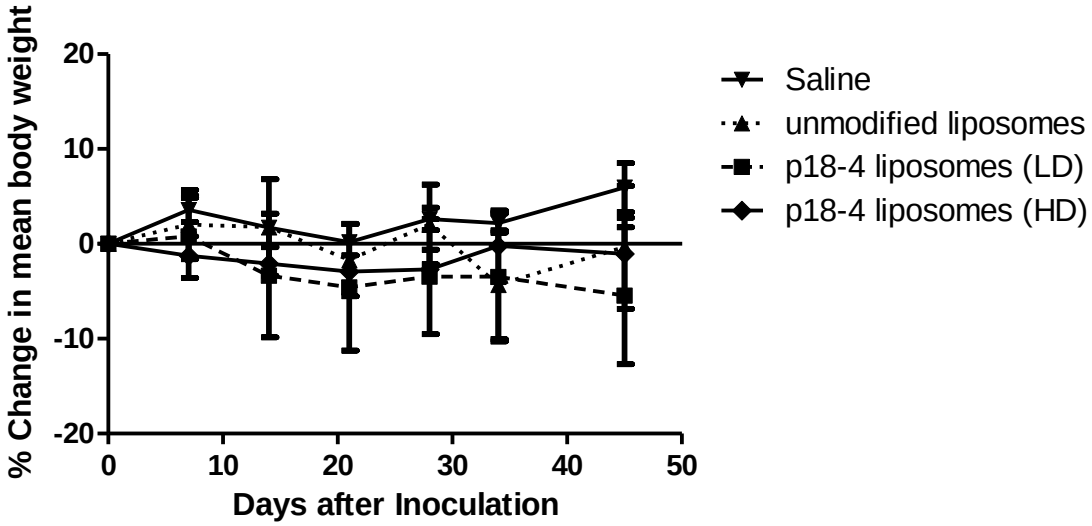

Figure 6-5. Percentage change in mean animal body weight for NOD-SCID mice bearing MDA-MB-435 xenograft treated with 6 i.v. injections of 2.5 mg/kg DOX formulations or saline. Each point represent mean % change in animal weight (n=3-6) ± SEM.

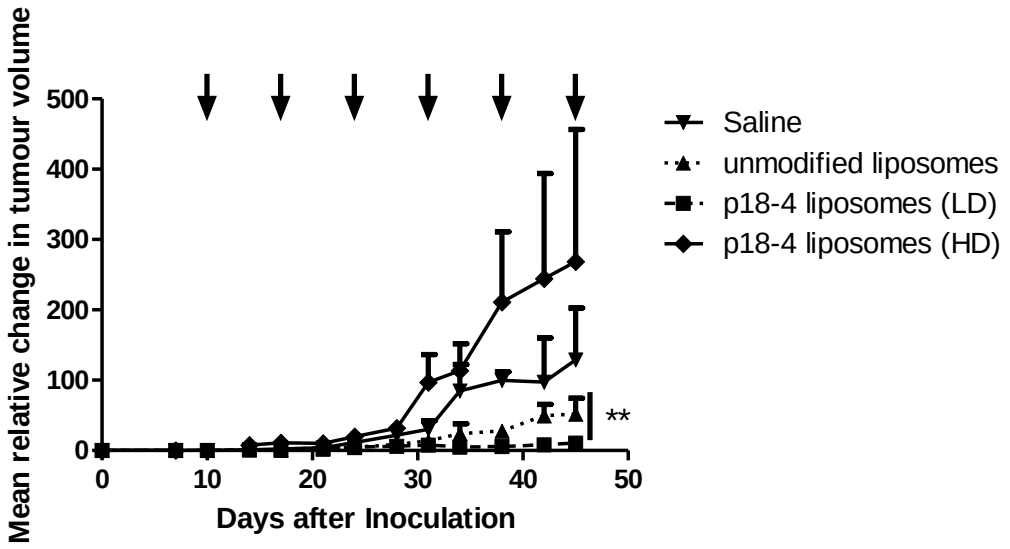

Figure 6-6. Mean relative change in tumor volume in NOD-SCID mice bearing MDA-MB-435 xenograft treated with 6 i.v. injections of 2.5 mg/kg DOX formulations or saline. Each point represent mean relative change in tumor volume (n=3-6) ± SEM. Arrow indicates onset of i.v. injection. ** denotes statistically significant difference (P<0.05).

6.4 Conclusion

We have successfully developed p18-4 peptide targeted stealth liposomal formulations with different peptide density on their surface to effectively deliver DOX to breast cancer. The p18-4 peptide was conjugated to the distal PEG terminus of PEG-DSPE through NHS chemistry. p18-4 decoration dramatically enhanced the cytotoxicity of DOX into MDA-MB-435 and MCF-7. This enhancement of cytotoxicity was dependant on the peptide conjugation level. The selective cytotoxicity of these liposomal formulations was improved by using a liposomal formulation with low density of the p18-4 peptide. The therapeutic efficacy of these carriers into NOD-SCID mice bearing MDA-MB-435 xenograft showed improved tumor volume inhibition dependant on the p18-4 peptide density. This study shows that peptide density plays a significant role determining

the cytotoxicity as well as therapeutic efficacy of formulation against target cells, also p18-4 targeted liposomes have a great potential in the treatment of patient with breast cancer.

Chapter 7
Conclusion and future directions

7.1 General conclusions

Cancer is a significant worldwide problem, and there is a significant need for development of effective specific and well-tolerated chemotherapeutic agent for its management. Considerable effort has been made toward the research of functionalized nanocarriers for cancer-targeted therapy that can fulfil this purpose. Among the functionalized nano-carrier platform, polymeric micelles and liposomes based systems have shown promise. FDA approval of Doxil® and several other on-going clinical trials on other nano-technology based medicines give confidence that more of these formulations will enter the clinic in the near future. There is a strong evidence that these formulations will solve several unsolved problem related to cancer treatment (e.g. drug toxicity). Several targeting modalities have been used to target cancer therapy to specific overexpressed receptors including antibodies, folate, carbohydrates, peptides, etc. Although antibodies are commonly used targeting agents, their use is limited by their large size that hampers tumour penetration, poor stability, and uptake by the RES especially liver and spleen. Peptides on the other hand represent a more fruitful targeting approach due to their small size that facilitate tumour penetration, ease of chemical modification that makes it possible to engineer better targeting ligands and better pharmacokinetic profile as they can stay unrecognized by mononuclear phagocytic cells. Recently, several peptides have been identified through phage display technique that has the capability to target receptor expressed on the surface of tumour cells, e.g. p160 peptide. These peptides can be further modified through chemical manipulation to achieve better

specific binding and improved metabolic stability, e.g. p18-4 peptide. The majority of publications involving the use of phage display peptides are mainly focused on their use in vivo as radio or optical imaging probes for cancer diagnostic applications. However, their use in cancer therapeutic application is still unexplored. Several peptide sequences have been shown in the literature to bind specifically to the tumour breast cancer cell line MDA-MB-435. Examples of these peptides are shown in (**Table 7-1).** Some of these peptides could target specific receptors e.g. (T-antigen, or nucleolin) or their target receptors are unknown (e.g. p160 peptides and its engineered derivative). The clear advantage of the p160 peptide and its derivative over these peptides is their small size (10-12 amino acids) (C.f. F3 peptide, 32 amino acids) this would reduce the chance of toxicity and immunogenicity of the peptide. The dissociation constant (Kd) (a constant describing the affinity and strength of binding between receptors and their ligands) shows the superiority of the p160 peptide (0.86 μM) in compare to T-antigen targeting peptides (10-200 μM). Engineered peptide with even higher binding affinity to the (i.e. p18-4) toward the MDA-MB-435 cells have been utilized in this study.

Table 7-1: Examples of peptides with affinity to the MDA-MB-435 cells.

Sequence	Peptide name	Tumour	Receptors	Cells	Comment	Reference
HGRFILPWWYAFSPS RFRGLISLSQVYLSP ARVSFWRYSSFAPTY GSWYAWSPLVPSAQI	P30 P89 P6 P10	Breast cancer	T-antigen	MDA-MB-435 cells	No data available about in vivo biodistribution and stability. Specificity to all T-antigen expressing tumours.	[539]
KDEPQRRSARLSAKPAPPKPEPKPKKAPAKKC	F3	Breast cancer	Nucleolin on tumour angiogenic endothelial cells	MDA-MB-435 breast carcinoma cells	Bind specifically to nucleolin expressing endothelial cells, and to MDA-435 cells. Long peptide sequence (32 amino acids), i.e. possibility for toxicity and immunogenicity. The peptide shows high renal clearance, in vivo studies showed moderate level of tumour uptake	[540, 541]
VPWMEPAYQRFL	p160	Breast cancer	unknown	MDA-MB-435, MCF-7 breast cancer cells, WAC2 neuroblastoma cells	High tumour to organ ratios compared to RGD-4C peptide. Low in vivo stability	[308, 310]
WXEAAYQRFL	p18	Breast cancer	unknown	Human breast cancer MDA-435, MCF-7	Three folds higher affinity to MDA-435 cells compared to p160 peptide.	[311]

Sequence	Peptide name	Tumour	Receptors	Cells	Comment	Reference
WxEAAYQrFL	p18-4	Breast cancer	unknown	Human breast cancer MDA-435, MCF-7	3.5 folds enhanced binding to MDA-435 cells in compare to p18, improved in vivo stability in human serum and liver homogenate.	[312]

In this thesis, we investigated the utilization of peptide decorated polymeric micelles and liposomes in cancer chemotherapy. The research presented in Chapter 2 investigated the potential of polymeric micelle delivery system based on amphiphilic block co-polymers of (ethylene oxide)-b-poly(ε-caprolactone) (PEO-b- PCL) containing different side groups, i.e, PEO-b-PBCL and PEO-b-P(PTX-CL), as carriers for physical encapsulation of (PTX). Due to the importance of the drug release rate on the pharmacokinetics, biodistribution, therapeutic efficacy and toxicity of nanocarriers, we aimed in that Chapter to determine the best core structure that could solubilize and control the release rate of physically encapsulated PTX. Although micelles composed of PEO-b-PCL showed low physically loading of PTX, they showed better control over the release rate of encapsulated PTX (**Figure 2-7**). On the other hand, micelles made out of the polymeric conjugate PEO-P(CL-PTX) revealed better solubilization capacity of PTX, yet they showed fast release of physically encapsulated PTX (**Figures 2-6 and 2-7**). Micelles of PEO-PBCL showed both intermediate solubilization and release rate control capacity. Based on these finding we proceed further with PCL, PBCL based micelles to prepared actively targeted micelles with p160 peptide on their surface. Chapter 3 provided the proof of concept research that show the potential of p160 peptide for active and selective drug targeting to human cancers using polymeric micelles. We showed the superiority of p160-based micelles over c(RGDfK) micelles in terms of cellular uptake and selective cytotoxicity against different cancer cells (**Figures 3-4 and 3-9**). Chapter 4 presented a new self-assembled polymeric conjugate of PTX,

p160-P(PCL-PTX). This conjugate showed 3.5 folds improved cytotoxicity against MDA-MB-435 cells in compare to unmodified PTX conjugate PEO-P(CL-PTX). Additional development of this conjugate through increasing the PTX conjugation level, and attachment of a higher affinity peptide (i.e. p18-4) was suggested. Further development of PTX loaded p160-PEO-PCL polymeric micelles for in vivo testing was associated with lots of obstacles related to the low solubility of PTX in the obtained micellar formulation (**Tables 2-2 and 3-2**) and difficulty to concentrate these micelles to a suitable therapeutically acceptable concentration. Also, difficulties related to the poor stability of the p160 peptide and its susceptibility to proteolytic degradation in human serum after short time of incubation (**Section 1.1.4.2**). To overcome these problems, we shifted our research toward a synthetic analogue of the biologically active p160 peptide that maintain the significant activity of the parent peptide and with even better biological stability, namely p18-4. In Chapter 5, we developed p18-4 decorated doxorubicin liposomal formulations. The development process of the p18-4 ligand modified liposomes involved investigation of the possible effect of the peptide coupling technique on the cytotoxicity and uptake of the carrier by cancer cells. The peptide coupling technique could significantly affect the way the peptide is presented on the liposomal surface and how it interacts with its target receptors on the tumor cells. In an attempt to find out the best conjugation method; herein, we studied three different techniques to incorporate the p18-4 peptide to the liposomal bilayer: the conventional, post conjugation, and post insertion methods. Overall, the conventional and post conjugation methods led to the production of

comparable DOX liposomal formulation with similar characteristics and behaviour in terms of liposomal size, DOX release, cell uptake and cytotoxicity (**Table 5-1, Figures 5-3 , 5-4, and 5-6**). The p18-4 decorated liposomal DOX formulations were superior to their unmodified counterparts in terms of DOX uptake and cytotoxicity in breast tumor cells (**Figures 5-4 and 5-6**). For in vivo studies, we decided to proceed further with the conventional method due to the ease of that process that excluded the need for use of complex bio-conjugation procedures that is required for the post conjugation method. Since the density of the targeting ligand on the surface of the liposomes plays a huge effect on the targeting efficiency of the carrier both in vitro and in vivo. So, we aimed in Chapter 6 to study the possible effect of the p18-4 ligand density on the cellular uptake and selective cytotoxicity in vitro, as well as its impact on the in vivo therapeutic efficacy in tumour bearing SCID mice. Our results showed that liposomes with high peptide density had lower selective cytotoxicity compared to liposomes decorated with liposomes bearing low peptide density (**Figure 6-4**). These results have been confirmed with in vivo therapeutic efficacy experiment which showed that almost 5 folds decrease in the mean relative tumour volume compared to non-targeted liposomes (**Figure 6-6**). These data could be due to the involvement of non-specific uptake mechanism by increasing the p18-4 ligand density on the liposomes surface. These data suggest that liposomes with a p18-4 density as low as 0.3 mole % is necessary to achieve acceptable targeting efficiency in vivo. This reduced selectivity may be due to increased binding to the non-target cells and decreased binding to target receptors. The deceased

binding to the target receptor at high ligand density may be due to several factor s, including but not limited to steric interference stemming from peptide size, peptide size, packing density, peptide orientation, and receptor mobility. Steric interference between the peptide molecules on the surface of the liposomes may occur due to their tight packing at high density. Small size molecules e.g. folate may allow high packing density on the surface of the nanocarriers without affecting the binding capacity to its receptors. However, the scenario is completely different with bigger molecules e.g. antibodies and peptides. Increasing the average number of ligand per nanocarriers would increase the probability that two peptide molecules exist in close vicinity to each other's. This would create competition between these peptides for a single receptor and will in turn limit the access that ligand has to the receptor. Overcrowding of the peptide would also prevent the peptide from obtaining the necessary orientating for binding to the receptor. Also some receptors may exist as clusters, targeting these clusters may be achieved only by certain ligand avidity (reflected by the density of the peptide on the carrier). However, using high peptide density may consume too much of the available receptors in a way that prevent other particles to bind to that cluster. Many receptors in their active or inactive states have shown this clustering effect, including folate [542], ICAM-1 [543], $\alpha_v\beta_3$ integrins [544], and transferrin receptors [545]. The increased binding to non-target receptor could be due to the low expression level of these receptors on non-target sites, binding of these carriers to non-target receptors occurs only at high density levels. The improved in vivo targeting efficiency that we have seen could be possibly

explained by the improved pharmacokinetic properties of low density targeted liposomes due to reduced systemic clearance and uptake by the RES. Reviewing the available literature studying the in vivo performance of peptide targeted nanocarriers in different tumour model, shows variability in the percentage reduction in the tumour volume; ranging from 20 up 80% with peptide targeted nanocarriers in comparison to untargeted control [240, 546, 547]. This variability could be attributed to difference in tumour models, target receptor type and its degree of expression, and peptide affinity. Herein, our p18-4 targeted liposomal formulation showed 80% reduction in relative tumour volume. To the best of our knowledge, both p160 and p18-4 are up-taken through receptor mediated endocytosis, further investigations on the mechanism involved in the peptide receptor interaction, and the nature of these receptors is still required. Further improvement of the results of the in vivo experiment could be performed through injecting less frequent higher doses of DOX liposomal formulation (i.e. 5 mg/Kg biweekly). This improvement in the therapeutic efficacy has been reported by Charrois and Allen [548] who demonstrated that DOX loaded stealth liposomes at doses of 9 mg/Kg every week or 18 mg/Kg would result in higher peak concentration in the tumour tissue of female Balb/c mice, and had better therapeutic efficacy compared to smaller doses (4.5 mg/Kg) given more frequently. Of note, we have utilized p160 and its engineered derivative p18-4 with several nanocarriers (e.g. polymeric micelles, polymeric conjugate, liposomes), comparing the folds increase in the cytotoxicity of peptide decorated carrier to unmodified carrier shows 1.5 to 3.5 folds decrease in the IC_{50} value.

This comparison shows similarity in the performance of these peptides with different classes of nanocarriers in terms of cytotoxicity improvement. Overall, actively targeted nanocarriers with improved selectivity of anticancer agent delivery have been explored. Here, we have shown peptide type, peptide conjugation technique and peptide density can have a significant impact on the performance of actively targeted nanocarriers.

7.2 Future directions

In this study, we explored multifunctional nanocarriers decorated with breast cancer targeting peptides for anticancer agent's delivery. Future development of these carriers might take several avenues. We might think about investigating the molecular mechanism of both p160, and p18-4 selectivity. To the best of our knowledge, these peptides are uptake into the cells through receptor mediated endocytosis. However, the exact binding receptors for internalization of these peptides into the cells are still unknown. Cell binding assays could be used to determine possible target receptors. Usually receptors are detected and measured by their ability to bind radioactive ligand (peptide) to the cell or cell fragments. Utilization of cell binding assays will help of find the degree of specific binding and non-specific binding as well [549].

Other possible avenues include further investigation on the pharmacokinetics and biodistribution profile of p160 and p18-4 PEO-PEO-P(CL-PTX) polymeric conjugate of paclitaxel. Further increase in the PTX conjugation level (i.e. > 16% by weight) reported in Chapter 4 is suggested.

Another area for future development is studying the pharmacokinetics and biodistribution of p18-4 modified DOX liposomal carrier in an attempt to explore how they behave inside the body. This would allow us to properly optimize the carrier in a way that improves its therapeutic outcome.

Multidrug resistance is still one of the biggest obstacles that hinder successful chemotherapy. The delivery of drugs through targeted nanocarriers that are internalizable by an alternative way to simple diffusion may allow targeted delivery system to bypass the activity of membrane efflux pump, known as MDR transporters. These transporter carry a variety of anticancer drugs out of the cancer cell to produce resistance against chemotherapy. Folate mediated cell uptake of DOX loaded liposomes into MDR cell lines have previously shown to be unaffected by p-glycoprotein mediated drug efflux, in contrast to free DOX [418]. Also, Vincristine loaded lipid nanoparticles modified with anti-Pgp mAbs (MAK-16) showed greater cytotoxicity in resistant myelogenous leukemia cells compared to non-targeted particles [222]. Our preliminary data on the development of functionalized polymeric micelles of p160-PEO_{5k}-PCL_{5k}, p160-PEO_{5k}-$PBCL_{5k}$, c(RGDfK)-PEO_{5k}-PCL_{5k}, and c(RGDfK)-PEO_{5k}-$PBCL_{5k}$ containing PTX against MDA-MB-435 MDR cells showed great potential for micelles having PCL core over micelles having PBCL core (data not shown). This finding is supported by the results obtained by Elmanchili et al. [550] who reported the potential of PEO-PCL diblock copolymer to reverse multidrug resistance in MDR cancer cells through inhibition of the p-glycoprotein function. Low MW PEO-b-PCL block copolymer showed the capability to increase the

accumulation of P-gp substrates above the CMC and little activity below the CMC, however the mechanism of this inhibition was attributed to the unimers with similar inhibition mechanism to pluronics (PEO-PPO-PEO) [551-553]. Also, combination therapy with MDR pump inhibitor (e.g. PSC 833, VX-710, S9788, SR 33557, Elacridar, Zosuquidar, Rariquidar, and ontogeny) might be alternative approach to address the problem of development of multidrug resistance. We have tested this approach with free PTX, free DOX and Doxil and we have found that 30 minutes pre-treatment of the MDA-435 MDR cells with 1 µg/mL of valspodar, an analogue of cyclosporine-A with potential P-gp inhibition activity, resulted in a significant increase in the cytotoxicity of free drugs and liposomal carrier against MDA-435 MDR cells after 24 h incubation (**Table 7-2, Figure 7-1, Figure 7-2)** . The next challenge would be co-encapsulation of both doxorubicin and valspodar into the same carrier.

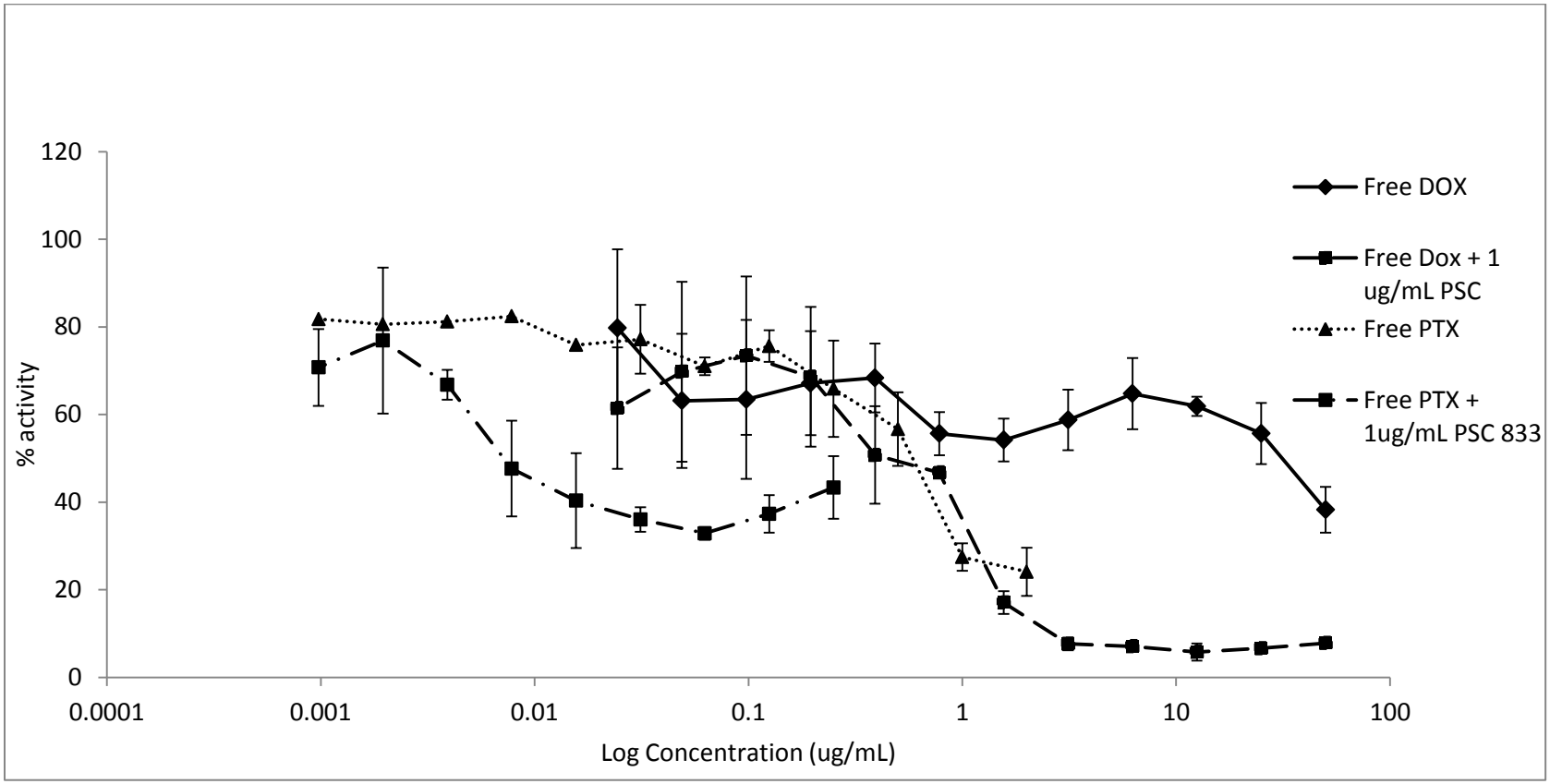

Figure 7-1: Cytotoxicity of free DOX and PTX after 24 h incubation against MDA-435 MDR before and after pre-treatment with 1 µg/mL PSC833.

Table 7-2: Cytotoxicity of Free DOX and PTX and modulation of drug resistance by PSC833 in human MDA-MB-435 MDR cancer cells.

Treatment	Pre-treatment	MDA-435 cell type	Absolute IC_{50} (ug/mL)	RF[a]	FS[b]
Free DOX	none	WT	0.34± 0.05	N/A	
	none	MDR	23.44 ± 7.96	69.3	
Free DOX	PSC 833 (1µg/mL) 30 min	MDR	0.46± 0.06	1.4	50.95
Free PTX	none	WT	0.01 ± 0.004	N/A	
	none	MDR	0.51± 0.15	51	
Free PTX	PSC 833 (1µg/mL) 30 min	MDR	0.01±0.01	0.9	51

[a] Resistance factor: IC_{50} of DOX or PTX in MDR cells divided by IC_{50} of the same drug in WT cells.

[b] Fold sensitization: IC_{50} of DOX or PTX in MDR cells divided by IC_{50} after pre-treatment with PSC833.

N/A : not applicable.

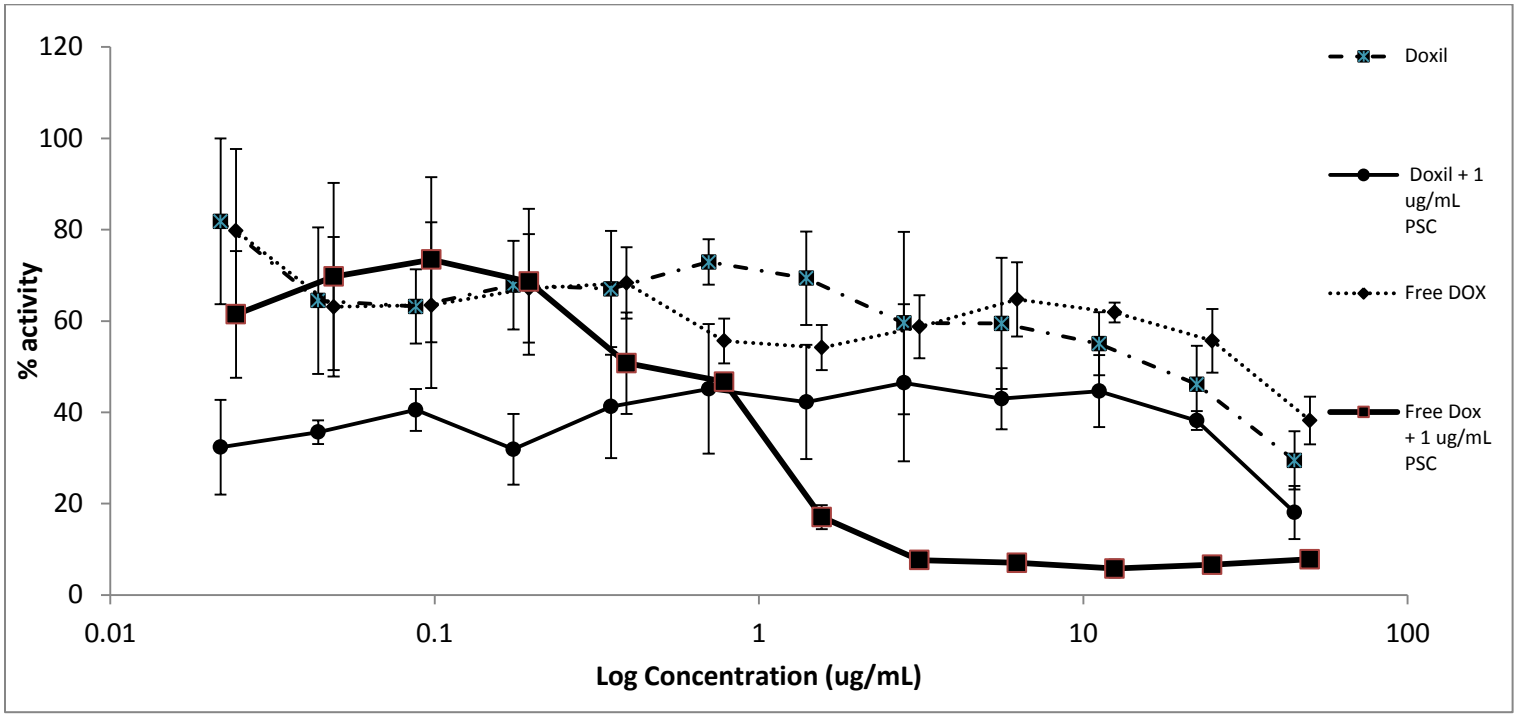

Figure 7-2: The Cytotoxicity profile of Doxil, and free DOX after 24 h incubation with MDA-435 MDR cells before and after pre-treatment with 1 µg/mL PSC 833.

Another future avenue is the utilization of these carrier for effective delivery of large molecules e.g. siRNA. Nowadays, one of the most challenging task in the development of therapeutic for siRNA is the lack of specificity of siRNA to the tissues and cells [554]. The targeted delivery not only minimizes the chances of development of side effects, but also reduces the amount of doses required to achieve the desired therapeutic effect. Cell specific ligand (e.g. antibodies [555], sugar, vitamins, peptides [556, 557]) have been largely employed to confer cell specificity on siRNA delivery system. Active targeting mechanism takes the advantage of high specific interaction between the targeting ligand and cell receptors in a way that increase the cellular uptake by the tumour and increase tumour retention. In general, peptides are more preferred for this purpose due to high stability, high purity, ease of production through synthetic routes, and non-immunogenicity. We might think about delivery of siRNA through PEGylated PEI, cationic liposomes, or polymeric micelles functionalized with polyamine core for efficient encapsulation and delivery of siRNA.

Although several reports have shown the advantages of targeted therapeutic versus non targeted formulation, yet in clinical practice there is no easy answer to whether targeted formulation will be superior to untargeted one. This would be due to variability the degree of receptor expression on the surface of the tumour cells among different patients [558]. Therefore, in clinical setting when a new targeted therapeutic enter clinical trials, it is important to determine if there is enough cell population that could express the target receptors are available or not. This way we will determine whether a targeted therapeutics will perform better

compared to non-targeted one. In other words, a customized treatment plan for each patient is our goal. Another way to solve this problem of heterogeneous target expression is to utilize a dual ligand approach, in which we will decorate the liposomes with two different types of targeting ligands to increase the targeting specificity and affinity. Some of our initial work with double targeted DiI loaded polymeric micelles of PEO-b-PBCL with both c(RGDfK) and p160 showed some promising results revealing increased cellular uptake of the p160-RGD- double targeted micelles in compare to micelle targeted with a single ligand c(RGDfK). This approach necessitates a better knowledge of the p160 receptors and other receptors located in close proximity to properly choose the two ligands.

Although we are still far from Nobel prize winner Paul Ehrlich's magic bullet [559], many believe that we might enter an era in which targeted nanocarriers approach will represent an important modality for therapeutic and diagnostic therapy.

7.3 References

1. Jemal, A., et al., *Global cancer statistics.* CA: A Cancer Journal for Clinicians, 2011. **61**(2): p. 69-90.
2. Singhal, S., S. Nie, and M.D. Wang, *Nanotechnology applications in surgical oncology.* Annual Review of Medicine, 2010. **61**: p. 359-73.
3. Das, M., C. Mohanty, and S.K. Sahoo, *Ligand-based targeted therapy for cancer tissue.* Expert Opinion on Drug Delivery, 2009. **6**(3): p. 285-304.
4. Parveen, S. and S.K. Sahoo, *Nanomedicine: clinical applications of polyethylene glycol conjugated proteins and drugs.* Clinical Pharmacokinetics, 2006. **45**(10): p. 965-88.
5. Parveen, S. and S.K. Sahoo, *Polymeric nanoparticles for cancer therapy.* J Drug Target, 2008. **16**(2): p. 108-23.
6. Adiseshaiah, P.P., J.B. Hall, and S.E. McNeil, *Nanomaterial standards for efficacy and toxicity assessment.* Wiley Interdiscip Rev Nanomed Nanobiotechnol, 2010. **2**(1): p. 99-112.
7. Bhushan, B., *Springer Handbook of Nanotechnology*. 2004: Springer-Verlag.
8. Cai, W., et al., *Applications of gold nanoparticles in cancer nanotechnology.* Nanotechnology, Science and Applications, 2008. **1**: p. 17-32.
9. Misra, R., S. Acharya, and S.K. Sahoo, *Cancer nanotechnology: application of nanotechnology in cancer therapy.* Drug Discovery Today, 2010. **15**(19-20): p. 842-50.
10. Smith, A.M., et al., *Multicolor quantum dots for molecular diagnostics of cancer.* Expert Review of Molecular Diagnostics, 2006. **6**(2): p. 231-244.
11. Gabizon, A., *Application of liposomal drug delivery in cancer therapy*, in *Nanotechnology for Cancer Therapy*, M.M. Amiji, Editor. 2007, CRC/Taylor & Francis. p. 595-607.
12. James, J., *DOXIL approved for KS.* AIDS Treatment News, 1995(236): p. 6.
13. Swenson, C., et al., *Liposome technology and the development of Myocet™(liposomal doxorubicin citrate).* The Breast, 2001. **10**: p. 1-7.
14. Matsumura, Y., et al., *Phase I and pharmacokinetic study of MCC-465, a doxorubicin (DXR) encapsulated in PEG immunoliposome, in patients with metastatic stomach cancer.* Annals of Oncology, 2004. **15**(3): p. 517-25.
15. Wood, B., et al. *Phase I study of thermally sensitive liposomes containing doxorubicin (ThermoDox) given during radiofrequency ablation (RFA) in patients with unresectable hepatic malignancies (Abstract)*. 2007.
16. ClinicalTrials.gov. *Phase 3 Study of ThermoDox With Radiofrequency Ablation (RFA) in Treatment of Hepatocellular Carcinoma (HCC).* June 7, 2011 June 25, 2012]; Available from: http://www.clinicaltrials.gov/ct2/show/NCT00617981?term=thermodox&rank=3.

17. Forssen, E.A., *The design and development of DaunoXome® for solid tumor targeting in vivo.* Advanced Drug Delivery Reviews, 1997. **24**(2-3): p. 133-150.
18. Glantz, M.J., et al., *A randomized controlled trial comparing intrathecal sustained-release cytarabine (DepoCyt) to intrathecal methotrexate in patients with neoplastic meningitis from solid tumors.* Clin Cancer Res, 1999. **5**(11): p. 3394-402.
19. Jaeckle, K.A., et al., *An open label trial of sustained-release cytarabine (DepoCyt) for the intrathecal treatment of solid tumor neoplastic meningitis.* Journal of Neuro-Oncology, 2002. **57**(3): p. 231-9.
20. Phuphanich, S., et al., *A pharmacokinetic study of intra-CSF administered encapsulated cytarabine (DepoCyt) for the treatment of neoplastic meningitis in patients with leukemia, lymphoma, or solid tumors as part of a phase III study.* Journal of Neuro-Oncology, 2007. **81**(2): p. 201-8.
21. Duffaud, F., et al., *Phase II study of OSI-211 (liposomal lurtotecan) in patients with metastatic or loco-regional recurrent squamous cell carcinoma of the head and neck. An EORTC New Drug Development Group study.* European Journal of Cancer, 2004. **40**(18): p. 2748-52.
22. Seiden, M.V., et al., *A phase II study of liposomal lurtotecan (OSI-211) in patients with topotecan resistant ovarian cancer.* Gynecologic Oncology, 2004. **93**(1): p. 229-32.
23. Dragovich, T., et al., *A Phase 2 trial of the liposomal DACH platinum L-NDDP in patients with therapy-refractory advanced colorectal cancer.* Cancer Chemotherapy and Pharmacology, 2006. **58**(6): p. 759-64.
24. Fetterly, G.J., et al., *Pharmacokinetic/pharmacodynamic modeling and simulation of neutropenia during phase I development of liposome-entrapped paclitaxel.* Clin Cancer Res, 2008. **14**(18): p. 5856-63.
25. Schuch, G., *EndoTAG-1. MediGene.* Current Opinion in Investigational Drugs, 2005. **6**(12): p. 1259-65.
26. Ko, A., et al., *A multinational phase II study of liposome irinotecan (PEP02) for patients with gemcitabine-refractory metastatic pancreatic cancer. 2011 Gastrointestinal Cancers Symposium.* Journal of Clinical Oncology, 2011. **29**(4): p. 237.
27. Chen, L., et al. *Phase I study of liposome encapsulated irinotecan (PEP02) in advanced solid tumor patients*. 2008.
28. Mylonakis, N., et al., *Phase II study of liposomal cisplatin (Lipoplatin™) plus gemcitabine versus cisplatin plus gemcitabine as first line treatment in inoperable (stage IIIB/IV) non-small cell lung cancer.* Lung Cancer, 2010. **68**(2): p. 240-247.
29. Stathopoulos, G.P., et al., *Pharmacokinetics and adverse reactions of a new liposomal cisplatin (Lipoplatin): phase I study.* Oncology Reports, 2005. **13**(4): p. 589-596.
30. Phan, A. *Open label phase I study of MBP-426, a novel formulation of oxalipatin, in patients with advanced or metastatic solid tumors*. 2007.

31. Sankhala, K., et al., *A phase I pharmacokinetic (PK) study of MBP-426, a novel liposome encapsulated oxaliplatin.* J. Clin. Oncol, 2009. **27**(15): p. 2535.
32. Wu, H., et al., *Population Pharmacokinetics of Pegylated Liposomal CKD-602 (S-CKD602) in Patients With Advanced Malignancies.* Journal of Clinical Pharmacology, 2011.
33. Zamboni, W.C., et al., *Bidirectional pharmacodynamic interaction between pegylated liposomal CKD-602 (S-CKD602) and monocytes in patients with refractory solid tumors.* Journal of Liposome Research, 2011. **21**(2): p. 158-65.
34. Zamboni, W.C., et al., *Phase I and pharmacokinetic study of pegylated liposomal CKD-602 in patients with advanced malignancies.* Clin Cancer Res, 2009. **15**(4): p. 1466-72.
35. Zamboni, W.C., et al., *Pharmacokinetic study of pegylated liposomal CKD-602 (S-CKD602) in patients with advanced malignancies.* Clinical Pharmacology and Therapeutics, 2009. **86**(5): p. 519-26.
36. Kim, D.W., et al., *Multicenter phase II trial of Genexol-PM, a novel Cremophor-free, polymeric micelle formulation of paclitaxel, with cisplatin in patients with advanced non-small-cell lung cancer.* Annals of Oncology, 2007. **18**(12): p. 2009-14.
37. Lee, K.S., et al., *Multicenter phase II trial of Genexol-PM, a Cremophor-free, polymeric micelle formulation of paclitaxel, in patients with metastatic breast cancer.* Breast Cancer Research and Treatment, 2008. **108**(2): p. 241-50.
38. Lim, W.T., et al., *Phase I pharmacokinetic study of a weekly liposomal paclitaxel formulation (Genexol-PM) in patients with solid tumors.* Annals of Oncology, 2010. **21**(2): p. 382-8.
39. Hamaguchi, T., et al., *A phase I and pharmacokinetic study of NK105, a paclitaxel-incorporating micellar nanoparticle formulation.* British Journal of Cancer, 2007. **97**(2): p. 170-6.
40. Kato, K., et al., *Phase II study of NK105, a paclitaxel-incorporating micellar nanoparticle, for previously treated advanced or recurrent gastric cancer.* Investigational New Drugs, 2011.
41. Peterson, C., *Drug therapy of cancer.* European Journal of Clinical Pharmacology, 2011. **67**(5): p. 437-447.
42. Lammers, T., et al., *Drug targeting to tumors: principles, pitfalls and (pre-) clinical progress.* Journal of Controlled Release, 2011.
43. Matsumura, Y., *Poly (amino acid) micelle nanocarriers in preclinical and clinical studies.* Adv Drug Deliv Rev, 2008. **60**(8): p. 899-914.
44. Plummer, R., et al., *A Phase I clinical study of cisplatin-incorporated polymeric micelles (NC-6004) in patients with solid tumours.* British Journal of Cancer, 2011. **104**(4): p. 593-8.
45. Nishiyama, N., H. Cabral, and K. Kataoka, *Micellar Structures as Drug Delivery Systems.* Drug Delivery in Oncology, 2012: p. 1051-1069.

46. Hamaguchi, T., et al., *Phase I study of NK012, a novel SN-38-incorporating micellar nanoparticle, in adult patients with solid tumors.* Clin Cancer Res, 2010. **16**(20): p. 5058-66.
47. Elsadek, B. and F. Kratz, *Impact of albumin on drug delivery - New applications on the horizon.* J Control Release, 2012. **157**(1): p. 4-28.
48. Montana, M., et al., *Albumin-bound paclitaxel: the benefit of this new formulation in the treatment of various cancers.* Journal of Chemotherapy, 2011. **23**(2): p. 59-66.
49. Montero, A.J., et al., *Nab-paclitaxel in the treatment of metastatic breast cancer: a comprehensive review.* Expert Rev Clin Pharmacol, 2011. **4**(3): p. 329-34.
50. Socinski, M.A., et al., *Weekly nab-Paclitaxel in Combination With Carboplatin Versus Solvent-Based Paclitaxel Plus Carboplatin as First-Line Therapy in Patients With Advanced Non-Small-Cell Lung Cancer: Final Results of a Phase III Trial.* Journal of Clinical Oncology, 2012. **30**(17): p. 2055-62.
51. Yamamoto, Y., I. Kawano, and H. Iwase, *Nab-paclitaxel for the treatment of breast cancer: efficacy, safety, and approval.* Onco Targets Ther, 2011. **4**: p. 123-36.
52. Sanna, V. and M. Sechi, *Nanoparticle therapeutics for prostate cancer treatment.* Nanomedicine, 2012.
53. Zhao, P. and D. Astruc, *Docetaxel nanotechnology in anticancer therapy.* Chemmedchem, 2012. **7**(6): p. 952-72.
54. Beija, M., et al., *Colloidal systems for drug delivery: from design to therapy.* Trends in Biotechnology, 2012.
55. Gaur, S., et al., *Preclinical study of the cyclodextrin-polymer conjugate of camptothecin CRLX101 for the treatment of gastric cancer.* Nanomedicine, 2011.
56. Svenson, S., et al., *Preclinical to clinical development of the novel camptothecin nanopharmaceutical CRLX101.* J Control Release, 2011. **153**(1): p. 49-55.
57. Young, C., et al., *CRLX101 (formerly IT-101)-A Novel Nanopharmaceutical of Camptothecin in Clinical Development.* Current Bioactive Compounds, 2011. **7**(1): p. 8-14.
58. Dinndorf, P.A., et al., *FDA drug approval summary: Pegaspargase (Oncaspar®) for the first-line treatment of children with acute lymphoblastic leukemia (ALL).* The Oncologist, 2007. **12**(8): p. 991-998.
59. Alconcel, S.N.S., A.S. Baas, and H.D. Maynard, *FDA-approved poly (ethylene glycol)–protein conjugate drugs.* Polymer Chemistry, 2011.
60. Graham, C., et al., *A Phase I/II Study of Xyotax (CT-2103), A Tumor-Targeted Taxane, in Patients With Recurrent Ovarian Cancer.* 2011.
61. Beer, T.M., et al., *A phase II study of paclitaxel poliglumex in combination with transdermal estradiol for the treatment of metastatic castration-resistant prostate cancer after docetaxel chemotherapy.* Anticancer Drugs, 2010. **21**(4): p. 433-8.

62. Langer, C.J., et al., *Phase III trial comparing paclitaxel poliglumex (CT-2103, PPX) in combination with carboplatin versus standard paclitaxel and carboplatin in the treatment of PS 2 patients with chemotherapy-naive advanced non-small cell lung cancer.* Journal of Thoracic Oncology, 2008. **3**(6): p. 623-30.
63. Lin, N.U., et al., *Phase II study of CT-2103 as first- or second-line chemotherapy in patients with metastatic breast cancer: unexpected incidence of hypersensitivity reactions.* Investigational New Drugs, 2007. **25**(4): p. 369-75.
64. Paz-Ares, L., et al., *Phase III trial comparing paclitaxel poliglumex vs docetaxel in the second-line treatment of non-small-cell lung cancer.* British Journal of Cancer, 2008. **98**(10): p. 1608-13.
65. Homsi, J., et al., *Phase I trial of poly-L-glutamate camptothecin (CT-2106) administered weekly in patients with advanced solid malignancies.* Clin Cancer Res, 2007. **13**(19): p. 5855-61.
66. Posey, J.A., 3rd, et al., *Phase 1 study of weekly polyethylene glycol-camptothecin in patients with advanced solid tumors and lymphomas.* Clin Cancer Res, 2005. **11**(21): p. 7866-71.
67. Scott, L.C., et al., *A phase II study of pegylated-camptothecin (pegamotecan) in the treatment of locally advanced and metastatic gastric and gastro-oesophageal junction adenocarcinoma.* Cancer Chemotherapy and Pharmacology, 2009. **63**(2): p. 363-70.
68. Miele, E., et al., *Albumin-bound formulation of paclitaxel (Abraxane® ABI-007) in the treatment of breast cancer.* International Journal of Nanomedicine, 2009. **4**: p. 99.
69. Gradishar, W.J., et al., *Phase III trial of nanoparticle albumin-bound paclitaxel compared with polyethylated castor oil–based paclitaxel in women with breast cancer.* Journal of Clinical Oncology, 2005. **23**(31): p. 7794-7803.
70. Bartels, C.L. and A. Wilson, *How does a novel formulation of paclitaxel affect drug delivery in metastatic breast cancer.* US Pharm, 2004. **29**.
71. Green, M., et al., *Abraxane®, a novel Cremophor®-free, albumin-bound particle form of paclitaxel for the treatment of advanced non-small-cell lung cancer.* Annals of Oncology, 2006. **17**(8): p. 1263-1268.
72. Ibrahim, N.K., et al., *Multicenter phase II trial of ABI-007, an albumin-bound paclitaxel, in women with metastatic breast cancer.* Journal of Clinical Oncology, 2005. **23**(25): p. 6019-6026.
73. Damascelli, B., et al., *Intraarterial chemotherapy with polyoxyethylated castor oil free paclitaxel, incorporated in albumin nanoparticles (ABI-007).* Cancer, 2001. **92**(10): p. 2592-2602.
74. Kratz, F., *Albumin as a drug carrier: Design of prodrugs, drug conjugates and nanoparticles.* Journal of Controlled Release, 2008. **132**(3): p. 171-183.
75. Perez, A.T., et al., *Pegylated liposomal doxorubicin (Doxil) for metastatic breast cancer: the Cancer Research Network, Inc., experience.* Cancer Investigation, 2002. **20 Suppl 2**: p. 22-9.

76. Porche, D.J., *Liposomal doxorubicin (Doxil).* Journal of the Association of Nurses in AIDS Care, 1996. **7**(2): p. 55-9.
77. Tejada-Berges, T., et al., *Caelyx/Doxil for the treatment of metastatic ovarian and breast cancer.* Expert Review of Anticancer Therapy, 2002. **2**(2): p. 143-50.
78. Northfelt, D.W., et al., *Doxorubicin encapsulated in liposomes containing surface-bound polyethylene glycol: pharmacokinetics, tumor localization, and safety in patients with AIDS-related Kaposi's sarcoma.* Journal of Clinical Pharmacology, 1996. **36**(1): p. 55-63.
79. Barenholz, Y.C., *Doxil(R) - The first FDA-approved nano-drug: Lessons learned.* J Control Release, 2012. **160**(2): p. 117-34.
80. Safra, T., et al., *Pegylated liposomal doxorubicin (doxil): reduced clinical cardiotoxicity in patients reaching or exceeding cumulative doses of 500 mg/m2.* Annals of Oncology, 2000. **11**(8): p. 1029-33.
81. Hoffman, A.S., *The origins and evolution of "controlled" drug delivery systems.* J Control Release, 2008. **132**(3): p. 153-63.
82. Batist, G., et al., *Myocet (liposome-encapsulated doxorubicin citrate): a new approach in breast cancer therapy.* Expert Opinion on Pharmacotherapy, 2002. **3**(12): p. 1739-1751.
83. Mross, K., et al., *Pharmacokinetics of liposomal doxorubicin (TLC-D99; Myocet) in patients with solid tumors: an open-label, single-dose study.* Cancer Chemotherapy and Pharmacology, 2004. **54**(6): p. 514-524.
84. Fassas, A., et al., *Safety and early efficacy assessment of liposomal daunorubicin (DaunoXome) in adults with refractory or relapsed acute myeloblastic leukaemia: a phase I–II study.* British Journal of Haematology, 2002. **116**(2): p. 308-315.
85. O'Byrne, K., et al., *A phase I dose-escalating study of DaunoXome, liposomal daunorubicin, in metastatic breast cancer.* British Journal of Cancer, 2002. **87**(1): p. 15-20.
86. Drugs.com. *DaunoXome® (daunorubicin citrate liposome injection)*. 2012 05/2012 28/06/2012]; Available from: http://www.drugs.com/pro/daunoxome.html.
87. Drugs.com. *DepoCyt® (cytarabine liposome injection)*. 2012 09/2011 28/06/2012]; Available from: http://www.drugs.com/pro/depocyt.html.
88. Craig, C., *Current treatment approaches for neoplastic meningitis: nursing management of patients receiving intrathecal DepoCyt.* Oncology Nursing Forum, 2000. **27**(8): p. 1225-30; quiz 1231-2.
89. Phuphanich, S. and C. Brock, *Neurologic improvement after high-dose intravenous immunoglobulin therapy in patients with paraneoplastic cerebellar degeneration associated with anti-Purkinje cell antibody.* Journal of Neuro-Oncology, 2007. **81**(1): p. 67-9.
90. Kim, T.Y., et al., *Phase I and pharmacokinetic study of Genexol-PM, a cremophor-free, polymeric micelle-formulated paclitaxel, in patients with advanced malignancies.* Clinical Cancer Research, 2004. **10**(11): p. 3708-3716.

91. Kim, S.C., et al., *In vivo evaluation of polymeric micellar paclitaxel formulation: toxicity and efficacy.* Journal of Controlled Release, 2001. **72**(1-3): p. 191-202.
92. Kim, D.W., et al., *Multicenter phase II trial of Genexol-PM, a novel Cremophor-free, polymeric micelle formulation of paclitaxel, with cisplatin in patients with advanced non-small-cell lung cancer.* Annals of Oncology, 2007. **18**(12): p. 2009-2014.
93. Rizzari, C., *Asparaginase treatment.* Acute Leukemias, 2003: p. 381.
94. Bader, H., H. Ringsdorf, and B. Schmidt, *Watersoluble polymers in medicine.* Die Angewandte Makromolekulare Chemie, 1984. **123**(1): p. 457-485.
95. Masayuki, Y., et al., *Polymer micelles as novel drug carrier: Adriamycin-conjugated poly (ethylene glycol)-poly (aspartic acid) block copolymer.* Journal of Controlled Release, 1990. **11**(1-3): p. 269-278.
96. Kwon, G., et al., *Enhanced tumor accumulation and prolonged circulation times of micelle-forming poly (ethylene oxide-aspartate) block copolymer-adriamycin conjugates.* Journal of Controlled Release, 1994. **29**(1): p. 17-23.
97. Nishiyama, N. and K. Kataoka, *Current state, achievements, and future prospects of polymeric micelles as nanocarriers for drug and gene delivery.* Pharmacology & Therapeutics, 2006. **112**(3): p. 630-648.
98. Kabanov, A.V., et al., *The neuroleptic activity of haloperidol increases after its solubilization in surfactant micelles. Micelles as microcontainers for drug targeting.* FEBS Letters, 1989. **258**(2): p. 343-5.
99. Aliabadi, H.M. and A. Lavasanifar, *Polymeric micelles for drug delivery.* Expert Opinion on Drug Delivery, 2006. **3**(1): p. 139-62.
100. Jones, M.C. and J.C. Leroux, *Polymeric micelles-a new generation of colloidal drug carriers.* European Journal of Pharmaceutics and Biopharmaceutics, 1999. **48**(2): p. 101-111.
101. Adams, M.L., A. Lavasanifar, and G.S. Kwon, *Amphiphilic block copolymers for drug delivery.* J Pharm Sci, 2003. **92**(7): p. 1343-55.
102. Trubetskoy, V.S., *Polymeric micelles as carriers of diagnostic agents.* Advanced Drug Delivery Reviews, 1999. **37**(1-3): p. 81-88.
103. Torchilin, V.P., *Targeted polymeric micelles for delivery of poorly soluble drugs.* Cellular and Molecular Life Sciences, 2004. **61**(19-20): p. 2549-59.
104. Gao, Z., et al., *Diacyllipid-polymer micelles as nanocarriers for poorly soluble anticancer drugs.* Nano Letters, 2002. **2**(9): p. 979-982.
105. Sutton, D., et al., *Functionalized micellar systems for cancer targeted drug delivery.* Pharmaceutical Research, 2007. **24**(6): p. 1029-1046.
106. Patel, S.K., A. Lavasanifar, and P. Choi, *Prediction of the solubility of cucurbitacin drugs in self-associating poly (ethylene oxide)-b-poly ([alpha]-benzyl carboxylate-caprolactone) block copolymer with different tacticities using molecular dynamics simulation.* Biomaterials, 2010. **31**(2): p. 345-357.

107. Kabanov, A.V., E.V. Batrakova, and V.Y. Alakhov, *Pluronic® block copolymers as novel polymer therapeutics for drug and gene delivery.* Journal of Controlled Release, 2002. **82**(2): p. 189-212.
108. Torchilin, V.P., *Structure and design of polymeric surfactant-based drug delivery systems.* Journal of Controlled Release, 2001. **73**(2): p. 137-172.
109. Maeda, H., et al., *Tumor vascular permeability and the EPR effect in macromolecular therapeutics: a review.* Journal of Controlled Release, 2000. **65**(1-2): p. 271-284.
110. Duncan, R., *Polymer conjugates as anticancer nanomedicines.* Nature Reviews Cancer, 2006. **6**(9): p. 688-701.
111. Iwai, K., H. Maeda, and T. Konno, *Use of oily contrast medium for selective drug targeting to tumor: enhanced therapeutic effect and X-ray image.* Cancer Research, 1984. **44**(5): p. 2115.
112. Matsumura, Y. and H. Maeda, *A new concept for macromolecular therapeutics in cancer chemotherapy: mechanism of tumoritropic accumulation of proteins and the antitumor agent smancs.* Cancer Res, 1986. **46**(12 Pt 1): p. 6387-92.
113. Maeda, H., T. Sawa, and T. Konno, *Mechanism of tumor-targeted delivery of macromolecular drugs, including the EPR effect in solid tumor and clinical overview of the prototype polymeric drug SMANCS.* J Control Release, 2001. **74**(1-3): p. 47-61.
114. Maeda, H., *Enhanced permeability and retention (EPR) effect: basis for drug targeting to tumor*. 2002: Kluwer Academic Publishers: Norwell, MA.
115. Fang, J., H. Nakamura, and H. Maeda, *The EPR effect: Unique features of tumor blood vessels for drug delivery, factors involved, and limitations and augmentation of the effect.* Advanced Drug Delivery Reviews, 2011. **63**(3): p. 136-151.
116. Litzinger, D.C., et al., *Effect of liposome size on the circulation time and intraorgan distribution of amphipathic poly(ethylene glycol)-containing liposomes.* Biochimica et Biophysica Acta, 1994. **1190**(1): p. 99-107.
117. Takakura, Y. and M. Hashida, *Macromolecular carrier systems for targeted drug delivery: pharmacokinetic considerations on biodistribution.* Pharm Res, 1996. **13**(6): p. 820-31.
118. Illum, L., et al., *The organ distribution and circulation time of intravenously injected colloidal carriers sterically stabilized with a block copolymer--poloxamine 908.* Life Sciences, 1987. **40**(4): p. 367-74.
119. Bae, K.H., H.J. Chung, and T.G. Park, *Nanomaterials for cancer therapy and imaging.* Molecules and Cells, 2011. **31**(4): p. 295-302.
120. Yokoyama, M., *Clinical Applications of Polymeric Micelle Carrier Systems in Chemotherapy and Image Diagnosis of Solid Tumors.* Journal of Experimental & Clinical Medicine, 2011.
121. Yokoyama, M., et al., *Toxicity and antitumor activity against solid tumors of micelle-forming polymeric anticancer drug and its extremely long circulation in blood.* Cancer Research, 1991. **51**(12): p. 3229.

122. Kazunori, K., et al., *Block copolymer micelles as vehicles for drug delivery.* Journal of Controlled Release, 1993. **24**(1): p. 119-132.
123. Hamaguchi, T., et al., *NK105, a paclitaxel-incorporating micellar nanoparticle formulation, can extend in vivo antitumour activity and reduce the neurotoxicity of paclitaxel.* British Journal of Cancer, 2005. **92**(7): p. 1240-6.
124. Kato, K., et al., *Phase I study of NK105, a paclitaxel-incorporating micellar nanoparticle, in patients with advanced cancer.* J. Clin. Oncol, 2006. **24**: p. 2018.
125. Nishiyama, N., et al., *Novel cisplatin-incorporated polymeric micelles can eradicate solid tumors in mice.* Cancer Research, 2003. **63**(24): p. 8977.
126. Wilson, R., et al., *Phase I and pharmacokinetic study of NC-6004, a new platinum entity of cisplatin-conjugated polymer forming micelles.* Journal of Clinical Oncology, 2008. **26**: p. 2573.
127. nanocarrier.co.jp. *NC-4016 DACH-Platin Micelle*. 2012 17/06/11 04/07/12]; Available from: http://www.nanocarrier.co.jp/en/research/pipeline/03.html.
128. Koizumi, F., et al., *Novel SN-38–Incorporating Polymeric Micelles, NK012, Eradicate Vascular Endothelial Growth Factor–Secreting Bulky Tumors.* Cancer Research, 2006. **66**(20): p. 10048.
129. Sumitomo, M., et al., *Novel SN-38–incorporated polymeric micelle, NK012, strongly suppresses renal cancer progression.* Cancer Research, 2008. **68**(6): p. 1631.
130. Saito, Y., et al., *Enhanced distribution of NK012, a polymeric micelle-encapsulated SN-38, and sustained release of SN-38 within tumors can beat a hypovascular tumor.* Cancer Science, 2008. **99**(6): p. 1258-1264.
131. Eguchi Nakajima, T., et al., *Antitumor Effect of SN-38–Releasing Polymeric Micelles, NK012, on Spontaneous Peritoneal Metastases from Orthotopic Gastric Cancer in Mice Compared with Irinotecan.* Cancer Research, 2008. **68**(22): p. 9318.
132. Kato, K., et al., *Phase I study of NK012, polymer micelle SN-38, in patients with advanced cancer.* Am Soc Clin Oncol GI, 2008: p. Abs#485.
133. Burris, H., et al., *A phase I dose-escalation study of NK012.* Am Soc Clin Oncol GI, 2008: p. Abs#2538.
134. Weitman, S.D., et al., *Cellular localization of the folate receptor: potential role in drug toxicity and folate homeostasis.* Cancer Res, 1992. **52**(23): p. 6708-11.
135. Wang, S., et al., *Synthesis, purification, and tumor cell uptake of 67Ga-deferoxamine--folate, a potential radiopharmaceutical for tumor imaging.* Bioconjug Chem, 1996. **7**(1): p. 56-62.
136. Sudimack, J. and R.J. Lee, *Targeted drug delivery via the folate receptor.* Adv Drug Deliv Rev, 2000. **41**(2): p. 147-62.
137. Yoo, H.S. and T.G. Park, *Folate receptor targeted biodegradable polymeric doxorubicin micelles.* Journal of Controlled Release, 2004. **96**(2): p. 273-283.

138. Park, E.K., et al., *Folate-conjugated methoxy poly (ethylene glycol)/poly (ε-caprolactone) amphiphilic block copolymeric micelles for tumor-targeted drug delivery.* Journal of Controlled Release, 2005. **109**(1): p. 158-168.
139. Cook, S.E., et al., *Galactosylated polyethylenimine-< i> graft</i>-poly (vinyl pyrrolidone) as a hepatocyte-targeting gene carrier.* Journal of Controlled Release, 2005. **105**(1): p. 151-163.
140. Lim, D.W., Y.I. Yeom, and T.G. Park, *Poly (DMAEMA-NVP)-b-PEG-galactose as gene delivery vector for hepatocytes.* Bioconjugate Chemistry, 2000. **11**(5): p. 688-695.
141. Yang, R., et al., *Galactose-decorated cross-linked biodegradable poly(ethylene glycol)-b-poly(epsilon-caprolactone) block copolymer micelles for enhanced hepatoma-targeting delivery of paclitaxel.* Biomacromolecules, 2011. **12**(8): p. 3047-55.
142. Wakebayashi, D., et al., *Lactose-conjugated polyion complex micelles incorporating plasmid DNA as a targetable gene vector system: their preparation and gene transfecting efficiency against cultured HepG2 cells.* Journal of Controlled Release, 2004. **95**(3): p. 653-664.
143. Wu, A.M. and P.D. Senter, *Arming antibodies: prospects and challenges for immunoconjugates.* Nature Biotechnology, 2005. **23**(9): p. 1137-1146.
144. Schrama, D., R.A. Reisfeld, and J.C. Becker, *Antibody targeted drugs as cancer therapeutics.* Nature Reviews Drug Discovery, 2006. **5**(2): p. 147-159.
145. Li, W., et al., *Chemotherapy for gastric cancer by finely tailoring anti-Her2 anchored dual targeting immunomicelles.* Biomaterials, 2012. **33**(21): p. 5349-5362.
146. Hoang, B., R.M. Reilly, and C. Allen, *Block copolymer micelles target auger electron radiotherapy to the nucleus of HER2-positive breast cancer cells.* Biomacromolecules, 2012. **13**(2): p. 455-65.
147. Sarisozen, C., et al., *PEG-PE-based micelles co-loaded with paclitaxel and cyclosporine A or loaded with paclitaxel and targeted by anticancer antibody overcome drug resistance in cancer cells.* Drug Deliv, 2012. **19**(4): p. 169-76.
148. Jin, C., et al., *Preparation and characterization of targeted DOX-PLGA-PEG micelles decorated with bivalent fragment HAb18 F(ab')2 for treatment of hepatocellular carcinoma.* J Control Release, 2011. **152 Suppl 1**: p. e14-5.
149. Palanca-Wessels, M.C., et al., *Anti-CD22 antibody targeting of pH-responsive micelles enhances small interfering RNA delivery and gene silencing in lymphoma cells.* Molecular Therapy, 2011. **19**(8): p. 1529-37.
150. Song, H., et al., *Anti-HIF-1alpha antibody-conjugated pluronic triblock copolymers encapsulated with Paclitaxel for tumor targeting therapy.* Biomaterials, 2010. **31**(8): p. 2302-12.
151. Liao, C., et al., *Targeting EGFR-overexpressing tumor cells using Cetuximab-immunomicelles loaded with doxorubicin and*

superparamagnetic iron oxide. European Journal of Radiology, 2011. **80**(3): p. 699-705.
152. Vega, J., et al., *Targeting doxorubicin to epidermal growth factor receptors by site-specific conjugation of C225 to poly(L-glutamic acid) through a polyethylene glycol spacer.* Pharm Res, 2003. **20**(5): p. 826-32.
153. Torchilin, V.P., et al., *Immunomicelles: targeted pharmaceutical carriers for poorly soluble drugs.* Proceedings of the National Academy of Sciences, 2003. **100**(10): p. 6039.
154. Graff, C.P. and K.D. Wittrup, *Theoretical analysis of antibody targeting of tumor spheroids.* Cancer Research, 2003. **63**(6): p. 1288.
155. Parmley, S.F. and G.P. Smith, *Antibody-selectable filamentous fd phage vectors: affinity purification of target genes.* Gene, 1988. **73**(2): p. 305-18.
156. Smith, G.P., *Filamentous fusion phage: novel expression vectors that display cloned antigens on the virion surface.* Science, 1985. **228**(4705): p. 1315.
157. Scott, J.K. and G.P. Smith, *Searching for peptide ligands with an epitope library.* Science, 1990. **249**(4967): p. 386-390.
158. Bangham, A., *Liposome letters*, ed. A. Bangham. 1983: Academic press.
159. Vanniasinghe, A.S., V. Bender, and N. Manolios, *The Potential of Liposomal Drug Delivery for the Treatment of Inflammatory Arthritis.* Seminars in Arthritis and Rheumatism, 2009. **39**(3): p. 182-196.
160. Lasic, D.D., *Novel applications of liposomes.* Trends Biotechnol, 1998. **16**(7): p. 307-21.
161. Düzgüneş, N., *Liposomes*. 2009: Elsevier Academic Press.
162. Szoka, F., et al., *Preparation of unilamellar liposomes of intermediate size (0.1–0.2 μm) by a combination of reverse phase evaporation and extrusion through polycarbonate membranes.* Biochimica et Biophysica Acta (BBA) - Biomembranes, 1980. **601**(0): p. 559-571.
163. Olson, F., et al., *Preparation of liposomes of defined size distribution by extrusion through polycarbonate membranes.* Biochimica et Biophysica Acta (BBA) - Biomembranes, 1979. **557**(1): p. 9-23.
164. Sriwongsitanont, S. and M. Ueno, *Effect of a PEG lipid (DSPE-PEG2000) and freeze-thawing process on phospholipid vesicle size and lamellarity.* Colloid and Polymer Science, 2004. **282**(7): p. 753-760.
165. Castile, J.D. and K.M.G. Taylor, *Factors affecting the size distribution of liposomes produced by freeze–thaw extrusion.* International Journal of Pharmaceutics, 1999. **188**(1): p. 87-95.
166. Schwendener, R.A., P.A. Lagocki, and Y.E. Rahman, *The effects of charge and size on the interaction of unilamellar liposomes with macrophages.* Biochimica et Biophysica Acta (BBA) - Biomembranes, 1984. **772**(1): p. 93-101.
167. Gregoriadis, G., B. McCormack, and N.A.T.O.S.A. Division, *Targeting of Drugs 6: Strategies for Stealth Therapeutic Systems*. 1998: Plenum Press.
168. Devine, D.V. and J.M. Marjan, *The role of immunoproteins in the survival of liposomes in the circulation.* Critical Reviews in Therapeutic Drug Carrier Systems, 1997. **14**(2): p. 105-31.

169. Chonn, A., S.C. Semple, and P.R. Cullis, *Association of blood proteins with large unilamellar liposomes in vivo. Relation to circulation lifetimes.* J Biol Chem, 1992. **267**(26): p. 18759-65.
170. Papahadjopoulos, D., et al., *Sterically stabilized liposomes: improvements in pharmacokinetics and antitumor therapeutic efficacy.* Proceedings of the National Academy of Sciences, 1991. **88**(24): p. 11460.
171. Blume, G. and G. Cevc, *Liposomes for the sustained drug release in vivo.* Biochimica et Biophysica Acta (BBA)-Biomembranes, 1990. **1029**(1): p. 91-97.
172. Blume, G. and G. Cevc, *Molecular mechanism of the lipid vesicle longevity in vivo.* Biochimica et Biophysica Acta (BBA)-Biomembranes, 1993. **1146**(2): p. 157-168.
173. Allen, T. and C. Hansen, *Pharmacokinetics of stealth versus conventional liposomes: effect of dose.* Biochimica et Biophysica Acta (BBA)-Biomembranes, 1991. **1068**(2): p. 133-141.
174. Woodle, M., et al., *Versatility in lipid compositions showing prolonged circulation with sterically stabilized liposomes.* Biochimica et Biophysica Acta (BBA)-Biomembranes, 1992. **1105**(2): p. 193-200.
175. Kenworthy, A.K., S.A. Simon, and T.J. McIntosh, *Structure and phase behavior of lipid suspensions containing phospholipids with covalently attached poly(ethylene glycol).* Biophysical Journal, 1995. **68**(5): p. 1903-20.
176. Gabizon, A. and D. Papahadjopoulos, *Liposome formulations with prolonged circulation time in blood and enhanced uptake by tumors.* Proceedings of the National Academy of Sciences of the United States of America, 1988. **85**(18): p. 6949-53.
177. Gabizon, A., et al., *Prolonged circulation time and enhanced accumulation in malignant exudates of doxorubicin encapsulated in polyethylene-glycol coated liposomes.* Cancer Research, 1994. **54**(4): p. 987.
178. Allen, T.M., et al., *Pharmacokinetics and pharmacodynamics of lipidic nano-particles in cancer.* Anti-Cancer Agents in Medicinal Chemistry, 2006. **6**(6): p. 513-23.
179. Charrois, G.J. and T.M. Allen, *Drug release rate influences the pharmacokinetics, biodistribution, therapeutic activity, and toxicity of pegylated liposomal doxorubicin formulations in murine breast cancer.* Biochimica et Biophysica Acta, 2004. **1663**(1-2): p. 167-77.
180. Allen, T.M., D.R. Mumbengegwi, and G.J. Charrois, *Anti-CD19-targeted liposomal doxorubicin improves the therapeutic efficacy in murine B-cell lymphoma and ameliorates the toxicity of liposomes with varying drug release rates.* Clin Cancer Res, 2005. **11**(9): p. 3567-73.
181. Johnston, M.J., et al., *Therapeutically optimized rates of drug release can be achieved by varying the drug-to-lipid ratio in liposomal vincristine formulations.* Biochimica et Biophysica Acta, 2006. **1758**(1): p. 55-64.
182. Torchilin, V.P., *Recent advances with liposomes as pharmaceutical carriers.* Nature Reviews Drug Discovery, 2005. **4**(2): p. 145-160.

183. Allen, T.M., C.B. Hansen, and D.E.L. de Menezes, *Pharmacokinetics of long-circulating liposomes.* Advanced Drug Delivery Reviews, 1995. **16**(2–3): p. 267-284.
184. Wicki, A., et al., *Targeting tumor-associated endothelial cells: anti-VEGFR2 immunoliposomes mediate tumor vessel disruption and inhibit tumor growth.* Clin Cancer Res, 2012. **18**(2): p. 454-64.
185. Nishikawa, K., et al., *Development of anti-HB-EGF immunoliposomes for the treatment of breast cancer.* J Control Release, 2012. **160**(2): p. 274-80.
186. Koren, E., et al., *Multifunctional PEGylated 2C5-immunoliposomes containing pH-sensitive bonds and TAT peptide for enhanced tumor cell internalization and cytotoxicity.* J Control Release, 2012. **160**(2): p. 264-73.
187. Hantel, C., et al., *Anti insulin-like growth factor I receptor immunoliposomes: a single formulation combining two anticancer treatments with enhanced therapeutic efficiency.* Journal of Clinical Endocrinology and Metabolism, 2010. **95**(2): p. 943-52.
188. Brignole, C., et al., *Development of Fab' fragments of anti-GD(2) immunoliposomes entrapping doxorubicin for experimental therapy of human neuroblastoma.* Cancer Lett, 2003. **197**(1-2): p. 199-204.
189. Knudsen, N.O., et al., *Design of cyclic RKKH peptide-conjugated PEG liposomes targeting the integrin alpha(2)beta(1) receptor.* Int J Pharm, 2012. **428**(1-2): p. 171-7.
190. Accardo, A., et al., *Peptide-modified liposomes for selective targeting of bombesin receptors overexpressed by cancer cells: a potential theranostic agent.* International Journal of Nanomedicine, 2012. **7**: p. 2007-17.
191. Garg, A. and E. Kokkoli, *pH-Sensitive PEGylated liposomes functionalized with a fibronectin-mimetic peptide show enhanced intracellular delivery to colon cancer cell.* Current Pharmaceutical Biotechnology, 2011. **12**(8): p. 1135-43.
192. Fretz, M.M. and G. Storm, *TAT-peptide modified liposomes: preparation, characterization, and cellular interaction.* Methods in Molecular Biology, 2010. **605**: p. 349-59.
193. Dubey, P.K., D. Singodia, and S.P. Vyas, *Liposomes modified with YIGSR peptide for tumor targeting.* J Drug Target, 2010. **18**(5): p. 373-80.
194. Song, S., et al., *Novel peptide ligand directs liposomes toward EGF-R high-expressing cancer cells in vitro and in vivo.* FASEB Journal, 2009. **23**(5): p. 1396-404.
195. Garg, A., et al., *Targeting colon cancer cells using PEGylated liposomes modified with a fibronectin-mimetic peptide.* Int J Pharm, 2009. **366**(1-2): p. 201-10.
196. Rezler, E.M., et al., *Peptide-mediated targeting of liposomes to tumor cells.* Methods in Molecular Biology, 2007. **386**: p. 269-98.
197. Gupta, B., T.S. Levchenko, and V.P. Torchilin, *TAT peptide-modified liposomes provide enhanced gene delivery to intracranial human brain tumor xenografts in nude mice.* Oncology Research, 2007. **16**(8): p. 351-9.

198. Yamamoto, M., et al., *Utility of liposomes coated with polysaccharide bearing 1-amino-lactose as targeting chemotherapy for AH66 hepatoma cells.* Oncology Reports, 2000. **7**(1): p. 107-11.
199. Yamauchi, H., et al., *Characterization and tissue distribution of liposomes containing lactose mono-fatty acid derivatives.* Journal of Microencapsulation, 1994. **11**(2): p. 179-88.
200. Eliaz, R.E. and F.C. Szoka, *Liposome-encapsulated Doxorubicin Targeted to CD44.* Cancer Research, 2001. **61**(6): p. 2592-2601.
201. Soares, D.C., et al., *Antitumoral activity and toxicity of PEG-coated and PEG-folate-coated pH-sensitive liposomes containing ^{159}Gd-DTPA-BMA in Ehrlich tumor bearing mice.* European Journal of Pharmaceutical Sciences, 2012. **45**(1-2): p. 58-64.
202. Xiong, S., et al., *Preparation, therapeutic efficacy and intratumoral localization of targeted daunorubicin liposomes conjugating folate-PEG-CHEMS.* Biomedicine and Pharmacotherapy, 2011. **65**(1): p. 2-8.
203. Tyagi, N. and P.C. Ghosh, *Folate receptor mediated targeted delivery of ricin entrapped into sterically stabilized liposomes to human epidermoid carcinoma (KB) cells: effect of monensin intercalated into folate-tagged liposomes.* European Journal of Pharmaceutical Sciences, 2011. **43**(4): p. 343-53.
204. Li, X., et al., *In vitro and in vivo evaluation of folate receptor-targeting amphiphilic copolymer-modified liposomes loaded with docetaxel.* International Journal of Nanomedicine, 2011. **6**: p. 1167-84.
205. Xiang, G., et al., *Synthesis and evaluation of a novel ligand for folate-mediated targeting liposomes.* Int J Pharm, 2008. **356**(1-2): p. 29-36.
206. Ahmad, I., et al., *Antibody-targeted delivery of doxorubicin entrapped in sterically stabilized liposomes can eradicate lung cancer in mice.* Cancer Research, 1993. **53**(7): p. 1484.
207. Park, J.W., et al., *Anti-HER2 immunoliposomes for targeted therapy of human tumors.* Cancer Letters, 1997. **118**(2): p. 153-160.
208. Carter, P., *IMPROVING THE EFFICACY OF ANTIBODY-BASED CANCER THERAPIES.* Nature Reviews Cancer, 2001. **1**(2): p. 118.
209. Sapra, P. and T.M. Allen, *Ligand-targeted liposomal anticancer drugs.* Progress in Lipid Research, 2003. **42**(5): p. 439-62.
210. Gabizon, A., et al., *Tumor cell targeting of liposome-entrapped drugs with phospholipid-anchored folic acid-PEG conjugates.* Adv Drug Deliv Rev, 2004. **56**(8): p. 1177-92.
211. Lu, Y. and P.S. Low, *Folate-mediated delivery of macromolecular anticancer therapeutic agents.* Adv Drug Deliv Rev, 2002. **54**(5): p. 675-93.
212. Leamon, C.P. and P.S. Low, *Delivery of macromolecules into living cells: a method that exploits folate receptor endocytosis.* Proceedings of the National Academy of Sciences of the United States of America, 1991. **88**(13): p. 5572-6.

213. Lee, R.J. and P.S. Low, *Delivery of liposomes into cultured KB cells via folate receptor-mediated endocytosis.* J Biol Chem, 1994. **269**(5): p. 3198-204.
214. Ni, S., S.M. Stephenson, and R.J. Lee, *Folate receptor targeted delivery of liposomal daunorubicin into tumor cells.* Anticancer Research, 2002. **22**(4): p. 2131-5.
215. Pan, X.Q., H. Wang, and R.J. Lee, *Antitumor activity of folate receptor-targeted liposomal doxorubicin in a KB oral carcinoma murine xenograft model.* Pharm Res, 2003. **20**(3): p. 417-22.
216. Gupta, Y., et al., *Design and development of folate appended liposomes for enhanced delivery of 5-FU to tumor cells.* J Drug Target, 2007. **15**(3): p. 231-40.
217. Lopes de Menezes, D.E., L.M. Pilarski, and T.M. Allen, *In vitro and in vivo targeting of immunoliposomal doxorubicin to human B-cell lymphoma.* Cancer Research, 1998. **58**(15): p. 3320.
218. Lopes de Menezes, D.E., et al., *Selective targeting of immunoliposomal doxorubicin against human multiple myeloma in vitro and ex vivo.* Biochimica et Biophysica Acta (BBA)-Biomembranes, 2000. **1466**(1-2): p. 205-220.
219. Park, J.W., et al., *Anti-HER2 immunoliposomes: enhanced efficacy attributable to targeted delivery.* Clin Cancer Res, 2002. **8**(4): p. 1172-81.
220. Kullberg, M., K. Mann, and T.J. Anchordoquy, *Targeting Her-2+ Breast Cancer Cells with Bleomycin Immunoliposomes Linked to LLO.* Mol Pharm, 2012.
221. Yamamoto, Y., et al., *Feasibility of tailored, selective and effective anticancer chemotherapy by direct injection of docetaxel-loaded immunoliposomes into Her2/neu positive gastric tumor xenografts.* International Journal of Oncology, 2011. **38**(1): p. 33-9.
222. Matsuo, H., et al., *Possibility of the reversal of multidrug resistance and the avoidance of side effects by liposomes modified with MRK-16, a monoclonal antibody to P-glycoprotein.* J Control Release, 2001. **77**(1-2): p. 77-86.
223. Sugano, M., et al., *Antibody Targeting of Doxorubicin-loaded Liposomes Suppresses the Growth and Metastatic Spread of Established Human Lung Tumor Xenografts in Severe Combined Immunodeficient Mice.* Cancer Research, 2000. **60**(24): p. 6942-6949.
224. Koning, G., et al., *Antiproliferative effect of immunoliposomes containing 5-fluorodeoxyuridine-dipalmitate on colon cancer cells.* British Journal of Cancer, 1999. **80**(11): p. 1718.
225. Pagnan, G., et al., *GD2-mediated melanoma cell targeting and cytotoxicity of liposome-entrapped fenretinide.* International Journal of Cancer, 1999. **81**(2): p. 268-74.
226. Nam, S.M., et al., *Sterically stabilized anti-G(M3), anti-Le(x) immunoliposomes: targeting to B16BL6, HRT-18 cancer cells.* Oncology Research, 1999. **11**(1): p. 9-16.

227. Marty, C., et al., *Cytotoxic targeting of F9 teratocarcinoma tumours with anti-ED-B fibronectin scFv antibody modified liposomes.* British Journal of Cancer, 2002. **87**(1): p. 106.
228. Guin, S., et al., *Targeting acute hypoxic cancer cells by doxorubicin-immunoliposomes directed by monoclonal antibodies specific to RON receptor tyrosine kinase.* Cancer Chemotherapy and Pharmacology, 2011. **67**(5): p. 1073-83.
229. Simard, P. and J.C. Leroux, *In vivo evaluation of pH-sensitive polymer-based immunoliposomes targeting the CD33 antigen.* Mol Pharm, 2010. **7**(4): p. 1098-107.
230. Lee, R.J. and P.S. Low, *Folate-mediated tumor cell targeting of liposome-entrapped doxorubicin in vitro.* Biochimica et Biophysica Acta (BBA) - Biomembranes, 1995. **1233**(2): p. 134-144.
231. Gabizon, A., et al., *Targeting Folate Receptor with Folate Linked to Extremities of Poly(ethylene glycol)-Grafted Liposomes: In Vitro Studies.* Bioconjugate Chemistry, 1999. **10**(2): p. 289-298.
232. Rui, Y., et al., *Diplasmenylcholine−Folate Liposomes: An Efficient Vehicle for Intracellular Drug Delivery†.* Journal of the American Chemical Society, 1998. **120**(44): p. 11213-11218.
233. Pan, X.Q., et al., *Strategy for the treatment of acute myelogenous leukemia based on folate receptor β–targeted liposomal doxorubicin combined with receptor induction using all-trans retinoic acid.* Blood, 2002. **100**(2): p. 594-602.
234. Shockley, T.R., et al., *Penetration of tumor tissue by antibodies and other immunoproteins.* Annals of the New York Academy of Sciences, 1991. **618**: p. 367-82.
235. Heldin, C.H., et al., *High interstitial fluid pressure - an obstacle in cancer therapy.* Nature Reviews. Cancer, 2004. **4**(10): p. 806-13.
236. Wu, H.C., D.K. Chang, and C.T. Huang, *Targeted-therapy for cancer.* Journal of Cancer Molecules, 2006. **2**(2): p. 57-66.
237. Lee, T.Y., et al., *Peptide-mediated targeting to tumor blood vessels of lung cancer for drug delivery.* Cancer Research, 2007. **67**(22): p. 10958.
238. Chang, D.K., et al., *Antiangiogenic targeting liposomes increase therapeutic efficacy for solid tumors.* Journal of Biological Chemistry, 2009. **284**(19): p. 12905.
239. Lo, A., C.-T. Lin, and H.-C. Wu, *Hepatocellular carcinoma cell-specific peptide ligand for targeted drug delivery.* Molecular Cancer Therapeutics, 2008. **7**(3): p. 579-589.
240. Lee, T.Y., et al., *A novel peptide specifically binding to nasopharyngeal carcinoma for targeted drug delivery.* Cancer Research, 2004. **64**(21): p. 8002.
241. Shahin, M., et al., *Decoration of polymeric micelles with cancer-specific peptide ligands for active targeting of paclitaxel.* Biomaterials, 2011. **32**(22): p. 5123-33.

242. Chang, D.K., et al., *A novel peptide enhances therapeutic efficacy of liposomal anti-cancer drugs in mice models of human lung cancer.* PLoS ONE, 2009. **4**(1): p. e4171.
243. Akita, N., et al., *Identification of oligopeptides binding to peritoneal tumors of gastric cancer.* Cancer Science, 2006. **97**(10): p. 1075-1081.
244. Wang, X., et al., *Truncated bFGF-mediated cationic liposomal paclitaxel for tumor-targeted drug delivery: improved pharmacokinetics and biodistribution in tumor-bearing mice.* J Pharm Sci, 2011. **100**(3): p. 1196-205.
245. Chen, X., et al., *Improved tumor-targeting drug delivery and therapeutic efficacy by cationic liposome modified with truncated bFGF peptide.* J Control Release, 2010. **145**(1): p. 17-25.
246. Sugahara, K.N., et al., *Tissue-penetrating delivery of compounds and nanoparticles into tumors.* Cancer Cell, 2009. **16**(6): p. 510-20.
247. Turowski, P., P. Adamson, and J. Greenwood, *Pharmacological targeting of ICAM-1 signaling in brain endothelial cells: potential for treating neuroinflammation.* Cellular and Molecular Neurobiology, 2005. **25**(1): p. 153-70.
248. Pavalko, F.M. and C.A. Otey, *Role of adhesion molecule cytoplasmic domains in mediating interactions with the cytoskeleton.* Proceedings of the Society for Experimental Biology and Medicine, 1994. **205**(4): p. 282-93.
249. Haass, N.K., et al., *Adhesion, migration and communication in melanocytes and melanoma.* Pigment Cell Research, 2005. **18**(3): p. 150-9.
250. Christofori, G., *Changing neighbours, changing behaviour: cell adhesion molecule-mediated signalling during tumour progression.* EMBO Journal, 2003. **22**(10): p. 2318-23.
251. Maaser, K., et al., *Functional hierarchy of simultaneously expressed adhesion receptors: integrin alpha2beta1 but not CD44 mediates MV3 melanoma cell migration and matrix reorganization within three-dimensional hyaluronan-containing collagen matrices.* Molecular Biology of the Cell, 1999. **10**(10): p. 3067-79.
252. Andrews, R.K. and M.C. Berndt, *Platelet physiology and thrombosis.* Thrombosis Research, 2004. **114**(5-6): p. 447-53.
253. Gibbins, J.M., *Platelet adhesion signalling and the regulation of thrombus formation.* Journal of Cell Science, 2004. **117**(Pt 16): p. 3415-25.
254. Hynes, R.O., *A reevaluation of integrins as regulators of angiogenesis.* Nature Medicine, 2002. **8**(9): p. 918-21.
255. Hynes, R.O. and Q. Zhao, *The evolution of cell adhesion.* Journal of Cell Biology, 2000. **150**(2): p. F89-96.
256. Ruoslahti, E., *Fibronectin and its integrin receptors in cancer.* Advances in Cancer Research, 1999. **76**: p. 1-20.
257. Luna, E.J. and A.L. Hitt, *Cytoskeleton--plasma membrane interactions.* Science, 1992. **258**(5084): p. 955-64.

258. Cai, W. and X. Chen, *Anti-angiogenic cancer therapy based on integrin alphavbeta3 antagonism.* Anti-Cancer Agents in Medicinal Chemistry, 2006. **6**(5): p. 407-28.
259. Mizejewski, G.J., *Role of integrins in cancer: survey of expression patterns.* Proceedings of the Society for Experimental Biology and Medicine, 1999. **222**(2): p. 124-38.
260. Jin, H. and J. Varner, *Integrins: roles in cancer development and as treatment targets.* British Journal of Cancer, 2004. **90**(3): p. 561-5.
261. Pierschbacher, M.D. and E. Ruoslahti, *Variants of the cell recognition site of fibronectin that retain attachment-promoting activity.* Proceedings of the National Academy of Sciences of the United States of America, 1984. **81**(19): p. 5985-8.
262. Pierschbacher, M.D. and E. Ruoslahti, *Cell attachment activity of fibronectin can be duplicated by small synthetic fragments of the molecule.* Nature, 1984. **309**(5963): p. 30-3.
263. Ruoslahti, E., *The RGD story: a personal account.* Matrix Biology, 2003. **22**(6): p. 459-65.
264. Enback, J. and P. Laakkonen, *Tumour-homing peptides: tools for targeting, imaging and destruction.* Biochemical Society Transactions, 2007. **35**(Pt 4): p. 780-3.
265. Maubant, S., et al., *Blockade of alpha v beta3 and alpha v beta5 integrins by RGD mimetics induces anoikis and not integrin-mediated death in human endothelial cells.* Blood, 2006. **108**(9): p. 3035-44.
266. Temming, K., et al., *RGD-based strategies for selective delivery of therapeutics and imaging agents to the tumour vasculature.* Drug Resistance Updates, 2005. **8**(6): p. 381-402.
267. Bogdanowich-Knipp, S.J., et al., *Solution stability of linear vs. cyclic RGD peptides.* Journal of Peptide Research, 1999. **53**(5): p. 530-41.
268. Goodman, S.L., et al., *Nanomolar small molecule inhibitors for alphav(beta)6, alphav(beta)5, and alphav(beta)3 integrins.* J Med Chem, 2002. **45**(5): p. 1045-51.
269. Koivunen, E., B. Wang, and E. Ruoslahti, *Phage libraries displaying cyclic peptides with different ring sizes: ligand specificities of the RGD-directed integrins.* Bio/Technology, 1995. **13**(3): p. 265-70.
270. Holig, P., et al., *Novel RGD lipopeptides for the targeting of liposomes to integrin-expressing endothelial and melanoma cells.* Protein Engineering, Design and Selection, 2004. **17**(5): p. 433-41.
271. Mitra, A., et al., *Targeting tumor angiogenic vasculature using polymer–RGD conjugates.* Journal of Controlled Release, 2005. **102**(1): p. 191-201.
272. Chen, K. and X. Chen, *Integrin targeted delivery of chemotherapeutics.* Theranostics, 2011. **1**: p. 189-200.
273. Assa-Munt, N., et al., *Solution structures and integrin binding activities of an RGD peptide with two isomers.* Biochemistry, 2001. **40**(8): p. 2373-8.
274. Haubner, R., et al., *Radiolabeled alpha(v)beta3 integrin antagonists: a new class of tracers for tumor targeting.* Journal of Nuclear Medicine, 1999. **40**(6): p. 1061-71.

275. Dechantsreiter, M.A., et al., *N-Methylated cyclic RGD peptides as highly active and selective alpha(V)beta(3) integrin antagonists.* J Med Chem, 1999. **42**(16): p. 3033-40.
276. www.cancer.gov. *Cilengitide, Temozolomide, and Radiation Therapy in Treating Patients With Newly Diagnosed Glioblastoma and Methylated Gene Promoter Status*. 2012 8/03/2012 16/07/2012].
277. Teesalu, T., et al., *C-end rule peptides mediate neuropilin-1-dependent cell, vascular, and tissue penetration.* Proceedings of the National Academy of Sciences of the United States of America, 2009. **106**(38): p. 16157-62.
278. Sugahara, K.N., et al., *Coadministration of a tumor-penetrating peptide enhances the efficacy of cancer drugs.* Science, 2010. **328**(5981): p. 1031-5.
279. Schiffelers, R.M., et al., *Anti-tumor efficacy of tumor vasculature-targeted liposomal doxorubicin.* J Control Release, 2003. **91**(1-2): p. 115-22.
280. Xiong, X.B., et al., *Intracellular delivery of doxorubicin with RGD-modified sterically stabilized liposomes for an improved antitumor efficacy: in vitro and in vivo.* J Pharm Sci, 2005. **94**(8): p. 1782-93.
281. Naik, S., et al., *In vitro mechanistic study of cell death and in vivo performance evaluation of RGD grafted PEGylated docetaxel liposomes in breast cancer.* Nanomedicine, 2011.
282. Zhang, Y.F., et al., *Targeted delivery of RGD-modified liposomes encapsulating both combretastatin A-4 and doxorubicin for tumor therapy: in vitro and in vivo studies.* European Journal of Pharmaceutics and Biopharmaceutics, 2010. **74**(3): p. 467-73.
283. Jiang, J., et al., *Sequential treatment of drug-resistant tumors with RGD-modified liposomes containing siRNA or doxorubicin.* European Journal of Pharmaceutics and Biopharmaceutics, 2010. **76**(2): p. 170-8.
284. Zhao, H., et al., *RGD-based strategies for improving antitumor activity of paclitaxel-loaded liposomes in nude mice xenografted with human ovarian cancer.* J Drug Target, 2009. **17**(1): p. 10-8.
285. Xiong, X.B., et al., *Enhanced intracellular delivery and improved antitumor efficacy of doxorubicin by sterically stabilized liposomes modified with a synthetic RGD mimetic.* J Control Release, 2005. **107**(2): p. 262-75.
286. Dubey, P.K., et al., *Liposomes modified with cyclic RGD peptide for tumor targeting.* J Drug Target, 2004. **12**(5): p. 257-64.
287. Wang, R.E., et al., *Development of NGR peptide-based agents for tumor imaging.* Am J Nucl Med Mol Imaging, 2011. **1**(1): p. 36-46.
288. Arap, W., R. Pasqualini, and E. Ruoslahti, *Cancer treatment by targeted drug delivery to tumor vasculature in a mouse model.* Science, 1998. **279**(5349): p. 377.
289. Curnis, F., et al., *Differential binding of drugs containing the NGR motif to CD13 isoforms in tumor vessels, epithelia, and myeloid cells.* Cancer Res, 2002. **62**(3): p. 867-74.

290. Pasqualini, R., et al., *Aminopeptidase N is a receptor for tumor-homing peptides and a target for inhibiting angiogenesis.* Cancer Res, 2000. **60**(3): p. 722-7.
291. Healy, J.M., et al., *Peptide ligands for integrin alpha v beta 3 selected from random phage display libraries.* Biochemistry, 1995. **34**(12): p. 3948-55.
292. Luan, Y. and W. Xu, *The structure and main functions of aminopeptidase N.* Current Medicinal Chemistry, 2007. **14**(6): p. 639-47.
293. Riemann, D., A. Kehlen, and J. Langner, *CD13—not just a marker in leukemia typing.* Immunology Today, 1999. **20**(2): p. 83-88.
294. Razak, K. and A.C. Newland, *The significance of aminopeptidases and haematopoietic cell differentiation.* Blood Reviews, 1992. **6**(4): p. 243-50.
295. Moffatt, S., S. Wiehle, and R.J. Cristiano, *Tumor-specific gene delivery mediated by a novel peptide-polyethylenimine-DNA polyplex targeting aminopeptidase N/CD13.* Human Gene Therapy, 2005. **16**(1): p. 57-67.
296. Corti, A., et al., *The neovasculature homing motif NGR: more than meets the eye.* Blood, 2008. **112**(7): p. 2628-35.
297. Curnis, F., et al., *Spontaneous formation of L-isoaspartate and gain of function in fibronectin.* J Biol Chem, 2006. **281**(47): p. 36466-76.
298. Majhen, D., et al., *Disulfide bond formation in NGR fiber-modified adenovirus is essential for retargeting to aminopeptidase N.* Biochemical and Biophysical Research Communications, 2006. **348**(1): p. 278-87.
299. Colombo, G., et al., *Structure-activity relationships of linear and cyclic peptides containing the NGR tumor-homing motif.* J Biol Chem, 2002. **277**(49): p. 47891-7.
300. Curnis, F., A. Sacchi, and A. Corti, *Improving chemotherapeutic drug penetration in tumors by vascular targeting and barrier alteration.* Journal of Clinical Investigation, 2002. **110**(4): p. 475-82.
301. Yang, K.L., et al., *Antagonizing TGF-beta induced liver fibrosis by a retinoic acid derivative through regulation of ROS and calcium influx.* Biochemical and Biophysical Research Communications, 2008. **365**(3): p. 484-9.
302. Curnis, F., et al., *Targeted delivery of IFNgamma to tumor vessels uncouples antitumor from counterregulatory mechanisms.* Cancer Res, 2005. **65**(7): p. 2906-13.
303. Sacchi, A., et al., *Crucial role for interferon gamma in the synergism between tumor vasculature-targeted tumor necrosis factor alpha (NGR-TNF) and doxorubicin.* Cancer Res, 2004. **64**(19): p. 7150-5.
304. Pastorino, F., et al., *Vascular damage and anti-angiogenic effects of tumor vessel-targeted liposomal chemotherapy.* Cancer Res, 2003. **63**(21): p. 7400-9.
305. Pastorino, F., et al., *Targeting liposomal chemotherapy via both tumor cell-specific and tumor vasculature-specific ligands potentiates therapeutic efficacy.* Cancer Res, 2006. **66**(20): p. 10073-82.
306. Dunne, M., et al., *APN/CD13-targeting as a strategy to alter the tumor accumulation of liposomes.* J Control Release, 2011. **154**(3): p. 298-305.

307. Takara, K., et al., *Size-controlled, dual-ligand modified liposomes that target the tumor vasculature show promise for use in drug-resistant cancer therapy.* J Control Release, 2012.
308. Zhang, J., H. Spring, and M. Schwab, *Neuroblastoma tumor cell-binding peptides identified through random peptide phage display.* Cancer Lett, 2001. **171**(2): p. 153-64.
309. Askoxylakis, V., et al., *Characterization and development of a peptide (p160) with affinity for neuroblastoma cells.* Journal of Nuclear Medicine, 2006. **47**(6): p. 981-8.
310. Askoxylakis, V., et al., *Preclinical evaluation of the breast cancer cell-binding peptide, p160.* Clin Cancer Res, 2005. **11**(18): p. 6705-12.
311. Ahmed, S., et al., *Peptide arrays for screening cancer specific peptides.* Analytical Chemistry, 2010. **82**(18): p. 7533-41.
312. Soudy, R., et al., *Proteolytically stable cancer targeting peptides with high affinity for breast cancer cells.* J Med Chem, 2011. **54**(21): p. 7523-34.
313. Torchilin, V.P., *Tat peptide-mediated intracellular delivery of pharmaceutical nanocarriers.* Adv Drug Deliv Rev, 2008. **60**(4-5): p. 548-58.
314. Breunig, M., S. Bauer, and A. Goepferich, *Polymers and nanoparticles: intelligent tools for intracellular targeting?* European Journal of Pharmaceutics and Biopharmaceutics, 2008. **68**(1): p. 112-28.
315. Kale, A.A. and V.P. Torchilin, *"Smart" drug carriers: PEGylated TATp-modified pH-sensitive liposomes.* Journal of Liposome Research, 2007. **17**(3-4): p. 197-203.
316. Marty, C., et al., *Enhanced heparan sulfate proteoglycan-mediated uptake of cell-penetrating peptide-modified liposomes.* Cellular and Molecular Life Sciences, 2004. **61**(14): p. 1785-94.
317. Oba, M., et al., *Cyclic RGD peptide-conjugated polyplex micelles as a targetable gene delivery system directed to cells possessing alphavbeta3 and alphavbeta5 integrins.* Bioconjug Chem, 2007. **18**(5): p. 1415-23.
318. Torchilin, V.P., et al., *Cell transfection in vitro and in vivo with nontoxic TAT peptide-liposome-DNA complexes.* Proceedings of the National Academy of Sciences of the United States of America, 2003. **100**(4): p. 1972-7.
319. Tseng, Y.L., J.J. Liu, and R.L. Hong, *Translocation of liposomes into cancer cells by cell-penetrating peptides penetratin and tat: a kinetic and efficacy study.* Mol Pharmacol, 2002. **62**(4): p. 864-72.
320. Naor, D., et al., *CD44 in cancer.* Critical Reviews in Clinical Laboratory Sciences, 2002. **39**(6): p. 527-79.
321. Rezler, E.M., et al., *Targeted drug delivery utilizing protein-like molecular architecture.* J Am Chem Soc, 2007. **129**(16): p. 4961-72.
322. Aota, S., M. Nomizu, and K.M. Yamada, *The short amino acid sequence Pro-His-Ser-Arg-Asn in human fibronectin enhances cell-adhesive function.* Journal of Biological Chemistry, 1994. **269**(40): p. 24756-61.

323. Mardilovich, A. and E. Kokkoli, *Biomimetic peptide-amphiphiles for functional biomaterials: the role of GRGDSP and PHSRN.* Biomacromolecules, 2004. **5**(3): p. 950-7.
324. Mardilovich, A., et al., *Design of a novel fibronectin-mimetic peptide-amphiphile for functionalized biomaterials.* Langmuir, 2006. **22**(7): p. 3259-64.
325. Demirgoz, D., A. Garg, and E. Kokkoli, *PR_b-targeted PEGylated liposomes for prostate cancer therapy.* Langmuir, 2008. **24**(23): p. 13518-24.
326. Sparano, J.A., et al., *Phase II trial of doxorubicin and paclitaxel plus granulocyte colony-stimulating factor in metastatic breast cancer: an Eastern Cooperative Oncology Group Study.* Journal of Clinical Oncology, 1999. **17**(12): p. 3828-34.
327. Sparano, J.A., et al., *Phase I trial of escalating doses of paclitaxel plus doxorubicin and dexrazoxane in patients with advanced breast cancer.* Journal of Clinical Oncology, 1999. **17**(3): p. 880-6.
328. Kramer, J.A., et al., *Randomised trial of paclitaxel versus doxorubicin as first-line chemotherapy for advanced breast cancer: quality of life evaluation using the EORTC QLQ-C30 and the Rotterdam symptom checklist.* European Journal of Cancer, 2000. **36**(12): p. 1488-97.
329. Paridaens, R., et al., *Paclitaxel versus doxorubicin as first-line single-agent chemotherapy for metastatic breast cancer: a European Organization for Research and Treatment of Cancer Randomized Study with cross-over.* Journal of Clinical Oncology, 2000. **18**(4): p. 724-33.
330. Jassem, J., et al., *Doxorubicin and paclitaxel versus fluorouracil, doxorubicin, and cyclophosphamide as first-line therapy for women with metastatic breast cancer: final results of a randomized phase III multicenter trial.* Journal of Clinical Oncology, 2001. **19**(6): p. 1707-15.
331. Panchagnula, R., *Pharmaceutical aspects of paclitaxel.* International Journal of Pharmaceutics, 1998. **172**(1): p. 1-15.
332. Liggins, R.T., W.L. Hunter, and H.M. Burt, *Solid-state characterization of paclitaxel.* Journal of Pharmaceutical Sciences, 1997. **86**(12): p. 1458-1463.
333. Kingston, D.G., *Taxol: the chemistry and structure-activity relationships of a novel anticancer agent.* Trends Biotechnol, 1994. **12**(6): p. 222-7.
334. Amos, L.A. and J. Lowe, *How Taxol stabilises microtubule structure.* Chemistry and Biology, 1999. **6**(3): p. R65-9.
335. Xiao, H., et al., *Insights into the mechanism of microtubule stabilization by Taxol.* Proceedings of the National Academy of Sciences of the United States of America, 2006. **103**(27): p. 10166-73.
336. Yusuf, R.Z., et al., *Paclitaxel resistance: molecular mechanisms and pharmacologic manipulation.* Current Cancer Drug Targets, 2003. **3**(1): p. 1-19.
337. Hawkins, M.J., P. Soon-Shiong, and N. Desai, *Protein nanoparticles as drug carriers in clinical medicine.* Advanced Drug Delivery Reviews, 2008. **60**(8): p. 876-885.

338. Knutsen, T., et al., *Cytogenetic and molecular characterization of random chromosomal rearrangements activating the drug resistance gene, MDR1/P-glycoprotein, in drug-selected cell lines and patients with drug refractory ALL.* Genes, Chromosomes and Cancer, 1998. **23**(1): p. 44-54.
339. Sparreboom, A., et al., *Limited oral bioavailability and active epithelial excretion of paclitaxel (Taxol) caused by P-glycoprotein in the intestine.* Proceedings of the National Academy of Sciences of the United States of America, 1997. **94**(5): p. 2031-5.
340. Spencer, C.M. and D. Faulds, *Paclitaxel. A review of its pharmacodynamic and pharmacokinetic properties and therapeutic potential in the treatment of cancer.* Drugs, 1994. **48**(5): p. 794-847.
341. Gelderblom, H., et al., *Cremophor EL: the drawbacks and advantages of vehicle selection for drug formulation.* European Journal of Cancer, 2001. **37**(13): p. 1590-8.
342. Fjallskog, M.L., L. Frii, and J. Bergh, *Is Cremophor EL, solvent for paclitaxel, cytotoxic?* Lancet, 1993. **342**(8875): p. 873.
343. Liebmann, J., J.A. Cook, and J.B. Mitchell, *Cremophor EL, solvent for paclitaxel, and toxicity.* Lancet, 1993. **342**(8884): p. 1428.
344. Stinchcombe, T.E., *Nanoparticle albumin-bound paclitaxel: a novel Cremphor-EL-free formulation of paclitaxel.* Nanomedicine (Lond), 2007. **2**(4): p. 415-23.
345. www.abraxane.com. *Abraxane for injectable suspension (paclitaxel-protein bound particle for injectable suspension) (albumin bound).* 2012 19/7/2012 [cited 2012 19/7/2012]; Available from: http://www.abraxane.com/dtc/.
346. Singer, J.W., *Paclitaxel poliglumex (XYOTAX, CT-2103): a macromolecular taxane.* J Control Release, 2005. **109**(1-3): p. 120-6.
347. Singer, J.W., et al., *Paclitaxel poliglumex (XYOTAX; CT-2103): an intracellularly targeted taxane.* Anticancer Drugs, 2005. **16**(3): p. 243-54.
348. Constantinides, P.P., et al., *Formulation development and antitumor activity of a filter-sterilizable emulsion of paclitaxel.* Pharm Res, 2000. **17**(2): p. 175-82.
349. Aubel-Sadron, G. and D. Londos-Gagliardi, *Daunorubicin and doxorubicin, anthracycline antibiotics, a physicochemical and biological review.* Biochimie, 1984. **66**(5): p. 333-352.
350. Arcamone, F., et al., *Adriamycin (14-hydroxydaunomycin), a novel antitumor antibiotic.* Tetrahedron Letters, 1969. **13**(13): p. 1007-1010.
351. www.drugbank.ca. *Drug Bank/Doxorubicin*. 2012 12/07/2012 [cited 2012; Available from: http://www.drugbank.ca/drugs/DB00997.
352. www.lclabs.com. *Material Safety data sheet (Doxorubicin HCL)*. 2012 [cited 2012 19/07/2012]; Available from: http://www.lclabs.com/MSDS/D-4000MSDS.php4.
353. Friedenberg, W.R., et al., *Modified vincristine, doxorubicin, and dexamethasone regimen in the treatment of resistant or relapsed chronic lymphocytic leukemia. An Eastern Cooperative Oncology Group study.* Cancer, 1993. **71**(10): p. 2983-9.

354. Frost, B.M., et al., *Pharmacokinetics of doxorubicin in children with acute lymphoblastic leukemia: multi-institutional collaborative study.* Medical and Pediatric Oncology, 2002. **38**(5): p. 329-37.
355. Hunault-Berger, M., et al., *A randomized study of pegylated liposomal doxorubicin versus continuous-infusion doxorubicin in elderly patients with acute lymphoblastic leukemia: the GRAALL-SA1 study.* Haematologica, 2011. **96**(2): p. 245-52.
356. Morris, K., et al., *Outcome of treatment of adult acute lymphoblastic leukemia with hyperfractionated cyclophosphamide, doxorubicin, vincristine, dexamethasone/methotrexate, cytarabine: results from an Australian population.* Leukemia and Lymphoma, 2011. **52**(1): p. 85-91.
357. Parnes, H.L., et al., *Phase III study of cyclophosphamide, doxorubicin, and fluorouracil (CAF) plus leucovorin versus CAF for metastatic breast cancer: Cancer and Leukemia Group B 9140.* Journal of Clinical Oncology, 2003. **21**(9): p. 1819-24.
358. Robertson, L.E., et al., *Fludarabine plus doxorubicin in previously treated chronic lymphocytic leukemia.* Leukemia, 1995. **9**(6): p. 943-5.
359. Arakelyan, N., et al., *Early versus late intensification for patients with high-risk Hodgkin lymphoma-3 cycles of intensive chemotherapy plus low-dose lymph node radiation therapy versus 4 cycles of combined doxorubicin, bleomycin, vinblastine, and dacarbazine plus myeloablative chemotherapy with autologous stem cell transplantation: five-year results of a randomized trial on behalf of the GOELAMS Group.* Cancer, 2008. **113**(12): p. 3323-30.
360. Boll, B., et al., *Phase 2 study of PVAG (prednisone, vinblastine, doxorubicin, gemcitabine) in elderly patients with early unfavorable or advanced stage Hodgkin lymphoma.* Blood, 2011. **118**(24): p. 6292-8.
361. Cabras, M.G., et al., *Long term outcome of localized aggressive non-Hodgkin lymphoma treated with a short weekly chemotherapy regimen (doxorubicin, cyclophosphamide, bleomycin, vincristine, and prednisone) and involved field radiotherapy: result of a Gruppo Italiano Multiregionale per lo Studio dei Linfomi e Leucenie (GIMURELL) study.* Leukemia and Lymphoma, 2009. **50**(9): p. 1475-81.
362. Dell'Olio, M., et al., *Non-pegylated liposomal doxorubicin (Myocet(R)) in patients with poor-risk aggressive B-cell non-Hodgkin lymphoma.* Leukemia and Lymphoma, 2011. **52**(7): p. 1222-9.
363. Pavlovsky, S., et al., *Risk-adapted therapy with three or six cycles of doxorubicin/bleomycin/vinblastine/dacarbazine plus involved-field radiation therapy in Hodgkin lymphoma, based on prognosis at diagnosis and early response: results from the GATLA study.* Clin Lymphoma Myeloma Leuk, 2010. **10**(3): p. 181-5.
364. Straus, D.J., et al., *Doxorubicin, vinblastine, and gemcitabine (CALGB 50203) for stage I/II nonbulky Hodgkin lymphoma: pretreatment prognostic factors and interim PET.* Blood, 2011. **117**(20): p. 5314-20.
365. Tobinai, K., et al., *Randomized phase II study of concurrent and sequential combinations of rituximab plus CHOP (cyclophosphamide,*

doxorubicin, vincristine and prednisolone) chemotherapy in untreated indolent B-cell non-Hodgkin lymphoma: 7-year follow-up results. Cancer Science, 2010. **101**(12): p. 2579-85.
366. Blay, J.Y., et al., *Phase I combination study of trabectedin and doxorubicin in patients with soft-tissue sarcoma.* Clin Cancer Res, 2008. **14**(20): p. 6656-62.
367. De Pas, T., et al., *Optimizing clinical care in patients with advanced soft tissue sarcoma: a phase II study of a new schedule of high-dose continuous infusion ifosfamide and doxorubicin combination.* Chemotherapy, 2011. **57**(3): p. 217-24.
368. Di Filippo, F., et al., *Hyperthermic isolated perfusion with tumor necrosis factor-alpha and doxorubicin for the treatment of limb-threatening soft tissue sarcoma: the experience of the Italian Society of Integrated Locoregional Treatment in Oncology (SITILO).* In Vivo, 2009. **23**(2): p. 363-7.
369. Fayette, J., et al., *Phase III trial of standard versus dose-intensified doxorubicin, ifosfamide and dacarbazine (MAID) in the first-line treatment of metastatic and locally advanced soft tissue sarcoma.* Investigational New Drugs, 2009. **27**(5): p. 482-9.
370. Ganjoo, K.N., et al., *A phase I study of the safety and pharmacokinetics of the hypoxia-activated prodrug TH-302 in combination with doxorubicin in patients with advanced soft tissue sarcoma.* Oncology, 2011. **80**(1-2): p. 50-6.
371. Mir, O., et al., *Doxorubicin and ifosfamide for high-grade sarcoma during pregnancy.* Cancer Chemotherapy and Pharmacology, 2012. **69**(2): p. 357-67.
372. Sessa, C., et al., *Phase I clinical and pharmacokinetic study of trabectedin and doxorubicin in advanced soft tissue sarcoma and breast cancer.* European Journal of Cancer, 2009. **45**(7): p. 1153-61.
373. Garaventa, A., et al., *A phase II study of topotecan with vincristine and doxorubicin in children with recurrent/refractory neuroblastoma.* Cancer, 2003. **98**(11): p. 2488-94.
374. George, R.E., et al., *Phase I study of decitabine with doxorubicin and cyclophosphamide in children with neuroblastoma and other solid tumors: a Children's Oncology Group study.* Pediatric Blood and Cancer, 2010. **55**(4): p. 629-38.
375. Nitschke, R., et al., *Doxorubicin and cisplatin therapy in children with neuroblastoma resistant to conventional therapy: a Southwest Oncology Group Study.* Cancer Treatment Reports, 1981. **65**(11-12): p. 1105-8.
376. Arcuri, C., et al., *A phase II study of liposomal doxorubicin in recurrent epithelial ovarian carcinoma.* Tumori, 2004. **90**(6): p. 556-61.
377. Cattel, L., et al., *Pegylated liposomal doxorubicin and vinorelbine in recurrent ovarian carcinoma: a pharmacokinetic study on alternate administration sequences.* Anticancer Research, 2006. **26**(1B): p. 745-50.
378. Chou, H.H., et al., *Pegylated liposomal doxorubicin (Lipo-Dox) for platinum-resistant or refractory epithelial ovarian carcinoma: a*

Taiwanese gynecologic oncology group study with long-term follow-up. Gynecologic Oncology, 2006. **101**(3): p. 423-8.
379. Hess, V., et al., *Phase I study of carboplatin, doxorubicin and weekly paclitaxel in patients with advanced ovarian carcinoma.* Annals of Oncology, 2003. **14**(4): p. 638-42.
380. Pectasides, D., et al., *Gemcitabine and pegylated liposomal doxorubicin alternating with cisplatin plus cyclophosphamide in platinum refractory/resistant, paclitaxel-pretreated, ovarian carcinoma.* Gynecologic Oncology, 2008. **108**(1): p. 47-52.
381. Valerio, M.R., et al., *A phase II study of pegylated liposomal doxorubicin oxaliplatin and cyclophosphamide as second-line treatment in relapsed ovarian carcinoma.* International Journal of Gynecological Cancer, 2006. **16 Suppl 1**: p. 79-85.
382. Brain, E.G., et al., *Impact of liposomal doxorubicin-based adjuvant chemotherapy on autonomy in women over 70 with hormone-receptor-negative breast carcinoma: A French Geriatric Oncology Group (GERICO) phase II multicentre trial.* Critical Reviews in Oncology/Hematology, 2011. **80**(1): p. 160-70.
383. Langer, C.J., et al., *Phase II evaluation of methotrexate, vinblastine, doxorubicin, and cisplatin (M-VAC) in advanced, measurable breast carcinoma.* Cancer Investigation, 1995. **13**(2): p. 150-9.
384. Lluch, A., et al., *Doxorubicin and paclitaxel in advanced breast carcinoma: importance of prior adjuvant anthracycline therapy.* Cancer, 2000. **89**(11): p. 2169-75.
385. Pawlicki, M., et al., *A phase II study of intravenous navelbine and doxorubicin combination in previously untreated advanced breast carcinoma.* Oncologist, 2002. **7**(3): p. 205-9.
386. Twelves, C.J. and A.M. Seymour, *Mouth cooling to prevent doxorubicin-induced stomatitis.* Annals of Oncology, 1991. **2**(9): p. 695.
387. Kaczmarek, A., et al., *Severity of doxorubicin-induced small intestinal mucositis is regulated by the TLR-2 and TLR-9 pathways.* Journal of Pathology, 2012. **226**(4): p. 598-608.
388. Hesketh, P.J. and P. Sanz-Altamira, *Aprepitant, dexamethasone, and palonosetron in the prevention of doxorubicin/cyclophosphamide-induced nausea and vomiting.* Supportive Care in Cancer, 2012. **20**(3): p. 653-6.
389. Chatterjee, K., et al., *Doxorubicin cardiomyopathy.* Cardiology, 2010. **115**(2): p. 155-62.
390. Kumar, S., et al., *Doxorubicin-induced cardiomyopathy 17 years after chemotherapy.* Texas Heart Institute Journal, 2012. **39**(3): p. 424-7.
391. Murali, A., et al., *Reversible cardiomyopathy due to doxorubicin.* National Medical Journal of India, 2010. **23**(6): p. 377-8.
392. Octavia, Y., et al., *Doxorubicin-induced cardiomyopathy: from molecular mechanisms to therapeutic strategies.* Journal of Molecular and Cellular Cardiology, 2012. **52**(6): p. 1213-25.

393. Takemura, G. and H. Fujiwara, *Doxorubicin-induced cardiomyopathy from the cardiotoxic mechanisms to management.* Progress in Cardiovascular Diseases, 2007. **49**(5): p. 330-52.
394. Durand, R.E. and P.L. Olive, *Flow cytometry studies of intracellular adriamycin in single cells in vitro.* Cancer Res, 1981. **41**(9 Pt 1): p. 3489-94.
395. Karukstis, K.K., et al., *Deciphering the fluorescence signature of daunomycin and doxorubicin.* Biophysical Chemistry, 1998. **73**(3): p. 249-63.
396. Perez-Ruiz, T., et al., *Simultaneous determination of doxorubicin, daunorubicin, and idarubicin by capillary electrophoresis with laser-induced fluorescence detection.* Electrophoresis, 2001. **22**(1): p. 134-8.
397. Minotti, G., et al., *Anthracyclines: molecular advances and pharmacologic developments in antitumor activity and cardiotoxicity.* Pharmacological Reviews, 2004. **56**(2): p. 185-229.
398. Robert, J., *Epirubicin. Clinical pharmacology and dose-effect relationship.* Drugs, 1993. **45 Suppl 2**: p. 20-30.
399. Andrivon, W., et al., *Enhanced topoisomerase II-induced DNA breaks and free radical production by a new anthracycline with potent antileukemic activity.* Leukemia Research, 1996. **20**(2): p. 119-26.
400. Danesi, R., et al., *Pharmacokinetic-pharmacodynamic relationships of the anthracycline anticancer drugs.* Clinical Pharmacokinetics, 2002. **41**(6): p. 431-44.
401. Minchin, R.F., et al., *Pharmacokinetics of doxorubicin in isolated lung of dogs and humans perfused in vivo.* Journal of Pharmacology and Experimental Therapeutics, 1984. **229**(1): p. 193-8.
402. Bongard, R.D., et al., *Influence of temperature and plasma protein on doxorubicin uptake by isolated lungs.* Drug Metabolism and Disposition, 1993. **21**(3): p. 428-34.
403. Kiyomiya, K., S. Matsuo, and M. Kurebe, *Mechanism of specific nuclear transport of adriamycin: the mode of nuclear translocation of adriamycin-proteasome complex.* Cancer Res, 2001. **61**(6): p. 2467-71.
404. Chen, V.Y., et al., *The role of the VPS4A-exosome pathway in the intrinsic egress route of a DNA-binding anticancer drug.* Pharm Res, 2006. **23**(8): p. 1687-95.
405. Fornari, F.A., et al., *Interference by doxorubicin with DNA unwinding in MCF-7 breast tumor cells.* Mol Pharmacol, 1994. **45**(4): p. 649-56.
406. Kudoh, K., et al., *Monitoring the expression profiles of doxorubicin-induced and doxorubicin-resistant cancer cells by cDNA microarray.* Cancer Res, 2000. **60**(15): p. 4161-6.
407. Lee, S., et al., *Mechanism of doxorubicin-induced cell death and expression profile analysis.* Biotechnology Letters, 2002. **24**(14): p. 1147-1151.
408. Cleator, S., et al., *Gene expression patterns for doxorubicin (Adriamycin) and cyclophosphamide (cytoxan) (AC) response and resistance.* Breast Cancer Research and Treatment, 2006. **95**(3): p. 229-33.

409. Song, J.H., et al., *Monitoring the gene expression profiles of doxorubicin-resistant acute myelocytic leukemia cells by DNA microarray analysis.* Life Sciences, 2006. **79**(2): p. 193-202.
410. Patil, R.R., S.A. Guhagarkar, and P.V. Devarajan, *Engineered nanocarriers of doxorubicin: a current update.* Critical Reviews in Therapeutic Drug Carrier Systems, 2008. **25**(1): p. 1-61.
411. George, J.W., et al., *Inhibition of DNA helicase II unwinding and ATPase activities by DNA-interacting ligands. Kinetics and specificity.* J Biol Chem, 1992. **267**(15): p. 10683-9.
412. Ueda, K., et al., *Expression of a full-length cDNA for the human "MDR1" gene confers resistance to colchicine, doxorubicin, and vinblastine.* Proceedings of the National Academy of Sciences of the United States of America, 1987. **84**(9): p. 3004-8.
413. Nielsen, D., C. Maare, and T. Skovsgaard, *Cellular resistance to anthracyclines.* General Pharmacology, 1996. **27**(2): p. 251-5.
414. Liu, Z.L., et al., *Induction of multidrug resistance in MOLT-4 cells by anticancer agents is closely related to increased expression of functional P-glycoprotein and MDR1 mRNA.* Cancer Chemotherapy and Pharmacology, 2002. **49**(5): p. 391-7.
415. Yasunami, T., et al., *Multidrug resistance protein expression of adult T-cell leukemia/lymphoma.* Leukemia Research, 2007. **31**(4): p. 465-70.
416. Juliano, R.L. and V. Ling, *A surface glycoprotein modulating drug permeability in Chinese hamster ovary cell mutants.* Biochimica et Biophysica Acta, 1976. **455**(1): p. 152-62.
417. Zaman, G.J., et al., *The human multidrug resistance-associated protein MRP is a plasma membrane drug-efflux pump.* Proceedings of the National Academy of Sciences of the United States of America, 1994. **91**(19): p. 8822-6.
418. Goren, D., et al., *Nuclear delivery of doxorubicin via folate-targeted liposomes with bypass of multidrug-resistance efflux pump.* Clin Cancer Res, 2000. **6**(5): p. 1949-57.
419. Park, J.W., et al., *Tumor targeting using anti-her2 immunoliposomes.* Journal of Controlled Release, 2001. **74**(1-3): p. 95-113.
420. Gregory, R.E. and A.F. DeLisa, *Paclitaxel: a new antineoplastic agent for refractory ovarian cancer.* Clinical Pharmacy, 1993. **12**(6): p. 401-15.
421. Wall, M.E. and M.C. Wani, *Camptothecin and taxol: discovery to clinic--thirteenth Bruce F. Cain Memorial Award Lecture.* Cancer Research, 1995. **55**(4): p. 753-60.
422. Chen, Q., et al., *Multi-center prospective randomized trial on paclitaxel liposome and traditional taxol in the treatment of breast cancer and non-small-cell lung cancer.* Chin. J. Oncol., 2003. **25**(2): p. 190-192.
423. Goldspiel, B.R., *Clinical overview of the taxanes.* Pharmacotherapy, 1997. **17**(5 Pt 2): p. 110S-125S.
424. Sharma, U.S., S.V. Balasubramanian, and R.M. Straubinger, *Pharmaceutical and physical properties of paclitaxel (Taxol) complexes*

with cyclodextrins. Journal of Pharmaceutical Sciences, 1995. **84**(10): p. 1223-30.
425. Singla, A., A. Garg, and D. Aggarwal, *Paclitaxel and its formulations.* International Journal of Pharmaceutics, 2002. **235**(1-2): p. 179-92.
426. Mazzo, D.J., et al., *Compatibility of docetaxel and paclitaxel in intravenous solutions with polyvinyl chloride infusion materials.* Am. J. Health-Syst. Pharm., 1997. **54**(5): p. 566-9.
427. Boyle, D.A. and B.R. Goldspiel, *A review of paclitaxel (Taxol) administration, stability, and compatibility issues.* Clin. J.Oncol. Nurs, 1998. **2**(4): p. 141-5.
428. Onetto, N., et al., *Overview of Taxol safety.* Journal of the National Cancer Institute. Monographs., 1993(15): p. 131-139.
429. Sparreboom, A., et al., *Cremophor EL-mediated alteration of paclitaxel distribution in human blood: clinical pharmacokinetic implications.* Cancer Research, 1999. **59**(7): p. 1454-1457.
430. Edelman, M.J., *Novel taxane formulations and microtubule-binding agents in non-small-cell lung cancer.* Clin. Lung Cancer, 2009. **10** p. S30-34.
431. Duncan, R., *The dawning era of polymer therapeutics.* Nature Reviews. Drug Discovery, 2003. **2**(5): p. 347-60.
432. Meerum Terwogt, J.M., et al., *Phase I clinical and pharmacokinetic study of PNU166945, a novel water-soluble polymer-conjugated prodrug of paclitaxel.* Anticancer Drugs, 2001. **12**(4): p. 315-23.
433. Langer, C.J., *CT-2103: a novel macromolecular taxane with potential advantages compared with conventional taxanes.* Clin. Lung Cancer, 2004. **6** p. S85-S88.
434. Singer, J.W., et al., *Poly-(L)-glutamic acid-paclitaxel (CT-2103) [XYOTAX], a biodegradable polymeric drug conjugate: characterization, preclinical pharmacology, and preliminary clinical data.* Advances in Experimental Medicine and Biology, 2003. **519**: p. 81-99.
435. Singer, J.W., *Paclitaxel poliglumex (XYOTAX™, CT-2103): A macromolecular taxane.* Journal of Controlled Release, 2005. **109**(1): p. 120-126.
436. Mahmud, A., X.B. Xiong, and A. Lavasanifar, *Development of novel polymeric micellar drug conjugates and nano-containers with hydrolyzable core structure for doxorubicin delivery.* European Journal of Pharmaceutics and Biopharmaceutics, 2008. **69**(3): p. 923-34.
437. Mahmud, A., X.B. Xiong, and A. Lavasanifar, *Novel Self-Associating Poly (ethylene oxide)-block-poly ([epsilon]-caprolactone) Block Copolymers with Functional Side Groups on the Polyester Block for Drug Delivery.* Macromolecules, 2006. **39**(26): p. 9419-9428.
438. Li, Y. and G.S. Kwon, *Micelle-like structures of poly (ethylene oxide)-block-poly (2-hydroxyethyl aspartamide)-methotrexate conjugates.* Colloids Surf. B: Biointerfaces, 1999. **16**(1-4): p. 217-226.
439. Vaisman, B., A. Shikanov, and A.J. Domb, *Normal phase high performance liquid chromatography for determination of paclitaxel*

incorporated in a lipophilic polymer matrix. Journal of Chromatography A, 2005. **1064**(1): p. 85-95.
440. Letchford, K., et al., *In vitro human plasma distribution of nanoparticulate paclitaxel is dependent on the physicochemical properties of poly(ethylene glycol)-block-poly(caprolactone) nanoparticles.* European Journal of Pharmaceutics and Biopharmaceutics, 2009. **71**(2): p. 196-206.
441. Forrest, M.L., et al., *Paclitaxel prodrugs with sustained release and high solubility in poly(ethylene glycol)-b-poly(epsilon-caprolactone) micelle nanocarriers: pharmacokinetic disposition, tolerability, and cytotoxicity.* Pharmaceutical Research, 2008. **25**(1): p. 194-206.
442. Zhao, C.L., et al., *Fluorescence probe techniques used to study micelle formation in water-soluble block copolymers.* Langmuir, 1990. **6**(2): p. 514-516.
443. Lavasanifar, A., J. Samuel, and G.S. Kwon, *The effect of alkyl core structure on micellar properties of poly(ethylene oxide)-block-poly(L-aspartamide) derivatives.* Colloids Surf. B: Biointerfaces, 2001. **22**(2): p. 115-126.
444. Cho, Y., et al., *Hydrotropic agents for study of in vitro paclitaxel release from polymeric micelles.* Journal of Controlled Release, 2004. **97**(2): p. 249-57.
445. Hu, F.-Q., et al., *Shell cross-linked stearic acid grafted chitosan oligosaccharide self-aggregated micelles for controlled release of paclitaxel.* Colloids Surf. B: Biointerfaces, 2006. **50**(2): p. 97-103.
446. Costa, P. and J.M. Sousa Lobo, *Modeling and comparison of dissolution profiles.* European Journal of Pharmaceutical Sciences, 2001. **13**(2): p. 123-33.
447. Skwarczynski, M., Y. Hayashi, and Y. Kiso, *Paclitaxel prodrugs: toward smarter delivery of anticancer agents.* Journal of Medicinal Chemistry, 2006. **49**(25): p. 7253-69.
448. Greenwald, R.B., et al., *Highly water soluble taxol derivatives: 2'-polyethyleneglycol esters as potential prodrugs.* Bioorganic and Medicinal Chemistry Letters, 1994. **4**(20): p. 2465-2470.
449. Ringel, I. and S.B. Horwitz, *Taxol is converted to 7-epitaxol, a biologically active isomer, in cell culture medium.* J. Pharm. Exper. Ther., 1987. **242**(2): p. 692-698.
450. Greenwald, R.B., et al., *Drug delivery systems: water soluble taxol 2'-polyethylene glycol ester prodrugs-design and in vivo effectiveness.* Journal of Medicinal Chemistry, 1996. **39**(2): p. 424-31.
451. Pendri, A., C.D. Conover, and R.B. Greenwald, *Antitumor activity of paclitaxel-2'-glycinate conjugated to poly(ethylene glycol): a water-soluble prodrug.* Anticancer Drug Des., 1998. **13**(5): p. 387-395.
452. Mahmud, A., et al., *Self-associating poly(ethylene oxide)-b-poly(alpha-cholesteryl carboxylate-epsilon-caprolactone) block copolymer for the solubilization of STAT-3 inhibitor cucurbitacin I.* Biomacromolecules, 2009.

453. Yao, J.H., et al., *Light scattering and luminescence studies on self-aggregation behavior of amphiphilic copolymer micelles.* Journal of Physical Chemistry. B, 2008. **112**(3): p. 749-755.
454. Hans, M., et al., *Synthesis and characterization of mPEG-PLA prodrug micelles.* Biomacromolecules, 2005. **6**(5): p. 2708-17.
455. Yokoyama, M., et al., *Characterization of physical entrapment and chemical conjugation of adriamycin in polymeric micelles and their design for in vivo delivery to a solid tumor.* J.Control. Release, 1998. **50**(1-3): p. 79-92.
456. Letchford, K., R. Liggins, and H. Burt, *Solubilization of hydrophobic drugs by methoxy poly(ethylene glycol)-block-polycaprolactone diblock copolymer micelles: theoretical and experimental data and correlations.* Journal of Pharmaceutical Sciences, 2008. **97**(3): p. 1179-90.
457. Shahin, M. and A. Lavasanifar, *Novel self-associating poly(ethylene oxide)-b-poly(epsilon-caprolactone) based drug conjugates and nano-containers for paclitaxel delivery.* Int J Pharm, 2010. **389**(1-2): p. 213-22.
458. Xiong, X.B., et al., *Conjugation of arginine-glycine-aspartic acid peptides to poly(ethylene oxide)-b-poly(epsilon-caprolactone) micelles for enhanced intracellular drug delivery to metastatic tumor cells.* Biomacromolecules, 2007. **8**(3): p. 874-84.
459. Xiong, X.B., et al., *Multifunctional polymeric micelles for enhanced intracellular delivery of doxorubicin to metastatic cancer cells.* Pharm Res, 2008. **25**(11): p. 2555-66.
460. Mahmud, A. and A. Lavasanifar, *The effect of block copolymer structure on the internalization of polymeric micelles by human breast cancer cells.* Colloids Surf B Biointerfaces, 2005. **45**(2): p. 82-9.
461. Wang, T., V.A. Petrenko, and V.P. Torchilin, *Paclitaxel-loaded polymeric micelles modified with MCF-7 cell-specific phage protein: enhanced binding to target cancer cells and increased cytotoxicity.* Mol Pharm, 2010. **7**(4): p. 1007-14.
462. Nasongkla, N., et al., *cRGD-functionalized polymer micelles for targeted doxorubicin delivery.* Angew Chem Int Ed Engl, 2004. **43**(46): p. 6323-7.
463. Danhier, F., et al., *Targeting of tumor endothelium by RGD-grafted PLGA-nanoparticles loaded with paclitaxel.* J Control Release, 2009. **140**(2): p. 166-73.
464. Yin, J., et al., *Cyclic RGDyK conjugation facilitates intracellular drug delivery of polymeric micelles to integrin-overexpressing tumor cells and neovasculature.* J Drug Target, 2011. **19**(1): p. 25-36.
465. Hu, Z., et al., *Arg-Gly-Asp (RGD) peptide conjugated poly(lactic acid)-poly(ethylene oxide) micelle for targeted drug delivery.* J Biomed Mater Res A, 2008. **85**(3): p. 797-807.
466. Vicent, M.J., *Polymer-drug conjugates as modulators of cellular apoptosis.* The AAPS journal, 2007. **9**(2): p. 200-207.
467. Duncan, R., *THE DAWNING ERA OF POLYMER.* NATURE REVIEWS| DRUG DISCOVERY, 2003. **2**: p. 347.

468. Li, C. and S. Wallace, *Polymer-drug conjugates: Recent development in clinical oncology.* Advanced Drug Delivery Reviews, 2008. **60**(8): p. 886-898.
469. Vicent, M.J. and R. Duncan, *Polymer conjugates: nanosized medicines for treating cancer.* Trends in Biotechnology, 2006. **24**(1): p. 39-47.
470. Greco, F. and M.J. Vicent, *Polymer-drug conjugates: current status and future trends.* Frontiers in bioscience: a journal and virtual library, 2008. **13**: p. 2744.
471. Kratz, F., K. Abu Ajaj, and A. Warnecke, *Anticancer carrier-linked prodrugs in clinical trials.* 2007.
472. Boddy, A.V., et al., *A phase I and pharmacokinetic study of paclitaxel poliglumex (XYOTAX), investigating both 3-weekly and 2-weekly schedules.* Clinical Cancer Research, 2005. **11**(21): p. 7834-7840.
473. Langer, C., et al., *Paclitaxel poliglumex (PPX)/carboplatin vs paclitaxel/carboplatin for the treatment of PS2 patients with chemotherapy-naïve advanced non-small cell lung cancer (NSCLC): A phase III study.* Journal of Clinical Oncology, 2005. **23**(16 suppl): p. 623s.
474. Hu, X. and X. Jing, *Biodegradable amphiphilic polymer-drug conjugate micelles.* 2009.
475. Xie, Z., et al., *A novel polymer–paclitaxel conjugate based on amphiphilic triblock copolymer.* Journal of Controlled Release, 2007. **117**(2): p. 210-216.
476. Mahmud, A., X.B. Xiong, and A. Lavasanifar, *Novel Self-Associating Poly (ethylene oxide)-b lock-poly (ε-caprolactone) Block Copolymers with Functional Side Groups on the Polyester Block for Drug Delivery.* Macromolecules, 2006. **39**(26): p. 9419-9428.
477. Leonessa, F., et al., *MDA435/LCC6 and MDA435/LCC6MDR1: ascites models of human breast cancer.* British Journal of Cancer, 1996. **73**(2): p. 154-61.
478. Sharifi, N. and R.A. Steinman, *Targeted chemotherapy: chronic myelogenous leukemia as a model.* Journal of Molecular Medicine, 2002. **80**(4): p. 219-32.
479. Vizel, M. and M.W. Oster, *Ocular side effects of cancer chemotherapy.* Cancer, 1982. **49**(10): p. 1999-2002.
480. Perrino, C., et al., *Cardiac Side Effects of Chemotherapy: State of Art and Strategies for a Correct Management.* Current Vascular Pharmacology, 2012. **10**(6).
481. Monsuez, J.J., et al., *Cardiac side-effects of cancer chemotherapy.* International Journal of Cardiology, 2010. **144**(1): p. 3-15.
482. Mavrogenis, A.F., et al., *Side effects of chemotherapy in musculoskeletal oncology.* Journal of Long-Term Effects of Medical Implants, 2010. **20**(1): p. 1-12.
483. Gosselin, M.A. and R.J. Lee, *Folate receptor-targeted liposomes as vectors for therapeutic agents.* Biotechnology Annual Review, 2002. **8**: p. 103-31.

484. Herbst, S.M., et al., *Delivery of stem cells to porcine arterial wall with echogenic liposomes conjugated to antibodies against CD34 and intercellular adhesion molecule-1.* Mol Pharm, 2010. **7**(1): p. 3-11.
485. Torchilin, V.P., et al., *p-Nitrophenylcarbonyl-PEG-PE-liposomes: fast and simple attachment of specific ligands, including monoclonal antibodies, to distal ends of PEG chains via p-nitrophenylcarbonyl groups.* Biochimica et Biophysica Acta, 2001. **1511**(2): p. 397-411.
486. Elbayoumi, T.A. and V.P. Torchilin, *Tumor-specific antibody-mediated targeted delivery of Doxil reduces the manifestation of auricular erythema side effect in mice.* Int J Pharm, 2008. **357**(1-2): p. 272-9.
487. Wei, M., et al., *Hepatocellular carcinoma targeting effect of PEGylated liposomes modified with lactoferrin.* European Journal of Pharmaceutical Sciences, 2012. **46**(3): p. 131-41.
488. Lv, P.P., et al., *Targeted Delivery of Insoluble Cargo (Paclitaxel) by PEGylated Chitosan Nanoparticles Grafted with Arg-Gly-Asp (RGD).* Mol Pharm, 2012. **9**(6): p. 1736-47.
489. Lin, R.Y., et al., *Targeted RGD nanoparticles for highly sensitive in vivo integrin receptor imaging.* Contrast Media and Molecular Imaging, 2012. **7**(1): p. 7-18.
490. Negussie, A.H., et al., *Synthesis and in vitro evaluation of cyclic NGR peptide targeted thermally sensitive liposome.* J Control Release, 2010. **143**(2): p. 265-73.
491. Chen, Y., J.J. Wu, and L. Huang, *Nanoparticles targeted with NGR motif deliver c-myc siRNA and doxorubicin for anticancer therapy.* Molecular Therapy, 2010. **18**(4): p. 828-34.
492. Wang, X., et al., *NGR-modified micelles enhance their interaction with CD13-overexpressing tumor and endothelial cells.* J Control Release, 2009. **139**(1): p. 56-62.
493. Garde, S.V., et al., *Binding and internalization of NGR-peptide-targeted liposomal doxorubicin (TVT-DOX) in CD13-expressing cells and its antitumor effects.* Anticancer Drugs, 2007. **18**(10): p. 1189-200.
494. Ruoslahti, E., *RGD and other recognition sequences for integrins.* Annual Review of Cell and Developmental Biology, 1996. **12**: p. 697-715.
495. Meyer, A., et al., *Targeting RGD recognizing integrins: drug development, biomaterial research, tumor imaging and targeting.* Current Pharmaceutical Design, 2006. **12**(22): p. 2723-47.
496. Janssen, A.P., et al., *Peptide-targeted PEG-liposomes in anti-angiogenic therapy.* Int J Pharm, 2003. **254**(1): p. 55-8.
497. Muggia, F.M., *Liposomal encapsulated anthracyclines: new therapeutic horizons.* Current Oncology Reports, 2001. **3**(2): p. 156-62.
498. Gabizon, A.A., *Pegylated liposomal doxorubicin: metamorphosis of an old drug into a new form of chemotherapy.* Cancer Investigation, 2001. **19**(4): p. 424-36.
499. Vail, D.M., et al., *Preclinical trial of doxorubicin entrapped in sterically stabilized liposomes in dogs with spontaneously arising malignant tumors.* Cancer Chemotherapy and Pharmacology, 1997. **39**(5): p. 410-6.

500. Ten Hagen, T.L., et al., *Low-dose tumor necrosis factor-alpha augments antitumor activity of stealth liposomal doxorubicin (DOXIL) in soft tissue sarcoma-bearing rats.* International Journal of Cancer, 2000. **87**(6): p. 829-37.
501. Gabizon, A., H. Shmeeda, and Y. Barenholz, *Pharmacokinetics of pegylated liposomal Doxorubicin: review of animal and human studies.* Clinical Pharmacokinetics, 2003. **42**(5): p. 419-36.
502. Sparano, J.A. and E.P. Winer, *Liposomal anthracyclines for breast cancer.* Seminars in Oncology, 2001. **28**(4 Suppl 12): p. 32-40.
503. Alberts, D.S., et al., *Efficacy and safety of liposomal anthracyclines in phase I/II clinical trials.* Seminars in Oncology, 2004. **31**(6 Suppl 13): p. 53-90.
504. Poveda, A., et al., *Phase II Clinical Trial With Pegylated Liposomal Doxorubicin (CAELYX(R)/Doxil(R)) and Quality of Life Evaluation (EORTC QLQ-C30) in Adult Patients With Advanced Soft Tissue Sarcomas: A study of the Spanish Group for Research in Sarcomas (GEIS).* Sarcoma, 2005. **9**(3-4): p. 127-32.
505. James, J.S., *DOXIL approved for KS.* AIDS Treatment News, 1995(236): p. 6.
506. Moreira, J.N., et al., *Use of the post-insertion technique to insert peptide ligands into pre-formed stealth liposomes with retention of binding activity and cytotoxicity.* Pharm Res, 2002. **19**(3): p. 265-9.
507. Allen, T.M., P. Sapra, and E. Moase, *Use of the post-insertion method for the formation of ligand-coupled liposomes.* Cellular and Molecular Biology Letters, 2002. **7**(3): p. 889-94.
508. Elbayoumi, T.A. and V.P. Torchilin, *Tumor-specific anti-nucleosome antibody improves therapeutic efficacy of doxorubicin-loaded long-circulating liposomes against primary and metastatic tumor in mice.* Mol Pharm, 2009. **6**(1): p. 246-54.
509. Iden, D.L. and T.M. Allen, *In vitro and in vivo comparison of immunoliposomes made by conventional coupling techniques with those made by a new post-insertion approach.* Biochimica et Biophysica Acta, 2001. **1513**(2): p. 207-16.
510. Li, C.L., et al., *Development of pegylated liposomal vinorelbine formulation using "post-insertion" technology.* Int J Pharm, 2010. **391**(1-2): p. 230-6.
511. Gubernator, J., *Active methods of drug loading into liposomes: recent strategies for stable drug entrapment and increased in vivo activity.* Expert Opinion on Drug Delivery, 2011. **8**(5): p. 565-80.
512. Ishida, T., D.L. Iden, and T.M. Allen, *A combinatorial approach to producing sterically stabilized (Stealth) immunoliposomal drugs.* FEBS Letters, 1999. **460**(1): p. 129-133.
513. Elbayoumi, T.A. and V.P. Torchilin, *Enhanced cytotoxicity of monoclonal anticancer antibody 2C5-modified doxorubicin-loaded PEGylated liposomes against various tumor cell lines.* European Journal of Pharmaceutical Sciences, 2007. **32**(3): p. 159-68.

514. Zunino, F. and G. Capranico, *DNA topoisomerase II as the primary target of anti-tumor anthracyclines.* Anti-Cancer Drug Design, 1990. **5**(4): p. 307-17.
515. Hortobagyi, G.N., *Anthracyclines in the treatment of cancer. An overview.* Drugs, 1997. **54 Suppl 4**: p. 1-7.
516. Igarashi, E., *Factors affecting toxicity and efficacy of polymeric nanomedicines.* Toxicology and applied pharmacology, 2008. **229**(1): p. 121-134.
517. Malam, Y., M. Loizidou, and A.M. Seifalian, *Liposomes and nanoparticles: nanosized vehicles for drug delivery in cancer.* Trends in Pharmacological Sciences, 2009. **30**(11): p. 592-599.
518. Ning, Y.M., et al., *Liposomal doxorubicin in combination with bortezomib for relapsed or refractory multiple myeloma.* Oncology (Williston Park), 2007. **21**(12): p. 1503-8; discussion 1511, 1513, 1516 passim.
519. Thigpen, J.T., et al., *Role of pegylated liposomal doxorubicin in ovarian cancer.* Gynecologic Oncology, 2005. **96**(1): p. 10-18.
520. Solomon, R. and A.A. Gabizon, *Clinical pharmacology of liposomal anthracyclines: focus on pegylated liposomal Doxorubicin.* Clinical Lymphoma, Myeloma & Leukemia, 2008. **8**(1): p. 21-32.
521. Sapra, P., et al., *Improved therapeutic responses in a xenograft model of human B lymphoma (Namalwa) for liposomal vincristine versus liposomal doxorubicin targeted via anti-CD19 IgG2a or Fab' fragments.* Clinical Cancer Research, 2004. **10**(3): p. 1100-1111.
522. Sapra, P. and T.M. Allen, *Improved outcome when B-cell lymphoma is treated with combinations of immunoliposomal anticancer drugs targeted to both the CD19 and CD20 epitopes.* Clinical Cancer Research, 2004. **10**(7): p. 2530-2537.
523. Pastorino, F., et al., *Targeting Liposomal Chemotherapy via Both Tumor Cell–Specific and Tumor Vasculature–Specific Ligands Potentiates Therapeutic Efficacy.* Cancer Research, 2006. **66**(20): p. 10073.
524. Reddy, J.A., et al., *Folate-targeted, cationic liposome-mediated gene transfer into disseminated peritoneal tumors.* Gene Therapy, 2002. **9**(22): p. 1542-50.
525. Saul, J.M., et al., *Controlled targeting of liposomal doxorubicin via the folate receptor in vitro.* J Control Release, 2003. **92**(1-2): p. 49-67.
526. Shmeeda, H., et al., *Intracellular uptake and intracavitary targeting of folate-conjugated liposomes in a mouse lymphoma model with up-regulated folate receptors.* Molecular Cancer Therapeutics, 2006. **5**(4): p. 818-24.
527. Kawano, K. and Y. Maitani, *Effects of polyethylene glycol spacer length and ligand density on folate receptor targeting of liposomal Doxorubicin in vitro.* J Drug Deliv, 2011. **2011**: p. 160967.
528. Olivier, V., et al., *Influence of targeting ligand flexibility on receptor binding of particulate drug delivery systems.* Bioconjug Chem, 2003. **14**(6): p. 1203-8.

529. Gindy, M.E., et al., *Preparation of poly(ethylene glycol) protected nanoparticles with variable bioconjugate ligand density.* Biomacromolecules, 2008. **9**(10): p. 2705-11.
530. Ferrari, M., *Nanogeometry: beyond drug delivery.* Nature Nanotechnology, 2008. **3**(3): p. 131-2.
531. Marty, C. and R.A. Schwendener, *Cytotoxic Tumor Targeting With scFv Antibody-Modified Liposomes*, in *Adoptive immunotherapy: methods and protocols*, B. Ludewig and M.W. Hoffmann, Editors. 2005, Humana Pr Inc. p. 389-401.
532. Huang, G., *Engineering RGD-Modified Liposomes for Targeted Drug Delivery to Activated Platelets*. 2006, Case Western Reserve University.
533. Kirpotin, D., et al., *Sterically stabilized anti-HER2 immunoliposomes: design and targeting to human breast cancer cells in vitro.* Biochemistry, 1997. **36**(1): p. 66-75.
534. Allen, T.M., et al., *A new strategy for attachment of antibodies to sterically stabilized liposomes resulting in efficient targeting to cancer cells.* Biochimica et Biophysica Acta (BBA) - Biomembranes, 1995. **1237**(2): p. 99-108.
535. Maruyama, K., et al., *Targetability of novel immunoliposomes modified with amphipathic poly(ethylene glycol)s conjugated at their distal terminals to monoclonal antibodies.* Biochimica et Biophysica Acta, 1995. **1234**(1): p. 74-80.
536. Allen, T.M., *Liposomal drug delivery.* Current Opinion in Colloid & Interface Science, 1996. **1**(5): p. 645-651.
537. Shmeeda, H., et al., *Her2-targeted pegylated liposomal doxorubicin: retention of target-specific binding and cytotoxicity after in vivo passage.* J Control Release, 2009. **136**(2): p. 155-60.
538. Gu, F., et al., *Precise engineering of targeted nanoparticles by using self-assembled biointegrated block copolymers.* Proceedings of the National Academy of Sciences of the United States of America, 2008. **105**(7): p. 2586-91.
539. Peletskaya, E.N., et al., *Characterization of peptides that bind the tumor-associated Thomsen-Friedenreich antigen selected from bacteriophage display libraries.* Journal of Molecular Biology, 1997. **270**(3): p. 374-84.
540. Bhojani, M.S., et al., *Synthesis and investigation of a radioiodinated F3 peptide analog as a SPECT tumor imaging radioligand.* PLoS ONE, 2011. **6**(7): p. e22418.
541. Numata, K., et al., *Silk-based nanocomplexes with tumor-homing peptides for tumor-specific gene delivery.* Macromolecular Bioscience, 2012. **12**(1): p. 75-82.
542. Smart, E.J., C. Mineo, and R.G. Anderson, *Clustered folate receptors deliver 5-methyltetrahydrofolate to cytoplasm of MA104 cells.* Journal of Cell Biology, 1996. **134**(5): p. 1169-77.
543. Fakhari, A., et al., *Controlling ligand surface density optimizes nanoparticle binding to ICAM-1.* J Pharm Sci, 2011. **100**(3): p. 1045-56.

544. Cluzel, C., et al., *The mechanisms and dynamics of (alpha)v(beta)3 integrin clustering in living cells.* Journal of Cell Biology, 2005. **171**(2): p. 383-92.
545. Liu, A.P., et al., *Local clustering of transferrin receptors promotes clathrin-coated pit initiation.* Journal of Cell Biology, 2010. **191**(7): p. 1381-93.
546. Arap, W., R. Pasqualini, and E. Ruoslahti, *Cancer treatment by targted drug delivery to tumor vasculature in a mouse model.* Science, 1998. **279**: p. 377-380.
547. Wang, H., et al., *Integrin-targeted imaging and therapy with RGD4C-TNF fusion protein.* Molecular Cancer Therapeutics, 2008. **7**(5): p. 1044.
548. Charrois, G.J. and T.M. Allen, *Multiple injections of pegylated liposomal Doxorubicin: pharmacokinetics and therapeutic activity.* Journal of Pharmacology and Experimental Therapeutics, 2003. **306**(3): p. 1058-67.
549. Lodish, H., et al., *Identification and Purification of Cell-Surface Receptors*, in *Molecular Cell Biology*. 2007, W. H. Freeman.
550. Elamanchili, P., C. McEachern, and H. Burt, *Reversal of multidrug resistance by methoxypolyethylene glycol-block-polycaprolactone diblock copolymers through the inhibition of P-glycoprotein function.* J Pharm Sci, 2009. **98**(3): p. 945-58.
551. Zastre, J., et al., *Methoxypolyethylene glycol-block-polycaprolactone diblock copolymers reduce P-glycoprotein efflux in the absence of a membrane fluidization effect while stimulating P-glycoprotein ATPase activity.* J Pharm Sci, 2007. **96**(4): p. 864-75.
552. Zastre, J., J. Jackson, and H. Burt, *Evidence for modulation of P-glycoprotein-mediated efflux by methoxypolyethylene glycol-block-Polycaprolactone amphiphilic diblock copolymers.* Pharm Res, 2004. **21**(8): p. 1489-97.
553. Zastre, J., et al., *Enhanced cellular accumulation of a P-glycoprotein substrate, rhodamine-123, by Caco-2 cells using low molecular weight methoxypolyethylene glycol-block-polycaprolactone diblock copolymers.* Eur J Pharm Biopharm, 2002. **54**(3): p. 299-309.
554. Shegokar, R., L. Al Shaal, and P.R. Mishra, *SiRNA delivery: challenges and role of carrier systems.* Pharmazie, 2011. **66**(5): p. 313-8.
555. Toloue, M.M. and L.P. Ford, *Antibody targeted siRNA delivery.* Methods in Molecular Biology, 2011. **764**: p. 123-39.
556. Tagalakis, A.D., et al., *Receptor-targeted liposome-peptide nanocomplexes for siRNA delivery.* Biomaterials, 2011. **32**(26): p. 6302-15.
557. Wang, X.L., R. Xu, and Z.R. Lu, *A peptide-targeted delivery system with pH-sensitive amphiphilic cell membrane disruption for efficient receptor-mediated siRNA delivery.* J Control Release, 2009. **134**(3): p. 207-13.
558. Allen, T.M., *Ligand-targeted therapeutics in anticancer therapy.* Nature Reviews Cancer, 2002. **2**(10): p. 750-763.

559. www.wikipedia.org. *Paul Ehrlich*. 2012 [cited 2012 24/06/2012]; Available from: http://en.wikipedia.org/wiki/Paul_Ehrlich.